THE HIGHLY PREORGANIZED LIGAND 2,9-DI-(2'-PYRIDYL)-1,10-PHENANTHROLINE, AND ITS COMPLEXATION PROPERTIES WITH METAL IONS

Gregory Mercer Cockrell

A Thesis Submitted to the
University of North Carolina Wilmington in Partial Fulfillment
Of the Requirements for the Degree of
Master of Science

Department of Chemistry and Biochemistry

University of North Carolina Wilmington

2007

Approved by

Advisory Committee

_____ _____

_____
Chair

Accepted by

_____
Dean, Graduate School

TABLE OF CONTENTS

ABSTRACT

The compound 2,9-di-(2'-pyridyl)-1,10-phenanthroline (DPP) has many potential uses in the fields of medicinal and environmental chemistry. The great stability possessed by complexes of DPP and heavier metal ions such as cadmium, lead, and mercury, is ideal when designing ligands for uses as fluorescence sensors or chelation therapies. This ligand, and others in its class, posses a high degree of preorganization. This means that they are designed to target specific metal ions by being in the correct conformation in its free form. UV/Vis spectroscopy was utilized to calculate stability constants with several different metal ions of varying ionic charges and radii. DPP was found to be highly selective for cadmium with a log K_1 = 12.21. Other metal ions that formed very stable complexes were bismuth (log K_1 = 15.72) and mercury (not measurable with available materials). Fluorescence studies were conducted and found that upon binding to cadmium, DPP has a dramatic increase in fluorescence intensity. Fluorescence studies also showed that cadmium could be detected in aqueous solution at concentrations as low as 1 x 10^{-10} M.

ACKNOWLEDGEMENTS

I would like to thank:

Dr. Hancock for being one of the best teachers I have ever had and for being a great research advisor. I have learned so much and I want to thank you for allowing me the opportunity to work on this project.

Dr. Jones for always knocking me down a notch so that I didn't get full of myself. Also, thanks for all of your help and time spent on this project.

Dr. Tyrell for being a great teacher and for all of your help with my organic chemistry related problems. I'll make you proud when I am up at Boston College.

The Inorganic Research Group: Crisp McDonald, Lindsay Boone, Ray Gephart, Nolan Dean, Jason Whitehead, Darren Melton, Neil Williams, and Marie Roth (MACRL) for all of the shenanigans and fun memories I will never forget.

My Family for their continued support throughout my education.

DEDICATION

I would like to dedicate this thesis to my hero Jack Bauer who taught me not to take crap from anyone: not my friends and especially not terrorists.

LIST OF TABLES

LIST OF FIGURES

INTRODUCTION

Selectivity of one metal ion over another is an important concept of coordination chemistry and has many potential uses in the fields of medicine and environmental chemistry. Ligands can be designed specifically for certain metals allowing them to be used as MRI (Magnetic Resonance Imaging) contrast agents, fluorescent detectors, and metal extractants.

MRI Contrast Agents

MRI is a powerful tool for visualizing internal body organs. Gadolinium (Gd^{3+}) is ideal for use as a contrast agent because of its seven unpaired electrons and long relaxation time (Pierre, 2006). However, Gd^{3+} is very toxic and must be strongly complexed to a ligand for in vivo applications. These Gd^{3+} based contrast agents function by catalytically relaxing water protons. They usually have one inner-sphere water molecule that is in fast exchange with the bulk solvent (Caravan, 2003). Clinically used MRI contrast agents have one water molecule coordinated directly to Gd^{3+} which limits its imaging enhancing capability. This is because the one water molecule exchanges too slowly with the bulk solvent (Pierre, 2006). Relaxivity depends on the electronic properties of the metal ion, the number of water molecules in the inner and second coordination spheres, and the ion-hydrogen distance (Caravan, 2003). Higher relaxivity, and thus a stronger MRI image, can be achieved by increasing the number of water molecules coordinated to Gd^{3+}. An example of a MRI contrast agent that is clinically used is a DTPA (diethylenetriamine pentaacetate) complex with Gd^{3+}. The

chemical structure of this complex is shown in Figure 1. This is used because DTPA forms a strong complex with Gd^{3+} (log K_1 22.39) (Martel, 2003).

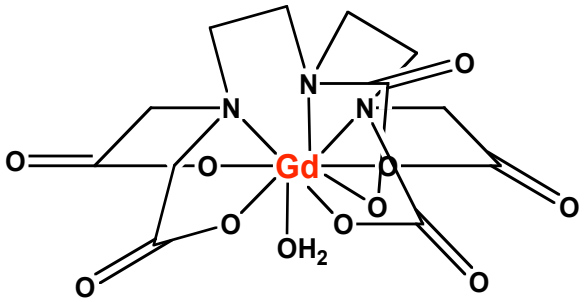

Figure 1. Chemical structure of [Gd(DTPA)OH_2] complex used as a MRI contrast agent.

This complex can only have one water attached because Gd^{3+} has a coordination number of nine and DTPA has eight points of attachment. When designing the ideal MRI contrast agent, the ligand must bind with as few points of attachment as possible without compromising complex stability, allowing more water molecules to be attached to Gd^{3+}.

Fluorescence Detectors

Chemosensors are molecules that transform chemical information, such as the presence of a specific metal ion, into an analytically useful signal (Lim, 2005). Such sensors take advantage of chelation-enhanced fluorescence (CHEF). This means that metal binding triggers intense fluorescence of the sensor and the unbound molecule is nonfluorescent (Lim, 2005). Ligands used as detectors must be designed for specific metal ions while the ligand itself weakly fluoresces. This can be achieved by amine donor groups. They will weakly fluoresce due to a photoelectron transfer (PET) quenching process caused by the lone pairs on the nitrogen donors (Lim, 2005). These CHEF-type sensors have both environmental and medicinal applications.

Lim *et al*. designed coumarin-based chemosensors that are zinc specific and can be used to describe the distribution patterns of zinc during biological events. One of the most important metals in biological systems is calcium (Ca^{2+}). Ca^{2+} can be called a universal switch because of its wide variety of functions in signal transduction. It turns on enzymes, releases neurotransmitters, and controls cell division. Ca^{2+} also activates a cysteine protease called calpain, which is involved in neurodegeneration and apoptosis (Gomperts, 2004). Intracellular Ca^{2+} in almost every kind of cell can be monitored by a fluorescent indicator called Fura2. The fluorescence of this compound is sensitive to Ca^{2+} concentration. Studies have been conducted using Fura2 to track Ca^{2+} in the neurons of Alzheimers patients (Mattson, 1998). The disadvantage to using Fura2 is the cost. Currently, Microprobes of California charges $150.00 for 5 mg of Fura2.

While ligands can be designed to detect zinc and calcium in the body, they can also be designed specifically for detection of heavy metals in ground and drinking waters. Cadmium is a dangerous metal with adverse health effects. Studies that show low-level cadmium exposure having negative health effects have led to efforts to reduce cadmium pollution in the environment (Hood, 2006). Cadmium occurs naturally in zinc, lead, and copper ores, in coal and fossil fuels, and is also released during volcanic action. Major industrial releases of cadmium come from many different sources. These include smelting and refining of zinc ores, casting of various cadmium alloy products for coating wires, manufacturing of nickel-cadmium batteries in convenience appliances and stand-by power and lighting, and also fossil fuel combustion, fertilizer application, and sewage sludge disposal (EPA, 2000). With the many ways cadmium can be introduced into the environment, it is important to detect its levels in ground and drinking waters.

Chelation therapy for cadmium, lead, and mercury poisoning

As discussed above, there are many ways people can come into contact with cadmium. It is known that high-level exposure to cadmium causes bone damage and new studies show that even low-level exposure can contribute to osteoporosis (Hood, 2006). Other health effects include nausea, vomiting, sensory disturbances, and potential to cause kidney and liver damage (EPA, 2000). Mercury and lead are two other metals that have dangerous health risks. Exposure to mercury may result in severe damage to the nervous and reproductive systems and may ultimately be fatal. Common symptoms of mercury poisoning are poor coordination and altered sensory perception (EPA, 2000). Mercury poisoning is most commonly caused by consumption of fish contaminated with methylmercury (EPA, 2000). Lead is a highly toxic metal that was used for many years in products found in and around homes. Lead may cause a range of health effects, from behavioral problems and learning disabilities, to seizures and death (EPA, 2000). When treating exposure to these three metals, a ligand selective for large metal ions can be used to separate these harmful metals from metals like calcium and zinc in the body. Once the ligand binds, the toxicity of the metal will be masked, much like how DTPA masks the toxicity of Gd^{3+} for MRI. Two case reports show that people exposed to fatal doses of both arsenic and mercury were healed after intense decontamination and the use of chelation therapy (Wang, 2006).

2,9-Di-(2'-pyridyl)-1,10-phenanthroline

The ligand investigated in this study was 2,9-di-(2'-pyridyl)-1,10-phenanthroline (DPP). DPP is just one of many phenanthroline derivatives being studied (Hancock *et. al.,* 2007; Melton, 2006). The structure of DPP is shown in Figure 2. This class of ligands is ideal for binding large metal ions because of several factors. Preorganization, type of donor atoms, chelate ring size, and hard and soft acid and base theory all play important roles in metal ion selectivity and designing ligands for the applications previously discussed.

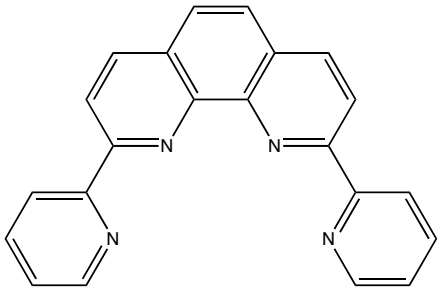

Figure 2. Chemical structure of DPP.

Preorganization

A ligand can be described as preorganized if the free ligand is in the correct conformation to bind to its target metal ion (Cram, 1988). Figure 3 illustrates the definition of preorganization with DPP and its straight chain analogue, Bis-2,2':6',2":6",2"'-quaterpyridine (QUATERPY).

a) 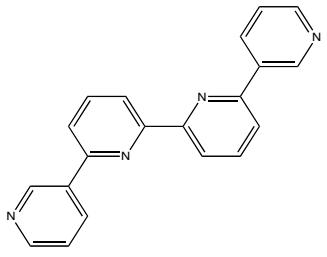

b) 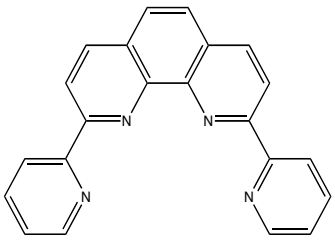

Figure 3. a) Chemical structure of QUATERPY compared to b) chemical structure of DPP to illustrate preorganization.

As shown above, QUATERPY can freely rotate along each single bond. This means it has to overcome more energy to bind a metal ion, resulting in a smaller stability constant (log K_1). With the addition of an ethylene bridge, forming DPP, the nitrogens in the 1,10-position are fixed and unable to rotate. Studies have shown that making it unnecessary for the ligand to rotate to form a complex leads to an increase in log K_1 (Hancock, 1989).

Chelate Ring Size and Metal Ion Selection

The chelate ring size rule states that the change from a five membered to a six membered chelate ring results in an increase in complex stability for small metal ions relative to large metal ions (Hancock, 1992). Figure 4 depicts the chelate ring size rule and also the effect preorganization has on designing ligands that form five and six membered rings with metal ions.

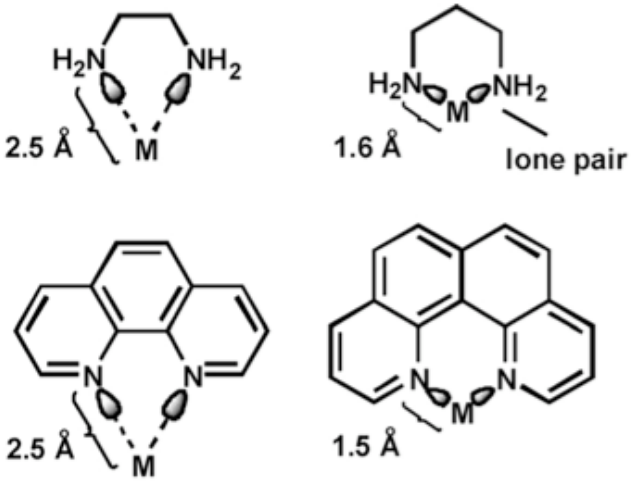

Figure 4. Illustration of the effect of the formation of chelate rings on metal ion selectivity. Ligands that form of 5-membered chelate rings upon complexing a metal ion are selective for large metals (left), where 6-membered rings are selective for small metal ions (right).

The reason for this increased stability can be easily explained by the low-strain chair conformation of cyclohexane. All torsional angles in this conformation are 60°, and the C-C-C bond angles are all 109.5°. By comparison a six membered ring made by a metal ligand complex will have a similar geometry. This means that the complex will have very low steric strain as long as the metal ion is similar in size to a sp^3 hybridized carbon atom. As seen in Figure 5, the ideal metal ion for formation of a six membered ring will result in an M-N bond length of 1.54 Å and an N-M-N bond angle of 109.5°. The lone pairs on the nitrogens in a five membered ring form an M-N bond of 2.5 Å, and create an N-M-N bond angle of 69°.

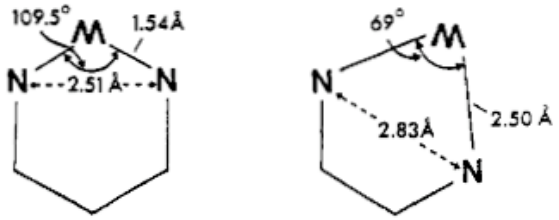

Figure 5. Illustration of bite size, bond lengths, and bond angles formed in a six membered and five membered chelate ring.

For both five and six membered rings there is a rapid rise in strain energy as the metal ion becomes less ideal in size and geometry, which results in lower complex stability. This effect can be seen in Figure 6, where there is a greater decrease in complex stability for large metal ions with an increase in chelate ring size in two different open chain ligands (Hancock, 1989).

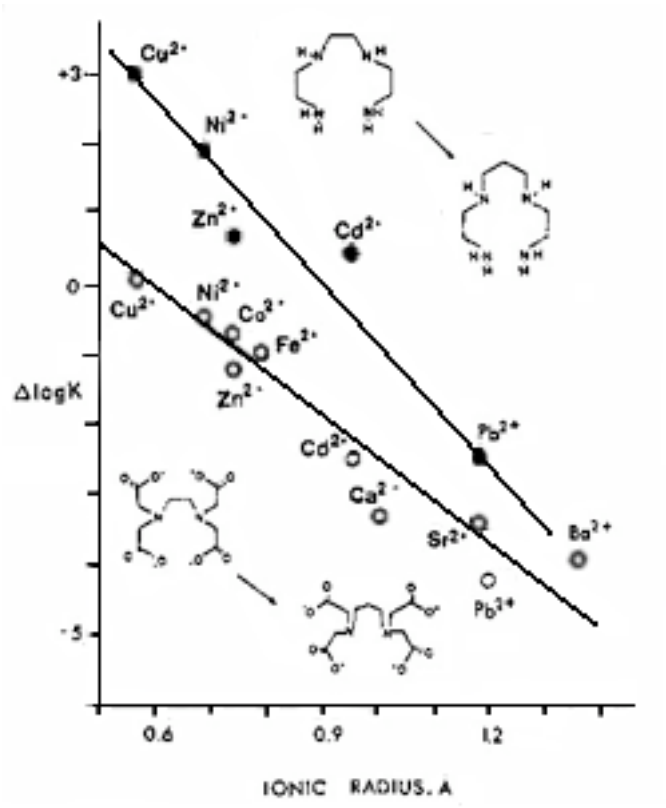

Figure 6. Plot of Δlog K versus ionic radius (Å) of two different open chain ligands to illustrate the effect on complex stability with an increase of chelate ring size from a five membered ring to a six membered ring.

Denticity and Nitrogen Donor atoms

The coordination number of a metal ion refers to the number of binding sites possessed by the metal. This is an important factor in designing ligands specifically for one metal ion. Coordination number is a good indication of how many donor atoms a ligand should have to form a strong complex. By increasing the denticity, or number of donor atoms, of a ligand, the stability constant also increases. This is illustrated in Table 1, where the stability constant of Ni^{2+} increases as the denticity increases in a series of polyamine ligands.

Table 1. Stability constants of Ni^{2+} complexes in a series of polyamine ligands to show the effect of increasing ligand denticity.

Polyamine	EN	DIEN	TRIEN	TETREN	PENTEN
denticity, n	2	3	4	5	6
log β_n (NH_3)	5.08	6.85	8.12	8.93	9.08
log K_1 (polyamine)	7.47	10.7	14.4	17.4	19.1

Ionic Strength =	0.5 M
EN	$NH_2CH_2CH_2NH_2$
DIEN	$NH_2(CH_2CH_2NH)_2H$
TRIEN	$NH_2(CH_2CH_2NH)_3H$
TETREN	$NH_2(CH_2CH_2NH)_4H$
PENTEN	$NH_2(CH_2CH_2NH)_5H$
Log $\beta_n(NH_3)$ =	log($K_1 \times K_2$ ----- $\times K_n$)

As denticity increases the number of chelate rings that are formed increases. The increase in stability of multidentate ligands over analogous monodentate ligands is due to the increase in number of chelate rings and is called the chelate effect.

Nitrogen donors are widely used in coordination chemistry because it is a synthetically convenient point of attachment, and displays stronger coordination properties with many metal ions than neutral oxygen donors (Hancock, 1989). The affinity of individual metal ions for neutral nitrogen donors can be characterized by the linear free energy relationship shown in Figure 7. Log K_1 values for ammonia are used as indicators of the affinity for nitrogen donors.

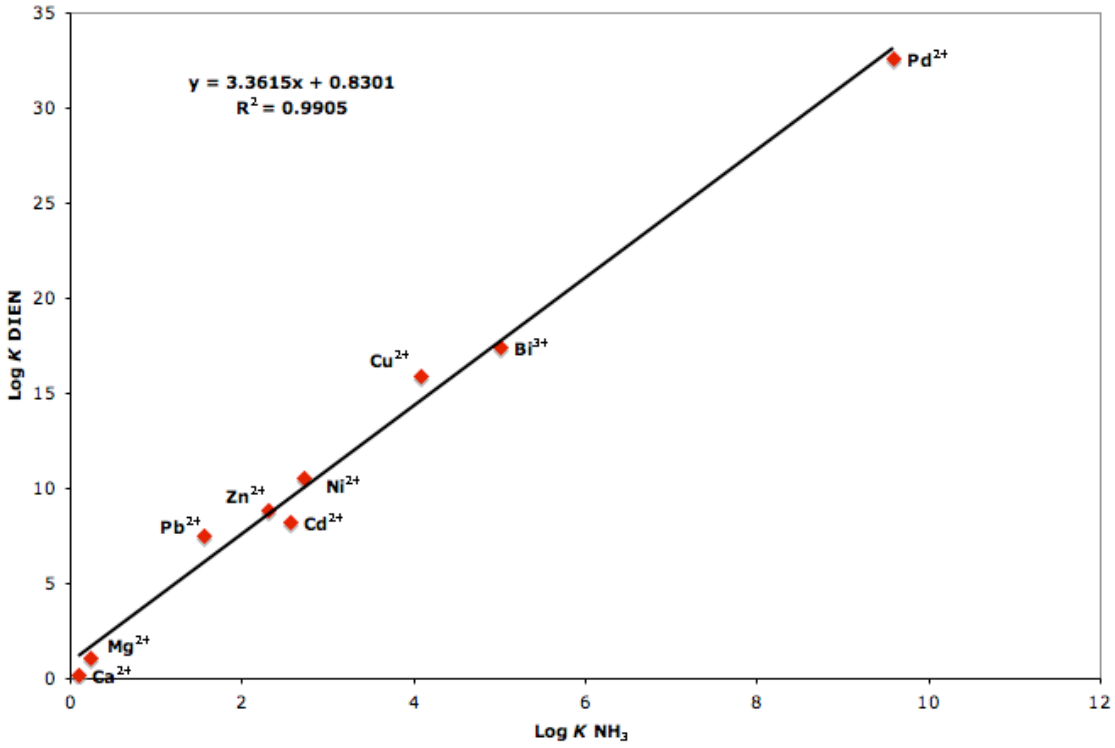

Figure 7. Plot of log K_1 DIEN versus log K_1 NH_3 for various metal ions to illustrate which metal ions form strong bonds with nitrogen donors.

DPP has four unsaturated nitrogen donor atoms. The nitrogens in this ligand are sp^2 hybridized which means that they will bind more covalently to a metal ion. Since these are unsaturated nitrogen donors there is a possibility of π-bonding between the ligand and the metal ion. Unsaturated nitrogen donors have low basicity, which is important because strong complexes not only rely on formation constants but also the relative difficulty to remove protons from donor groups in order to permit complex formation (Hancock, 1989).

Hard and soft acids and bases

Pearson proposed the principle of hard and soft acids and bases (HSAB) in 1963 based on patterns in the variation of log K_1 values. He devised a simple rule that states that hard acids bind strongly to hard bases and soft acids bind strongly to soft bases (Pearson, 1963). This principle is important in choosing donor atoms when designing ligands specific for certain metal ions. Table 2 shows the classification of hard and soft acids and bases proposed by Pearson. Figure 8 is the classification of Lewis acids as hard, soft, or intermediate and the trend in the periodic table.

The definition of a soft base, according to Pearson, is a donor atom that has high polarizability, low electronegativity, and is easily oxidized. A hard base is a donor atom that has low polarizability, high electronegativity, and is not easily oxidized. A soft acid is an acceptor atom that has a low positive charge, large size and outer electrons that are easily excited. A hard acid is an acceptor atom that has a large positive charge, small size, and lacks easily excited outer electrons.

Pearson explained the behavior of HSAB by various degrees of ionic and covalent σ-bonding, π-bonding, electron correlation phenomena, and solvation effects (Pearson, 1963).

Table 2. Classification of hard and soft acids and bases by Pearson's HSAB principle.

Classification of Lewis Acids	
Class (a)/Hard	Class (b)/Soft
H^+, Li^+, Na^+, K^+	Cu^+, Ag^+, Au^+, Tl^+, Hg^+, Cs^+
Be^{2+}, Mg^{2+}, Ca^{2+}, Sr^{2+}, Sn^{2+}	Pd^{2+}, Cd^{2+}, Pt^{2+}, Hg^{2+}
Al^{3+}, Se^{3+}, Ga^{3+}, In^{3+}, La^{3+}	CH_3Hg^+
Cr^{3+}, Co^{3+}, Fe^{3+}, As^{3+}, Ir^{3+}	Tl^{3+}, $Tl(CH_3)_3$, RH_3
Si^{4+}, Ti^{4+}, Zr^{4+}, Th^{4+}, Pu^{4+}, VO^{2+}	RS^+, RSe^+, RTe^+
UO_2^{2+}, $(CH_3)_2Sn^{2+}$	I^+, Br^+, HO^+, RO^+
$BeMe_2$, BF_3, BCl_3, $B(OR)_3$	I_2, Br_2, INC, etc.
$Al(CH_3)_3$, $Ga(CH_3)_3$, $In(CH_3)_3$	Trinitrobenzene, etc.
RPO_2^+, $ROPO_2^+$	Chloranil, quinones, etc.
RSO_2^+, $ROSO_2^+$, SO_3	Tetracyanoethylene, etc.
I^{7+}, I^{5+}, Cl^{7+}	O, Cl, Br, I, R_3C
R_3C^+, RCO^+, CO_2, NC^+	M^0 (metal atoms)
	Bulk metals
HX (hydrogen-bonding molecules)	
Borderline	
Fe^{2+}, Co^{2+}, Ni^{2+}, Cu^{2+}, Zn^{2+}, Pb^{2+}	
$B(CH_3)_3$, SO_2, NO^+	
Classification of Lewis Bases	
Hard	Soft
H_2O, OH^-, F^-	R_2S, RSH, RS^-
CH_3CO_2, PO_4^{3-}, SO_4^{2-}	I^-, SCN^-, $S_2O_3^{2-}$
Cl^-, CO_3^{2-}, ClO_4, NO_3^-	R_3P, R_3As, $(RO)_3P$
ROH, RO^-, R_2O	CN^-, RNC, CO
NH_3, RNH_2, N_2H_4	C_2H_4, C_6H_6
	H^-, R^-
Borderline	
$C_6H_5NH_2$, C_5H_5N, N_3^-, Br^-, NO_2^-, SO_3^{2-}, N_2	

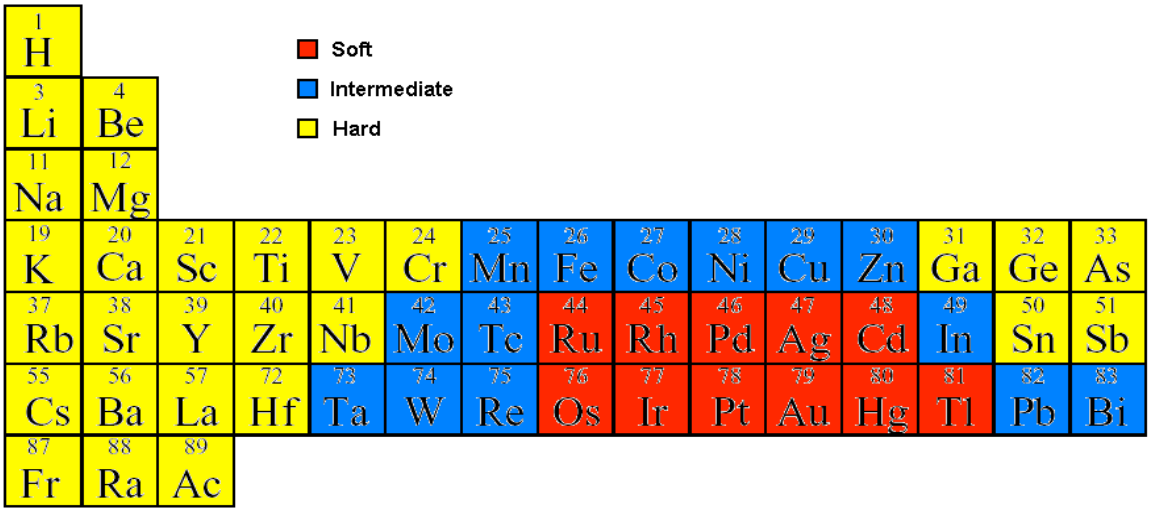

Figure 8. Classification of metals according to HSAB principle and illustration of periodic table trend.

METHODS AND MATERIALS

General

All metal and ligand stock solutions were prepared with deionized (DI) water. A Bruker 400 MHz NMR spectrometer was used to obtain ^{1}H-NMR spectra for analysis of all organic synthesis products (*see* Additional Research). All samples for ^{1}H-NMR analysis were prepared and referenced using DMSO-d_6. A Polaris IR-10410 FT-IR instrument (Mattson, Inc.) with WinFIRST software was used to obtain infrared absorption spectra of all organic products synthesized (*see* Additional Research). The samples for FT-IR analysis were prepared as KBr Pellets.

Chemicals

DPP and QUATERPY were synthesized by a research group supervised by Dr. Randolph P. Thummell (University of Houston). The purity of each was characterized by ^{1}H-NMR spectroscopy and the spectra are shown in Figure 9 and Figure 10. All other chemicals and reagents used were analytical grade and purchased commercially.

Stock Solutions

A 2 x 10^{-5} M stock solution of DPP (0.0042 g in 250 mL of DI water) at pH = 2 (0.01 M $HClO_4$) was prepared for all UV-vis spectroscopy experiments involving DPP. A 1.42 x 10^{-5} M stock solution of QUATERPY (0.0011 g in 250 mL of DI water) was prepared for all UV/Vis spectroscopy experiments involving QUATERPY. A 1 M $NaClO_4$ stock solution was prepared with 12.246 g in a 100 mL volumetric flask filled to volume. Stock solutions of each metal used in titration experiments were made in 50 mL volumetric flasks and filled to volume. Table 3 summarizes each metal stock solution.

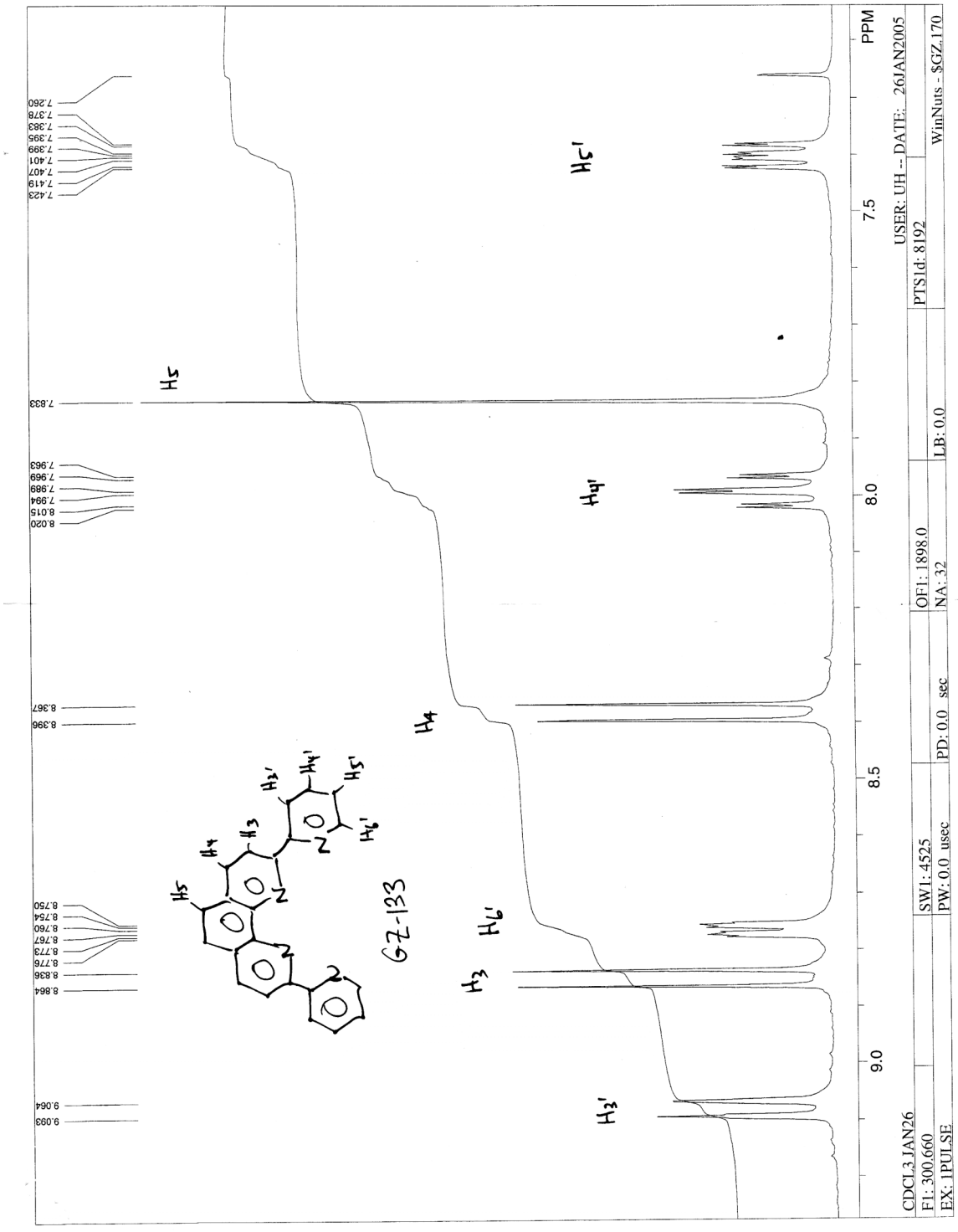

Figure 9. ^{1}H-NMR spectrum of DPP.

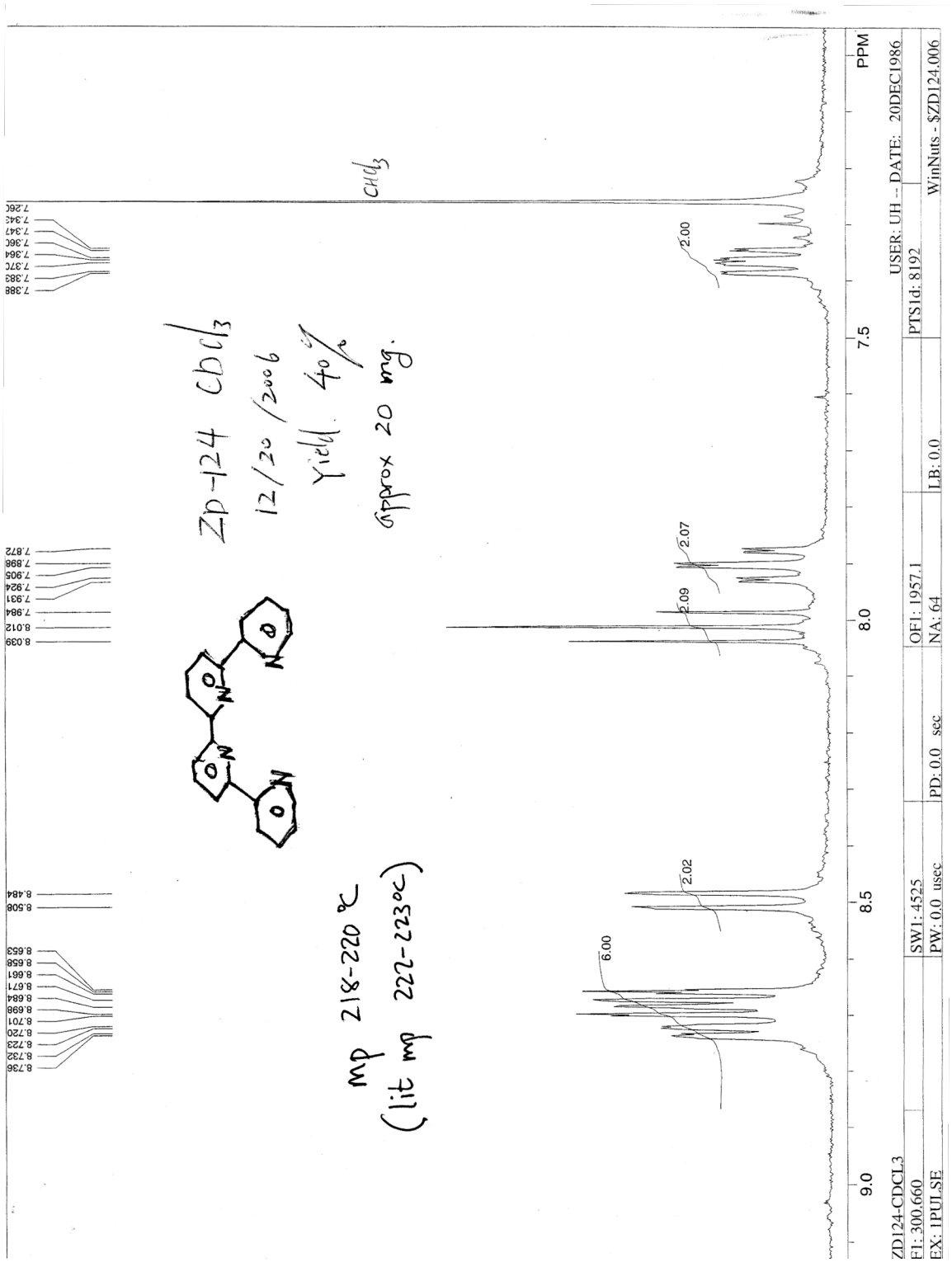

Figure 10. ^{1}H-NMR spectrum of QUATERPY.

Table 3. Summary of prepared metal stock solutions. Note: Cadmium and zinc stock solutions were diluted prior to use in titration experiments. No calcium solution was made. Reagent was weighed and dissolved directly in the UV solution.

Metal	Formula Weight (g/mol)	Mass (g)	Molarity
$Ni(ClO_4)_2 \cdot 6H_2O$	365.68	0.1828	0.01
$Mn(ClO_4)_2 \cdot 6H_2O$	361.93	0.1810	0.01
$Gd(ClO_4)_3 \cdot 6H_2O$	563.70	5.637 (50%(w/w))	0.1
$Th(NO_3)_3 \cdot 4H_2O$	552.15	0.2871	0.0104
$La(ClO_4)_3 \cdot 6H_2O$	437.26	0.2186	0.01
$Cd(ClO_4) \cdot 6H_2O$	419.40	0.2097	0.01 (stock diluted to 0.001 M for titration)
$Pb(ClO_4)_2 \cdot 3H_2O$	460.14	0.2301	0.01
$Ca(ClO_4)_2 \cdot 4H_2O$	311.04	0.5184 (added directly to titration solution)	0.03333 (titrated solution)
$Lu(ClO_4)_3 \cdot 6H_2O$	581.41	0.5814 (50%(w/w))	0.01
$Zn(ClO_4)_2 \cdot 6H_2O$	372.36	0.6200	0.0333 (stock diluted to 0.00333 M for titration)
$Hg(ClO_4)_2 \cdot H_2O$	399.49	0.1997	0.01
$In(ClO_4)_3 \cdot 8H_2O$	557.26	0.0412	0.001479

UV/Vis Spectroscopy

Aqueous metal-ligand titration experiments were carried out using a double beam Cary BIO 100 UV/Vis spectrophotometer (Varian, Inc.) with WinUV Version 2.00(25) software. All pH values for the titration experiments were recorded using an Accumet AB15 pH meter, which was calibrated prior to each titration experiment using pH 4.00, 7.00, and 10.00 buffer solutions. The titrant in each titration experiment was 0.1 M NaOH.

Flow Cell Set-up

A 1.0 cm quartz flow cell, fitted with a peristaltic pump, was used to mix the aqueous metal-ligand solution after each titrant addition was made to the solution. A

diagram of the flow cell apparatus is shown in Figure 11. An equilibration time of seven minutes was used for all titrant additions that were made. To ensure equilibration within a seven minute time period, the metal-ligand solution was placed on a stir plate and stirred with a magnetic stir bar. The absorbance scan range used was from 190 to 350 nm at a rate of 600.00 nm/min for all samples. All absorbance spectra were referenced by placing a 1.0 cm quartz cell filled with DI water in the path of the reference beam.

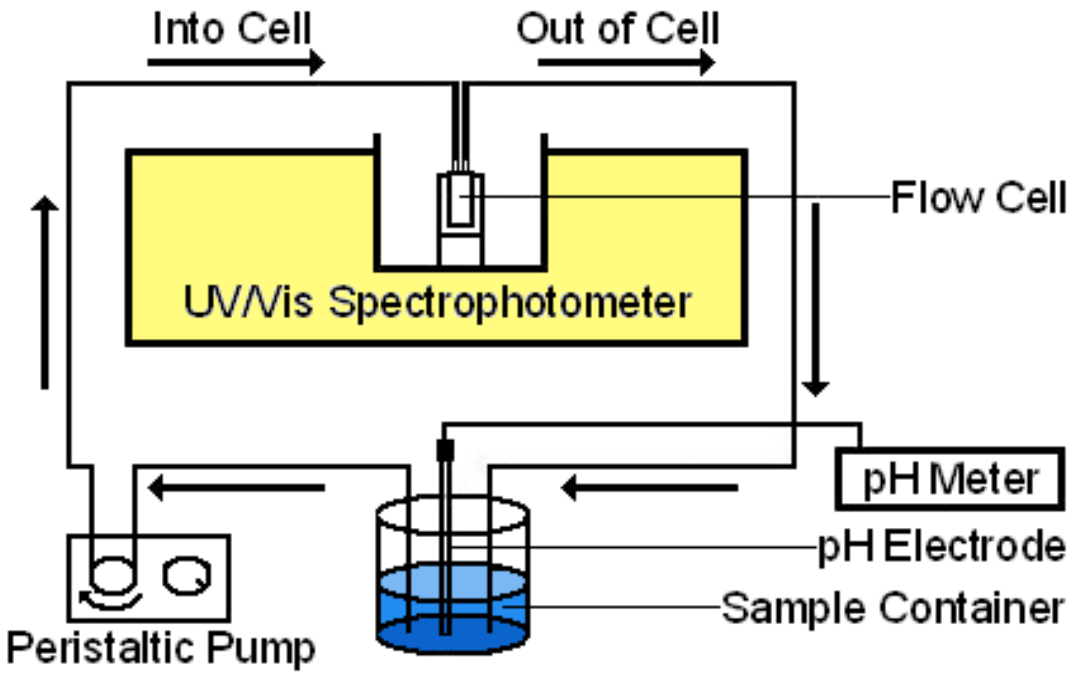

Figure 11. Schematic of flow cell apparatus.

Metal-Ligand Solution Preparation

Aqueous metal-ligand samples used in the titration experiments were of 0.10 *M* $NaClO_4$ for ionic strength and maintained at a constant temperature of 25.0 ± 0.1 °C throughout the experiment. Each titration solution was prepared from the ligand and metal stock solutions described above. Each metal-ligand solution was prepared in a 50

mL volumetric flask and filled to volume with water. Table 4 summarizes the preparation of each metal-ligand solution for titration.

Table 4. Experimental design for the preparation of metal-ligand solutions.

Metal	Molarity of DPP in titration solutions	Volume of metal stock in titration solutions (mL)	Molarity of metal in titration solutions
Zn^{2+}	4×10^{-6}	0.060	4×10^{-6}
Ca^{2+}	4×10^{-6}	-	0.03333
Gd^{3+}	4×10^{-6}	0.002	4×10^{-4}
	4×10^{-6}	0.020	4×10^{-5}
	4×10^{-6}	2.000	4×10^{-3}
Pb^{2+}	4×10^{-6}	0.020	4×10^{-6}
Th^{3+}	4×10^{-6}	0.095	2×10^{-5}
Ni^{2+}	4×10^{-6}	0.020	4×10^{-6}
In^{2+}	4×10^{-6}	0.135	4×10^{-6}
Mn^{2+}	4×10^{-6}	0.020	4×10^{-5}
Lu^{3+}	4×10^{-6}	2.000	4×10^{-4}
La^{3+}	4×10^{-6}	1.666	0.01666
Cd^{2+}	4×10^{-6}	0.200	4×10^{-6}
	8×10^{-7}	0.040	8×10^{-7}

3-D Fluorescence

Excitation-emission matrix (EEM) fluorescence properties were determined on a Jobin Yvon SPEX Fluoromax-3 scanning fluorometer equipped with a 150 W Xe arc lamp and a R928P detector. The instrument is configured to collect the signal in ratio mode with dark offset using 5nm bandpasses on both the excitation and emission monochromators. The EEMs were created by concatenating emission spectra measured every 5nm from 250 to 500nm at 51 separate excitation wavelengths. Scans are corrected for instrument configuration using factory supplied correction factors. Post processing of scans is performed using FLToolbox 1.91 developed by Wade Sheldon (University of

Georgia) for MATLAB® (Release 11). The software eliminates Rayleigh and Raman scattering peaks by excising portions (± 10-15 nm FW) of each scan centered on the respective scatter peak. The excised data is replaced using three-dimensional interpolation of the remaining data according to the Delaunay triangulation method and constraining the interpolation such that all nonexcised data is retained. Following removal of scatter peaks, data were normalized to a daily-determined water Raman intensity (275ex / 303em, 5 nm bandpasses) and converted to Raman normalized quinine sulfate equivalents (QSE) in ppb. For samples that required dilution, the scatter corrected fluorescence of the diluent Milli-Q was subtracted and the resultant fluorescence values were multiplied by the dilution factor to obtain the intensity for the original, undiluted sample. Replicate scans are generally within 5% agreement in terms of intensity and within bandpass resolution in terms of peak location.

Cadmium Crystal Synthesis

Crystals were prepared by dissolving 10 mg (3×10^{-5} mol) of DPP in *n*-butanol in a 50 mL beaker. An equimolar (2.54 mL of a 0.018 M solution) amount of $Cd(ClO_4)_2$ was placed in a separate 50 mL beaker and DI water was added until the volume of the aqueous metal solution was approximately the same as the volume of *n*-butanol. The DPP in *n*-butanol was then carefully pipetted to the beaker containing the aqueous metal solution, creating two separate layers. The beaker was then covered with parafilm and holes were poked through the top, allowing the DPP to diffuse into the aqueous layer and complex with cadmium. The beaker was allowed to sit so that the layers could evaporate. As the layers evaporated the complex crystallized on the interface of the two layers. Once

crystals were observed in the beaker, they were filtered and dried under vacuum. The crystals obtained were analyzed by x-ray crystallography and mass spectrometry.

Lead Crystal Synthesis

Crystals were prepared by dissolving 5 mg (1.5×10^{-5} mol) of DPP in *n*-butanol in a 50 mL beaker. An equimolar (1.5 mL of a 0.01 M solution) amount of $Pb(ClO_4)_2$ was placed in a separate beaker and DI water was added until the volume of the aqueous metal solution was approximately the same as the volume of *n*-butanol. Crystals were then synthesized by the method described above. Once crystals were observed on the interface of the layers they were filtered and dried under vacuum. The crystals were analyzed by x-ray crystallography and mass spectrometry.

Zinc Crystal Synthesis

Crystals were prepared by dissolving 5 mg (1.5×10^{-5} mol) of DPP in *n*-butanol in a 50 mL beaker. An equimolar (0.4504 mL of a 0.0333 M solution) amount of $Zn(ClO_4)_2$ was placed in a separate beaker and DI water was added until the volume of the aqueous metal solution was approximately the same as the volume of *n*-butanol. Crystals were then synthesized by the method described above. Once crystals were observed on the interface of the layers they were filtered and dried under vacuum. The crystals were analyzed by x-ray crystallography and mass spectrometry.

Mercury Crystal Synthesis

Crystals were prepared by dissolving 5 mg (1.5×10^{-5} mol) of DPP in *n*-butanol in a 50 mL beaker. An equimolar (1.5 mL of a 0.01 M solution) amount of $Hg(ClO_4)_2$ was placed in a separate beaker and DI water was added until the volume of the aqueous metal solution was approximately the same as the volume of *n*-butanol. Crystals were then synthesized by the method described above. Once crystals were observed on the interface of the layers they were filtered and dried under vacuum. The crystals were analyzed by x-ray crystallography and mass spectrometry.

Copper Crystal Synthesis

Crystals were prepared by dissolving 5 mg (1.5×10^{-5} mol) of DPP in *n*-butanol in a 50 mL beaker. An equimolar (1.5 mL of a 0.01 M solution) amount of $Cu(ClO_4)_2$ was placed in a separate beaker and DI water was added until the volume of the aqueous metal solution was approximately the same as the volume of *n*-butanol. Crystals were then synthesized by the method described above. Once crystals were observed on the interface of the layers they were filtered and dried under vacuum. The crystals were analyzed by x-ray crystallography and mass spectrometry.

X-ray Crystallography

Crystals synthesized were sent to The Molecular Structure Center at Clemson University for x-ray crystallographic analysis. A Rigaku Mercury diffractometer, using the ω scan mode, was employed for crystal screening, unit cell determination, and data

collection. The structure was solved by direct methods and refined to convergence. No absorption corrections were made.

Mass Spectrometry

The crystals synthesized were analyzed with a JEOL JMS-SX102 reverse geometry double focused sector mass spectrometer (JEOL Inc., Peabody, MA) using positive ion Fast Atom Bombardment (FAB^+). Xenon was used as the FAB gas at an accelerating voltage of 10 kV. Crystals were placed directly in the *p*-nitrobenzyl alcohol matrix.

Computer Software

Computer software was used in analyzing the mass spectra of the crystals synthesiszed and for constructing species distribution diagrams as a check for UV/Vis spectroscopy results. A program called iMass was used to create theoretical mass spectra of formulas entered by isotope distribution (Rockwood, 1995). These were compared to the actual mass spectra peaks to confirm the synthesized complex. Species distribution diagrams were constructed using Species 3.0 written by Robert D. Hancock in QBasic.

RESULTS AND DISCUSSION

DPP Protonation Constants

In order to determine the strength with which different metal ions will bind to DPP, the protonation constants (p*K*) of the ligand were first determined. UV/Vis spectroscopy was used as previously discussed. A 4 x 10^{-6} M solution of free DPP in 0.1 M $NaClO_4$ was prepared for the titration experiment. Starting at a pH of 1.99, NaOH was added to the solution until a final pH of 7.34 was reached. For each titrant addition of 0.1 *M* NaOH absorbance scans were taken from 190 nm to 350 nm. The spectra of the free ligand titration are shown in Figure 12. Absorbances were recorded at 277, 287, 292, 330, and 344 nm because these wavelengths showed the greatest change in absorbances. Absorbance data at these wavelengths were used to create plots of absorbance versus pH. DPP has two separate protonation events, pK_1 and pK_2. To determine the value of the protonation constants from the observed absorbances, it was first necessary to correct each absorbance for dilution using Eq(1).

$$Abs_{Corr} = \frac{Abs \cdot V_{Total}}{V_{initial}} \tag{1}$$

Plots of Abs_{corr} versus pH were constructed for each wavelength selected.

The total ligand concentration, $[L]_{total}$, in solution can be described by Eq(2).

$$L_{Total} = [L] + [LH^+] + [LH_2^{2+}] \tag{2}$$

Eq(2) can be rearranged by adding the following equilibrium constants to get Eq(5). Each Eq(3)-(4) represent a separate equilibrium expression.

$$K_1 = \frac{[LH^+]}{[L][H^+]} \tag{3}$$

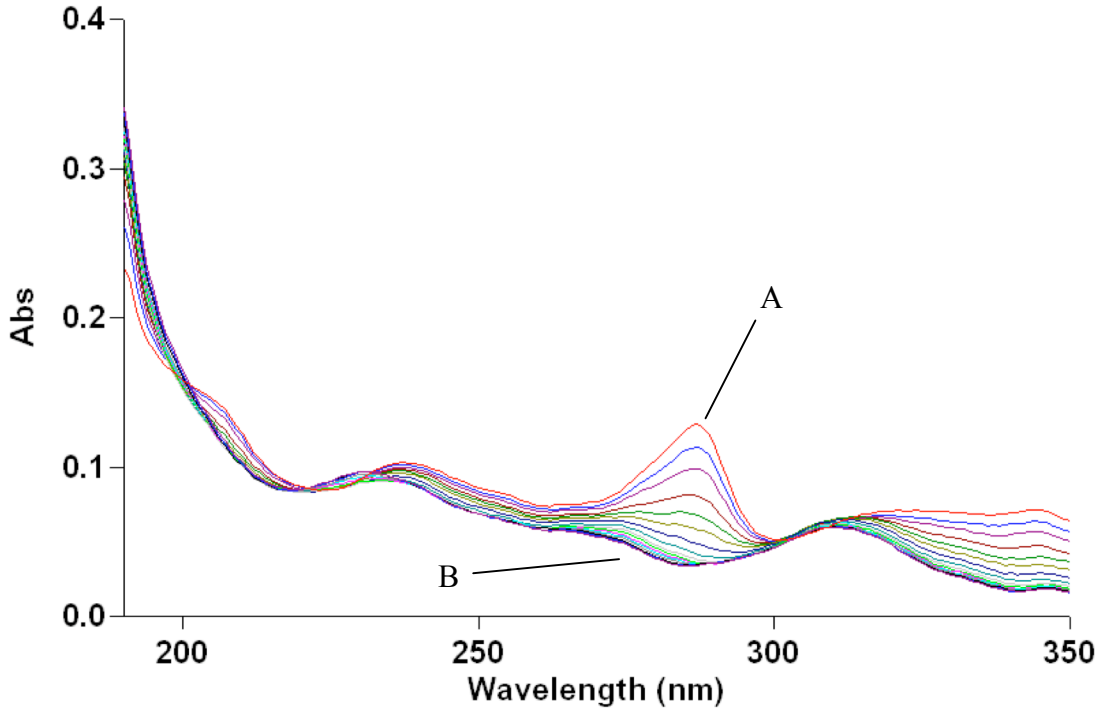

Figure 12. UV spectra of 4 x 10^{-6} M DPP in 0.01 M $HClO_4$ and 0.09 M $NaClO_4$ as a function of pH. Initial spectrum (A) of fully protonated DPP at pH=1.99. Final spectrum (B) of unprotonated DPP at pH=7.34.

$$K_1K_2 = \frac{[LH_2^{2+}]}{[L][H^+]^2} \quad (4)$$

$$L_{Total} = [L] + K_1[L][H^+] + K_1K_2[L][H^+]^2 \quad (5)$$

By dividing out the free ligand concentration, [L], Eq(5) can be simplified to Eq(6).

$$\frac{L_{Total}}{[L]} = 1 + K_1[H^+] + K_1K_2[H^+]^2 \quad (6)$$

Theoretical absorbance, Abs(theor), in Eq(7) was calculated by multiplying the concentration of the species present in solution [L, LH^+, LH_2^{2+}] by the absorbance of each of these species at a 4 x 10^{-6} M concentration, as shown in Eq(6).

$$Abs(theor) = \frac{1 \times [Abs(L)] + K_1[H^+][Abs(LH^+)] + K_1K_2[H^+]^2[Abs(LH_2^{2+})]}{1 + K_1[H^+] + K_1K_2[H^+]^2} \quad (7)$$

Abs(L) is the absorbance where only unprotonated ligand exists in the sample solution. Abs(LH^+), and Abs(LH_2^{2+}) describe the absorbances at each protonation event. These are labeled Abs(0), Abs(1), and Abs(2) respectively in each spreadsheet constructed to determine stability constants. To simplify Table 5, which is an example of the spreadsheet used to calculate protonation constants, each term in Eq(6) was described as a function, for example: $L(Func)1 = K_1[H^+] = \frac{1}{K_{a_2}}[H^+] = \left(10^{pK_{a2}}\right)\left(10^{-pH}\right)$, and $L(Func)2 = K_1K_2\left[H^+\right]^2 = \left(10^{pK_{a1}+pK_{a2}}\right)\left(10^{-pH}\right)^2$. With this conversion within the spreadsheet, the pK_a was calculated from the initial equilibrium expressions. Plots of pH versus corrected absorbance were fit with plots of pH versus Abs(theor) using the 'SOLVER' module of EXCEL to minimize the average sum of the squares of the residuals at each wavelength selected. Figure 13a shows the plot of the 287 nm fit from Table 5 and Figure 13b shows all of the wavelengths fit simultaneously to calculate pK_a.

Table 5. EXCEL spreadsheet for free ligand at 287 nm. pK1 and pK2 were solved by minimizing the average standard deviation of each scan using the 'SOLVER' module.

287 nm									
Amount of base	**Total base**	**pH**	**abs.**	**corr. Abs.**	**L(func)1**	**L(func)2**	**L(func)4**	**A(theor) (259)**	**diff**
0	0	1.99	0.12869	0.12869	277.6281192	588.5473541	867.1754733	0.127810281	7.73906E-07
1.5	1.5	2.15	0.1129998	0.116389794	192.0717313	281.6964744	474.7682057	0.116484571	8.98265E-09
1	2.5	2.31	0.09887213	0.103815737	132.8811723	134.8284096	268.7095819	0.104334636	2.69256E-07
1	3.5	2.55	0.08052804	0.086165003	76.46513348	44.64588247	122.1110159	0.086270769	1.11865E-08
0.5	4	2.74	0.06761451	0.073023671	49.3700368	18.6115015	68.9815383	0.073558397	2.85932E-07
0.3	4.3	2.92	0.05786972	0.062846516	32.61845984	8.124215066	41.74267491	0.06358411	5.44045E-07
0.3	4.6	3.21	0.04822788	0.052664845	16.72874846	2.136886285	19.86563474	0.052034314	3.97569E-07
0.15	4.75	3.47	0.04110563	0.045010665	9.193131047	0.645329341	10.83846039	0.045664333	4.27283E-07
0.1	4.85	3.83	0.03776469	0.041427865	4.01294725	0.122964971	5.135912221	0.040946574	2.31641E-07
0.05	4.9	4.25	0.03589658	0.039414445	1.525679992	0.017773846	2.543453838	0.038707787	4.99365E-07
0.015	4.915	4.77	0.03493674	0.038371022	0.460747992	0.001620994	1.462368986	0.037943376	1.82881E-07
0.005	4.92	4.96	0.03505899	0.038508795	0.297483889	0.000675743	1.298159632	0.037870043	4.08004E-07
0.005	4.925	5.23	0.03430196	0.037680703	0.159758308	0.000194886	1.159953194	0.037828229	2.1764E-08
0.005	4.93	6.36	0.03466237	0.03808008	0.011843047	1.07098E-06	1.011844118	0.037812898	7.13863E-08
0.005	4.935	6.88	0.03395275	0.037303886	0.003576543	9.76745E-08	1.003576641	0.03781321	2.59411E-07
0.005	4.94	7.34	0.03374802	0.037082324	0.001240119	1.17431E-08	1.001240131	0.037813324	5.34361E-07
		pK1	4.433463451					**$SS_{residuals}$**	4.92697E-06
		pK2	2.316317961						
		Abs(0)	0.03781339						
		Abs(1)	0.037759342						
		Abs(2)	0.170441803						

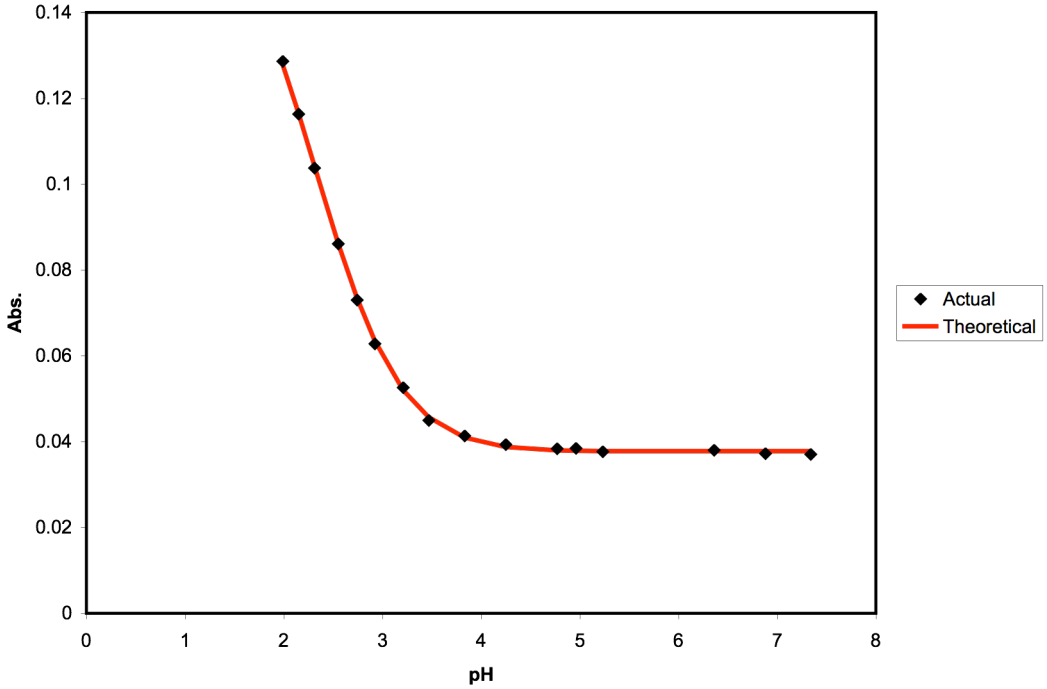

a)

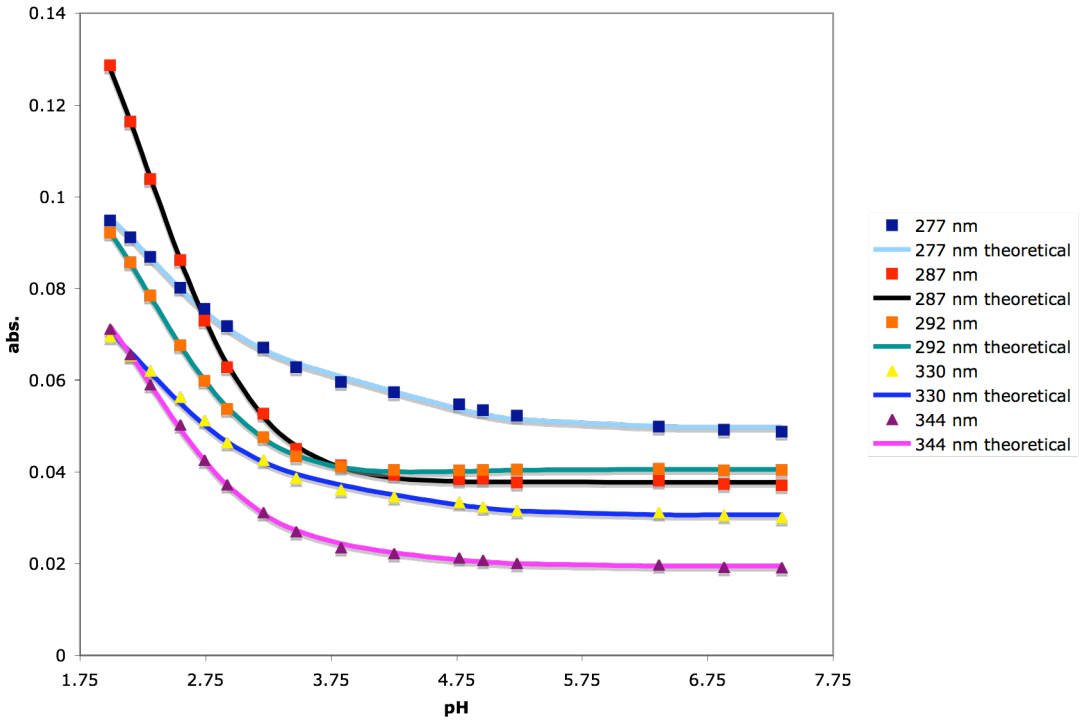

b)

Figure 13. Plot of measured and theoretical absorbance vs. pH for a) 287 nm as shown in Table 5 and b) all wavelengths recorded to calculate pK_a.

The 'SOLVER' module of EXCEL was utilized to perform non-linear least-squares curve fitting. The independent variable x (pH) and the dependent variable y (abs_{corr}) were plotted. The calculated variable y_{calc} (abs_{theor}) was determined by Equation (7), which includes the independent variable and the coefficients, pK_1, pK_2, abs(1), abs(2), and abs(3) to be varied. The square of the residual (diff) was calculated for each data point using Equation (8).

$$\text{diff} = \left(y_{obs} - y_{calc}\right)^2 \tag{8}$$

The square of the residual for the free ligand is shown in Table 5 at 287 nm and single wavelengths are shown for each metal titration (Appendix). The small value for the square of the residual was a good indication of the accuracy of each data point measured. The sum of the squares of the residuals, Equation (9), was minimized by 'SOLVER' by changing the coefficients of the functions listed above.

$$SS_{residuals} = \sum \left(y_{obs} - y_{calc}\right)^2 \tag{9}$$

The module 'SOLVER' is limited because it does not provide the standard deviations of the coefficients. The SolvStat.xls macro was used to determine the standard deviation of the coefficients and the coefficient of determination (Billo, 2001). The solver statistics macro calculates $SS_{residuals}$, $SS_{regression}$, and the standard error of the y estimate ($SE_{(y)}$) from the known y's (abs_{corr}) and calculated y's (abs_{Theor}). $SS_{regression}$ and $SE_{(y)}$ are defined by Equations (10) and (11) respectively.

$$SS_{regression} = \sum \left(y_{mean} - y_{calc}\right)^2 \tag{10}$$

$$SE_{(y)} = \sqrt{\frac{SS_{residuals}}{N - K}} \tag{11}$$

The variable N is defined by the number of data points and K is defined by the number of regression coefficients. Solver Statistics calculates the standard deviations using the diagonals from an inverted matrix of partial differentials for each of the *K* regression coefficients. Table 6 outlines the solutions of each parameter that was varied by 'SOLVER' and the standard deviation of each variable calculated by Solver Statistics.

The Solver Statistics macro is an important and necessary tool in calculating the protonation events of DPP and DPP metal complexes. Solver has other sources of error such as cross correlation and solvstat.xls was used as a statistical check. If solvstat.xls calculated any unreasonably high standard deviations for the varied coefficients, it was assumed that solver had produced a false minimum and the protonation events were recalculated. To reduce any error, all five wavelengths were fitted simultaneously and an overall pK_1 and pK_2 were calculated by Solver.

The coefficient of determination (R^2) measures the goodness of fit of the data and is calculated by Equation (12).

$$R^2 = 1 - \frac{SS_{residual}}{SS_{regression}} \tag{12}$$

If x and y are perfectly correlated, then $R^2 = 1$. An R^2 value of 0 means that there is no correlation between x and y and a value less than 0.9 corresponds to a poor fit. The value for R^2 is given in Table 6 for the free ligand titration and indicates a very good fit for all of the five wavelengths fitted simultaneously. The goodness of fit is also illustrated in Figure 13. The p*K*'s were recorded once all standard deviations were minimized and the R^2 value was close to one. Table 7 shows the equations of each protonation event observed for the free ligand titration of DPP and the pK_a calculated with minimal error.

Table 6. Solutions and standard deviation for each parameter solved by the 'SOLVER' module of EXCEL in determining pK_a of DPP. Note: Coefficient of determination and standard error calculated with 'Solver Statistics' macro.

	Parameter	Solution	Standard Deviation
Overall	pK_1	4.433463451	0.070928693
	pK_2	2.316317961	0.012427391
277 nm	Abs(0)	0.04978392	0.000316212
	Abs(1)	0.061995148	0.000509746
	Abs(2)	0.111205863	0.000844654
287 nm	Abs(0)	0.03781339	0.000282483
	Abs(1)	0.037759342	0.000479126
	Abs(2)	0.170441803	0.001563936
292 nm	Abs(0)	0.040620623	0.000281748
	Abs(1)	0.038781844	0.000394613
	Abs(2)	0.117528679	0.001071384
330 nm	Abs(0)	0.030656178	0.000289241
	Abs(1)	0.037275959	0.000430896
	Abs(2)	0.085921084	0.000826783
344 nm	Abs(0)	0.019524572	0.000281884
	Abs(1)	0.023422419	0.000428289
	Abs(2)	0.094622361	0.000992646

R^2: 0.999455885 **Standard Error:** 0.000597982

Table 7. Protonation events and constants for DPP free ligand; Equations written in terms of log K to complement initial equilibrium expressions.

					pK_a
DPP	+	H^+	$\rightleftharpoons$	$H(DPP)^+$	4.43
$H(DPP)^+$	+	H^+	$\rightleftharpoons$	$H_2(DPP)^{2+}$	2.31

Note: Because $K = \frac{1}{K_a}$, log K_1 = pK_{a2} and log K_2 = pK_{a1}

Stability Constant Determination

Upon binding a metal ion, peak shifts are observed in the absorbance versus wavelength UV/Vis spectra of the free ligand. The calculations previously discussed are performed on the data from each metal-ligand complex. The metal affects the protonation constants in two ways. In the first case, the protons on the ligand displace binding of the metal ion:

$$ML^{x+} + H^{+} \rightarrow M^{x+} + LH^{+} \tag{13}$$

Shown above is a simple case where one proton is attached to the ligand and log K_1 for the complex (ML) is calculated by the following steps. Evidence of a protonation of the free ligand with no metal present is shown by an inflection of absorbance versus pH. The pK_a is at the midpoint of this inflection. In the presence of the metal ion, if a complex is formed, an inflection in the absorbance versus pH curve is observed, but now at lower pH. This protonation event corresponds to Eq. (13). The reaction constant, Eq. (14) can be calculated from the position of the midpoint of the inflection corresponding to Eq (13).

$$K_{react} = \frac{[LH^{+}][M^{x+}]}{[ML^{x+}][H^{+}]} \tag{14}$$

If $[H^+]$ is the proton concentration at pH_{50}, this is the pH in Eq. (14) where [LH] = [ML]. In calculating K_{react}, the free metal ion concentration $[M^{x+}]$ must also be included. Thus, K_{react} equals the free metal ion concentration $[M^{x+}]$, which at pH_{50} will be 50% of the total metal ion concentration ($[ML^{x+}] = [M^{x+}]$), divided by $[H^+]$ at pH_{50}. K_1 for the metal ion complex now corresponds to the constant K_{react} for Eq. (14) combined with the protonation constant K_a:

$$K_1 = \frac{1}{K_a K_{react}} \tag{15}$$

$$= \left(\frac{[LH^+]}{[L][H^+]} \right) \left(\frac{[ML^{x+}][H^+]}{[LH^+][M^{x+}]} \right) = \frac{[ML^{x+}]}{[L][M^{x+}]} \quad (16)$$

because $\frac{1}{10^{-pK_1}} = 10^{pK_1}$. DPP is a dibasic ligand for which pK_a is calculated the same as above except that both of the protonation constants are involved.

$$ML^{x+} + 2H^+ \rightleftharpoons LH_2^{2+} + M^{x+} \quad (17)$$

$$K_{react} = \frac{[LH_2^{2+}][M^{x+}]}{[ML^{x+}][H^+]^2} \quad (18)$$

$$K_1 = \frac{1}{K_{a1}K_{a2}K_{react}} \quad (19)$$

$$= \left(\frac{[LH_2^{2+}]}{[L][H^+]^2} \right) \left(\frac{[ML^{x+}][H^+]^2}{[LH_2^{2+}][M^{x+}]} \right) = \frac{[ML^{x+}]}{[L][M^{x+}]} \quad (20)$$

Eq. (1)-(20) were used to calculate the protonation equilibria of each metal-ligand complex with minimal standard deviation. There is a difference in the pK_a values calculated for the free ligand and the complex because of the inflection at a lower pH as previously discussed. The protonation constants calculated for each metal titration are denoted by pK_{50}, and when discussed individually are labeled as pK_1, pK_2, and pK_3. In the presence of a metal ion log K_1 can be calculated by:

$$\log K_1 (ML^{x+}) = -\log[M^{x+}] + (pK_a - pK_{50}) + (pK_a - pK_{50}) \quad (21)$$

Other protonation events that are apparent from the UV/Vis spectra of several of the metals explored include formation of hydroxides on the complex.

$$MLOH^{x-1} + H^+ \rightleftharpoons ML^{x+} \quad (22)$$

The pK_1 was determined for these protonation events, however it was not used in determining complex stability.

Log K_1 Results for Metal Ions Studied

Metal ions complexed with DPP were chosen based on varying ionic radii and ionic charge. Studied metals varied in size from Nickel (Ni^{2+}), which has a radius of 0.69 Å to lead (Pb^{2+}) with a radius of 1.19 Å. Table 8 summarizes the log K_1 calculated for each metal-DPP complex compared to log K_1 for select metal-1,10-phenanthroline and metal-TERPY complexes.

Table 8. Comparison of log K_1 of DPP with various metal ions to log K_1 of 1,10-phen and TERPY complexes with select metals. Log K_1 data for 1,10-phenanthroline and TERPY from ref. Martel, 2003. *Log K_1 determined by Michael Anhorn, unpublished work, **2007**.

	Ionic Radii (Å)	**DPP**	**1,10-phen**	**Δlog K_1**	**TERPY**	**Δlog K_1**
Ni^{2+}	0.69	6.73	8.70	-1.97	10.7	-3.97
Zn^{2+}	0.74	8.40	6.38	+2.02	9.8*	-1.40
Mn^{2+}	0.80	5.84	4.09	+1.75	4.4	+1.44
In^{3+}	0.80	7.15	5.70	+1.45	-	-
Gd^{3+}	0.93	6.06	-	-	-	-
Th^{4+}	0.94	5.73	2.1	+3.63	-	-
Cd^{2+}	0.95	12.21	5.66	+6.55	6.1*	+6.11
Lu^{3+}	0.98	7.86	-	-	-	-
Ca^{2+}	1.00	2.69	1.00	+1.69	0.1	+2.58
Bi^{3+}	1.03	15.72	-	-	-	-
La^{3+}	1.05	4.05	-	-	1.8*	+2.25
Pb^{2+}	1.19	7.36	4.62	+2.74	6.0*	+1.36

Each titration experiment conducted resulted in p*K* values different from the free ligand and were used to calculate log K_1. Results for individual metal ions are discussed below.

Nickel Results

Nickel is an intermediate acid according to the HSAB principle. Nickel has an ionic radius of 0.69 Å and was the smallest of all metal ions explored. Because of its small radius, nickel was expected to bind weakly with DPP compared to some of the larger metals studied. Upon binding with DPP, nickel forms 5-membered rings, which is unfavorable for small metal ions (Hancock, 1992). This is according to the chelate ring size rule previously discussed. A solution of 4 x 10^{-6} M DPP and 4 x 10^{-6} M $Ni(ClO_4)_2$ was titrated with 0.1 M NaOH from pH = 2.02 to pH = 6.41. The UV/Vis spectra plotting absorbance versus wavelength are shown in Figure 14. Absorbances were recorded at 277, 287, 292, 330, and 344 nm because these wavelengths exhibited the largest change in absorbances. Theoretical and measured absorbances were plotted for every wavelength simultaneously by minimizing the sum of the squares of the residuals as previously discussed and shown in Figure 15. Table 9 outlines the solutions of each parameter that was varied by 'SOLVER' and the standard deviation of each variable calculated by Solver Statistics. The p*K*'s were recorded once all standard deviations were minimized and the R^2 value was close to one. Table 10 shows the equations of each protonation event observed for the DPP-Ni titration and the p*K*'s calculated with minimal error, which were a pK_1 and pK_2 of 3.42 and 2.29 respectively. These were used in Eq. (21) to calculate a log K_1 of 6.73. TERPY, which has a log K_1 of 10.7 with nickel, is much more stable because of its lack of preorganization. TERPY can rotate and strain to bind nickel to all three donor atoms where DPP is in a fixed position. This means that nickel cannot bind to all of the donor atoms of DPP. This is also apparent from the UV/Vis spectra.

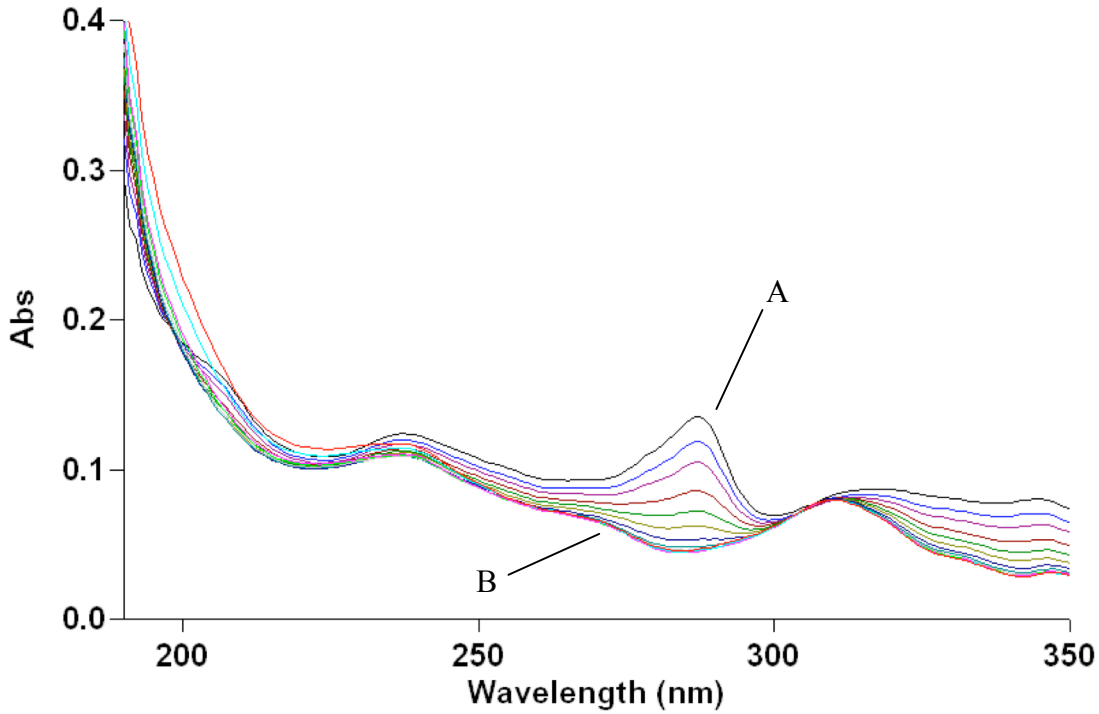

Figure 14. UV spectra of 4 x 10^{-6} M DPP and 4 x 10^{-6} M $Ni(ClO_4)_2$ in 0.01 M $HClO_4$ and 0.09 M $NaClO_4$. Initial spectrum (A) of free DPP at pH = 2.02. Final spectrum (B) of DPP- Ni complex at pH = 6.41.

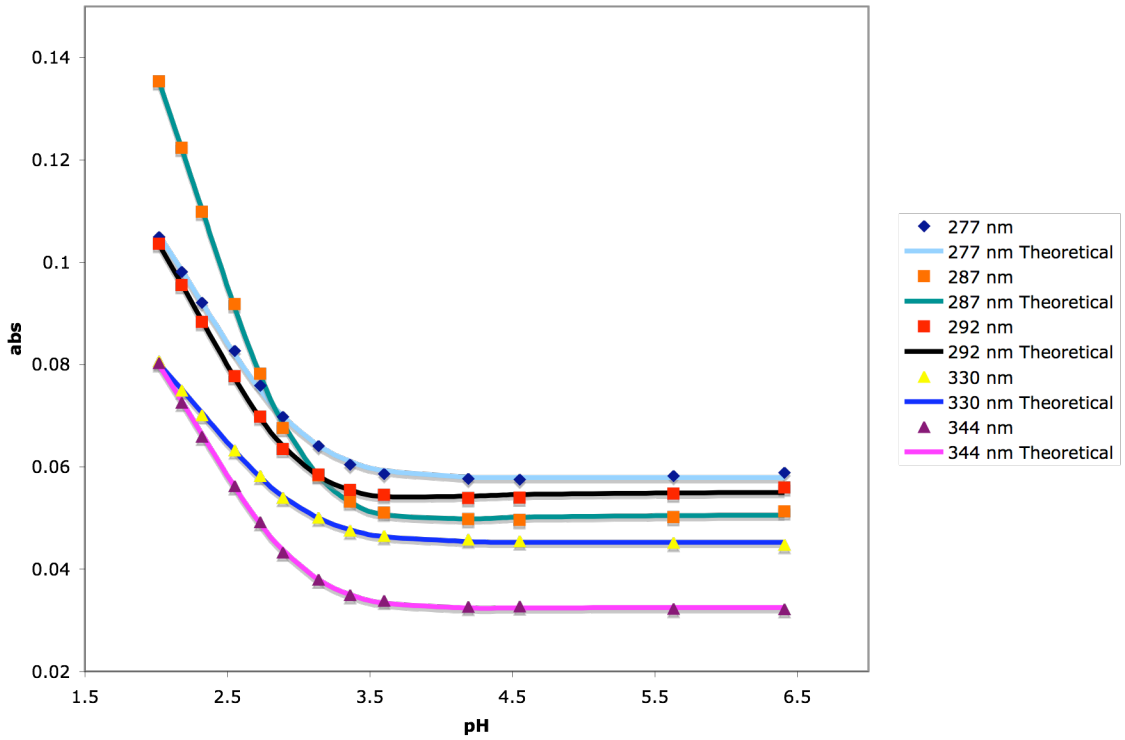

Figure 15. Plot of corrected absorbance (data points) and theoretical absorbance (lines) versus pH for titration of DPP and $Ni(ClO_4)_2$.

Table 9. Solutions and standard deviation for each parameter solved by the 'SOLVER' module of EXCEL in determining log K_1 of DPP-Ni complex. Note: Coefficient of determination and standard error calculated with 'Solver Statistics' macro.

	Parameter	Solution	Standard Deviation
Overall	pK_1	3.423660919	0.100747935
	pK_2	2.29404976	0.019432559
277 nm	Abs(0)	0.057910506	0.00025964
	Abs(1)	0.057808087	0.000747443
	Abs(2)	0.131467434	0.001461712
287 nm	Abs(0)	0.050547633	0.000284415
	Abs(1)	0.044071226	0.000847068
	Abs(2)	0.185641029	0.002325202
292 nm	Abs(0)	0.054983819	0.000273063
	Abs(1)	0.049189208	0.000579813
	Abs(2)	0.133323004	0.00141669
330 nm	Abs(0)	0.045264604	0.000258378
	Abs(1)	0.045391259	0.000647575
	Abs(2)	0.099444661	0.001173783
344 nm	Abs(0)	0.032534719	0.000261396
	Abs(1)	0.031038354	0.000689185
	Abs(2)	0.106784993	0.001440583

R^2: 0.999638782 **Standard Error:** 0.000483874

Table 10. Summary of equations at each protonation event of $[Ni(DPP)]^{2+}$; Equations written in terms of log K to complement initial equilibrium expressions.

							pK_{50}
$[Ni(DPP)]^{2+}$	+	H^+	$\rightleftharpoons$	$H(DPP)^+$	+	Ni^{2+}	3.42
$H(DPP)^+$	+	H^+	$\rightleftharpoons$	$H_2(DPP)^{2+}$			2.29

Although the spectra changed as pH was increased, no sharp peaks formed indicating that the complex was not as rigid as larger metal complexes. The $\Delta \log K_1$ of -1.97 between DPP and 1,10-phenanthroline is due to the denticity. DPP has more donor atoms than 1,10-phenanthroline but both are preorganized for large metal ions. Preorganization is the factor in which TERPY binds nickel stronger than either 1,10-phenanthroline or DPP.

Zinc Results

Zinc is slightly bigger than nickel with an ionic radius of 0.74 Å. Zinc is classified as an intermediate acid according to the HSAB principle. Figure 7 illustrates the affinity zinc has for nitrogen donors. The $\log K_1$ of the $[Zn(DPP)]^{2+}$ complex is expected to be higher than $[Ni(DPP)]^{2+}$ because of its difference in size. As previously reported nickel cannot bind to as many donor atoms of DPP, thus resulting in a lower $\log K_1$ than a larger metal ion, like zinc. A solution of 4×10^{-6} M DPP and 4×10^{-6} M $Zn(ClO_4)_2$ was titrated with 0.1 M NaOH from pH = 1.86 to pH = 6.17. The UV/Vis spectra plotting absorbance versus wavelength is shown in Figure 16. Absorbances were recorded at 277, 287, 292, and 330 nm because these wavelengths exhibited the largest change in absorbances. Theoretical and measured absorbances were plotted for every wavelength simultaneously by minimizing the sum of the squares of the residuals as previously discussed and shown in Figure 17. Table 11 outlines the solutions of each parameter that was varied by 'SOLVER' and the standard deviation of each variable calculated by Solver Statistics. The p*K*'s were recorded once all standard deviations were minimized and the R^2 value was close to one. Table 12 shows the equations of each

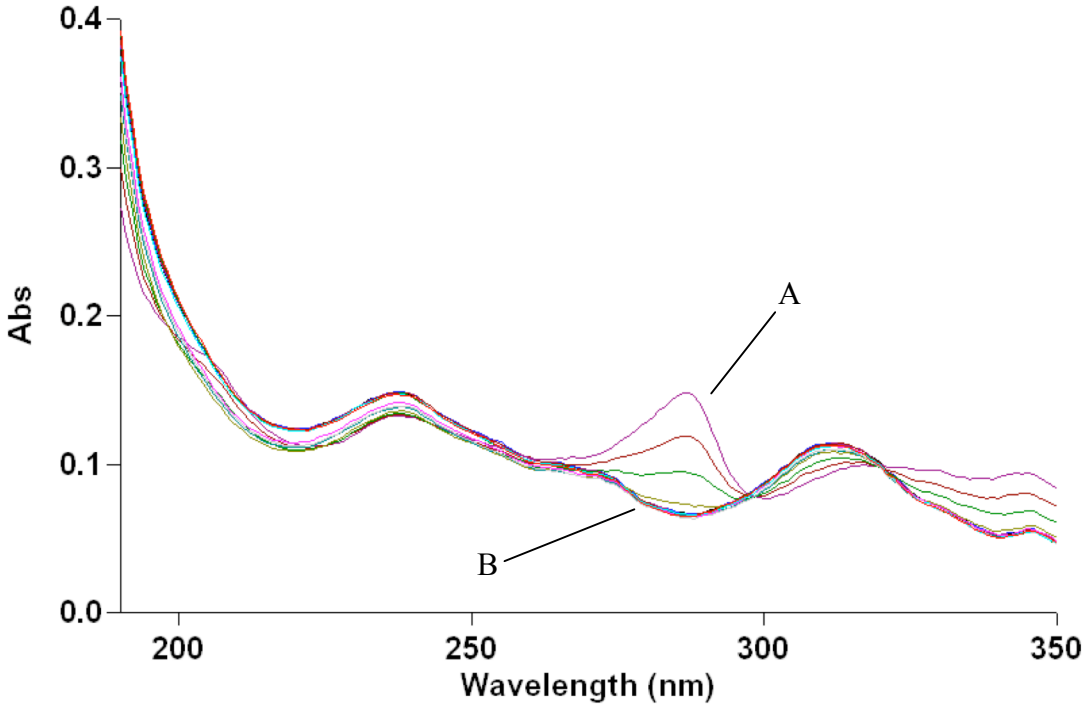

Figure 16. UV spectra of 4 x 10^{-6} M DPP and 4 x 10^{-6} M $Zn(ClO_4)_2$ in 0.01 M $HClO_4$ and 0.09 M $NaClO_4$ as a function of pH. Initial spectrum (A) of free DPP at pH = 1.86. Final spectrum (B) of DPP- zinc complex at pH = 6.17.

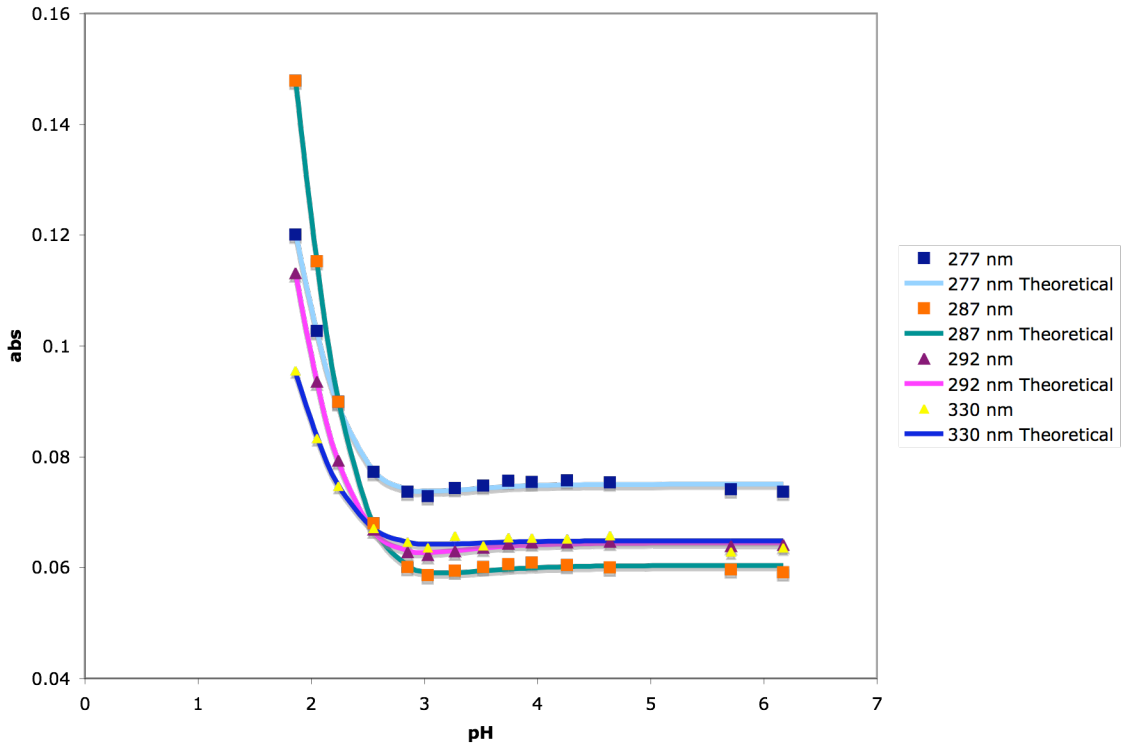

Figure 17. Plot of corrected absorbance (data points) and theoretical absorbance (lines) versus pH for titration of DPP and $Zn(ClO_4)_2$.

Table 11. Solutions and standard deviation for each parameter solved by the 'SOLVER' module of EXCEL in determining log K_1 of DPP-Zn complex. Note: Coefficient of determination and standard error calculated with 'Solver Statistics' macro.

	Parameter	Solution	Standard Deviation
Overall	pK_1	2.533834306	0.151598903
	pK_2	1.511344115	0.166613379
277 nm	Abs(0)	0.075274023	0.000339085
	Abs(1)	0.062252905	0.002571639
	Abs(2)	0.272079285	0.047146314
287 nm	Abs(0)	0.060388819	0.000352301
	Abs(1)	0.04471371	0.002857793
	Abs(2)	0.41781492	0.086229298
292 nm	Abs(0)	0.06475922	0.000346643
	Abs(1)	0.048362232	0.003065081
	Abs(2)	0.282658675	0.051912813
330 nm	Abs(0)	0.064914586	0.000328622
	Abs(1)	0.057893542	0.001866167
	Abs(2)	0.193445336	0.031200332

R^2: 0.99834326 **Standard Error:** 0.000822737

Table 12. Summary of equations at each protonation event of $[Zn(DPP)]^{2+}$; Equations written in terms of log K to complement initial equilibrium expressions.

							pK_{50}
$[Zn(DPP)]^{2+}$	+	H^+	$\rightleftharpoons$	$H(DPP)^+$	+	Zn^{2+}	2.53
$H(DPP)^+$	+	H^+	$\rightleftharpoons$	$H_2(DPP)^{2+}$			1.51

protonation event observed for the DPP-Zn titration and the pK's calculated with minimal error, which were a pK_1 and pK_2 of 2.53 and 1.51 respectively. These were used in Eq. (21) to calculate a log K_1 of 8.40. As predicted the stability of $[Zn(DPP)]^{2+}$ was greater than complexes with nickel. The stability was also greater than $[Zn(TERPY)]^{2+}$ (log K_1 = 6.0) and $[Zn(PHEN)]^{2+}$ (log K_1 = 6.38). This can be explained by preorganization and affinity for nitrogen donors. Although zinc is small it can bind to more donor atoms than nickel. TERPY must overcome folding energy to bind zinc, whereas DPP is in a fixed position leading to a greater log K_1. Denticity explains why DPP has a Δlog K_1 of +2.02 over PHEN. Three nitrogen donors bind zinc in DPP and only two are available in PHEN molecule. This was determined by Hyperchem PM3 energy minimization calculations. The lowest energy conformation found was -5120 kcal/mol and the structure is shown in Figure 18. This conformation also agrees with the UV/Vis spectra because of the similar shape of the spectra at high pH to nickel. The UV/Vis spectra of zinc (Figure 16) indicate the formation of a complex, but no sharp peaks are formed in the spectra when the metal binds. Therefore zinc is not expected to make the ligand as rigid as larger metals, as shown in Figure 18.

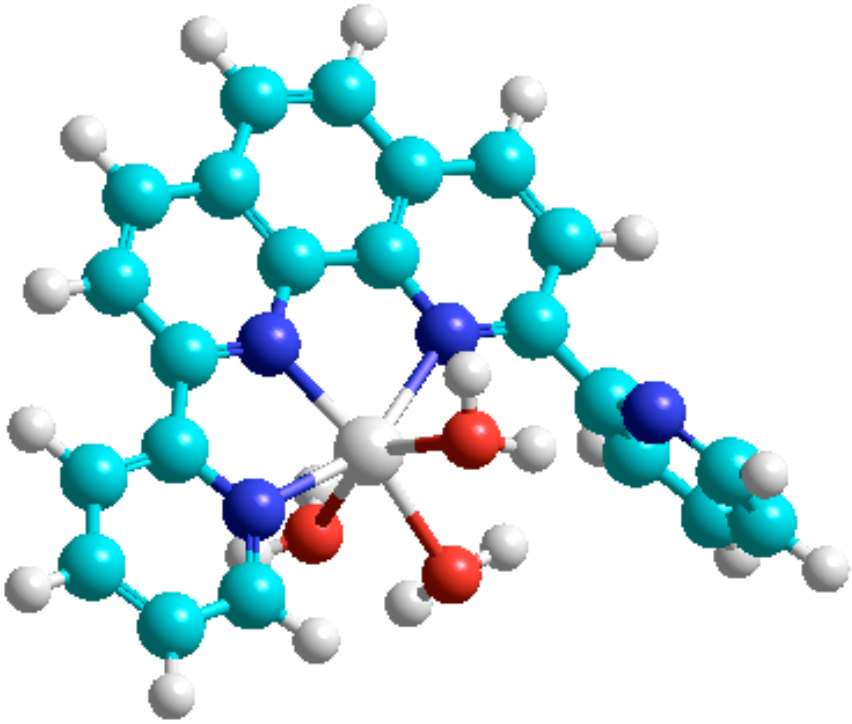

Figure 18. Hyperchem model of lowest energy conformation of $Zn[DPP]^{2+}$ complex. Energy minimized by PM3. Three water molecules were attached to give zinc a coordination number of six. Note: this conformation is also seen later in x-ray crystallography.

Manganese Results

Manganese has an ionic radius of 0.80 Å and is classified as an intermediate acid. Nitrogens are intermediate bases and therefore will be a source of extra stability of $[Mn(DPP)]^{2+}$. A solution of 4 x 10^{-6} M DPP and 4 x 10^{-5} M $Mn(ClO_4)_2$ was titrated with 0.1 M NaOH from pH = 1.98 to pH = 6.12. The UV/Vis spectra plotting absorbance versus wavelength is shown in Figure 19. Absorbances were recorded at 279, 283, 287, 292, and 344 nm because these wavelengths exhibited the largest change in absorbances. Theoretical and measured absorbances were plotted for every wavelength simultaneously by minimizing the sum of the squares of the residuals as previously discussed and shown in Figure 20. Table 13 outlines the solutions of each parameter that was varied by 'SOLVER' and the standard deviation of each variable calculated by Solver Statistics. The p*K*'s were recorded once all standard deviations were minimized and the R^2 value was close to one. Table 14 shows the equations of each protonation event observed for the DPP-Mn titration and the p*K*'s calculated with minimal error, which were a pK_1 and pK_2 of 2.80 and 2.80, respectively. These were used in Eq. (21) to calculate a log K_1 of 5.84. The log K_1 of $[Mn(TERPY)]^{2+}$ is 4.44. The Δlog K_1 between TERPY and DPP is +1.44. Comparing to 1,10-phenanthroline (log K_1 = 4.09), the DPP complex is more stable with a Δlog K_1 of +1.75. The change in log K_1 is not great between these three ligands. Since manganese has a coordination number of seven, the more donor atoms a ligand has, the more stable the manganese complex, as seen in this trend. So the increasing stability as the number of nitrogen donors increases is due to denticity and not preorganization. Hyperchem was used to explore the binding properties of the

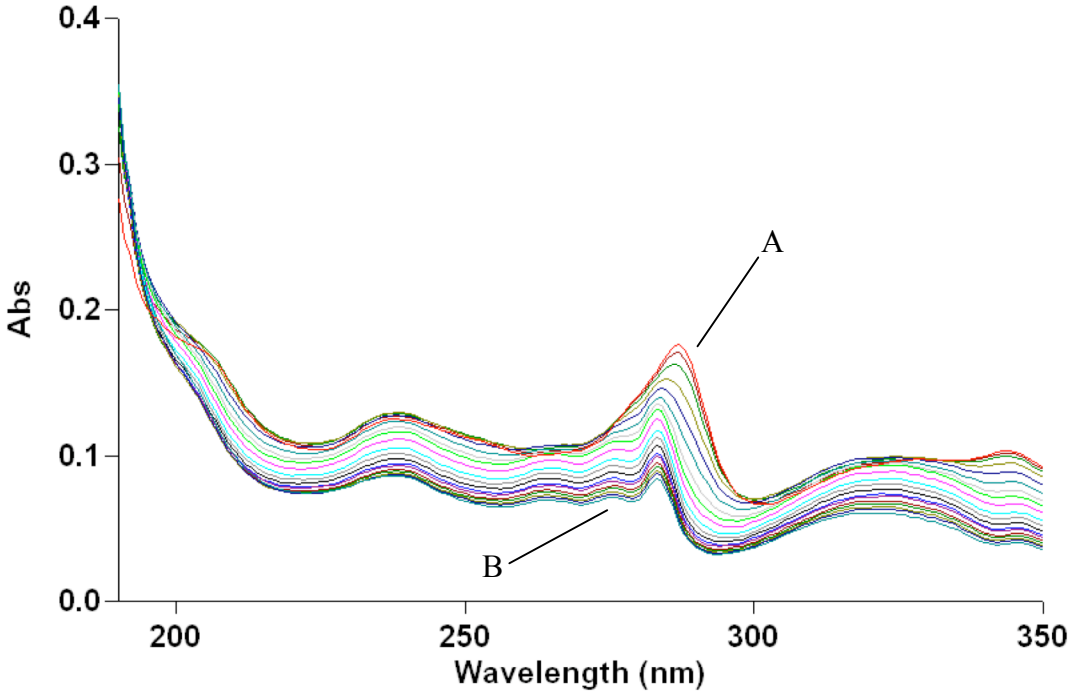

Figure 19. UV spectra of 4 x 10^{-6} M DPP and 4 x 10^{-5} M $Mn(ClO_4)_2$ in 0.01 M $HClO_4$ and 0.09 M $NaClO_4$. Initial spectrum (A) of free DPP at pH = 1.98. Final spectrum (B) of DPP- Mn complex at pH=6.12.

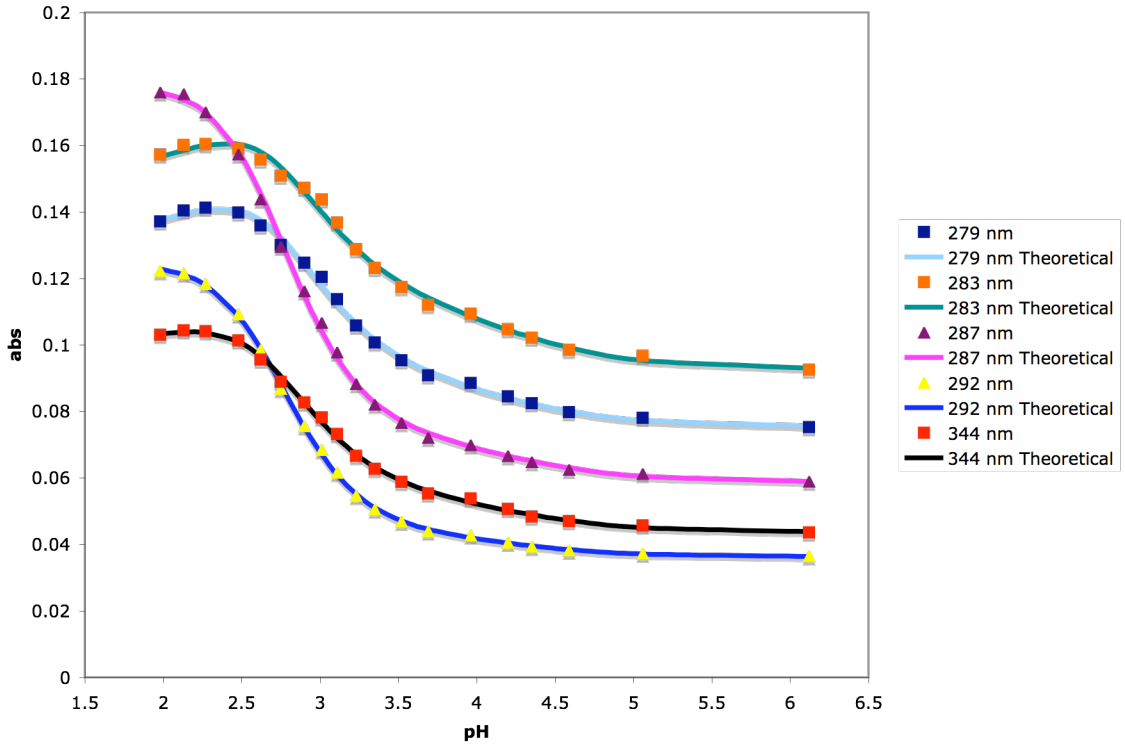

Figure 20. Plot of corrected absorbance (data points) and theoretical absorbance (lines) versus pH for titration of DPP and $Mn(ClO_4)_2$.

Table 13. Solutions and standard deviation for each parameter solved by the 'SOLVER' module of EXCEL in determining log K_1 of DPP-Mn complex. Note: Coefficient of determination and standard error calculated with 'Solver Statistics' macro.

	Parameter	Solution	Standard Deviation
Overall	pK_1	2.802814483	0.038905902
	pK_2	2.802814483	0.038905902
279 nm	Abs(0)	0.078660378	0.000754288
	Abs(1)	0.17462827	0.007972348
	Abs(2)	0.135105349	0.002491928
283 nm	Abs(0)	0.098024809	0.000765025
	Abs(1)	0.205717907	0.008101583
	Abs(2)	0.151447657	0.00273372
287 nm	Abs(0)	0.062020754	0.000773684
	Abs(1)	0.126714873	0.011967606
	Abs(2)	0.189655043	0.001725715
292 nm	Abs(0)	0.037578663	0.000767709
	Abs(1)	0.078138369	0.009138551
	Abs(2)	0.134789059	0.001665731
344 nm	Abs(0)	0.046244012	0.000742498
	Abs(1)	0.112496556	0.007302388
	Abs(2)	0.105069792	0.001996744

R^2: 0.99802681 **Standard Error:** 0.001814884

Table 14. Summary of equations at each protonation event of $[Mn(DPP)]^{2+}$; Equations written in terms of log K to complement initial equilibrium expressions.

							pK_{50}
$[Mn(DPP)]^{2+}$	+	H^+	$\rightleftharpoons$	$H(DPP)^+$	+	Mn^{2+}	2.80
$H(DPP)^+$	+	H^+	$\rightleftharpoons$	$H_2(DPP)^{2+}$			2.80

$[Mn(DPP)]^{2+}$ complex. According to the change in the absorbance spectra the molecule becomes very rigid. This is indicated by the sharp peaks visible at high pH. Manganese is seven coordinate and binds all four donor atoms with three water molecules attached to the metal. The lowest energy calculated using PM3 was -5232.6820 kcal/mol and the structure is shown in Figure 21. Although manganese binds all four donor atoms of DPP, it is smaller than the ideal size for a strong DPP complex. Log K_1 for the $[Mn(DPP)]^{2+}$ complex is lower than other metal ions that bind all four donor atoms because of the strain DPP has to overcome for manganese to bind.

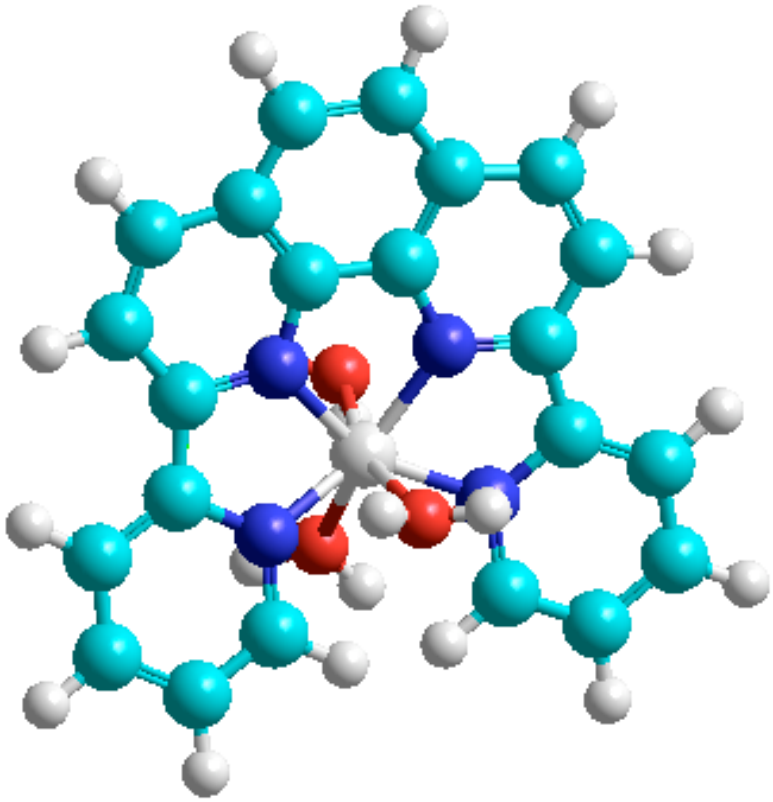

Figure 21. Minimum energy conformation of $[Mn(DPP)]^{2+}$ complex, calculated by PM3 semi empirical method.

Indium Results

Indium has an ionic radius of 0.80 Å and is classified as an intermediate acid, which will be ideal to bind to nitrogen donors. A solution of 4 x 10^{-6} M DPP and 4 x 10^{-6} M $In(ClO_4)_3$ was titrated with 0.1 M NaOH from pH = 2.05 to pH = 6.45. The UV/Vis spectra plotting absorbance versus wavelength is shown in Figure 22. Absorbances were recorded at 278, 282, 287, 330, and 344 nm because these wavelengths exhibited the largest change in absorbances. Theoretical and measured absorbances were plotted for every wavelength simultaneously by minimizing the sum of the squares of the residuals as previously discussed and shown in Figure 23. Table 15 outlines the solutions of each parameter that was varied by 'SOLVER' and the standard deviation of each variable calculated by Solver Statistics. The p*K*'s were recorded once all standard deviations were minimized and the R^2 value was close to one. Table 16 shows the equations of each protonation event observed for the DPP-In titration and the p*K*'s calculated with minimal error, which were a pK_1 and pK_2 of 3.20 and 2.10, respectively. These were used in Eq. (21) to calculate a log K_1 of 7.15. Comparing to 1,10-phenanthroline (log K_1 = 5.70), the DPP complex is more stable with a Δlog K_1 of +1.45. Increasing the number of donor atoms to bind to indium results in the increased stability of the complex.

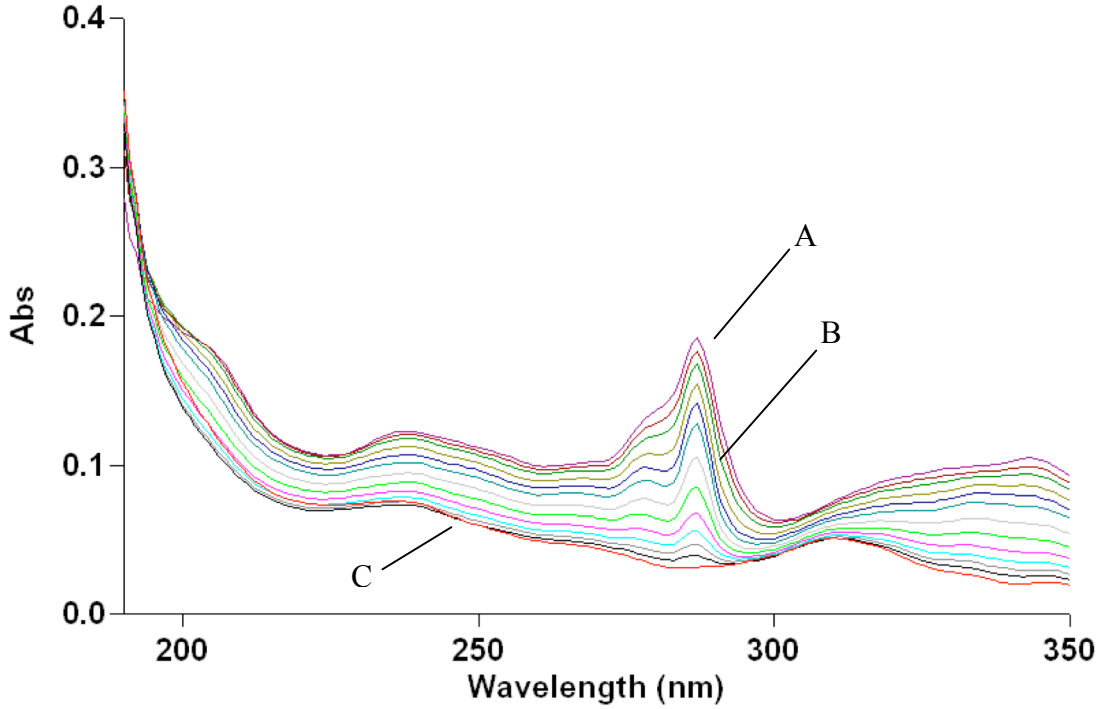

Figure 22. UV spectra of 4 x 10^{-6} M DPP and 4 x 10^{-6} M $In(ClO_4)_3$ in 0.01 M $HClO_4$ and 0.09 M $NaClO_4$. Initial spectrum (A) of free DPP at pH = 2.05. Spectrum (B) of DPP- In complex. Final spectrum (C) of deprotonated DPP at pH = 6.45 after precipitation of $In(OH)_3$.

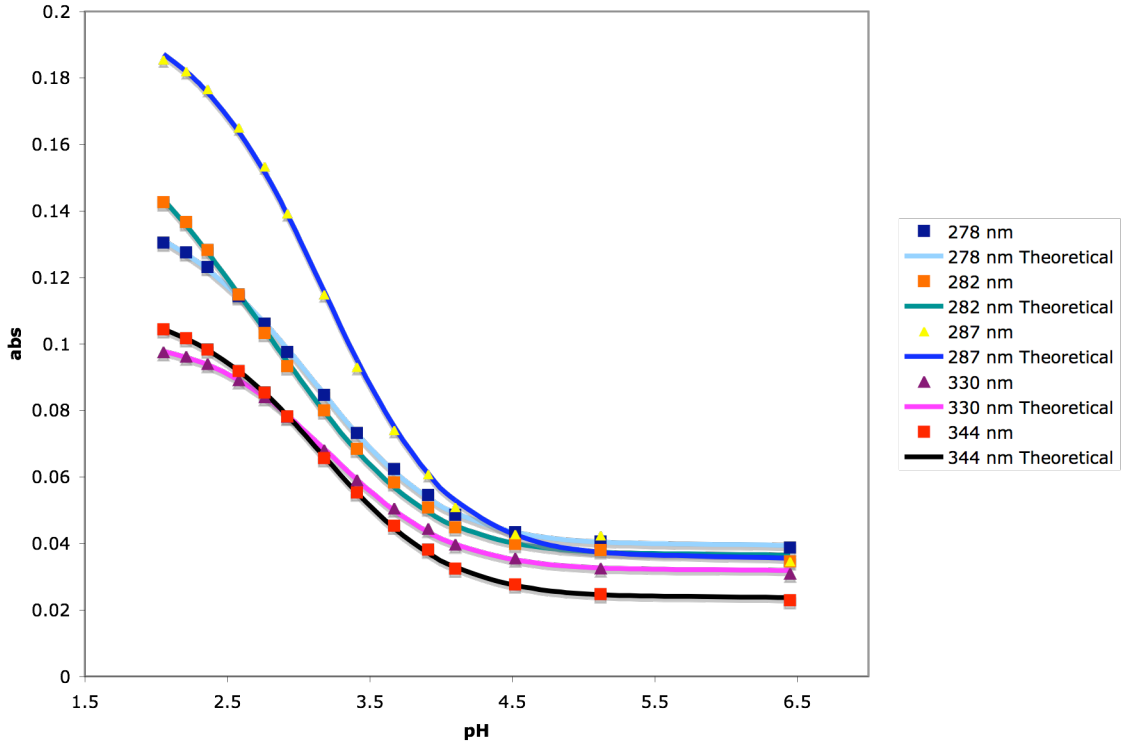

Figure 23. Plot of corrected absorbance (data points) and theoretical absorbance (lines) versus pH for titration of DPP and $In(ClO_4)_3$.

Table 15. Solutions and standard deviation for each parameter solved by the 'SOLVER' module of EXCEL in determining log K_1 of DPP-In complex. Note: Coefficient of determination and standard error calculated with 'Solver Statistics' macro.

	Parameter	Solution	Standard Deviation
Overall	pK_1	3.200461453	0.026736825
	pK_2	2.099535303	0.174435425
278 nm	Abs(0)	0.039702857	0.000545561
	Abs(1)	0.122620195	0.004439687
	Abs(2)	0.144185943	0.003363004
282 nm	Abs(0)	0.036622561	0.00057367
	Abs(1)	0.112742598	0.005623895
	Abs(2)	0.177955794	0.010728872
287 nm	Abs(0)	0.036083014	0.000592551
	Abs(1)	0.18436083	0.00687542
	Abs(2)	0.197775879	0.003263748
330 nm	Abs(0)	0.032132287	0.000544672
	Abs(1)	0.099934345	0.003125046
	Abs(2)	0.09943916	0.00300702
344 nm	Abs(0)	0.023987616	0.000545665
	Abs(1)	0.10223817	0.003832807
	Abs(2)	0.110993609	0.002583242

R^2: 0.999460446 **Standard Error:** 0.001096016

Table 16. Summary of equations at each protonation event of $[In(DPP)]^{3+}$; Equations written in terms of log K to complement initial equilibrium expressions.

							pK_{50}
$[In(DPP)]^{3+}$	+	H^+	⇌	$H(DPP)^+$	+	In^{3+}	3.20
$H(DPP)^+$	+	H^+	⇌	$H_2(DPP)^{2+}$			2.10

Gadolinium Results

Gadolinium was a metal where an extra protonation event occurred as the pH increased. This was predicted to be the formation of the hydroxide complex as shown in Eq. (22). To conclude that that this was the case, three separate titrations were performed at varying gadolinium concentrations while keeping the ligand concentration constant. By varying the metal concentration the pK_{50} should change as well, but the pK_1 of the hydroxide formation should remain the same for all three titrations. This is because the formation of the hydroxide complex is not dependent on the metal concentration as shown in Eq. (23).

$$K_1 = \frac{[ML^{x+}]}{[MLOH^{(x-1)+}][H^+]} \tag{23}$$

The first titration experiment was conducted with 4 x 10^{-5} M $Gd(ClO_4)_3$. The plot of absorbance versus wavelength is shown in Figure 24. Absorbances were recorded at 249, 276, 287, 295, and 332 nm because these wavelengths exhibited the largest change in absorbances. Theoretical and measured absorbances were plotted for every wavelength simultaneously by minimizing the sum of the squares of the residuals as previously discussed and shown in Figure 25. Table 17 outlines the solutions of each parameter that was varied by 'SOLVER' and the standard deviation of each variable calculated by Solver Statistics. The p*K*'s were recorded once all standard deviations were minimized and the R^2 value was close to one. The observed protonation events for the DPP-Gd titration were a pK_2 and pK_3 of 3.07 and 2.31, respectively. These were used in Eq. (21) to calculate a log K_1 of 6.06. A third protonation constant was calculated to be 5.37. This was the deprotonation of a water molecule coordinated to the metal ion.

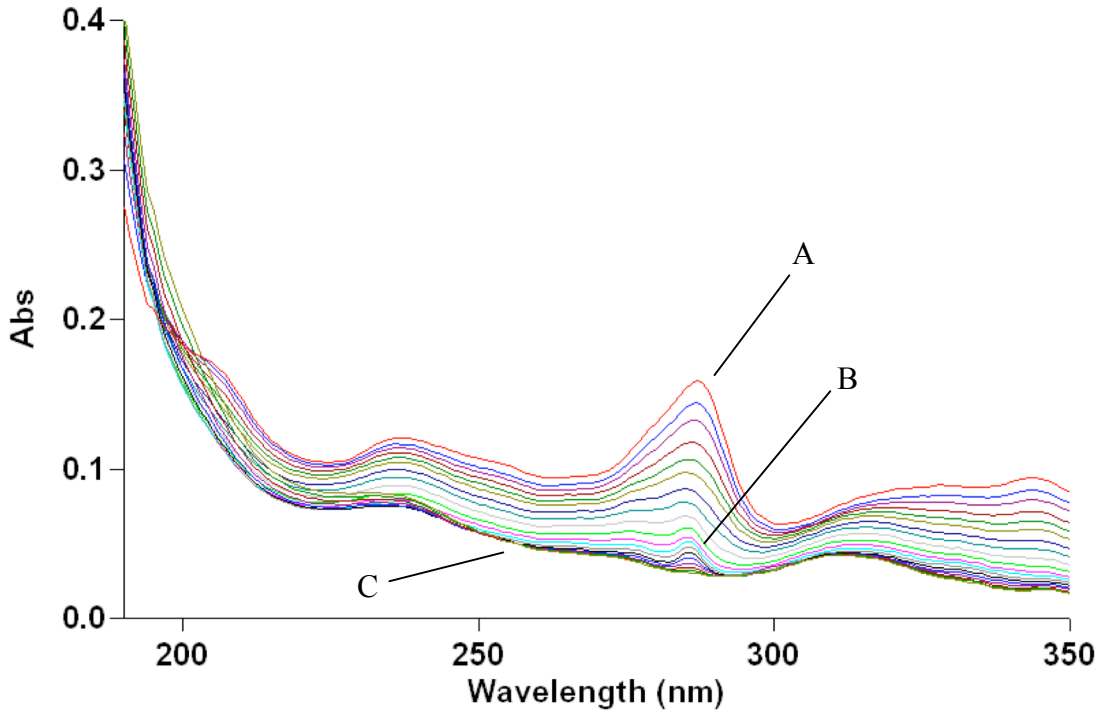

Figure 24. UV spectra of 4 x 10^{-6} M DPP and 4 x 10^{-5} M $Gd(ClO_4)_3$ in 0.01 M $HClO_4$ and 0.09 M $NaClO_4$. Initial spectrum (A) of free DPP at pH = 1.93. Spectrum (B) of DPP-Gd complex. Final spectrum (C) of DPP- Gd hydroxide complex at pH = 7.04.

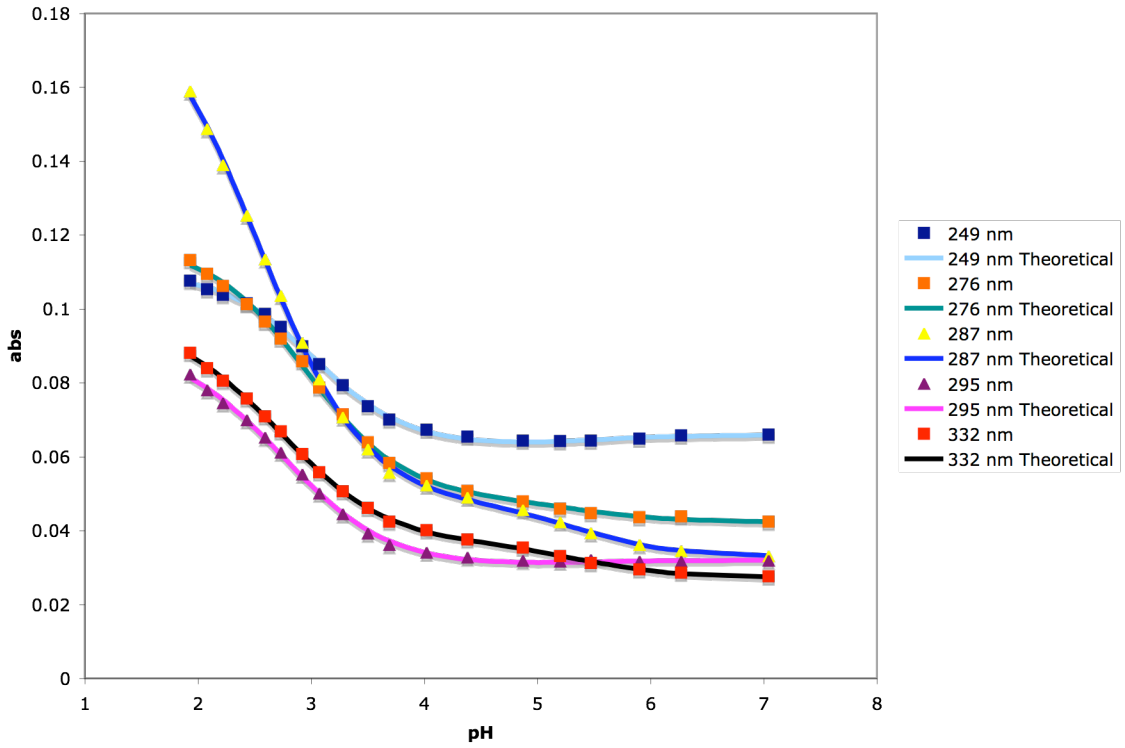

Figure 25. Plot of corrected absorbance (data points) and theoretical absorbance (lines) versus pH for titration of DPP and $Gd(ClO_4)_3$.

Table 17. Solutions and standard deviation for each parameter solved by the 'SOLVER' module of EXCEL in determining log K_1 of DPP-Gd complex (low concentration titration). Note: Coefficient of determination and standard error calculated with 'Solver Statistics' macro.

	Parameter	Solution	Standard Deviation
Overall	pK_1	5.374589495	0.065889443
	pK_2	3.06922914	0.039524544
	pK_3	2.31223054	0.050263588
249 nm	Abs(0)	0.065973297	0.000418168
	Abs(1)	0.062708834	0.000428923
	Abs(2)	0.103686805	0.002362909
	Abs(3)	0.109786538	0.001149483
276 nm	Abs(0)	0.042331096	0.000429246
	Abs(1)	0.048755836	0.000483248
	Abs(2)	0.101928833	0.003218605
	Abs(3)	0.118066371	0.001195348
287 nm	Abs(0)	0.032940365	0.000495095
	Abs(1)	0.047564291	0.000592892
	Abs(2)	0.096415229	0.00509649
	Abs(3)	0.186534396	0.002286954
295 nm	Abs(0)	0.032087482	0.000409796
	Abs(1)	0.030740424	0.000401591
	Abs(2)	0.062671752	0.002521369
	Abs(3)	0.090874155	0.00103792
332 nm	Abs(0)	0.027338272	0.000448229
	Abs(1)	0.036916226	0.000464634
	Abs(2)	0.068324129	0.00252777
	Abs(3)	0.09679516	0.001018114

R^2: 0.999622628 **Standard Error:** 0.000643425

The subsequent titrations were performed with 4 x 10^{-4} M and 4 x 10^{-3} M $Gd(ClO_4)_3$. The following table summarizes the results for the three gadolinium titrations.

Table 18. Summary of results from three DPP-gadolinium titrations and overall standard deviation of fit. pK_1 is the protonation event associated with the hydroxide complex.

[Gd^{3+}]	**pK_1 (OH)**	**pK_2**	**pK_3**	**Std. Deviation (Overall Fit)**
4 x 10^{-5} M	5.37	3.07	2.31	0.000643425
4 x 10^{-4} M	5.16	2.64	1.76	0.000955232
4 x 10^{-3} M	5.11	-	-	0.032877935

For the titration with 4 x 10^{-4} M $Gd(ClO_4)$, absorbances were recorded at 249, 276, 287, 295, and 332 nm because these wavelengths exhibited the largest change in absorbances. The UV/Vis spectra are shown in Figure 26. Theoretical and measured absorbances were plotted for every wavelength simultaneously by minimizing the sum of the squares of the residuals as previously discussed and shown in Figure 27. Table 19 outlines the solutions of each parameter that was varied by 'SOLVER' and the standard deviation of each variable calculated by Solver Statistics. The pK's were recorded once all standard deviations were minimized and the R^2 value was close to one. The observed protonation events for the DPP-Gd titration were a pK_2 and pK_3 of 2.64 and 1.76, respectively and Table 20 outlines the chemical equations observed at each event. These were used in Eq. (21) to calculate a log K_1 of 6.04.

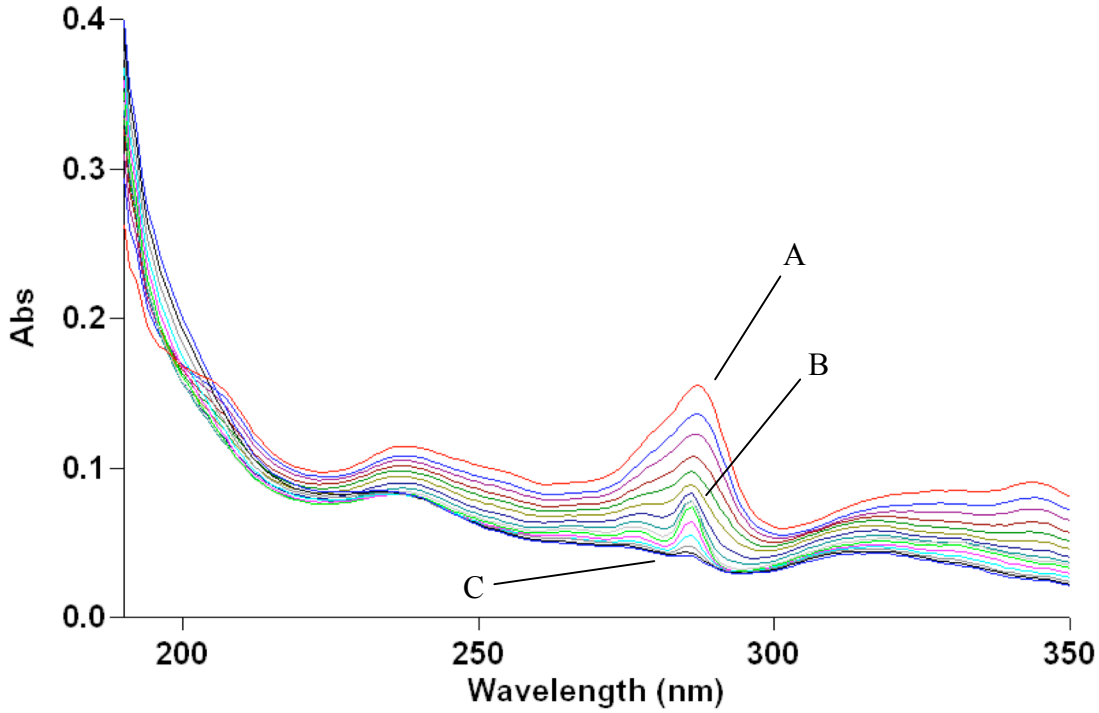

Figure 26. UV spectra of 4 x 10^{-6} M DPP and 4 x 10^{-4} M $Gd(ClO_4)_3$ in 0.01 M $HClO_4$ and 0.09 M $NaClO_4$. Initial spectrum (A) of free DPP at pH = 1.67. Spectrum (B) of DPP-Gd complex. Final spectrum (C) of DPP- Gd hydroxide complex at pH = 6.38.

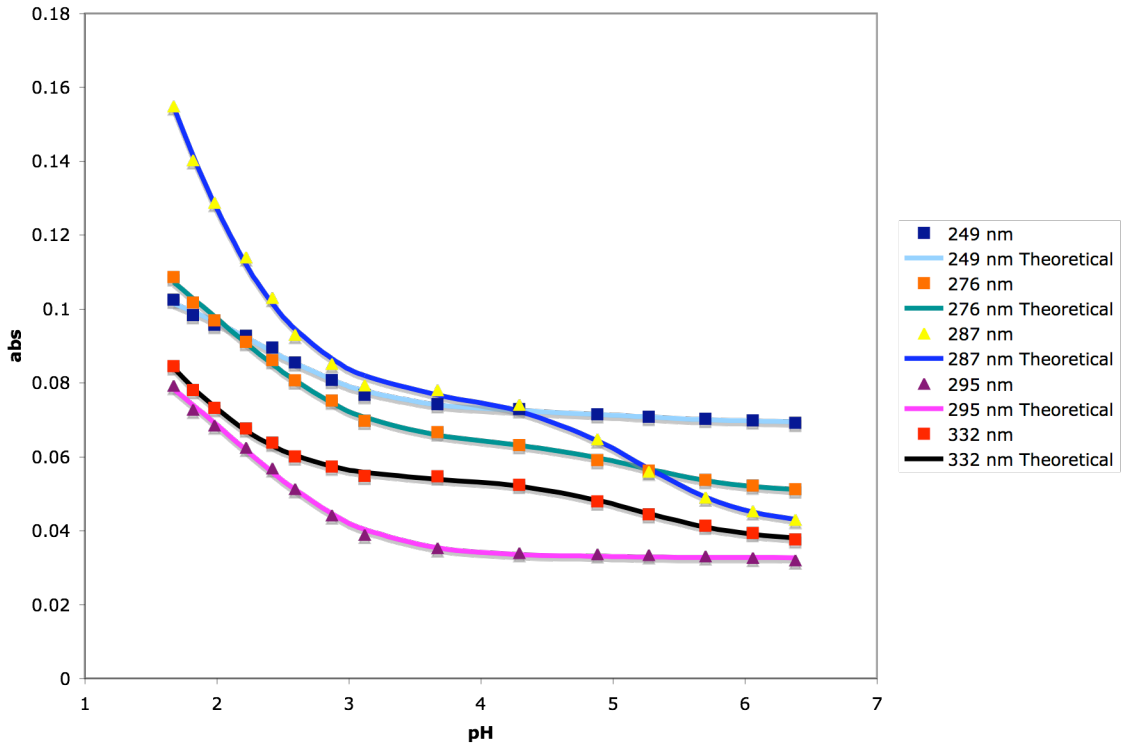

Figure 27. Plot of corrected absorbance (data points) and theoretical absorbance (lines) versus pH for titration of DPP and $Gd(ClO_4)_3$.

Table 19. Solutions and standard deviation for each parameter solved by the 'SOLVER' module of EXCEL in determining log K_1 of DPP-Gd complex. Note: Coefficient of determination and standard error calculated with 'Solver Statistics' macro.

	Parameter	Solution	Standard Deviation
Overall	pK_1	5.157878517	0.050314095
	pK_2	2.639445747	0.126261121
	pK_3	1.764679825	0.07874352
249 nm	Abs(0)	0.069377574	0.00062528
	Abs(1)	0.072394675	0.000706744
	Abs(2)	0.093362667	0.003920409
	Abs(3)	0.110601601	0.002979294
276 nm	Abs(0)	0.05046489	0.000661909
	Abs(1)	0.064228916	0.000741758
	Abs(2)	0.088759234	0.00507145
	Abs(3)	0.125688089	0.003531193
287 nm	Abs(0)	0.041032205	0.000840862
	Abs(1)	0.076797142	0.000943344
	Abs(2)	0.091861286	0.006628127
	Abs(3)	0.210319884	0.008433671
295 nm	Abs(0)	0.03271326	0.000625106
	Abs(1)	0.033091723	0.000720495
	Abs(2)	0.060398695	0.005409451
	Abs(3)	0.096689533	0.003684563
332 nm	Abs(0)	0.037095169	0.000676429
	Abs(1)	0.054148278	0.000729093
	Abs(2)	0.058731839	0.002799077
	Abs(3)	0.106151554	0.003940839

R^2: 0.999006406 **Standard Error:** 0.000955232

Table 20. Summary of equations at each protonation event of $[Gd(DPP)]^{3+}$; Equations written in terms of log K to complement initial equilibrium expressions.

							pK_{50}
$[Gd(DPP)OH]^{2+}$	+	H^+	$\rightleftharpoons$	$[Gd(DPP)]^{3+}$	+	H_2O	5.37
$[Gd(DPP)]^{3+}$	+	H^+	$\rightleftharpoons$	$H(DPP)^+$	+	Gd^{3+}	3.06
$H(DPP)^+$	+	H^+	$\rightleftharpoons$	$H_2(DPP)^{2+}$			2.31

The two titrations previously discussed produced the same log K_1 with very good fits. The UV/Vis spectra of the third experiment are shown in Figure 28. The third titration at higher concentration was fit by minimizing the sum of the squares of the residuals as the other titrations. Although the two protonation constants at the higher gadolinium concentration were not determined, the constant corresponding to the hydroxide complex was calculated to be 5.11. The plot of absorbance versus pH at 287 nm is shown in Figure 29. The pK_{50} for $[Gd(DPP)]^{3+}$ could not be determined because at low pH the complex was predominant in solution according to the UV/Vis spectrum. The data from all three titrations showed that pK_1 was constant with varying metal concentrations, while pK_2 and pK_3 changed, meaning the protonation event was in fact the formation of the hydroxide complex. The species distribution diagram was constructed to verify the results from the UV/Vis spectra. QBasic was used by inputting the pK data calculated, literature log K data for hydroxide and gadolinium, and solubility constants (Martel, 2003). The species distribution diagram is shown in Figure 30.

One important observation is that the hydroxide complex was formed at a pH lower than 7. The protonation event occurs at a pH of about 5.2, meaning this would be the form of the complex at biological pH. Using DPP as an MRI imaging agent would have hydroxides attached directly to the metal rather than waters. Further studies to determine the effect hydroxides have on shifting the MRI signals need to be explored. The log K_1 of $[Gd(DPP)]^{3+}$ is not as high as that of DTPA, but the hydroxide complex that is formed does add extra stability to the complex. The pK of the hydroxide did not contribute to the calculated log K_1 of 6.04.

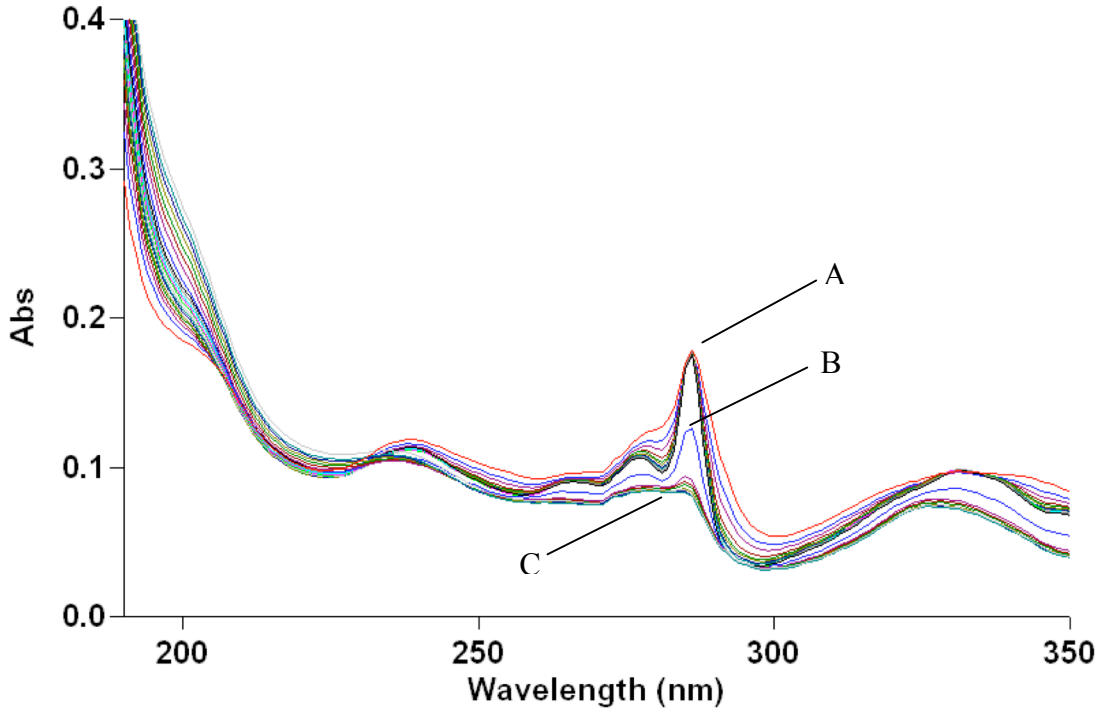

Figure 28. UV spectra of 4 x 10^{-6} M DPP and 4 x 10^{-3} M $Gd(ClO_4)_3$ in 0.01 M $HClO_4$ and 0.09 M $NaClO_4$. Initial spectrum (A) of DPP-Gd complex at pH = 1.89. Spectrum (B) shows initial formation of DPP-Gd hydroxide complex. Final spectrum (C) of DPP-Gd hydroxide complex at pH = 6.25.

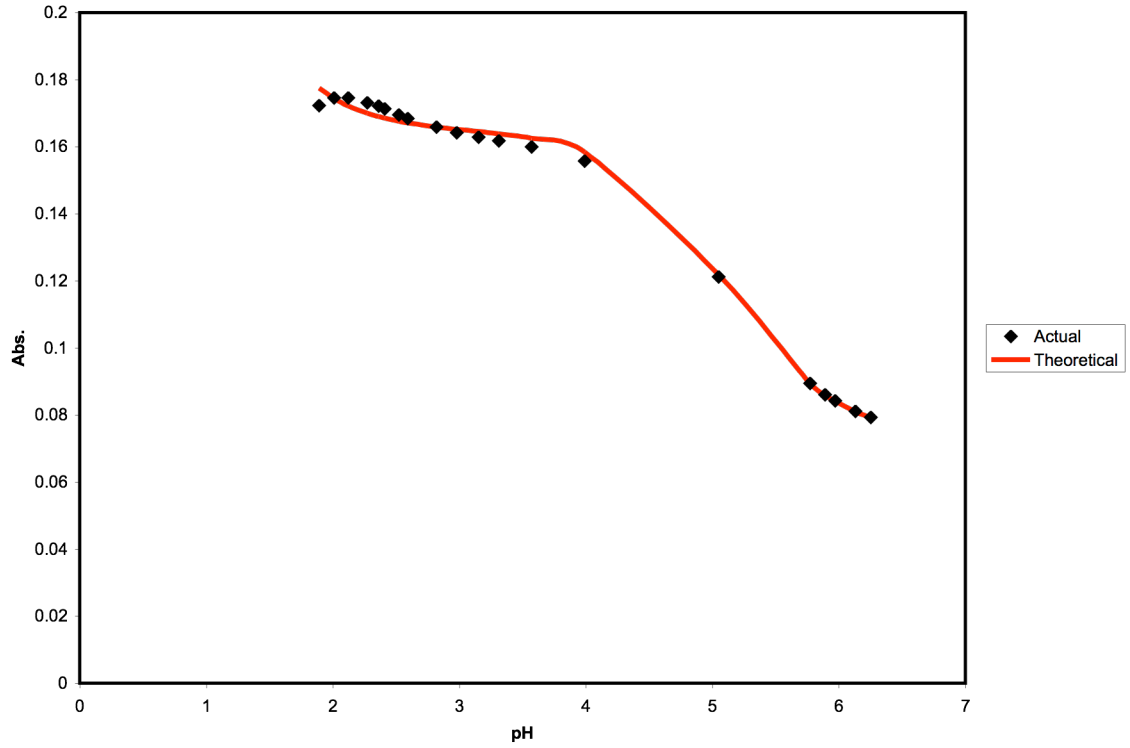

Figure 29. Observed absorbance and theoretical absorbance versus pH at 287 nm of 4 x 10^{-3} M $Gd(ClO_4)_3$ to show the protonation event corresponding to formation of the hydroxide complex.

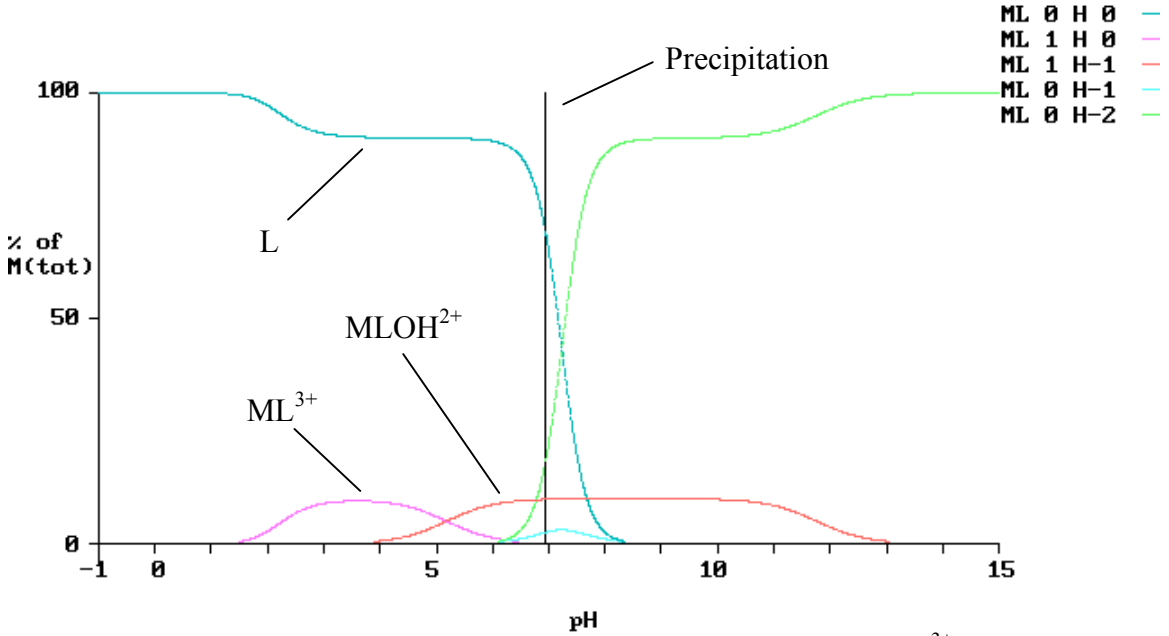

Figure 30. Species distribution diagram for the formation of $[Gd(DPP)]^{3+}$ and $[Gd(DPP)OH]^{2+}$. The vertical black line represents precipitation.

Thorium Results

Thorium was the only actinide studied for which a log K_1 could be calculated. A titration experiment involving uranium with DPP was performed but the complex was too strong to measure any log K_1 with available materials. Thorium has an ionic radius of 0.94 Å, which is about the size of gadolinium. Thorium is classified as a hard acid. It has a charge of 4+ and is the highest charge studied. The size of thorium is the only optimal attribute for binding with DPP. A solution of 4×10^{-6} M DPP and 2×10^{-5} M $Th(NO_3)_4$ was titrated with 0.1 M NaOH from pH = 2.02 to pH = 7.27. The UV/Vis spectra plotting absorbance versus wavelength is shown in Figure 31. Absorbances were recorded at 277, 287, 292, 335, and 345 nm because these wavelengths exhibited the largest change in absorbances. Theoretical and measured absorbances were plotted for every wavelength simultaneously by minimizing the sum of the squares of the residuals as previously discussed and shown in Figure 32. Table 21 outlines the solutions of each parameter that was varied by 'SOLVER' and the standard deviation of each variable calculated by Solver Statistics. The pK's were recorded once all standard deviations were minimized and the R^2 value was close to one. Table 22 shows the equations of each protonation event observed for the DPP-Th titration and the pK's calculated with minimal error, which were a pK_1 and pK_2 of 2.97 and 1.90, respectively. These were used in Eq. (21) to calculate a log K_1 of 6.58.

More studies need to be conducted on the stability of the thorium complex observed. No peak sharpening was apparent in the UV/Vis spectra. This would suggest that no complex was formed, but if no complex had formed the pK's calculated would have been the same as the free ligand. The change in the calculated pK_1 and pK_2 suggests

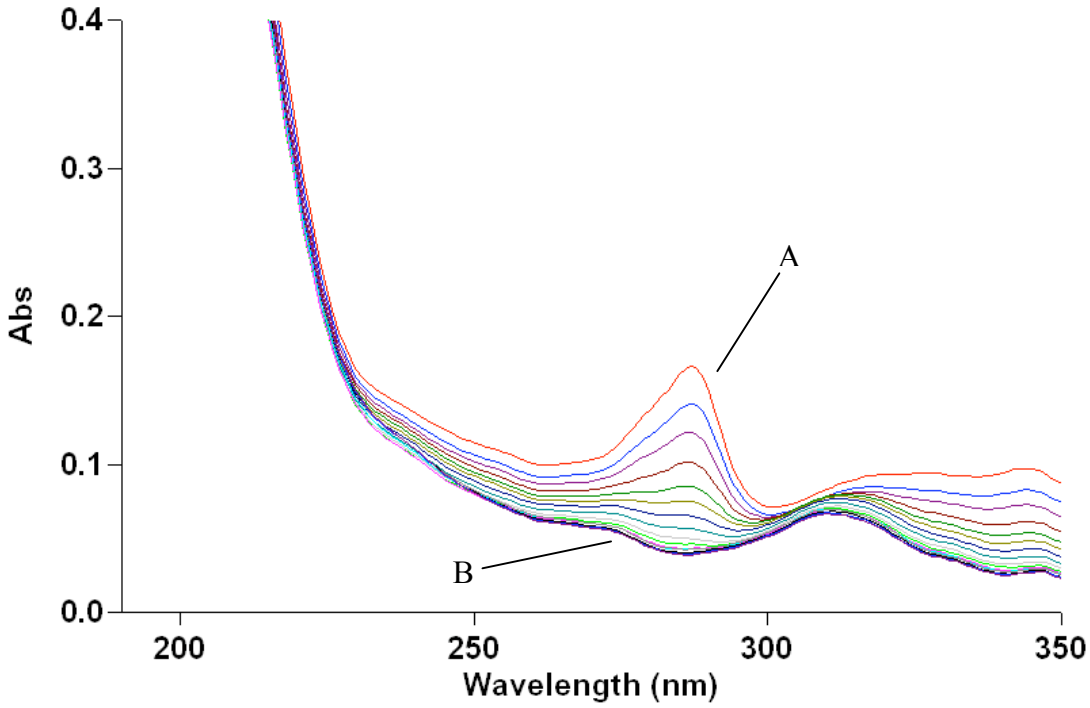

Figure 31. UV spectra of 4 x 10^{-6} M DPP and 4 x 10^{-6} M $Th(NO_3)_4$ in 0.01 M $HClO_4$ and 0.09 M $NaClO_4$. Initial spectrum (A) of free DPP at pH = 2.05. Final spectrum (B) of DPP- Th hydroxide complex at pH = 6.45.

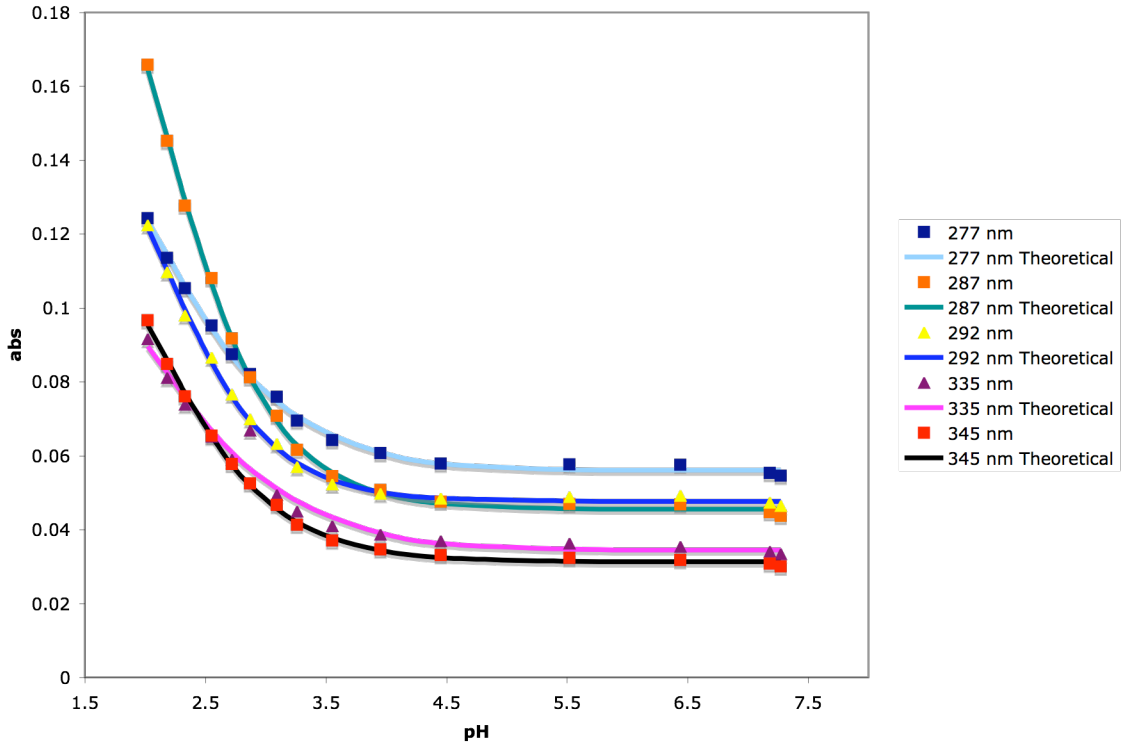

Figure 32. Plot of corrected absorbance (data points) and theoretical absorbance (lines) versus pH for titration of DPP and $Th(NO_3)_4$.

Table 21. Solutions and standard deviation for each parameter solved by the 'SOLVER' module of EXCEL in determining log K_1 of DPP-Th complex. Note: Coefficient of determination and standard error calculated with 'Solver Statistics' macro.

	Parameter	Solution	Standard Deviation
Overall	pK_1	2.972473581	0.159007737
	pK_2	1.895191617	0.117636277
277 nm	Abs(0)	0.056499726	0.000460137
	Abs(1)	0.092074572	0.009442901
	Abs(2)	0.175025843	0.007289028
287 nm	Abs(0)	0.045472979	0.000444567
	Abs(1)	0.088723803	0.014315426
	Abs(2)	0.286670711	0.022409678
292 nm	Abs(0)	0.04750564	0.000437834
	Abs(1)	0.074058553	0.008921479
	Abs(2)	0.19810912	0.014366229
335 nm	Abs(0)	0.035290041	0.000441878
	Abs(1)	0.060173924	0.007331432
	Abs(2)	0.138929598	0.008138493
345 nm	Abs(0)	0.031459139	0.000439258
	Abs(1)	0.057687212	0.008112958
	Abs(2)	0.156346236	0.010697662

R^2: 0.998948242 **Standard Error:** 0.001065588

Table 22. Summary of equations at each protonation event of $[Th(DPP)]^{4+}$; Equations written in terms of log K to complement initial equilibrium expressions.

	pK_{50}
$[Th(DPP)OH]^{3+} + 2H^+ \rightleftharpoons H(DPP)^+ + Th^{4+} + H_2O$	2.97
$H(DPP)^+ + H^+ \rightleftharpoons H_2(DPP)^{2+}$	1.89

that a complex was in fact formed. Thorium has a high affinity for hydroxides and is very acidic. DPP was not expected to have a high stability constant with thorium, but according to the calculated log K_1 it was a stable complex. This extra stability is predicted to be the immediate formation of a hydroxide complex. This would also agree with the characteristics of the UV/Vis spectra, where there was an obvious change in the spectra as pH was increased, but no sharp peaks. The species distribution diagram was constructed with QBasic by inputting the measured p*K*'s and the log *K* values thorium has for hydroxides, along with literature solubility constants. The species distribution diagram is shown in Figure 33.

Because of the preorganization DPP possesses, thorium is near the perfect size to bind to all four donor atoms. As previously reported, DPP causes acidic metal ions to behave even more acidicly, leading to the water molecules coordinated to the metal ion to become more acidic. This results in the loss of a proton and the formation of a hydroxide complex. Thorium, already being the most acidic metal ion studied, is predicted to form a hydroxide complex at very low pH and is confirmed by the species distribution diagram. Based on Figure 33, hardly any $[Th(DPP)]^{4+}$ was formed before $[Th(DPP)OH]^{3+}$ began to form, and $[Th(DPP)(OH)_2]^{2+}$ was the predominant product. The diagram shows a precipitate at a pH of about 2.5. This was not observed in the UV data. This is expected to be a kinetic effect due to the low concentrations of DPP and thorium.

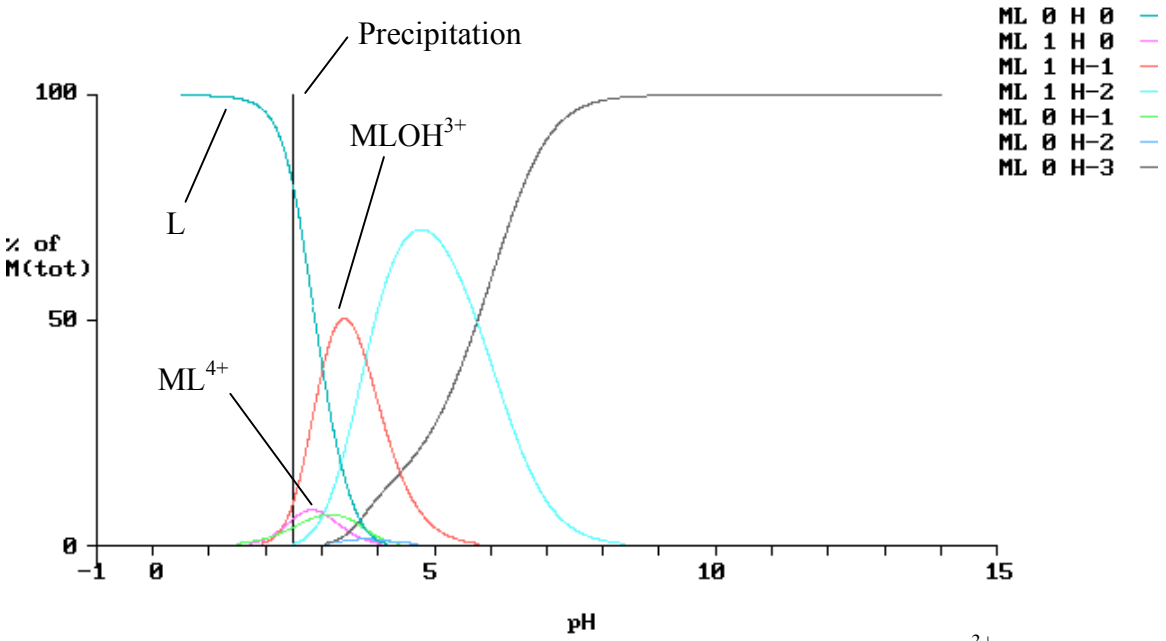

Figure 33. Species distribution diagram for the formation of $[Th(DPP)OH]^{3+}$ and $[Th(DPP)(OH)_2]^{4+}$. The vertical black line represents precipitation.

Cadmium Results

Cadmium has an ionic radius of 0.95 Å and is classified as a soft acid. DPP was found to be very selective for cadmium because of its ideal size. A solution of 4 x 10^{-6} M DPP and 4 x 10^{-6} M $Cd(ClO_4)_2$ was titrated with 0.1 M NaOH from pH = 2.93 to pH = 7.66. The UV/Vis spectra plotting absorbance versus wavelength is shown in Figure 34. Absorbances were recorded at 238, 264, 282, 325, and 345 nm because these wavelengths exhibited the largest change in absorbances. Theoretical and measured absorbances were plotted for every wavelength simultaneously by minimizing the sum of the squares of the residuals as previously discussed and shown in Figure 35. The parameter that was varied by 'SOLVER' and the standard deviation of each variable calculated by Solver Statistics. The pK's were recorded to be 6.15 $\pm$ 0.05 and 4.6 $\pm$ 0.2 once all standard deviations were minimized and the R^2 value was close to one. The R^2 value was 0.997 and the fit had an overall $SE_{(y)}$ of 0.003. No log K_1 was calculated from this experiment because both pK_{50} values calculated were deprotonation of a water molecule attached directly to the cadmium. According to the UV/Vis spectra, the complex had formed at the initial pH. The spectra change as pH is increased but the spectrum for the free ligand was never seen. It appears that the formation of the hydroxide complex resulted in the formation of a precipitate from the left side of the spectra.

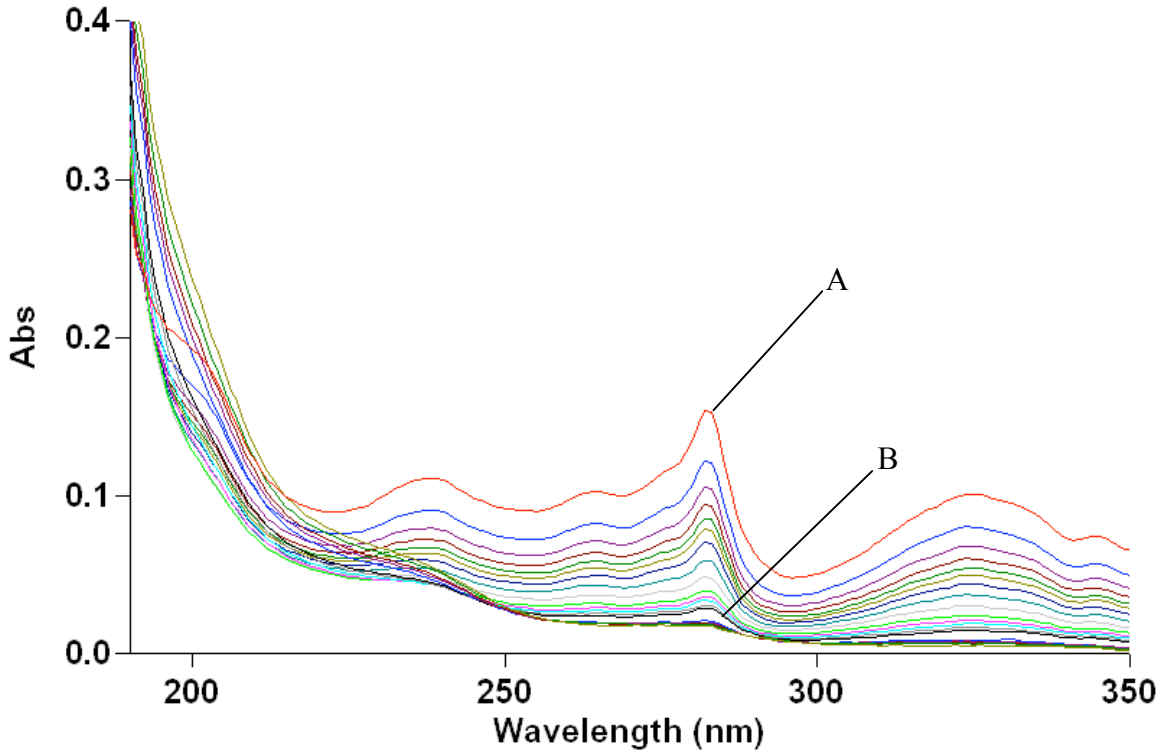

Figure 34. UV spectra of 4 x 10^{-6} M DPP and 4 x 10^{-6} M $Cd(ClO_4)_2$ in 0.01 M $HClO_4$ and 0.09 M $NaClO_4$. Initial spectrum (A) of DPP-Cd complex at pH = 2.93. Final spectrum (B) of DPP- Cd hydroxide complex at pH = 7.66.

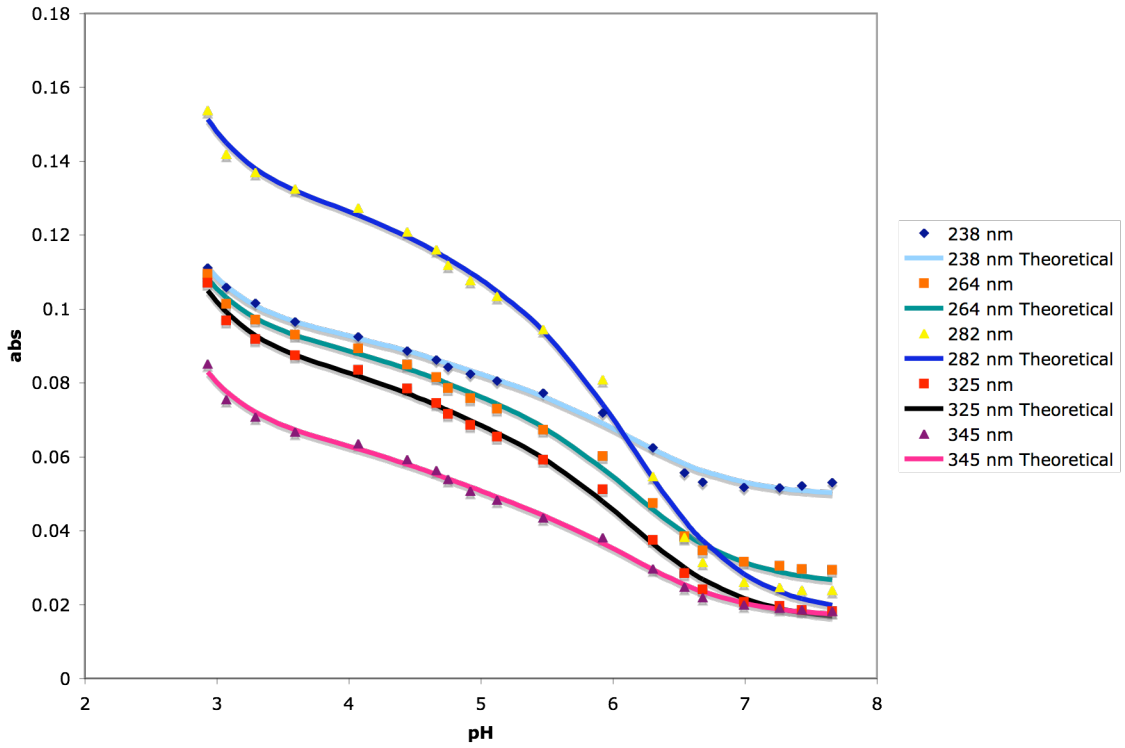

Figure 35. Plot of corrected absorbance (data points) and theoretical absorbance (lines) versus pH for titration of DPP and $Cd(ClO_4)_2$.

A second titration was conducted to calculate log K_1 of the $[Cd(DPP)]^{2+}$ complex. A solution of 4 x 10^{-6} M DPP and 4 x 10^{-6} M $Cd(ClO_4)_2$ was titrated with 11.6 M $HClO_4$ from pH = 3.04 to pH = 0.38. The UV/Vis spectra plotting absorbance versus wavelength is shown in Figure 36. Absorbances were recorded at 264, 282, 290, 325, and 345 nm because these wavelengths exhibited the largest change in absorbances. Theoretical and measured absorbances were plotted for every wavelength simultaneously by minimizing the sum of the squares of the residuals as previously discussed and shown in Figure 37. Table 23 outlines the solutions of each parameter that was varied by 'SOLVER' and the standard deviation of each variable calculated by Solver Statistics. The pK's were recorded once all standard deviations were minimized and the R^2 value was close to one. Observed protonation events for the DPP-Cd titration were at a pK_1 and pK_2 of 2.41 and 0.18, respectively. These were used in Eq. (21) to calculate a log K_1 of 12.21.

Cadmium has higher stability with DPP than most of the other metal ions explored. Cadmium is the ideal size and binds to all four donor atoms. Log K_1 with 1,10-phenanthroline is 5.66. DPP is much more stable than 1,10-phenanthroline with a Δlog K_1 of +6.55. DPP is also much more stable than TERPY (log K_1 = 6.1) with a Δlog K_1 of +6.11. Both denticity and preorganization are factors in the high stability of the $[Cd(DPP)]^{2+}$ complex.

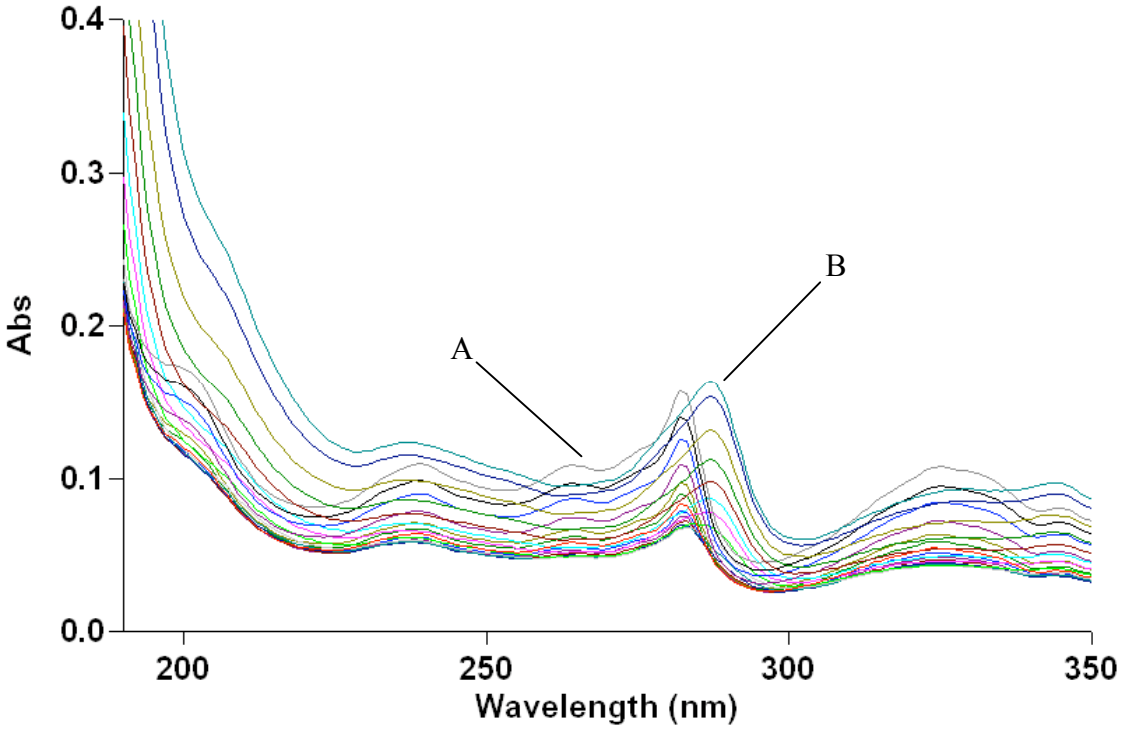

Figure 36. UV spectra of 4 x 10^{-6} M DPP and 4 x 10-^{6} M $Cd(ClO_4)_2$ in 0.10 M $NaClO_4$. Initial spectrum (A) of DPP-Cd complex at pH = 3.04. Final spectrum (B) of free ligand at pH = 0.38.

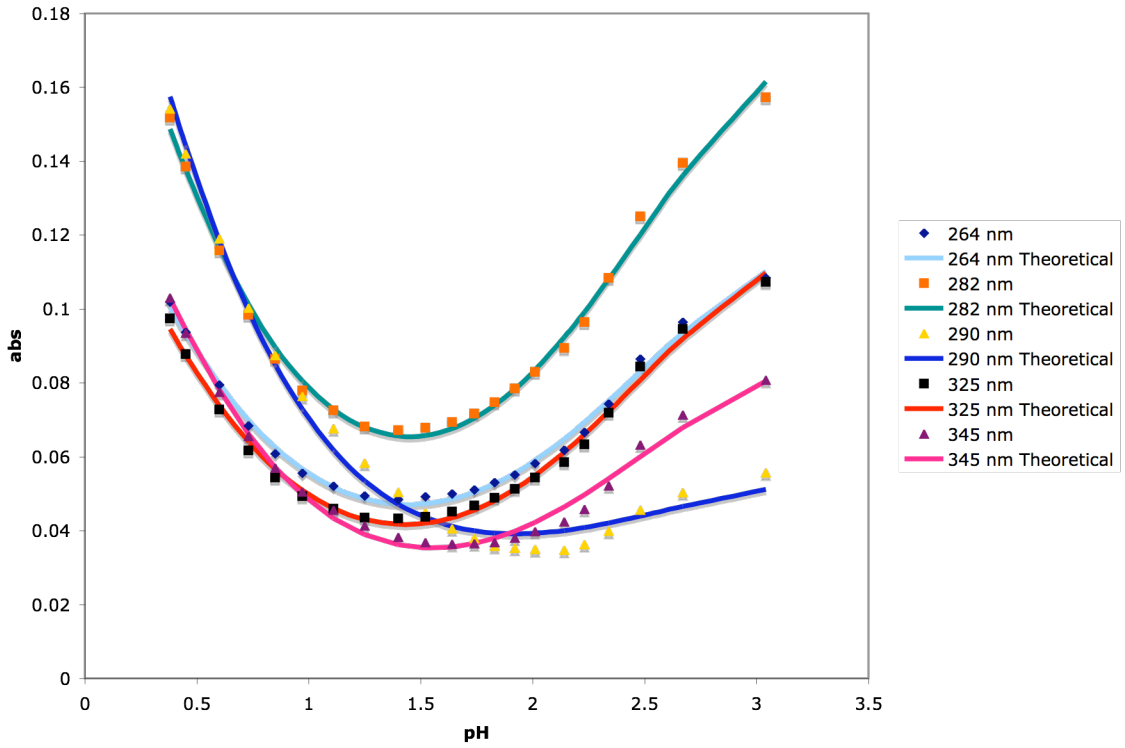

Figure 37. Plot of corrected absorbance (data points) and theoretical absorbance (lines) versus pH for titration of DPP and $Cd(ClO_4)_2$.

Table 23. Solutions and standard deviation for each parameter solved by the 'SOLVER' module of EXCEL in determining log K_1 of DPP-Cd complex. Note: Coefficient of determination and standard error calculated with 'Solver Statistics' macro.

	Parameter	Solution	Standard Deviation
Overall	pK_1	2.41891261	0.031480366
	pK_2	0.180341288	0.056779048
264 nm	Abs(0)	0.129467861	0.003050231
	Abs(1)	0.029230208	0.001660788
	Abs(2)	0.211778187	0.015199857
282 nm	Abs(0)	0.191040967	0.003846984
	Abs(1)	0.037964527	0.002071298
	Abs(2)	0.321714052	0.02279967
290 nm	Abs(0)	0.057337048	0.002380625
	Abs(1)	0.027033046	0.001630899
	Abs(2)	0.363253788	0.028142674
325 nm	Abs(0)	0.130463658	0.003153929
	Abs(1)	0.023238974	0.001692517
	Abs(2)	0.205765296	0.015144961
345 nm	Abs(0)	0.095382538	0.002727812
	Abs(1)	0.01840152	0.001608344
	Abs(2)	0.235508947	0.018100602

R^2: 0.993529278 **Standard Error:** 0.002566762

A third titration was conducted at a lower concentration of both ligand and metal ion. This was done to get more accurate results because at lower concentrations the protonation events would occur at higher pH. The log K_1 calculated from the titration at lower concentrations was also used to confirm the log K_1 from the previous titration. A solution of 8 x 10^{-7} M DPP and 8 x 10^{-7} M $Cd(ClO_4)_2$ was titrated with 11.6 M $HClO_4$ from pH = 5.14 to pH = 0.19. The UV/Vis spectra plotting absorbance versus wavelength are shown in Figure 38. Absorbances were recorded at 262, 277, 282, 325, and 345 nm because these wavelengths exhibited the largest change in absorbances. Theoretical and measured absorbances were plotted for every wavelength simultaneously by minimizing the sum of the squares of the residuals as previously discussed and shown in Figure 39. Table 24 outlines the solutions of each parameter that was varied by 'SOLVER' and the standard deviation of each variable calculated by Solver Statistics. The p*K*'s were recorded once all standard deviations were minimized and the R^2 value was close to one. Table 25 shows the equations of each protonation event observed for the DPP-Cd titration and the p*K*'s calculated with minimal error, which were a pK_1 and pK_2 of 3.61 and 0.64, respectively. These were used in Eq. (21) to calculate a log K_1 of 11.90. The two independent titrations were in good agreement and both had good fits with small standard deviations.

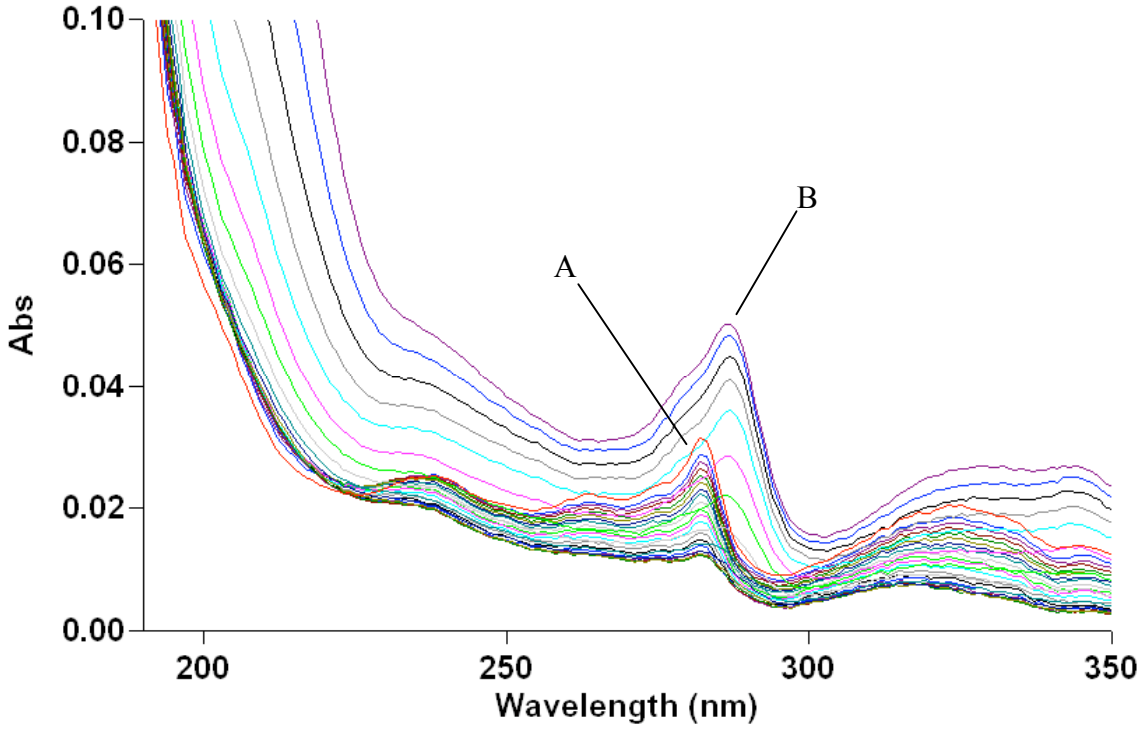

Figure 38. UV spectra of 8 x 10^{-7} M DPP and 8 x 10^{-7} M $Cd(ClO_4)_2$ in 0.10 M $NaClO_4$. Initial spectrum (A) of DPP-Cd complex at pH = 5.14. Final spectrum (B) of free ligand at pH = 0.19.

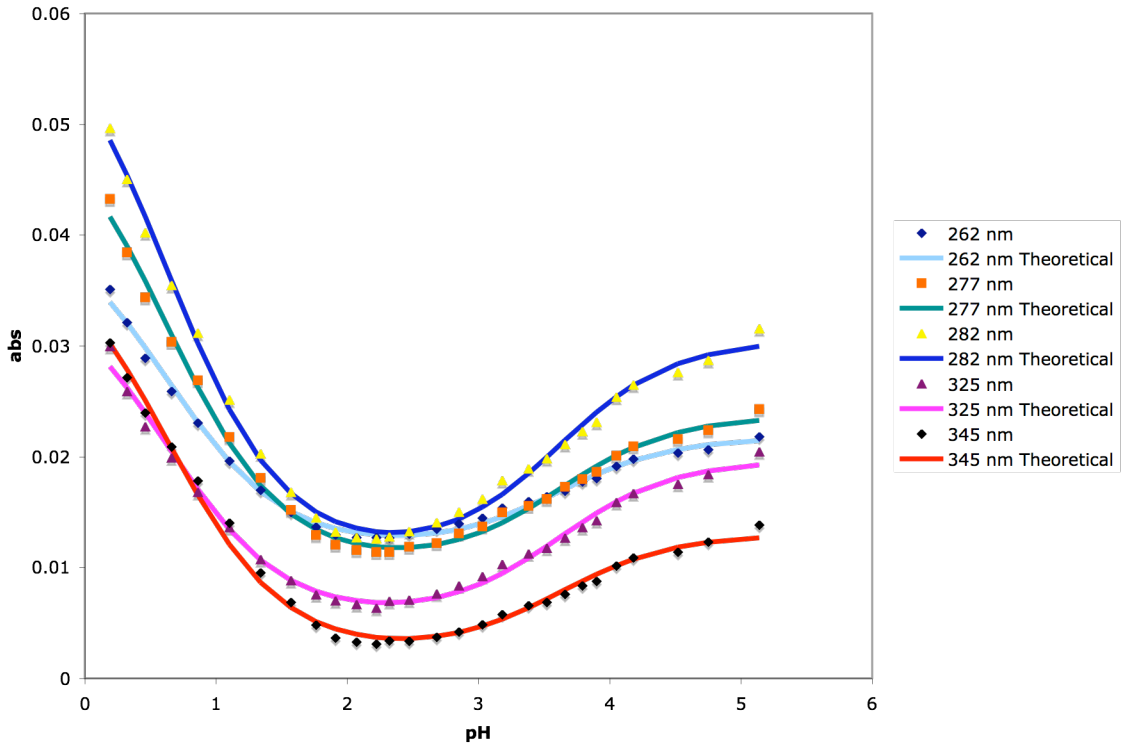

Figure 39. Plot of corrected absorbance (data points) and theoretical absorbance (lines) versus pH for titration of DPP and $Cd(ClO_4)_2$.

Table 24. Solutions and standard deviation for each parameter solved by the 'SOLVER' module of EXCEL in determining log K_1 of DPP-Cd complex. Note: Coefficient of determination and standard error calculated with 'Solver Statistics' macro.

	Parameter	Solution	Standard Deviation
Overall	pK_1	3.607201477	0.027401668
	pK_2	0.63867203	0.020725921
262 nm	Abs(0)	0.021740885	0.000327902
	Abs(1)	0.011839129	0.000235687
	Abs(2)	0.041821273	0.000737598
277 nm	Abs(0)	0.0236496	0.000342393
	Abs(1)	0.010320455	0.000248358
	Abs(2)	0.05280752	0.000895925
282 nm	Abs(0)	0.030503721	0.000375979
	Abs(1)	0.011263672	0.000266759
	Abs(2)	0.061846939	0.001005065
325 nm	Abs(0)	0.019672891	0.000347094
	Abs(1)	0.00555491	0.000243122
	Abs(2)	0.036180531	0.00074183
345 nm	Abs(0)	0.012985544	0.000330429
	Abs(1)	0.002370578	0.000240804
	Abs(2)	0.040157218	0.000835042

R^2: 0.994994465 **Standard Error:** 0.000673332

Table 25. Summary of equations at each protonation event of $[Cd(DPP)]^{2+}$; Equations written in terms of log K to complement initial equilibrium expressions.

							pK_{50}
$[Cd(DPP)(OH)_2]$	+	H^+	⇌	$[Cd(DPP)OH]^+$	+	H_2O	6.15
$[Cd(DPP)OH]^+$	+	H^+	⇌	$[Cd(DPP)]^{2+}$	+	H_2O	4.64
$[Cd(DPP)]^{2+}$	+	H^+	⇌	$[Cd(DPP)H]^{3+}$	+		2.43
$[Cd(DPP)H]^{3+}$	+	H^+	⇌	$H_2(DPP)^{2+}$	+	Cd^{2+}	0.12

The species distribution diagram was constructed by QBasic to confirm the UV/Vis spectra for the DPP-Cd complex. Figure 40 shows the species distribution diagram.

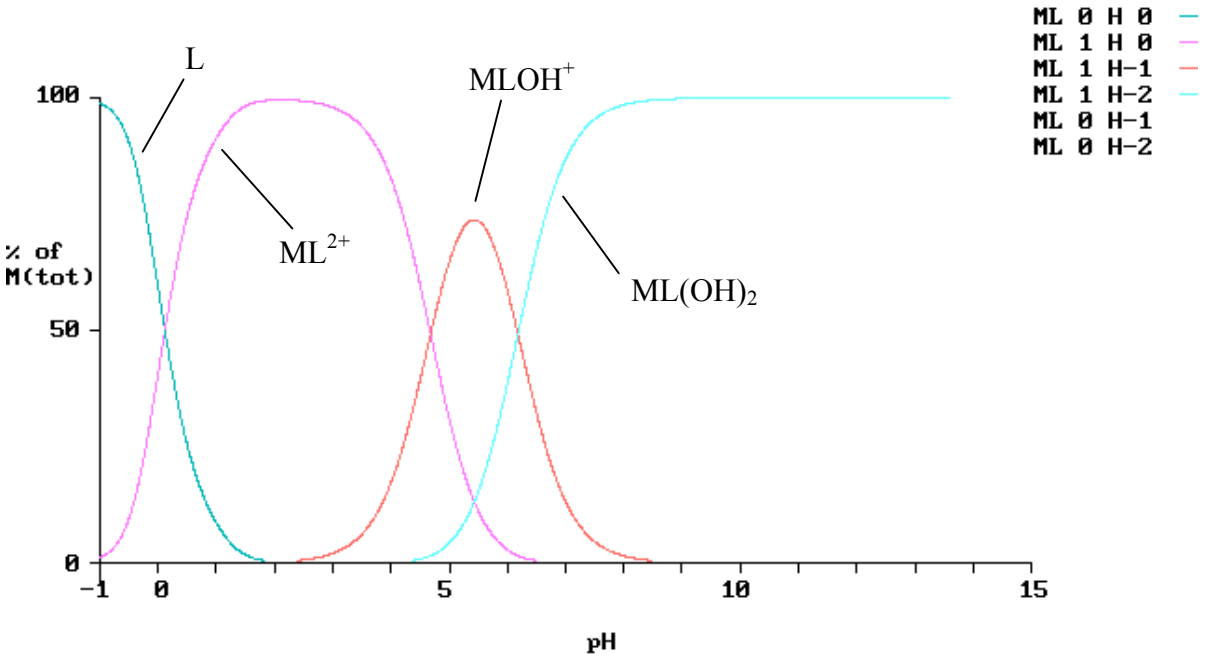

Figure 40. Species distribution diagram for the formation of $[Cd(DPP)]^{2+}$, $[Cd(DPP)OH]^{+}$, and $[Cd(DPP)(OH)_2]$. Concentration of DPP and Cd^{2+} were 4 x 10^{-6} M.

The diagram confirms that the complex is predominant at very low pH and the formation of the hydroxide complex at a pH of about 5.1.

Bismuth Results

Bismuth is an intermediate acid according to the HSAB principle and has a high affinity for nitrogen donors (Hancock, 1995). Bismuth shows great potential for cancer therapy. Bismuth has a very high affinity for hydroxides and the hydroxide complex is insoluble ($Ksp=10^{-40}$). This means that a different approach had to be taken to prevent precipitation of $Bi(OH)_3$. Through initial experiments following the procedures of previous metal ions reported, it was found that bismuth formed a more stable complex than cadmium. At low pH the DPP-Bi complex had formed and neither increasing nor decreasing the pH could drive the bismuth out. Increasing the pH led to precipitation as predicted. By keeping the pH constant and using 0.03333 M $Cd(ClO_4)_2$ as a titrant, it was possible to determine log K_1 of the DPP-Bi. A solution of 4 x 10^{-6} M DPP and 4 x 10^{-6} M $Bi(ClO_4)_3$ was titrated with 0.03333 M $Cd(ClO_4)_2$ at a pH around 3.00. The UV/Vis spectra are shown in Figure 41. The initial spectrum shows the bismuth complex and as $Cd(ClO_4)_2$ was titrated the peak shifts to a maximum of 282 nm, which was the peak maximum of the DPP-Cd complex. The spreadsheet used to calculate log K_1 is shown in Figure 26. Log K_1 was calculated for each data point and an average was taken. The average was added to the log K_1 calculated for cadmium and the result was the log K_1 for the DPP-Bi complex. The calculated log K_1 for DPP and bismuth was 15.72.

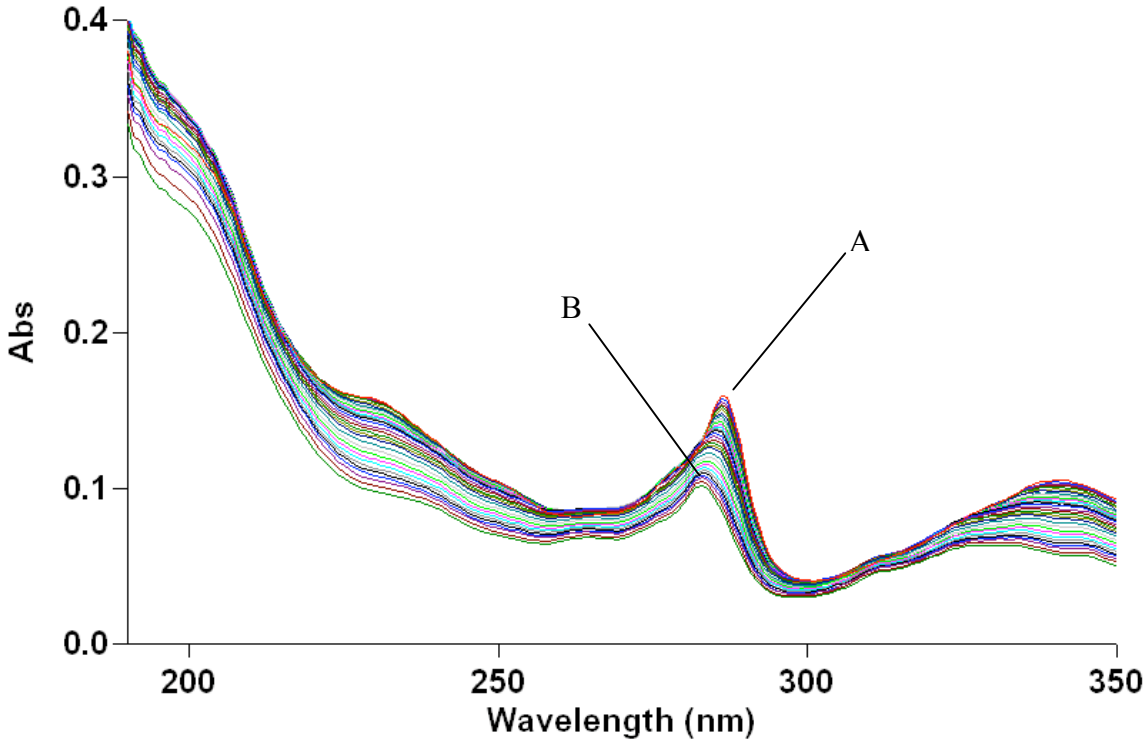

Figure 41. UV spectra of 4 x 10^{-6} M DPP and 4 x 10^{-6} M $Bi(ClO_4)_3$ in 0.10 M $NaClO_4$. Initial spectrum (A) of DPP-Bi complex. Final spectrum (B) of DPP-Cd complex.

Table 26. EXCEL spreadsheet in determining log K_1 for DPP-Bi complex

287 nm															
Amount Added	**Total**	**pH**	**[Cd]**	**Bi(total)**	**log[Cd]**	**Abs**	**abs(corr)**	**CdL/(L(total))**	**[CdL]**	**[Cd]**	**[BiL]**	**[Bi]**	**K**	**difference**	**log K**
0	0	2.86	0	0.000004		0.1581158	0.1581158	0	0	0	0.000004	0			
0.01	0.01	2.87	6.66467E-06	3.9992E-06	-5.176221541	0.1551309	0.155161926	0.090446204	3.61712E-07	6.30295E-06	3.63749E-06	3.61712E-07	0.00570665	2.92556E-05	-2.243618741
0.025	0.035	2.87	2.33147E-05	3.9972E-06	-4.632370546	0.1529037	0.153010733	0.154659946	6.18207E-07	2.26965E-05	3.37899E-06	6.18207E-07	0.004983357	2.19544E-05	-2.302478012
0.05	0.085	2.87	5.65648E-05	3.99321E-06	-4.247453439	0.15114	0.151396938	0.199948236	7.98436E-07	5.57664E-05	3.19478E-06	7.98436E-07	0.003578218	1.07611E-05	-2.446333257
0.1	0.185	2.87	0.000122866	3.98525E-06	-3.910566886	0.148868	0.149418812	0.252017242	1.00435E-06	0.000121862	2.9809E-06	1.00435E-06	0.002776876	6.14578E-06	-2.556443459
0.2	0.385	2.87	0.00025468	3.96944E-06	-3.59400522	0.1466341	0.147763183	0.285149708	1.13188E-06	0.000253548	2.83755E-06	1.13188E-06	0.001780734	2.19907E-06	-2.749400833
0.2	0.585	2.87	0.000385451	3.95374E-06	-3.414030575	0.1441867	0.145873684	0.326013699	1.28897E-06	0.000384162	2.66477E-06	1.28897E-06	0.001622984	1.75609E-06	-2.789685811
0.2	0.785	2.87	0.000515192	3.93817E-06	-3.288030486	0.1416344	0.14385806	0.37130965	1.46228E-06	0.00051373	2.47589E-06	1.46228E-06	0.001681106	1.91352E-06	-2.774404878
0.2	0.985	2.87	0.000643916	3.92272E-06	-3.191170879	0.139766	0.14251939	0.39574381	1.55239E-06	0.000642363	2.37033E-06	1.55239E-06	0.001582756	1.65109E-06	-2.800586107
0.3	1.285	2.87	0.000835118	3.89978E-06	-3.078251919	0.1373884	0.140919282	0.420069829	1.63818E-06	0.00083348	2.2616E-06	1.63818E-06	0.001423677	1.26758E-06	-2.846588416
0.3	1.585	2.88	0.001024097	3.8771E-06	-2.989658855	0.134996	0.139275373	0.446388376	1.73069E-06	0.001022366	2.14641E-06	1.73069E-06	0.001364962	1.13882E-06	-2.864879467
0.3	1.885	2.88	0.00121089	3.85468E-06	-2.916895153	0.1329721	0.137985148	0.461960148	1.78071E-06	0.00120911	2.07397E-06	1.78071E-06	0.001264495	9.34485E-07	-2.89808296
0.3	2.185	2.88	0.001395536	3.83252E-06	-2.855258933	0.1312915	0.137028939	0.467223366	1.79064E-06	0.001393745	2.04188E-06	1.79064E-06	0.001126691	6.87048E-07	-2.948195212
0.3	2.485	2.88	0.001578071	3.81061E-06	-2.801873495	0.1295921	0.136032827	0.474137763	1.80676E-06	0.001576264	2.00386E-06	1.80676E-06	0.001033482	5.41217E-07	-2.985697089
0.5	2.985	2.88	0.001877702	3.77465E-06	-2.72637329	0.127691	0.135314153	0.455609714	1.71977E-06	0.001875982	2.05488E-06	1.71977E-06	0.000767227	2.20355E-07	-3.115076123
1	3.985	2.89	0.002460314	3.70473E-06	-2.609009466	0.1244892	0.134410989	0.402040331	1.48945E-06	0.002458825	2.21528E-06	1.48945E-06	0.000407283	1.19851E-08	-3.390103296
1	4.985	2.9	0.003021734	3.63736E-06	-2.519743753	0.1221459	0.134323846	0.321819862	1.17057E-06	0.003020564	2.46678E-06	1.17057E-06	0.000183899	1.29752E-08	-3.735421586
1	5.985	2.91	0.003563098	3.57239E-06	-2.448172214	0.119291	0.133570133	0.26480305	9.45979E-07	0.003562152	2.62641E-06	9.45979E-07	9.56507E-05	4.08672E-08	-4.019311884
1	6.985	2.91	0.004085462	3.5097E-06	-2.388758828	0.1173508	0.133744707	0.175980719	6.17639E-07	0.004084844	2.89206E-06	6.17639E-07	3.22914E-05	7.04986E-08	-4.490913268
1	7.985	2.91	0.004589809	3.44917E-06	-2.338205427	0.1152411	0.133645104	0.096781552	3.33816E-07	0.004589475	3.11535E-06	3.33816E-07	7.7937E-06	8.41078E-08	-5.108256287
2	9.985	2.93	0.005548055	3.33417E-06	-2.25585928	0.1108395	0.132974148	-0.043733577	-1.45815E-07	0.0055482	3.47998E-06	-1.45815E-07	1.10122E-06	8.80344E-08	-5.958124451
2	11.985	2.95	0.006444463	3.22659E-06	-2.190813254	0.1071227	0.132800011	-0.201646683	-6.50631E-07	0.006445114	3.87722E-06	-6.50631E-07	1.69402E-05	7.88862E-08	-4.771081828
2	13.985	2.96	0.007284833	3.12573E-06	-2.13758039	0.1033415	0.132246118	-0.344090402	-1.07553E-06	0.007285909	4.20127E-06	-1.07553E-06	3.77907E-05	6.76086E-08	-4.422615265
2	15.985	2.97	0.00807426	3.03099E-06	-2.092897267	0.1001011	0.132103422	-0.501955253	-1.52142E-06	0.008075781	4.55241E-06	-1.52142E-06	6.29612E-05	5.51526E-08	-4.200926771
2	17.985	2.98	0.00881724	2.94183E-06	-2.054667346	0.09663784	0.131398471	-0.635809761	-1.87044E-06	0.00881911	4.81227E-06	-1.87044E-06	8.24354E-05	4.6385E-08	-4.083886292
2	19.985	3	0.009517755	2.85776E-06	-2.021465501	0.0936506	0.131082745	-0.784777661	-2.2427E-06	0.009519997	5.10046E-06	-2.2427E-06	0.000103585	3.77222E-08	-3.98470265
2	21.985	3.01	0.010179344	2.77836E-06	-1.992280225	0.09061942	0.130464779	-0.919498892	-2.5547E-06	0.010181898	5.33305E-06	-2.5547E-06	0.000120192	3.15473E-08	-3.920126214
2	23.985	3.02	0.010805164	2.70325E-06	-1.966368642	0.08763756	0.129677298	-1.044928399	-2.8247E-06	0.010807989	5.52795E-06	-2.8247E-06	0.000133548	2.69812E-08	-3.874363601
2	25.985	3.03	0.01139804	2.6321E-06	-1.943169833	0.08452009	0.128445181	-1.147498785	-3.02033E-06	0.01140106	5.65243E-06	-3.02033E-06	0.000141556	2.44144E-08	-3.849071565
3	28.985	3.04	0.012231057	2.53213E-06	-1.912536004	0.08082278	0.127675746	-1.348367525	-3.41424E-06	0.012234471	5.94636E-06	-3.41424E-06	0.000160233	1.89268E-08	-3.795249335
3	31.985	3.06	0.013003111	2.43947E-06	-1.885952732	0.07746116	0.127013064	-1.551795751	-3.78556E-06	0.013006896	6.22503E-06	-3.78556E-06	0.000176989	1.45971E-08	-3.752054883
												average:	0.000297807	1.5469E-07	
														average:	-3.522589318
		Abs BiL	**Abs(0)**			0.1581158								**stdev:**	0.891769946
		Abs CdL	**Abs(1)**			0.1258									
														log K1 =	15.72258932

Lutetium Results

Lutetium has an ionic radius of 0.98 Å and is the ideal size to bind the four donor atoms of DPP. A solution of 4 x 10^{-6} M DPP and 4 x 10^{-4} M $Lu(ClO_4)_3$ was titrated with 0.1 M NaOH from pH = 1.94 to pH = 6.90. The UV/Vis spectra plotting absorbance versus wavelength is shown in Figure 42. The UV/Vis spectra show a sharpening of peaks indicating the formation of a rigid complex. Absorbances were recorded at 273, 282, 293, 300, and 344 nm because these wavelengths exhibited the largest change in absorbances. Theoretical and measured absorbances were plotted for every wavelength simultaneously by minimizing the sum of the squares of the residuals as previously discussed and shown in Figure 43. Table 27 outlines the solutions of each parameter that was varied by 'SOLVER' and the standard deviation of each variable calculated by Solver Statistics. The p*K*'s were recorded once all standard deviations were minimized and the R^2 value was close to one. Table 28 shows the equations of each protonation event observed for the DPP-Lu titration and the p*K*'s calculated with minimal error, which were a pK_1 and pK_2 of 2.58 and 2.58, respectively. These were used in Eq. (21) to calculate a log K_1 of 7.86. The complex forms at a low pH according to the UV/Vis spectra with the formation of sharp peaks. A p*K* corresponding to the formation of a hydroxide complex was calculated to be 5.58. This is also apparent in the UV/Vis spectra where the absorbance remains constant but begins to drop and loose the sharpness of its peaks. This is the same deprotonation of a water molecule as seen in the $[Gd(DPP)]^{3+}$ complex and occurs at about the same pH.

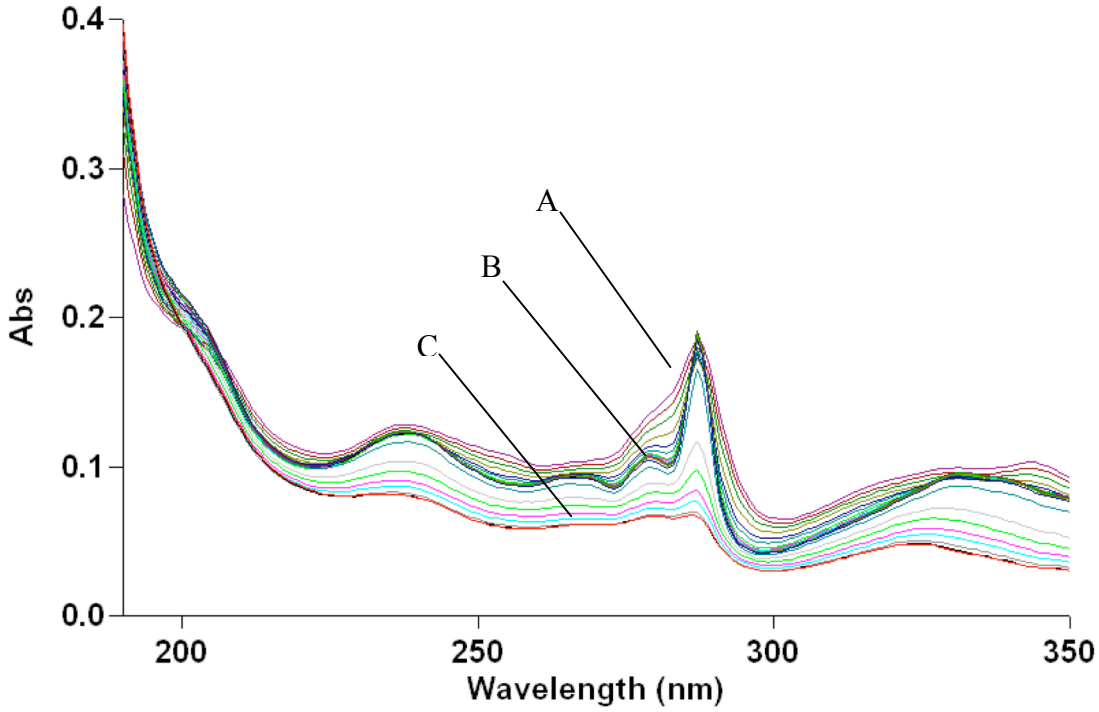

Figure 42. UV spectra of 4 x 10^{-6} M DPP and 4 x 10^{-4} M $Lu(ClO_4)_3$ in 0.01 M $HClO_4$ and 0.09 M $NaClO_4$. Initial spectrum (A) of free DPP at pH = 1.94. Spectrum (B) of DPP-Lu complex. Final spectrum (C) of DPP- Lu hydroxide complex at pH = 6.90.

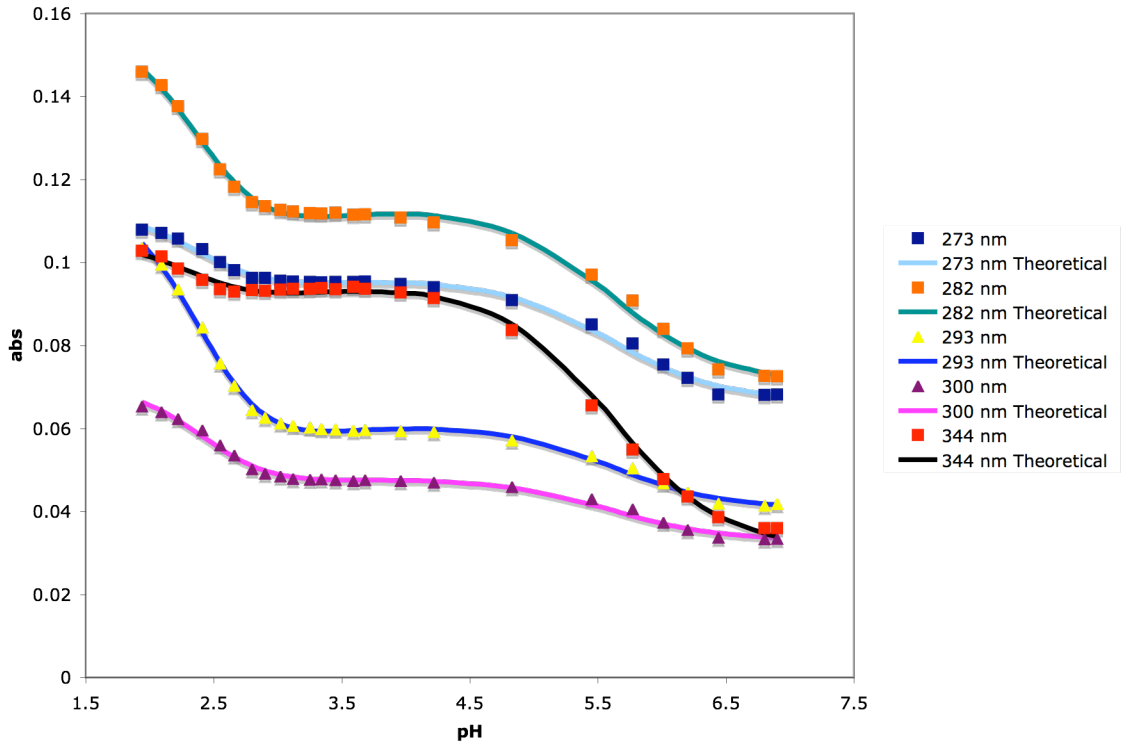

Figure 43. Plot of corrected absorbance (data points) and theoretical absorbance (lines) versus pH for titration of DPP and $Lu(ClO_4)_3$.

Table 27. Solutions and standard deviation for each parameter solved by the 'SOLVER' module of EXCEL in determining log K_1 of DPP-Lu complex. Note: Coefficient of determination and standard error calculated with 'Solver Statistics' macro.

	Parameter	Solution	Standard Deviation
Overall	pK_1	5.584533446	0.019510646
	pK_2	2.585760745	0.028927482
	pK_3	2.585760745	0.028927482
273 nm	Abs(0)	0.066722132	0.000529741
	Abs(1)	0.096042166	0.000497968
	Abs(2)	0.08837219	0.002397036
	Abs(3)	0.114086045	0.001236207
282 nm	Abs(0)	0.071088197	0.000564108
	Abs(1)	0.113433504	0.00056368
	Abs(2)	0.091157717	0.003034197
	Abs(3)	0.161113784	0.001511685
293 nm	Abs(0)	0.040739591	0.000512967
	Abs(1)	0.061138508	0.000565453
	Abs(2)	0.039455667	0.00348442
	Abs(3)	0.121813624	0.001586264
300 nm	Abs(0)	0.032996265	0.000503688
	Abs(1)	0.047973178	0.000492901
	Abs(2)	0.042862735	0.002548116
	Abs(3)	0.072750835	0.001237364
344 nm	Abs(0)	0.031248466	0.000646548
	Abs(1)	0.094631135	0.000531173
	Abs(2)	0.08299042	0.002357763
	Abs(3)	0.106665222	0.001250832

R^2: 0.998899177 **Standard Error:** 0.000986911

Table 28. Summary of equations at each protonation event of $[Lu(DPP)]^{3+}$; Equations written in terms of log K to complement initial equilibrium expressions.

							pK_{50}
$[Lu(DPP)OH]^{2+}$	+	H^+	$\rightleftharpoons$	$[Lu(DPP)]^{3+}$	+	H_2O	5.59
$[Lu(DPP)]^{3+}$	+	$2H^+$	$\rightleftharpoons$	$H_2(DPP)^{2+}$	+	Lu^{3+}	2.59

Calcium Results

Calcium has an ionic radius of 1.00 Å and is classified as a hard acid by Pearson's HSAB principle (Table 2). The nitrogen donors on DPP are borderline bases which means calcium would bind better to a hard base. As seen in Figure 7, calcium has a very low affinity for nitrogen donors. The log K_1 of $[Ca(DPP)]^{2+}$ was expected to be low. TERPY was used as a reference, which has a log K_1 with calcium of 0.1 (NIST). A solution of 4 x 10^{-6} M DPP and 0.0333 M $Ca(ClO_4)_2$ was titrated with 0.1 M NaOH from pH = 1.96 to pH = 6.15. The UV/Vis spectra plotting absorbance versus wavelength are shown in Figure 44. Absorbances were recorded at 260, 279, 283, 287, and 340 nm because these wavelengths exhibited the largest change in absorbances. Theoretical and measured absorbances were plotted for every wavelength simultaneously by minimizing the sum of the squares of the residuals as previously discussed and shown in Figure 45. Table 29 outlines the solutions of each parameter that was varied by 'SOLVER' and the standard deviation of each variable calculated by Solver Statistics. The pK's were recorded once all standard deviations were minimized and the R^2 value was close to one. Table 30 shows the equations of each protonation event observed for the DPP-Ca titration and the pK's calculated with minimal error, which were a pK_1 and pK_2 of 3.88 and 1.66, respectively. These were used in Eq. (21) to calculate a log K_1 of 2.69. The significant increase in log K_1 that DPP has over TERPY can be explained by preorganization. Despite its very low affinity for nitrogen donors, the ionic radius of 1.00 Å is an optimal size to span the cavity and bind to all four donor atoms of DPP. A Hyperchem model of the $[Ca(DPP)]^{2+}$ complex is shown in Figure 46 and illustrates how calcium binds to DPP.

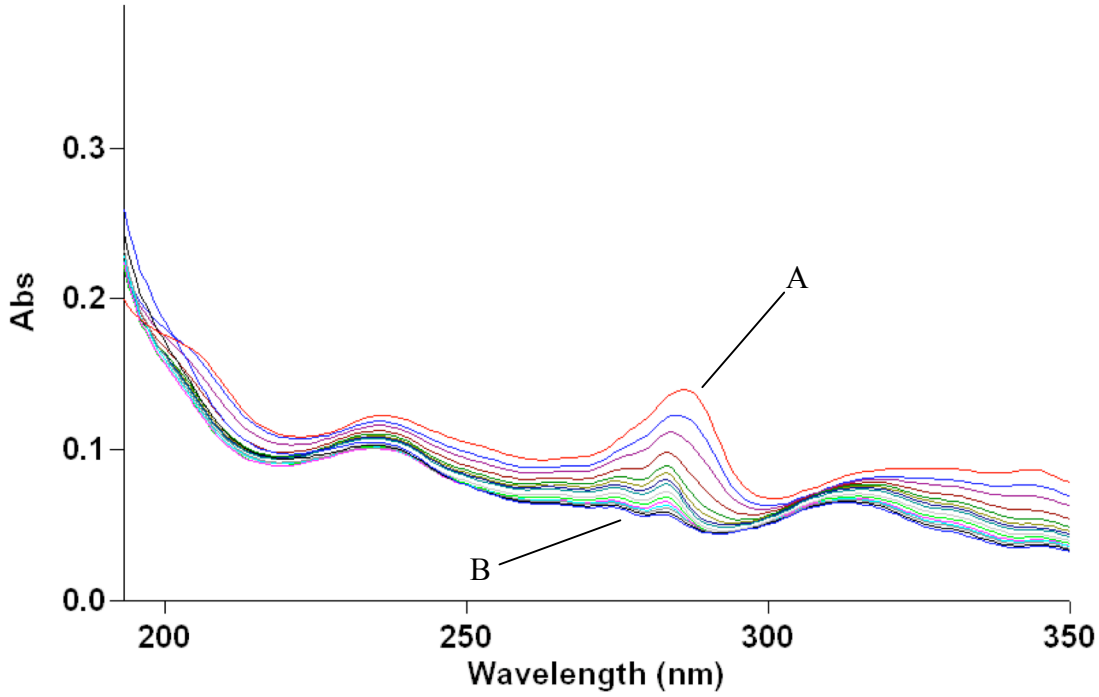

Figure 44. UV spectra of 4 x 10^{-6} M DPP and 0.03333 M $Ca(ClO_4)_2$ in 0.01 M $HClO_4$ and 0.09 M $NaClO_4$. Initial spectrum (A) of free DPP at pH = 1.96. Final spectrum (B) of DPP- Ca complex at pH = 6.15.

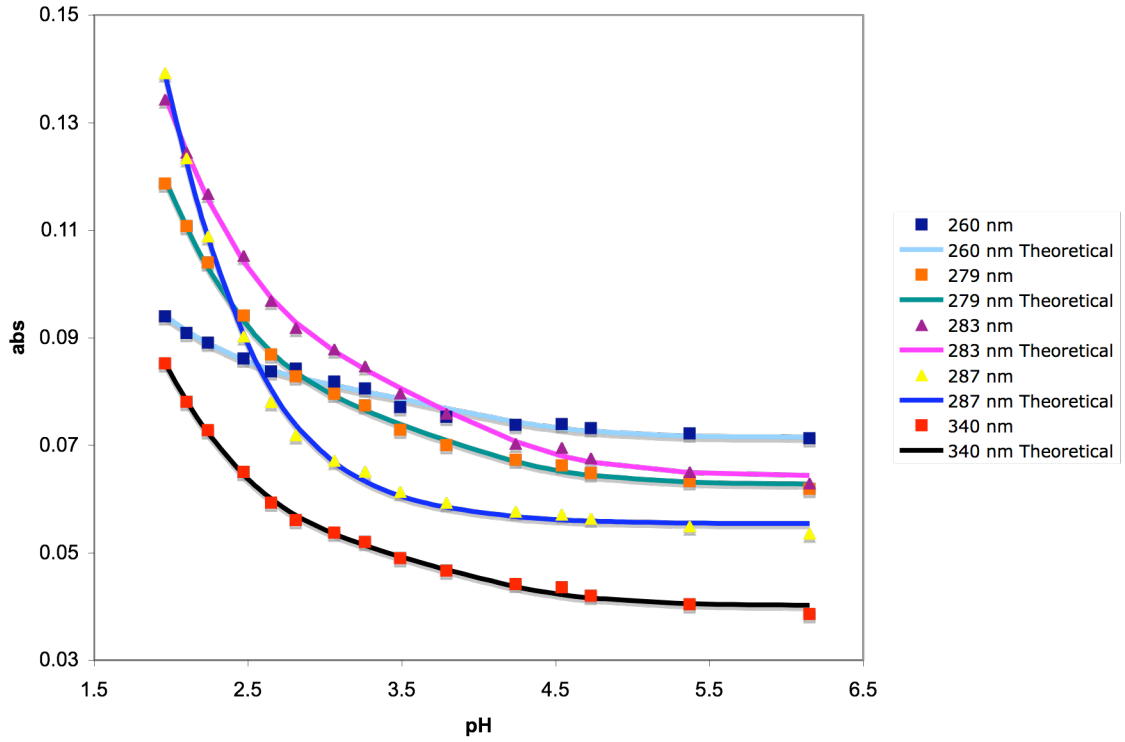

Figure 45. Plot of corrected absorbance (data points) and theoretical absorbance (lines) versus pH for titration of DPP and $Ca(ClO_4)_2$.

Table 29. Solutions and standard deviation for each parameter solved by the 'SOLVER' module of EXCEL in determining log K_1 of DPP-Ca complex. Note: Coefficient of determination and standard error calculated with 'Solver Statistics' macro.

	Parameter	Solution	Standard Deviation
Overall	pK_1	3.877171918	0.075126548
	pK_2	1.657485659	0.056766848
260 nm	Abs(0)	0.071422853	0.000535876
	Abs(1)	0.081046813	0.000707379
	Abs(2)	0.120665789	0.004302668
279 nm	Abs(0)	0.062679369	0.000551771
	Abs(1)	0.076680543	0.000931799
	Abs(2)	0.206979997	0.011437881
283 nm	Abs(0)	0.06422204	0.000598218
	Abs(1)	0.085128846	0.001132292
	Abs(2)	0.237020925	0.013082826
287 nm	Abs(0)	0.055395999	0.000524655
	Abs(1)	0.059336943	0.000950496
	Abs(2)	0.301271798	0.021534887
340 nm	Abs(0)	0.040140244	0.000540221
	Abs(1)	0.051601395	0.000830448
	Abs(2)	0.154051801	0.009150692

R^2: 0.998393848 **Standard Error:** 0.000990121

Table 30. Summary of equations at each protonation event of $[Ca(DPP)]^{2+}$; Equations written in terms of log K to complement initial equilibrium expressions.

							pK_{50}
$[Ca(DPP)]^{2+}$	+	H^+	$\rightleftharpoons$	$H(DPP)^+$	+	Ca^{2+}	3.88
$H(DPP)^+$	+	H^+	$\rightleftharpoons$	$H_2(DPP)^{2+}$			1.66

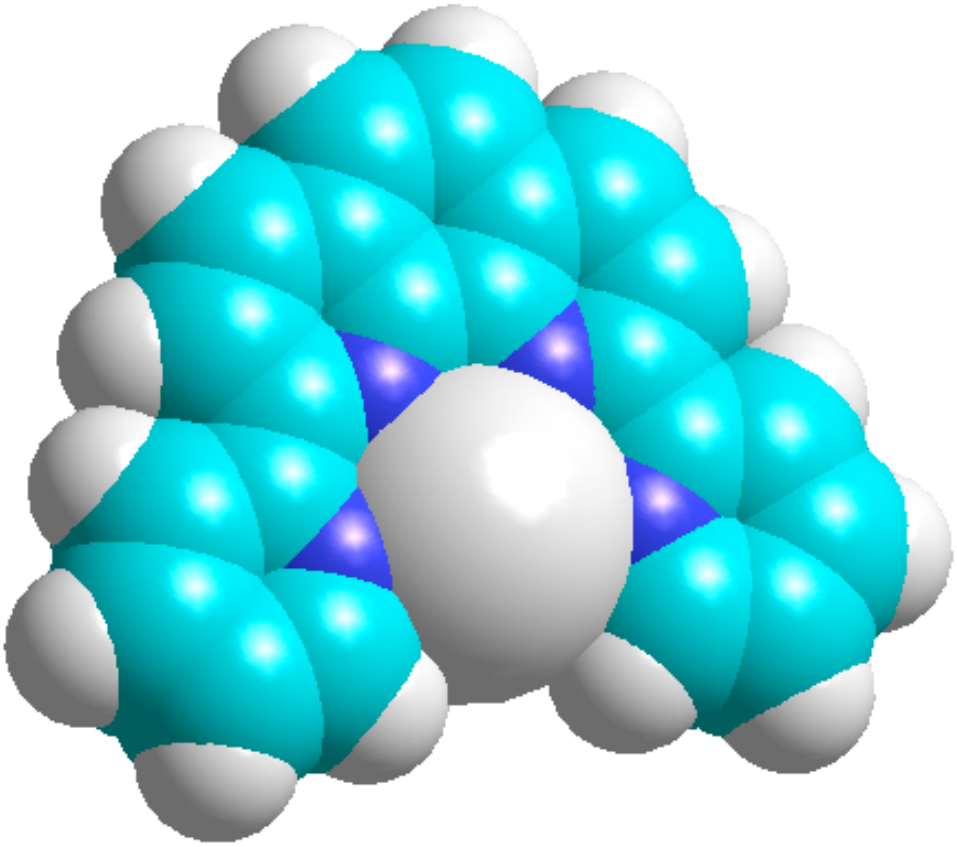

Figure 46. Hyperchem model of $[Ca(DPP)]^{2+}$ complex. Geometry was optimized by PM3.

Lanthanum Results

Lanthanum has an ionic radius of 1.05 Å and is classified as a hard acid by HSAB principle. A solution of 4 x 10^{-6} M DPP and 0.01666 M $La(ClO_4)_3$ was titrated with 0.1 M NaOH from pH = 1.94 to pH = 6.01. The UV/Vis spectra plotting absorbance versus wavelength are shown in Figure 47. Absorbances were recorded at 281, 287, 293, 335, and 345 nm because these wavelengths exhibited the largest change in absorbances. Theoretical and measured absorbances were plotted for every wavelength simultaneously by minimizing the sum of the squares of the residuals as previously discussed and shown in Figure 48. Table 31 outlines the solutions of each parameter that was varied by 'SOLVER' and the standard deviation of each variable calculated by Solver Statistics. The p*K*'s were recorded once all standard deviations were minimized and the R^2 value was close to one. Table 32 shows the equations of each protonation event observed for the DPP-La titration and the p*K*'s calculated with minimal error, which were a pK_1 and pK_2 of 2.24 and 2.24, respectively. These were used in Eq. (21) to calculate a log K_1 of 4.05. Lanthanum was the only lanthanide studied that did not exhibit any characteristics of hydroxide complex formation in the spectra. The metal ions that formed hydroxide complexes are very acidic and make waters attached more acidic as well. The log K_1 of lanthanum with TERPY is 1.8. The Δlog K_1 of +2.25 is due to preorganization. TERPY has to overcome more energy to bind lanthanum than DPP because it has to fold whereas DPP is already in the correct conformation.

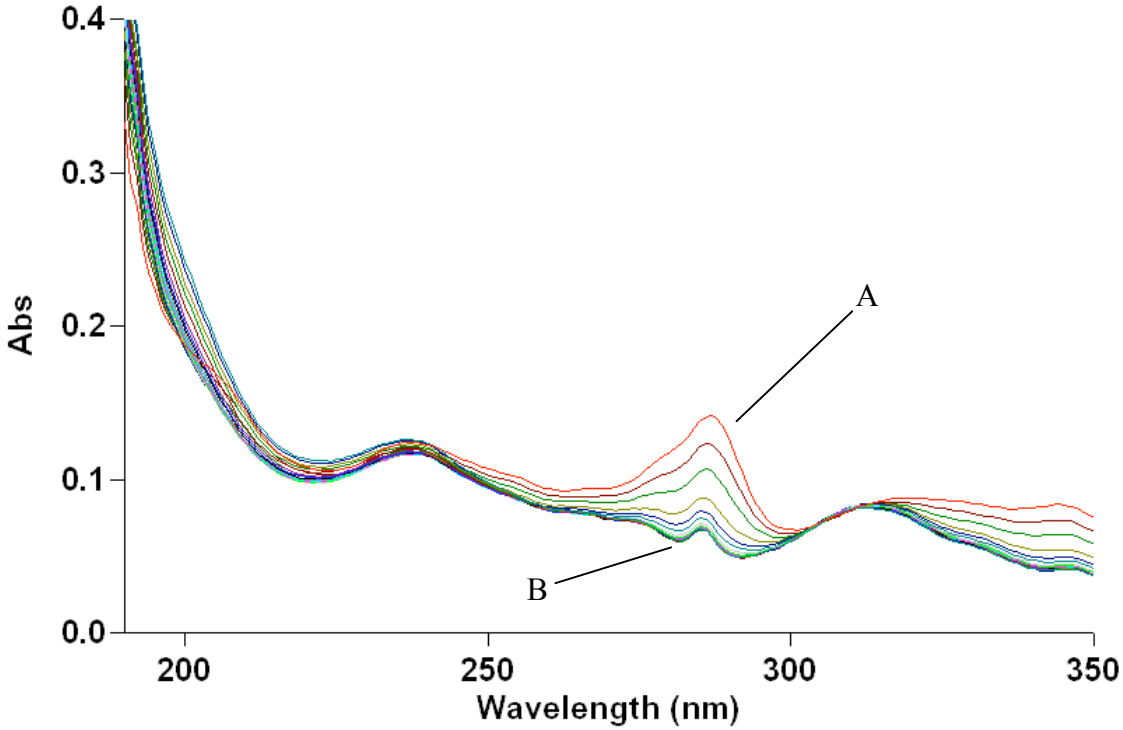

Figure 47. UV spectra of 4 x 10^{-6} M DPP and 4 x 10^{-5} M $La(ClO_4)_3$ in 0.01 M $HClO_4$ and 0.09 M $NaClO_4$. Initial spectrum (A) of free DPP at pH = 1.93. Final spectrum (B) of DPP- La complex at pH = 7.04.

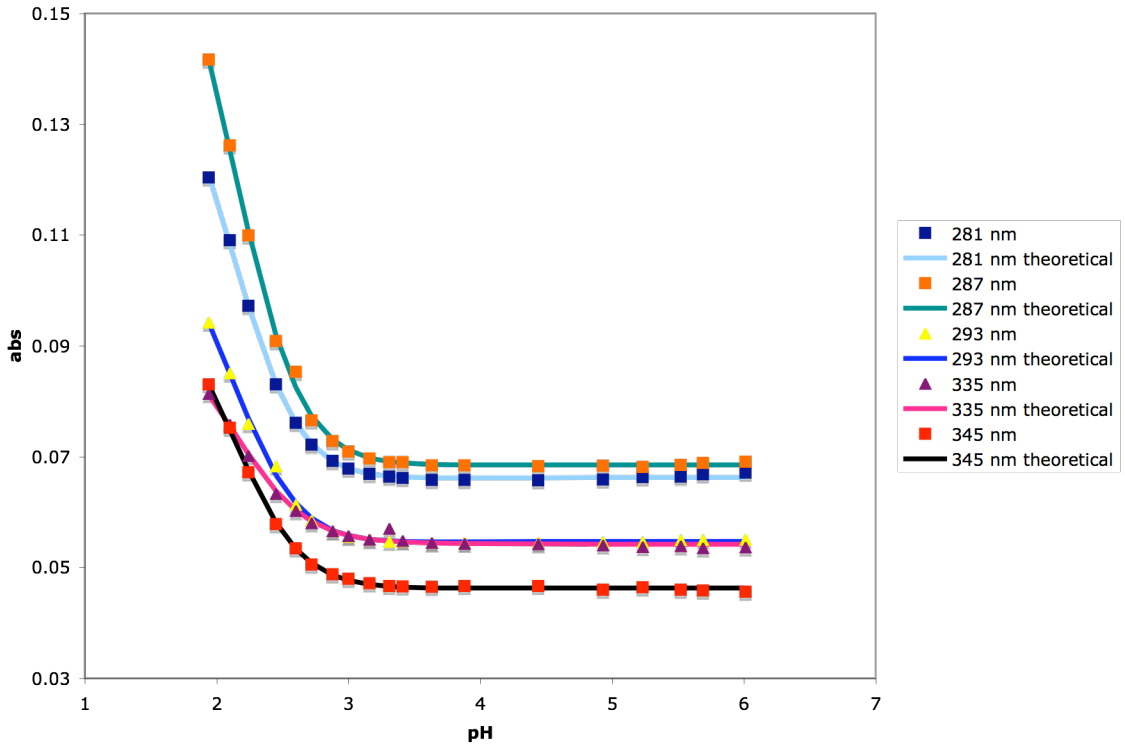

Figure 48. Plot of corrected absorbance (data points) and theoretical absorbance (lines) versus pH for titration of DPP and $La(ClO_4)_3$.

Table 31. Solutions and standard deviation for each parameter solved by the 'SOLVER' module of EXCEL in determining log K_1 of DPP-La complex. Note: Coefficient of determination and standard error calculated with 'Solver Statistics' macro.

	Parameter	Solution	Standard Deviation
Overall	pK_1	2.240587904	0.014544585
	pK_2	2.240587904	0.014544585
281 nm	Abs(0)	0.066257547	0.000202675
	Abs(1)	0.059954369	0.002248939
	Abs(2)	0.165286056	0.002007693
287 nm	Abs(0)	0.068526668	0.000206137
	Abs(1)	0.064107256	0.00267397
	Abs(2)	0.199177055	0.002291269
293 nm	Abs(0)	0.054730721	0.000200278
	Abs(1)	0.049149895	0.00198099
	Abs(2)	0.126684014	0.001760094
335 nm	Abs(0)	0.054206642	0.000198427
	Abs(1)	0.05705503	0.001866936
	Abs(2)	0.1000382	0.001499381
345 nm	Abs(0)	0.04627848	0.000199653
	Abs(1)	0.044476103	0.001972217
	Abs(2)	0.111640275	0.001662665

R^2: 0.999083686 **Standard Error:** 0.000584943

Table 32. Summary of equations at each protonation event of $[La(DPP)]^{3+}$; Equations written in terms of log K to complement initial equilibrium expressions.

							pK_{50}
$[La(DPP)]^{3+}$	+	$2H^+$	$\rightleftharpoons$	$H_2(DPP)^{2+}$	+	La^{3+}	2.24

To confirm the results from the UV/Vis spectra, the p*K* values calculated were input into QBasic along with stability constants of lanthanum with hydroxides and the solubility constants (Martel, 2003). The species distribution diagram is shown in Figure 49.

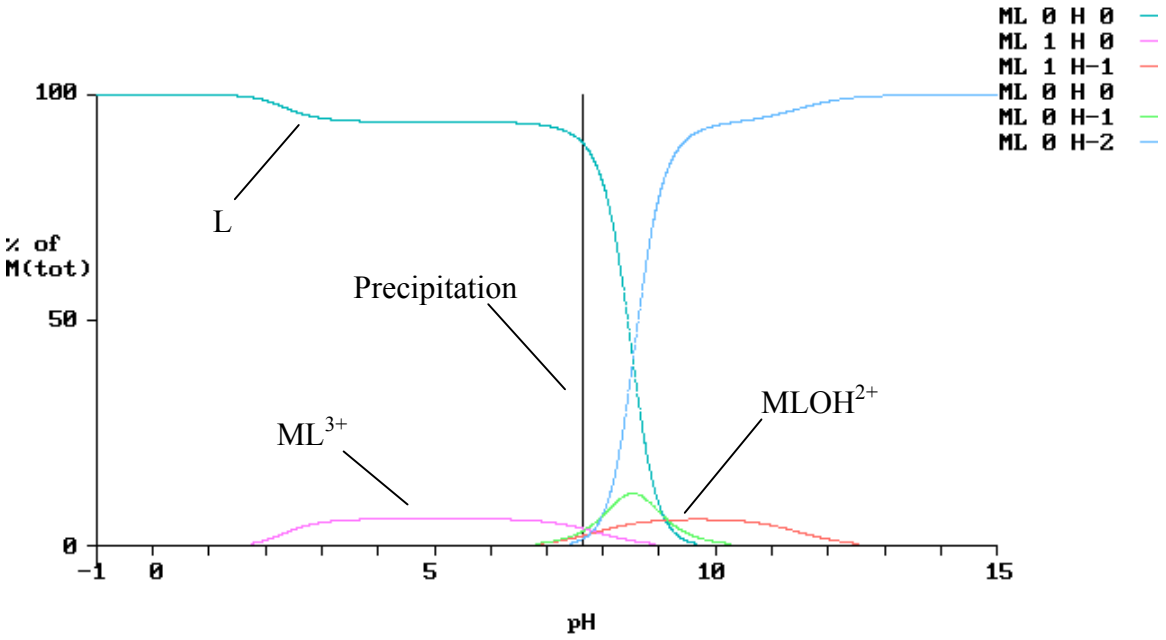

Figure 49. Species distribution diagram for the formation of $[La(DPP)]^{3+}$ and $[La(DPP)OH]^{2+}$. Black line represents formation of precipitate.

The species distribution diagram shows why the hydroxide complex was never seen in the UV/Vis spectra. Upon formation of the hydroxide complex, the compound becomes insoluble as indicated by the vertical black line.

Lead Results

Lead has an ionic radius of 1.19 and is the largest metal ion studied. Lead is an intermediate acid according to HSAB principle and is expected to bind well with nitrogen donor groups. A solution of 4 x 10^{-6} M DPP and 4 x 10^{-6} M $Pb(ClO_4)_2$ was titrated with 0.1 M NaOH from pH = 1.91 to pH = 7.06. The UV/Vis spectra plotting absorbance versus wavelength is shown in Figure 50. Absorbances were recorded at 250, 279, 287, 295, and 343 nm because these wavelengths exhibited the largest change in absorbances. Theoretical and measured absorbances were plotted for every wavelength simultaneously by minimizing the sum of the squares of the residuals as previously discussed and shown in Figure 51. Table 33 outlines the solutions of each parameter that was varied by 'SOLVER' and the standard deviation of each variable calculated by Solver Statistics. The p*K*'s were recorded once all standard deviations were minimized and the R^2 value was close to one. Table 34 shows the equations of each protonation event observed for the DPP-Pb titration and the p*K*'s calculated with minimal error, which were a pK_1 and pK_2 of 3.51 and 1.58, respectively. These were used in Eq. (21) to calculate a log K_1 of 7.36. Lead also has a protonation event corresponding to the formation of the hydroxide complex at 5.73. Although DPP is selective for large metal ions by the chelate ring size rule, lead is too large to strongly bind. Lead causes steric hindrance between hydrogens on the 3 and 3' positions of DPP. This is illustrated in Figure 52, which was energy minimized by Hyperchem PM3 calculations. For larger metals like lead, variations of DPP can be synthesized to correct for steric effects and thus increasing the log K_1 of the lead complex. An example of a ligand that should be more selective for lead is shown in Figure 53. This ligand called DPA (dipyridoacridine) can form more stable complexes

with larger metal ions because there is an increased cavity size and steric hindrance between hydrogens is minimized.

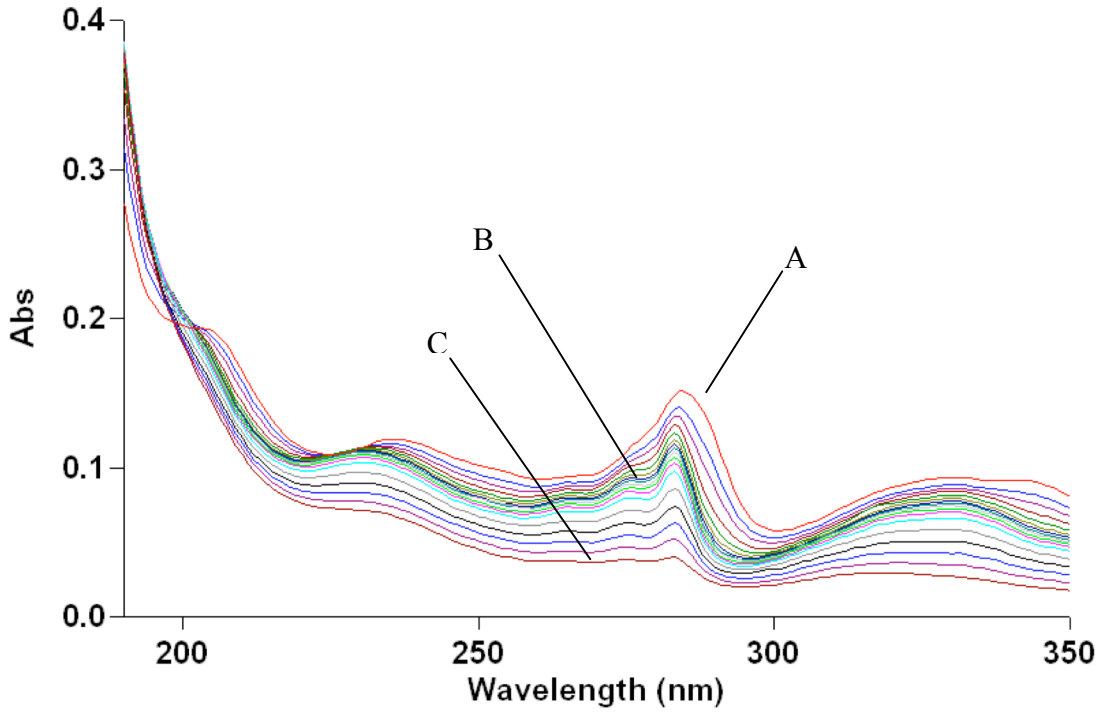

Figure 50. UV spectra of 4 x 10^{-6} M DPP and 4 x 10^{-6} M $Pb(ClO_4)_2$ in 0.01 M $HClO_4$ and 0.09 M $NaClO_4$. Initial spectrum (A) of free DPP at pH = 1.91. Spectrum (B) of DPP-Pb complex. Final spectrum (C) of DPP- Pb hydroxide complex at pH = 7.06.

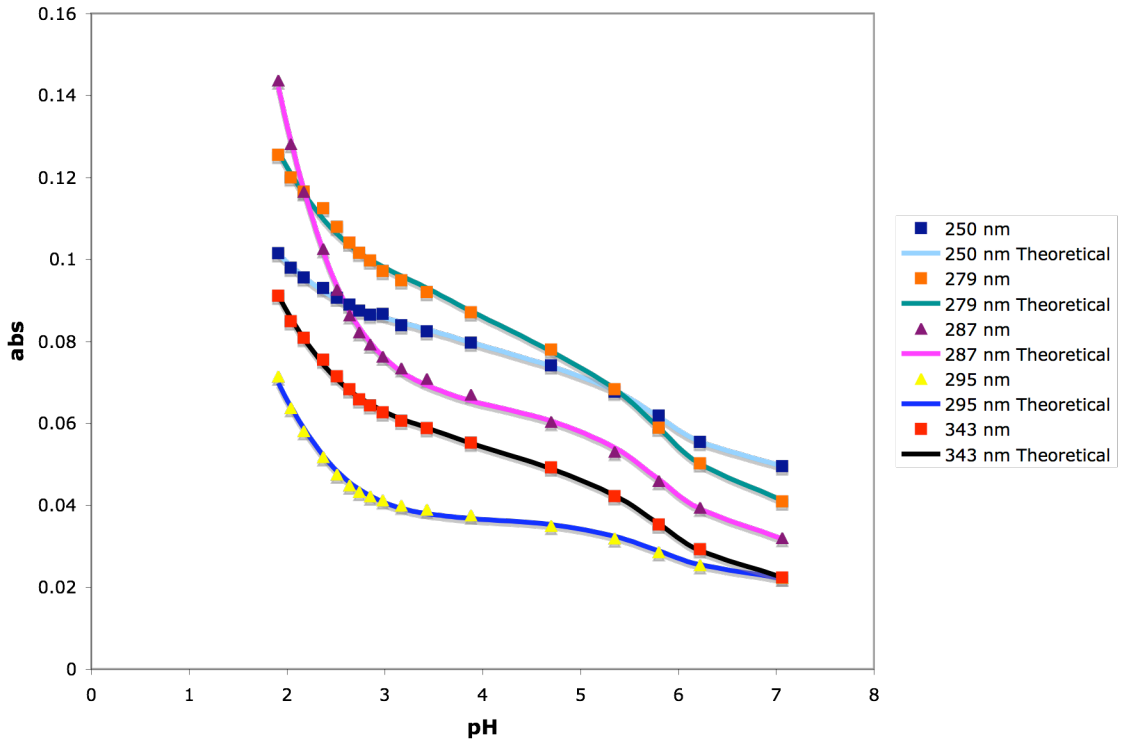

Figure 51. Plot of corrected absorbance (data points) and theoretical absorbance (lines) versus pH for titration of DPP and $Pb(ClO_4)_2$.

Table 33. Solutions and standard deviation for each parameter solved by the 'SOLVER' module of EXCEL in determining log K_1 of DPP-Pb complex. Note: Coefficient of determination and standard error calculated with 'Solver Statistics' macro.

	Parameter	Solution	Standard Deviation
Overall	pK_1	5.731925998	0.028170487
	pK_2	3.507654591	0.089671844
	pK_3	1.576803282	0.058995879
250 nm	Abs(0)	0.048513746	0.000639562
	Abs(1)	0.076057195	0.000720197
	Abs(2)	0.086928856	0.000760324
	Abs(3)	0.133632649	0.004643371
279 nm	Abs(0)	0.039630383	0.000687766
	Abs(1)	0.080421932	0.000913138
	Abs(2)	0.100385181	0.001167034
	Abs(3)	0.18404468	0.007512222
287 nm	Abs(0)	0.030767748	0.00066555
	Abs(1)	0.063361348	0.000702127
	Abs(2)	0.071604592	0.001253792
	Abs(3)	0.301951101	0.021169922
295 nm	Abs(0)	0.021571329	0.000612283
	Abs(1)	0.036713917	0.00060094
	Abs(2)	0.038078449	0.000665106
	Abs(3)	0.142552416	0.009935316
343 nm	Abs(0)	0.02131779	0.000647221
	Abs(1)	0.051188946	0.000735933
	Abs(2)	0.063136891	0.000918723
	Abs(3)	0.154022053	0.008334136

R^2: 0.999454039 **Standard Error:** 0.000744675

Table 34. Summary of equations at each protonation event of $[Pb(DPP)]^{2+}$; Equations written in terms of log K to complement initial equilibrium expressions.

							pK_{50}
$[Pb(DPP)OH]^+$	+	H^+	$\rightleftharpoons$	$[Pb(DPP)]^{2+}$	+	H_2O	5.81
$[Pb(DPP)]^{2+}$	+	H^+	$\rightleftharpoons$	$H(DPP)^+$	+	Pb^{2+}	3.92
$H(DPP)^+$	+	H^+	$\rightleftharpoons$	$H_2(DPP)^{2+}$			1.72

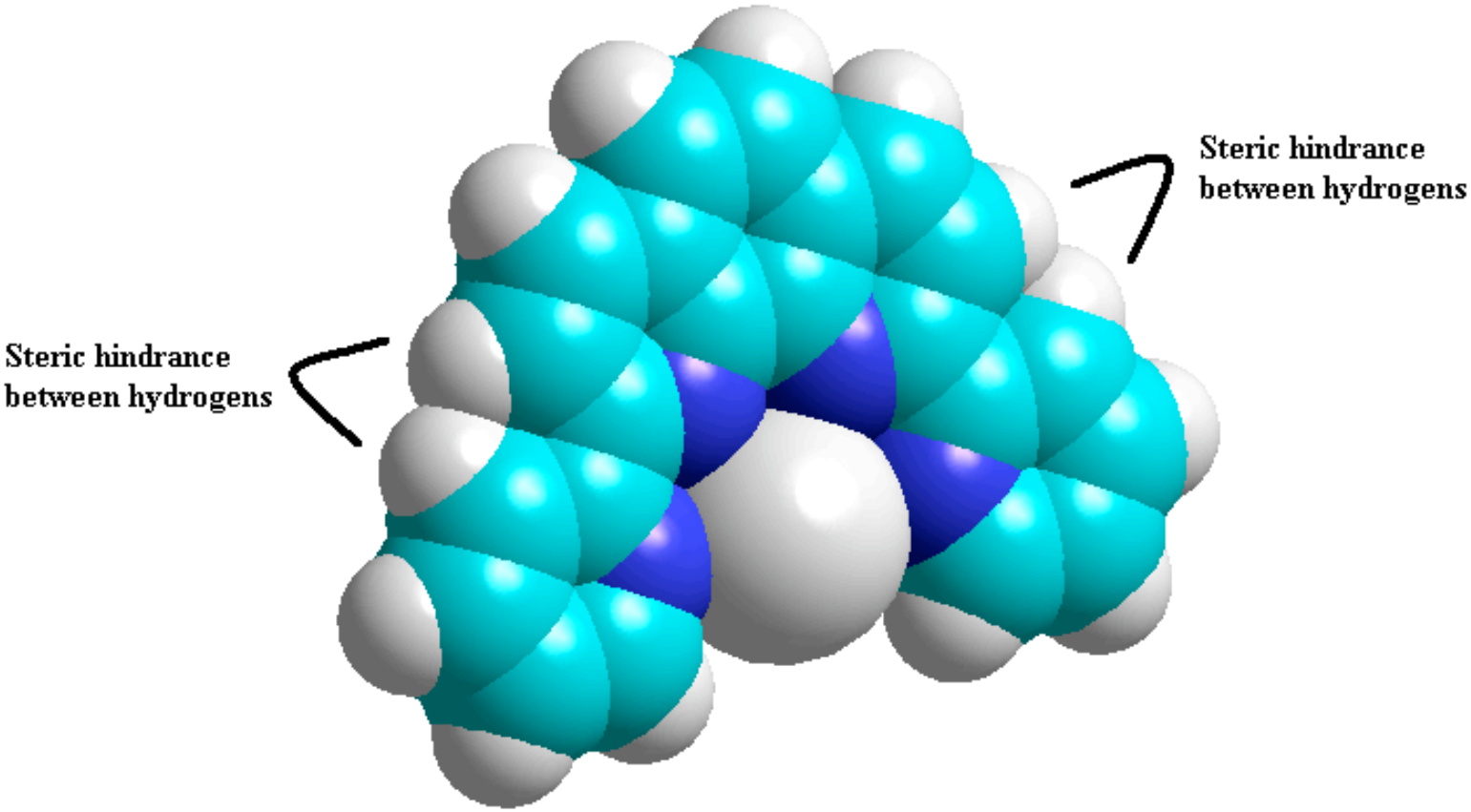

Figure 52. Lowest energy conformation of $[Pb(DPP)]^{2+}$ complex.

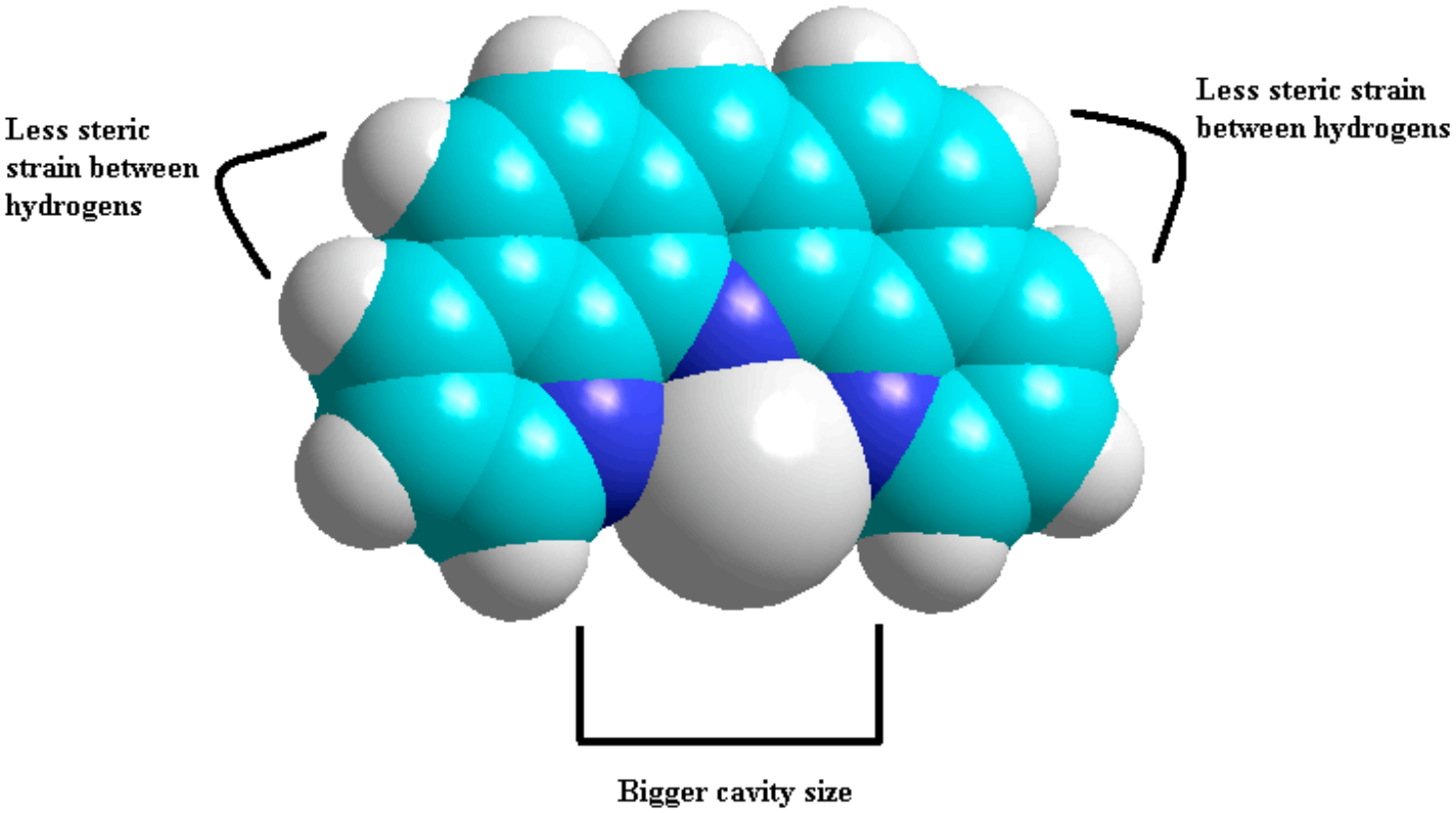

Figure 53. Energy minimized structure of more preorganized ligand DPA for binding large metal ions.

Preliminary Data for Protonation Constants of QUATERPY

In order to determine the stability constants QUATERPY has with various metal ions, it was first necessary to determine protonation constants of the free ligand. Preliminary titration experiments were performed and data was analyzed following the same procedure used to determine the protonation constants of DPP. A solution of 4×10^{-6} M QUATERPY was titrated with 0.1 M NaOH from pH = 1.91 to pH = 4.47. The UV/Vis spectra plotting absorbance versus wavelength is shown in Figure 54. Absorbances were recorded at 237, 244, 279, 300, 320, and 330 nm because these wavelengths exhibited the largest change in absorbances. Theoretical and measured absorbances were plotted for every wavelength simultaneously by minimizing the sum of the squares of the residuals as previously discussed and shown in Figure 55. Table 35 outlines the solutions of each parameter that was varied by 'SOLVER' and the standard deviation of each variable calculated by Solver Statistics. The pK's were recorded once all standard deviations were minimized and the R^2 value was close to one. The observed protonation events for the free ligand titration yielded a pK_1 and pK_2 of 5.01 and 1.51, respectively, which were calculated with minimized error.

Table 35 shows that there is a large amount of error associated with pK_1. This was because the titration experiment was stopped at pH=4.47. A higher pH was not reached because of what is predicted to be a kinetic effect or precipitation of the ligand. More experiments need to be conducted in order to reduce the error in each parameter before determining stability constants of metal-QUATERPY complexes.

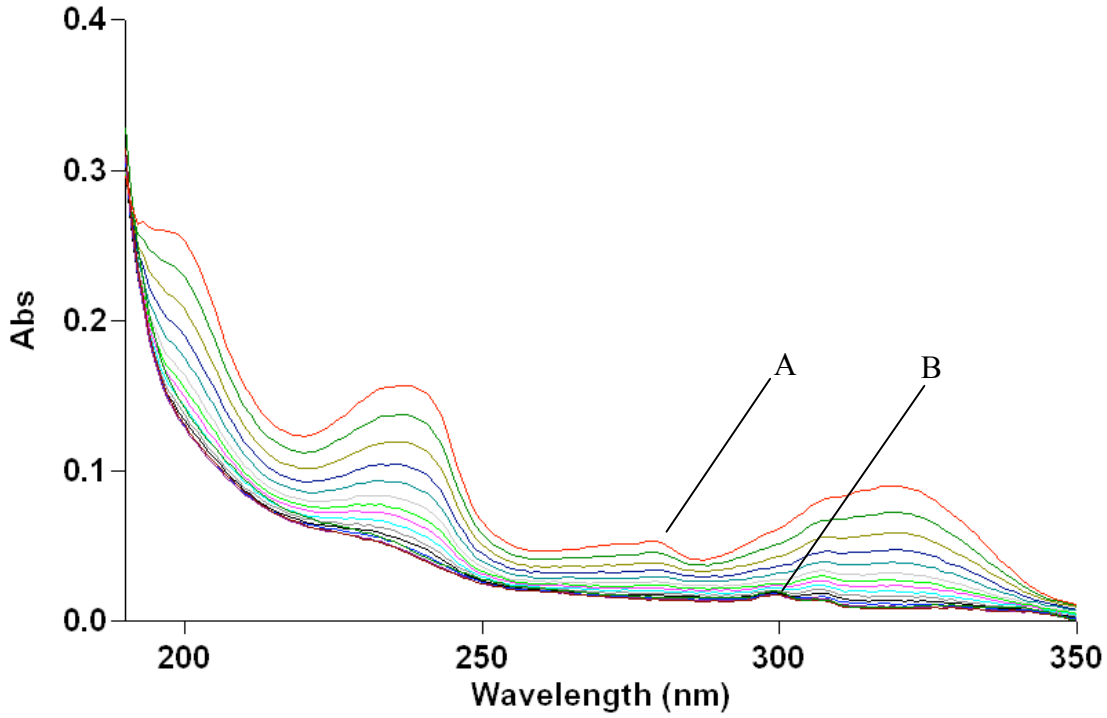

Figure 54. UV spectra of 4 x 10^{-6} M QUATERPY in 0.01 M $HClO_4$ and 0.09 M $NaClO_4$ as a function of pH. Initial spectrum (A) of fully protonated QUATERPY at pH=1.91. Final spectrum (B) of unprotonated QUATERPY at pH=4.47.

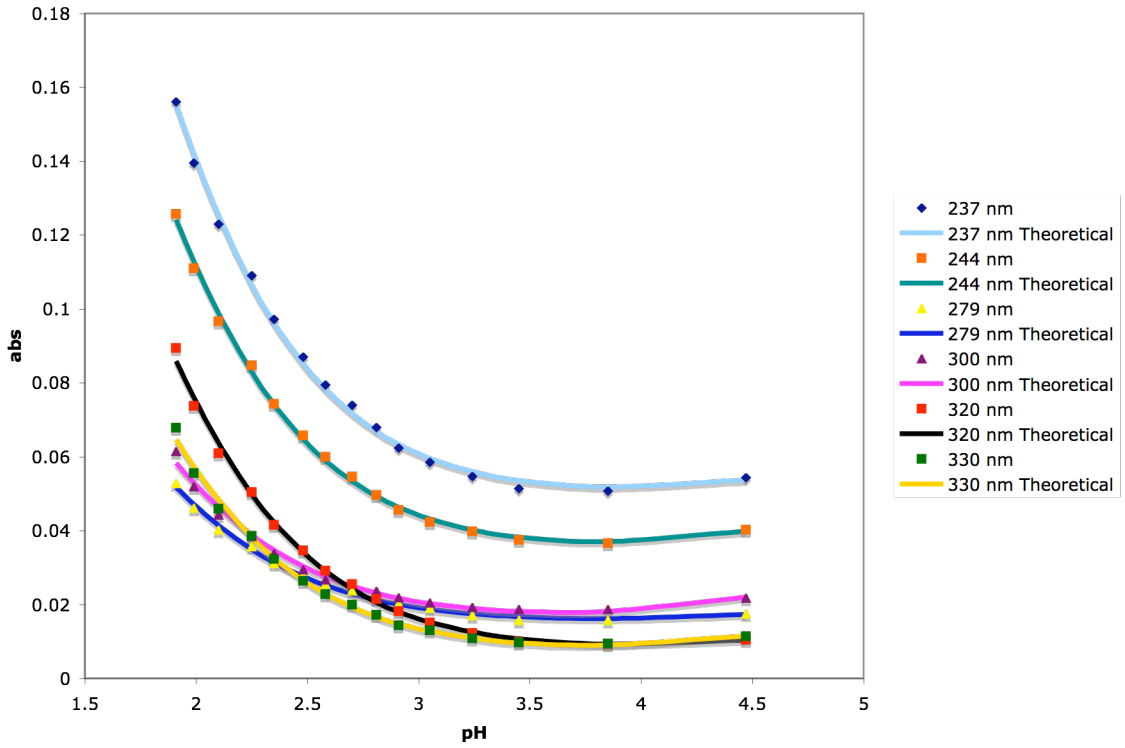

Figure 55. Plot of corrected absorbance (data points) and theoretical absorbance (lines) versus pH for titration of QUATERPY free ligand.

Table 35. Solutions and standard deviation for each parameter solved by the 'SOLVER' module of EXCEL in determining p*K* of QUATERPY free ligand. Note: Coefficient of determination and standard error calculated with 'Solver Statistics' macro.

	Parameter	Solution	Standard Deviation
Overall	pK_1	5.013752475	1.699914252
	pK_2	1.51807603	0.048535399
237 nm	Abs(0)	0.059333962	0.076301681
	Abs(1)	0.034062991	0.000751024
	Abs(2)	0.346779646	0.025164904
244 nm	Abs(0)	0.069149732	0.060950265
	Abs(1)	0.048933184	0.000766048
	Abs(2)	0.417847802	0.029820839
279 nm	Abs(0)	0.026735661	0.060045977
	Abs(1)	0.006929962	0.000697844
	Abs(2)	0.207027597	0.01630679
300 nm	Abs(0)	0.019742888	0.037556459
	Abs(1)	0.007390654	0.00070971
	Abs(2)	0.279712223	0.022242769
320 nm	Abs(0)	0.043272055	0.083285219
	Abs(1)	0.015799654	0.000726481
	Abs(2)	0.163266925	0.012037115
330 nm	Abs(0)	0.024727858	0.029756287
	Abs(1)	0.015100434	0.000658834
	Abs(2)	0.142247504	0.010880862

R^2: 0.998427889 **Standard Error:** 0.001413316

Crystal Synthesis Results

$[Pb(DPP)(ClO_4)(H_2O)](ClO_4)$

The crystals formed on the interface of the butanol/H_2O layers were thick, yellow, and needle-like. Figure 56 is a microscopic photograph of the crystals synthesized. Crystal structures were determined by both x-ray crystallography and mass spectrometry. The crystal structure of $[Pb(DPP)(ClO_4)(H_2O)](ClO_4)$ consists of a lead metal ion coordinated with one DPP molecule through all four donor atoms along with one perchlorate molecule and one water molecule as in Figure 57 and Figure 58. A 3D representation of the crystal structure is shown in Figure 59. The lead was coordinated to all four neutral nitrogen donor atoms of DPP, giving it a coordination number of six including the coordinated perchlorate and water molecules.

The crystal data and structural refinement parameters for the $[Pb(DPP)(ClO_4)(H_2O)](ClO_4)$ complex are listed in Table 36. The bond distances and angles for the $[Pb(DPP)(ClO_4)(H_2O)](ClO_4)$ complex are shown in Table 37 and 38 respectively. In addition, the spatial coordinates of the atoms for the $[Pb(DPP)(ClO_4)(H_2O)](ClO_4)$ complex are given in Tables 39 and 40. Each unit cell of the crystal contained two complexes with corresponding perchlorate and water molecules. The bond distances between the lead and nitrogens of DPP were 2.382, 2.487, 2.522, and 2.621 Å. These were compared to an average Pb-N bond length of 2.56 $\pm$ 0.08 Å determined by 36 structures containing bipyridyl and lead from the Cambridge Crystallographic Database. The measured Pb-N bond lengths were in good agreement with the expected average bond length.

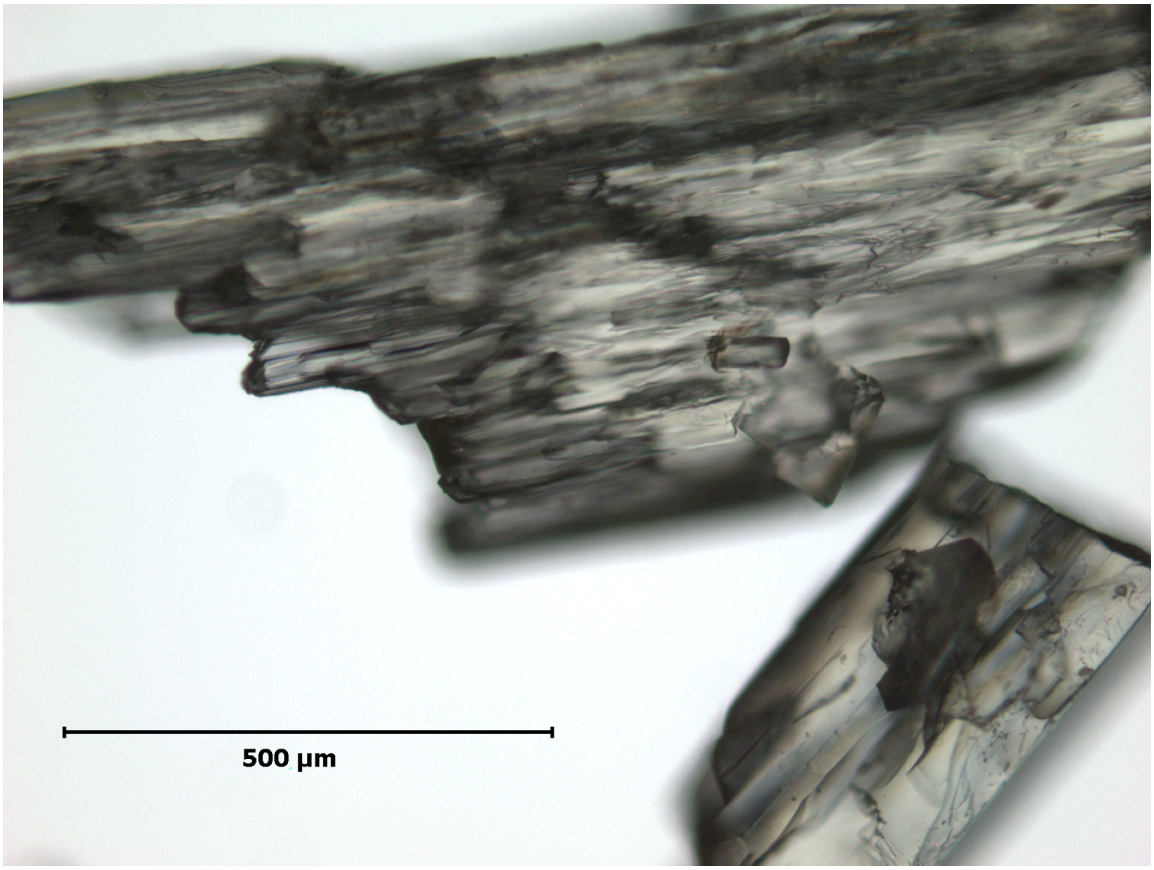

Figure 56. Microscopic view (10x) of crystals formed with equimolar amounts of DPP and $Pb(ClO_4)_2$

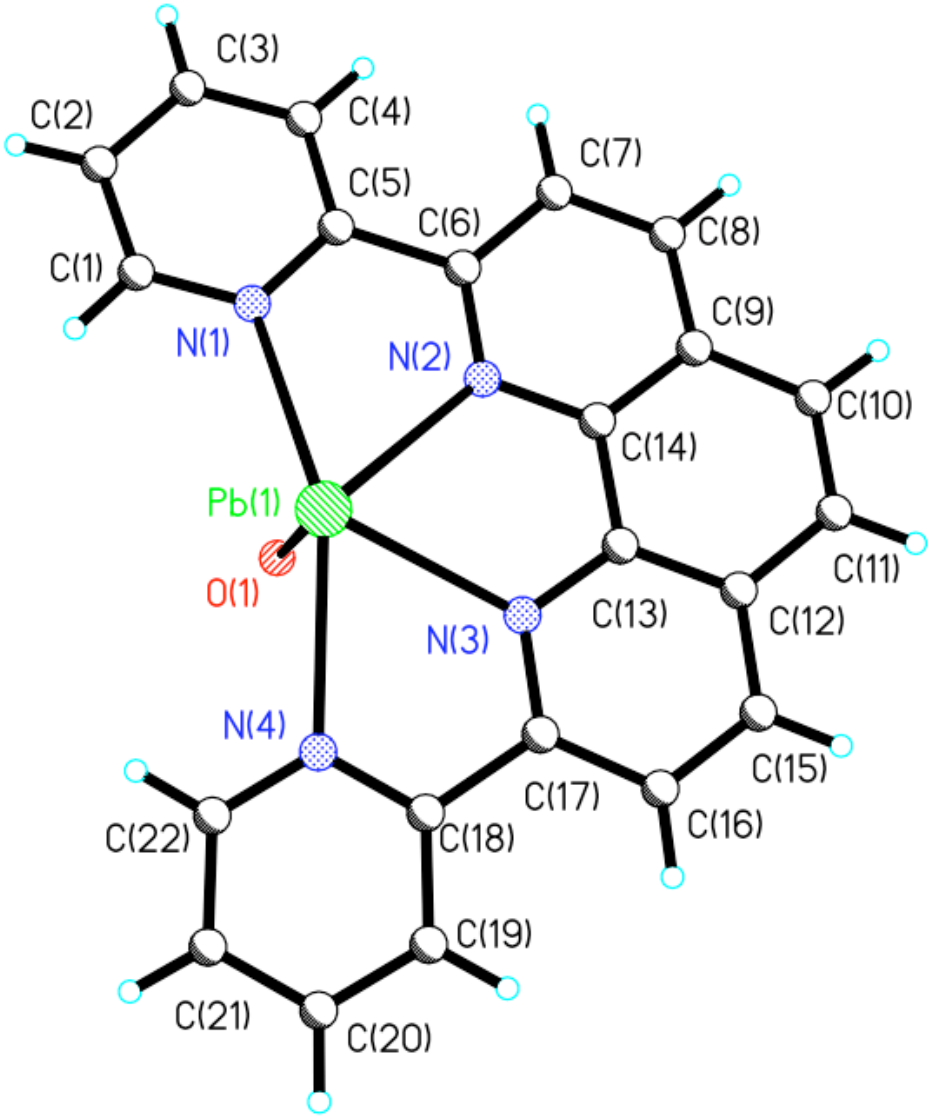

Figure 57. Molecular structure of [Pb(DPP)(ClO_4)(H_2O)](ClO_4) as determined by x-ray crystallography.

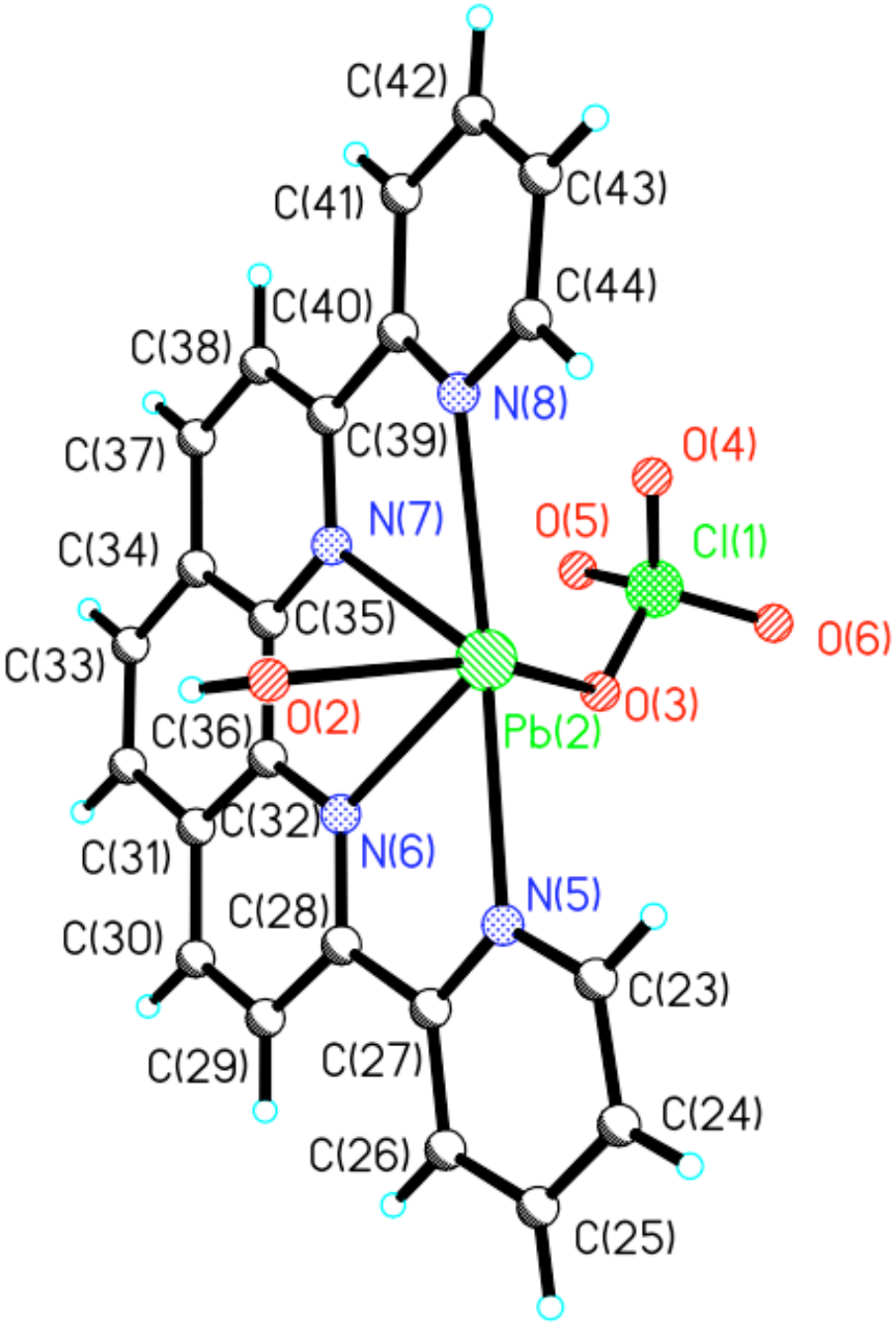

Figure 58. [Pb(DPP)(ClO_4)(H_2O)](ClO_4) structure coordinated to a perchlorate and one water.

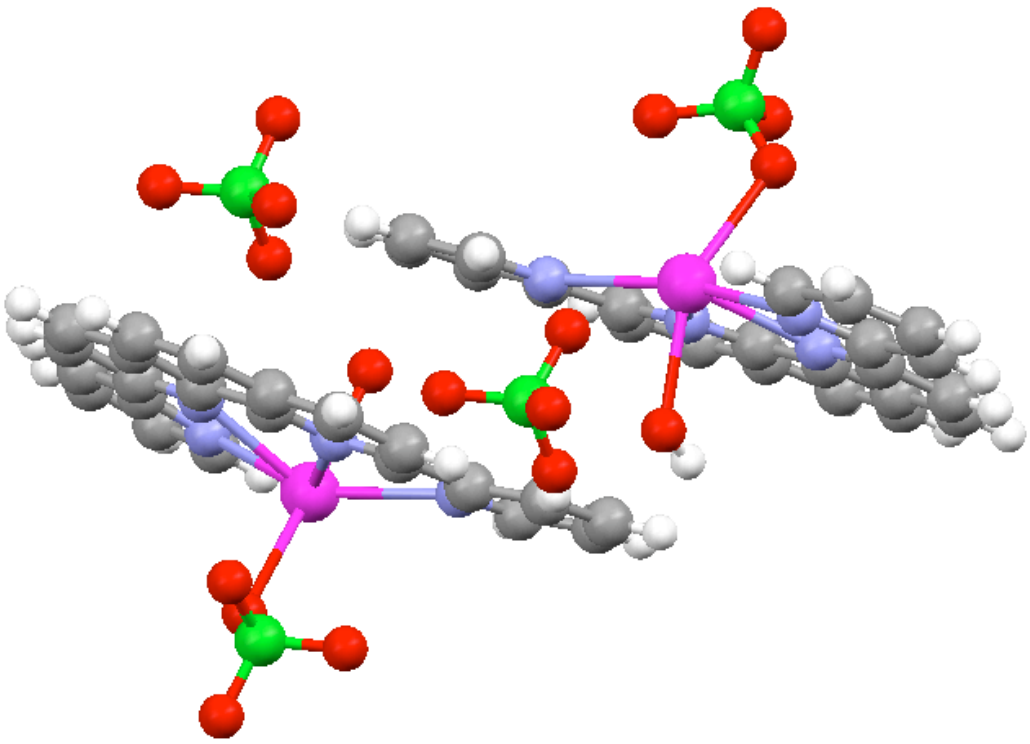

Figure 59. Three dimensional illustration of lead complex to see orientation of coordinated perchlorate ions and water molecule.

Table 36. Crystal data and structure refinement for the $[Pb(DPP)(ClO_4)(H_2O)](ClO_4)$ complex.

Identification code	dpppb	
Empirical formula	C22 H14.50 Cl2 N4 O9 Pb	
Formula weight	756.97	
Temperature	158(2) K	
Wavelength	0.71073 Å	
Crystal system	Monoclinic	
Space group	P 2_1/c	
Unit cell dimensions	a = 15.715(3) Å	α= 90.00°
	b = 11.425(2) Å	β= 104.72(3)°
	c = 27.309(6) Å	γ = 90.00°
Volume	4742.0(16) $Å^3$	
Z	8	
Density (calculated)	2.121 Mg/m^3	
Absorption coefficient	0.740 mm^{-1}	
F(000)	2900	
Crystal size	0.24 x 0.17 x 0.12 mm^3	
Theta range for data collection	2.90 to 25.05°	
Index ranges	$-17 \leq h \leq 18$, $-13 \leq k \leq 12$, $-28 \leq l \leq 32$	
Reflections collected	8350	
Independent reflections	7610 [R(int) = 0.0548]	
Completeness to theta = 25.05°	99.3 %	
Absorption correction	Semi-empirical from equivalents	
Max. and min. transmission	0.4703 and 0.2695	
Refinement method	Full-matrix least-squares on F^2	
Data / restraints / parameters	8350 / 0 / 686	
Goodness-of-fit on F^2	1.208	
Final R indices [I>2sigma(I)]	R1 = 0.0515, wR2 = 0.0985	
R indices (all data)	R1 = 0.0597, wR2 = 0.1016	
Largest diff. peak and hole	2.805 and -1.100 e.$Å^{-3}$	

Table 37. Bond lengths of [Pb(DPP)(ClO_4)(H_2O)](ClO_4) crystal structures.

Bond	Bond Length (Å)	Bond	Bond Length (Å)
Pb(1)-O(1)	2.382(7)	C(8)-C(9)	1.383(14)
Pb(1)-N(3)	2.487(7)	C(9)-C(14)	1.429(13)
Pb(1)-N(2)	2.522(7)	C(9)-C(10)	1.443(14)
Pb(1)-N(4)	2.621(8)	C(10)-C(11)	1.346(15)
Pb(1)-N(1)	2.661(7)	C(11)-C(12)	1.420(15)
Pb(2)-O(2)	2.477(6)	C(12)-C(15)	1.384(14)
Pb(2)-N(7)	2.533(8)	C(12)-C(13)	1.392(13)
Pb(2)-N(6)	2.560(7)	C(13)-C(14)	1.451(13)
Pb(2)-O(3)	2.642(7)	C(15)-C(16)	1.377(16)
Pb(2)-N(5)	2.644(8)	C(16)-C(17)	1.419(14)
Pb(2)-N(8)	2.657(8)	C(17)-C(18)	1.502(15)
Cl(1)-O(4)	1.404(8)	C(18)-C(19)	1.405(14)
Cl(1)-O(6)	1.406(8)	C(19)-C(20)	1.365(17)
Cl(1)-O(5)	1.407(9)	C(20)-C(21)	1.371(17)
Cl(1)-O(3)	1.437(8)	C(21)-C(22)	1.401(15)
N(1)-C(1)	1.333(11)	C(23)-C(24)	1.402(14)
N(1)-C(5)	1.349(11)	C(24)-C(25)	1.378(13)
N(2)-C(6)	1.325(11)	C(25)-C(26)	1.355(13)
N(2)-C(14)	1.363(11)	C(26)-C(27)	1.400(12)
N(3)-C(17)	1.337(12)	C(27)-C(28)	1.479(13)
N(3)-C(13)	1.347(12)	C(28)-C(29)	1.408(13)
N(4)-C(22)	1.326(13)	C(29)-C(30)	1.352(14)
N(4)-C(18)	1.333(12)	C(30)-C(31)	1.408(14)
N(5)-C(23)	1.330(13)	C(31)-C(36)	1.388(13)
N(5)-C(27)	1.342(11)	C(31)-C(32)	1.457(14)
N(6)-C(28)	1.337(12)	C(32)-C(33)	1.325(16)
N(6)-C(36)	1.370(11)	C(33)-C(34)	1.435(16)
N(7)-C(35)	1.338(13)	C(34)-C(37)	1.414(15)
N(7)-C(39)	1.356(12)	C(34)-C(35)	1.428(14)
N(8)-C(44)	1.327(13)	C(35)-C(36)	1.463(13)
N(8)-C(40)	1.344(13)	C(37)-C(38)	1.352(16)
C(1)-C(2)	1.399(13)	C(38)-C(39)	1.409(14)
C(2)-C(3)	1.389(14)	C(39)-C(40)	1.468(15)
C(3)-C(4)	1.370(14)	C(40)-C(41)	1.403(13)
C(4)-C(5)	1.403(13)	C(41)-C(42)	1.378(17)
C(5)-C(6)	1.495(13)	C(42)-C(43)	1.372(16)
C(6)-C(7)	1.414(13)	C(43)-C(44)	1.390(14)
C(7)-C(8)	1.371(14)		

Table 38. Bond angles of [Pb(DPP)(ClO_4)(H_2O)](ClO_4) complexes.

Bond	Bond Angle (°)	Bond	Bond Angle (°)	Bond	Bond Angle (°)
O(1)-Pb(1)-N(3)	86.3(2)	C(23) N(5)-C(27)	118.3(8)	N(4)-C(18)-C(17)	116.4(8)
O(1)-Pb(1)-N(2)	83.9(2)	C(23) N(5)-Pb(2)	120.6(6)	C(19)-C(18)-C(17)	122.8(9)
N(3)-Pb(1)-N(2)	65.7(2)	C(27) N(5)-Pb(2)	120.8(6)	C(20)-C(19)-C(18)	119.3(11)
O(1)-Pb(1)-N(4)	74.3(2)	C(28) N(6)-C(36)	118.8(8)	C(19)-C(20)-C(21)	120.0(10)
N(3)-Pb(1)-N(4)	63.4(3)	C(28) N(6)-Pb(2)	123.7(6)	C(20)-C(21)-C(22)	117.8(11)
N(2)-Pb(1)-N(4)	125.3(2)	C(36) N(6)-Pb(2)	117.4(6)	N(4)-C(22)-C(21)	122.4(11)
O(1)-Pb(1)-N(1)	74.8(2)	C(35) N(7)-C(39)	120.3(8)	N(5)-C(23)-C(24)	123.9(9)
N(3)-Pb(1)-N(1)	126.2(2)	C(35) N(7)-Pb(2)	117.6(6)	C(25)-C(24)-C(23)	116.4(9)
N(2)-Pb(1)-N(1)	62.5(2)	C(39) N(7)-Pb(2)	121.8(7)	C(26)-C(25)-C(24)	121.0(9)
N(4)-Pb(1)-N(1)	146.7(2)	C(44) N(8)-C(40)	119.8(9)	C(25)-C(26)-C(27)	119.2(9)
O(2)-Pb(2)-N(7)	81.0(2)	C(44) N(8)-Pb(2)	120.8(6)	N(5)-C(27)-C(26)	121.3(9)
O(2)-Pb(2)-N(6)	75.5(2)	C(40) N(8)-Pb(2)	117.7(7)	N(5)-C(27)-C(28)	116.3(8)
N(7)-Pb(2)-N(6)	66.1(2)	N(1) C(1)-C(2)	123.9(9)	C(26)-C(27)-C(28)	122.4(8)
O(2)-Pb(2)-O(3)	147.8(2)	C(3) C(2)-C(1)	117.0(9)	N(6)-C(28)-C(29)	121.1(9)
N(7)-Pb(2)-O(3)	78.1(3)	C(4) C(3)-C(2)	119.8(9)	N(6)-C(28)-C(27)	117.0(8)
N(6)-Pb(2)-O(3)	73.7(2)	C(3) C(4)-C(5)	119.9(9)	C(29)-C(28)-C(27)	121.9(8)
O(2)-Pb(2)-N(5)	82.6(3)	N(1) C(5)-C(4)	120.8(9)	C(30)-C(29)-C(28)	120.2(9)
N(7)-Pb(2)-N(5)	127.9(3)	N(1) C(5)-C(6)	116.3(8)	C(29)-C(30)-C(31)	119.9(9)
N(6)-Pb(2)-N(5)	62.0(2)	C(4) C(5)-C(6)	122.9(9)	C(36)-C(31)-C(30)	117.5(9)
O(3)-Pb(2)-N(5)	91.2(2)	N(2) C(6)-C(7)	122.8(9)	C(36)-C(31)-C(32)	120.8(10)
O(2)-Pb(2)-N(8)	85.8(2)	N(2) C(6)-C(5)	116.8(8)	C(30)-C(31)-C(32)	121.7(9)
N(7)-Pb(2)-N(8)	63.1(3)	C(7) C(6)-C(5)	120.4(8)	C(33)-C(32)-C(31)	119.7(10)
N(6)-Pb(2)-N(8)	127.8(3)	C(8) C(7)-C(6)	117.9(9)	C(32)-C(33)-C(34)	121.8(10)
O(3)-Pb(2)-N(8)	105.9(2)	C(7) C(8)-C(9)	121.5(9)	C(37)-C(34)-C(35)	117.1(10)
N(5)-Pb(2)-N(8)	161.9(3)	C(8) C(9)-C(14)	117.0(9)	C(37)-C(34)-C(33)	122.1(10)
O(4)-Cl(1)-O(6)	114.6(6)	C(8) C(9)-C(10)	124.5(9)	C(35)-C(34)-C(33)	120.8(10)
O(4)-Cl(1)-O(5)	108.7(7)	C(14) C(9)-C(10)	118.4(9)	N(7)-C(35)-C(34)	122.4(9)
O(6)-Cl(1)-O(5)	108.4(7)	C(11) C(10)-C(9)	121.1(10)	N(7)-C(35)-C(36)	120.7(8)
O(4)-Cl(1)-O(3)	108.6(5)	C(10) C(11)-C(12)	121.5(9)	C(34)-C(35)-C(36)	116.9(9)
O(6)-Cl(1)-O(3)	109.0(5)	C(15) C(12)-C(13)	117.3(10)	N(6)-C(36)-C(31)	122.6(9)
O(5)-Cl(1)-O3	107.3(6)	C(15) C(12)-C(11)	122.5(10)	N(6)-C(36)-C(35)	117.4(8)
Cl(1)-O(3)-Pb(2)	122.4(4)	C(13) C(12)-C(11)	120.1(9)	C(31)-C(36)-C(35)	120.0(9)
C(1)-N(1)-C(5)	118.6(8)	N(3) C(13)-C(12)	123.8(8)	C(38)-C(37)-C(34)	118.8(9)
C(1)-N(1)-Pb(1)	122.5(6)	N(3) C(13)-C(14)	116.6(8)	C(37)-C(38)-C(39)	122.3(10)
C(5)-N(1)-Pb(1)	118.6(6)	C(12) C(13)-C(14)	119.5(9)	N(7)-C(39)-C(38)	119.2(10)
C(6)-N(2)-C(14)	119.1(8)	N(2) C(14)-C(9)	121.7(8)	N(7)-C(39)-C(40)	117.7(8)
C(6)-N(2)-Pb(1)	123.8(6)	N(2) C(14)-C(13)	119.1(8)	C(38)-C(39)-C(40)	123.1(9)
C(14)-N(2)-Pb(1)	115.7(6)	C(9) C(14)-C(13)	119.2(8)	N(8)-C(40)-C(41)	120.9(10)
C(17)-N(3)-C(13)	117.8(8)	C(16) C(15)-C(12)	120.7(10)	N(8)-C(40)-C(39)	117.4(8)
C(17)-N(3)-Pb(1)	121.5(6)	C(15) C(16)-C(17)	117.9(10)	C(41)-C(40)-C(39)	121.7(10)
C(13)-N(3)-Pb(1)	118.5(6)	N(3) C(17)-C(16)	122.4(10)	C(42)-C(41)-C(40)	118.5(10)
C(22)-N(4)-C(18)	119.7(9)	N(3) C(17)-C(18)	116.2(8)	C(43)-C(42)-C(41)	120.1(10)
C(22)-N(4)-Pb(1)	122.0(7)	C(16) C(17)-C(18)	121.4(9)	C(42)-C(43)-C(44)	118.3(11)
C(18)-N(4)-Pb(1)	117.4(6)	N(4) C(18)-C(19)	120.7(10)	N(8)-C(44)-C(43)	122.3(11)

Symmetry transformations used to generate equivalent atoms

1: -x, -y+½, z+½ **2:** -x, -y+½, z-½ **3:** -x, -y+1, z

Table 39. Atomic coordinates and equivalent isotropic displacement parameters ($Å^2$) for $[Pb(DPP)(ClO_4)(H_2O)](ClO_4)$. U(eq) is defined as one third of the trace of the orthogonalized U^{ij} tensor.

	x	y	z	U(eq)
Pb(1)	0.99003(2)	0.65042(3)	0.157232(12)	0.02350(10)
Pb(2)	1.48237(2)	0.92471(3)	0.109172(13)	0.02439(10)
Cl(1)	1.48014(14)	0.8011(2)	-0.01322(8)	0.0315(5)
O(1)	1.0252(4)	0.5944(6)	0.0807(2)	0.0380(17)
O(2)	1.4718(5)	0.9083(6)	0.1979(2)	0.0387(17)
O(3)	1.5389(5)	0.8334(8)	0.0343(3)	0.054(2)
N(1)	0.8392(5)	0.5765(6)	0.0966(3)	0.0237(16)
N(2)	0.8936(5)	0.8005(6)	0.1018(3)	0.0234(16)
N(3)	1.0656(5)	0.8383(7)	0.1495(3)	0.0279(17)
N(4)	1.1623(5)	0.6447(7)	0.1783(3)	0.0325(18)
N(5)	1.6416(5)	1.0034(7)	0.1533(3)	0.0321(18)
N(6)	1.6007(5)	0.7751(6)	0.1496(3)	0.0232(16)
N(7)	1.4261(5)	0.7165(7)	0.1068(3)	0.0316(18)
N(8)	1.3090(5)	0.8957(8)	0.0838(3)	0.036(2)
O(4)	1.3948(5)	0.8375(10)	-0.0133(4)	0.078(3)
O(6)	1.5122(6)	0.8470(9)	-0.0528(3)	0.071(3)
C(1)	0.8161(6)	0.4640(8)	0.0927(4)	0.031(2)
C(2)	0.7337(6)	0.4235(9)	0.0652(4)	0.036(2)
C(3)	0.6734(6)	0.5072(9)	0.0410(4)	0.033(2)
C(4)	0.6964(6)	0.6231(9)	0.0443(4)	0.035(2)
C(5)	0.7804(6)	0.6569(8)	0.0725(3)	0.0263(19)
C(6)	0.8107(6)	0.7814(8)	0.0771(3)	0.027(2)
C(7)	0.7522(6)	0.8725(9)	0.0558(4)	0.033(2)
C(8)	0.7836(7)	0.9850(8)	0.0610(4)	0.034(2)
C(9)	0.8699(7)	1.0095(8)	0.0860(4)	0.032(2)
C(10)	0.9070(7)	1.1256(9)	0.0935(4)	0.037(2)
C(11)	0.9915(8)	1.1427(9)	0.1187(4)	0.041(3)
C(12)	1.0481(6)	1.0475(8)	0.1382(3)	0.030(2)
C(13)	1.0160(6)	0.9334(8)	0.1328(3)	0.027(2)
C(14)	0.9246(6)	0.9125(8)	0.1067(3)	0.0237(19)
C(15)	1.1352(7)	1.0631(10)	0.1641(4)	0.042(3)
C(16)	1.1883(7)	0.9682(10)	0.1816(4)	0.041(3)
C(17)	1.1504(6)	0.8550(9)	0.1729(4)	0.034(2)
C(18)	1.2048(6)	0.7465(9)	0.1876(3)	0.032(2)
C(19)	1.2965(7)	0.7495(11)	0.2073(4)	0.042(3)
C(20)	1.3421(7)	0.6468(13)	0.2167(4)	0.052(3)
C(21)	1.2985(7)	0.5422(12)	0.2062(4)	0.047(3)
C(22)	1.2069(7)	0.5452(10)	0.1876(4)	0.039(2)
O(5)	1.4810(7)	0.6782(8)	-0.0163(4)	0.081(3)
C(23)	1.6604(7)	1.1166(9)	0.1519(4)	0.042(3)
C(24)	1.7446(6)	1.1636(8)	0.1711(4)	0.033(2)
C(25)	1.8106(6)	1.0851(8)	0.1916(3)	0.029(2)
C(26)	1.7934(6)	0.9691(8)	0.1933(3)	0.028(2)
C(27)	1.7074(5)	0.9291(8)	0.1734(3)	0.0236(19)
C(28)	1.6841(6)	0.8035(8)	0.1719(3)	0.026(2)
C(29)	1.7468(6)	0.7168(8)	0.1922(4)	0.031(2)
C(30)	1.7238(7)	0.6025(9)	0.1885(4)	0.035(2)
C(31)	1.6368(7)	0.5701(8)	0.1642(3)	0.030(2)
C(32)	1.6095(8)	0.4479(9)	0.1587(4)	0.042(3)
C(33)	1.5268(8)	0.4214(9)	0.1359(4)	0.046(3)
C(34)	1.4623(7)	0.5102(9)	0.1170(4)	0.040(3)
C(35)	1.4855(6)	0.6313(8)	0.1215(3)	0.030(2)
C(36)	1.5774(6)	0.6593(8)	0.1457(3)	0.027(2)
C(37)	1.3734(8)	0.4827(9)	0.0940(4)	0.045(3)
C(38)	1.3154(7)	0.5712(10)	0.0792(4)	0.040(3)
C(39)	1.3404(7)	0.6897(9)	0.0862(4)	0.034(2)
C(40)	1.2779(6)	0.7868(9)	0.0723(3)	0.031(2)
C(41)	1.1884(7)	0.7675(11)	0.0496(4)	0.043(3)
C(42)	1.1335(7)	0.8631(12)	0.0375(4)	0.047(3)
C(43)	1.1662(7)	0.9740(11)	0.0486(4)	0.043(3)
C(44)	1.2552(6)	0.9867(10)	0.0719(4)	0.037(2)

Table 40. Anisotropic displacement parameters ($Å^2$) for $[Pb(DPP)(ClO_4)(H_2O)](ClO_4)$. The anisotropic displacement factor exponent takes the form:
$-2\pi^2[h^2 a^{*2}U^{11} + ... + 2 h k a^* b^* U^{12}]$

	U^{11}	U^{22}	U^{33}	U^{23}	U^{13}	U^{12}
Pb(1)	0.02521(18)	0.02108(17)	0.02300(18)	-0.00111(14)	0.00391(13)	-0.00205(13)
Pb(2)	0.02074(17)	0.02584(18)	0.02526(18)	0.00067(14)	0.00339(13)	-0.00280(13)
Cl(1)	0.0275(12)	0.0368(13)	0.0287(12)	-0.0018(10)	0.0044(9)	-0.0041(10)
O(1)	0.030(4)	0.051(4)	0.027(4)	0.001(3)	-0.005(3)	-0.005(3)
O(2)	0.060(5)	0.035(4)	0.026(4)	0.015(3)	0.019(3)	0.017(3)
O(3)	0.031(4)	0.092(7)	0.037(4)	-0.019(4)	0.003(3)	0.005(4)
N(1)	0.026(4)	0.025(4)	0.020(4)	-0.002(3)	0.005(3)	-0.005(3)
N(2)	0.021(4)	0.024(4)	0.026(4)	0.000(3)	0.008(3)	-0.003(3)
N(3)	0.029(4)	0.024(4)	0.030(4)	-0.004(3)	0.007(3)	-0.005(3)
N(4)	0.031(4)	0.039(5)	0.026(4)	0.006(4)	0.004(3)	0.003(4)
N(5)	0.029(4)	0.022(4)	0.040(5)	0.000(4)	-0.001(4)	-0.002(3)
N(6)	0.032(4)	0.022(4)	0.017(4)	-0.003(3)	0.010(3)	-0.002(3)
N(7)	0.033(4)	0.033(5)	0.030(4)	0.001(4)	0.011(4)	-0.011(4)
N(8)	0.032(5)	0.044(5)	0.030(4)	-0.002(4)	0.004(4)	-0.010(4)
O(4)	0.029(4)	0.133(9)	0.068(6)	0.006(6)	0.007(4)	0.021(5)
O(6)	0.079(6)	0.095(7)	0.041(5)	0.022(5)	0.017(5)	-0.015(6)
C(1)	0.033(5)	0.028(5)	0.030(5)	0.001(4)	0.004(4)	-0.005(4)
C(2)	0.039(6)	0.033(5)	0.039(6)	-0.007(5)	0.013(5)	-0.015(5)
C(3)	0.024(5)	0.044(6)	0.030(5)	-0.009(5)	0.005(4)	-0.011(4)
C(4)	0.021(5)	0.042(6)	0.040(6)	0.002(5)	0.002(4)	-0.003(4)
C(5)	0.030(5)	0.028(5)	0.023(5)	-0.002(4)	0.012(4)	0.000(4)
C(6)	0.028(5)	0.036(5)	0.019(4)	0.000(4)	0.011(4)	0.002(4)
C(7)	0.023(5)	0.041(6)	0.037(6)	-0.001(5)	0.009(4)	0.004(4)
C(8)	0.043(6)	0.023(5)	0.042(6)	0.008(4)	0.020(5)	0.008(4)
C(9)	0.043(6)	0.029(5)	0.029(5)	0.001(4)	0.019(4)	0.004(4)
C(10)	0.056(7)	0.023(5)	0.038(6)	-0.002(4)	0.023(5)	0.001(5)
C(11)	0.064(7)	0.023(5)	0.049(6)	-0.006(5)	0.037(6)	-0.006(5)
C(12)	0.043(6)	0.033(5)	0.018(5)	0.001(4)	0.013(4)	-0.009(4)
C(13)	0.031(5)	0.028(5)	0.025(5)	-0.001(4)	0.010(4)	-0.010(4)
C(14)	0.040(5)	0.023(5)	0.014(4)	-0.003(3)	0.017(4)	-0.003(4)
C(15)	0.050(7)	0.042(6)	0.041(6)	-0.017(5)	0.024(5)	-0.025(5)
C(16)	0.041(6)	0.044(6)	0.039(6)	-0.009(5)	0.014(5)	-0.021(5)
C(17)	0.035(5)	0.039(6)	0.028(5)	-0.001(4)	0.012(4)	-0.016(5)
C(18)	0.031(5)	0.045(6)	0.021(5)	0.003(4)	0.005(4)	-0.010(4)
C(19)	0.032(6)	0.070(8)	0.027(5)	0.002(5)	0.008(4)	-0.016(5)
C(20)	0.022(5)	0.089(10)	0.041(6)	0.002(7)	0.002(5)	-0.008(6)
C(21)	0.038(6)	0.072(9)	0.035(6)	0.005(6)	0.015(5)	0.018(6)
C(22)	0.036(6)	0.051(7)	0.028(5)	-0.005(5)	0.003(4)	0.002(5)
O(5)	0.077(7)	0.044(6)	0.124(10)	-0.017(6)	0.031(6)	-0.021(5)
C(23)	0.040(6)	0.028(6)	0.051(7)	0.001(5)	0.001(5)	0.008(5)
C(24)	0.035(5)	0.018(5)	0.040(6)	-0.004(4)	0.000(4)	-0.005(4)
C(25)	0.027(5)	0.034(5)	0.021(5)	-0.004(4)	-0.002(4)	-0.004(4)
C(26)	0.024(5)	0.033(5)	0.027(5)	0.004(4)	0.004(4)	0.003(4)
C(27)	0.023(4)	0.031(5)	0.016(4)	0.000(4)	0.004(3)	0.006(4)
C(28)	0.032(5)	0.026(5)	0.022(5)	0.001(4)	0.009(4)	0.006(4)
C(29)	0.035(5)	0.030(5)	0.029(5)	0.006(4)	0.012(4)	0.007(4)
C(30)	0.040(6)	0.040(6)	0.027(5)	0.009(4)	0.013(4)	0.017(5)
C(31)	0.050(6)	0.027(5)	0.021(5)	0.000(4)	0.023(4)	0.006(4)
C(32)	0.060(7)	0.027(6)	0.051(7)	-0.001(5)	0.035(6)	0.006(5)
C(33)	0.065(8)	0.028(6)	0.058(7)	-0.004(5)	0.039(6)	-0.008(5)
C(34)	0.055(7)	0.034(6)	0.039(6)	-0.006(5)	0.025(5)	-0.007(5)
C(35)	0.037(5)	0.032(5)	0.023(5)	-0.006(4)	0.014(4)	-0.014(4)
C(36)	0.036(5)	0.032(5)	0.014(4)	-0.004(4)	0.010(4)	-0.003(4)
C(37)	0.064(8)	0.026(6)	0.047(7)	-0.009(5)	0.017(6)	-0.028(5)
C(38)	0.042(6)	0.046(7)	0.031(5)	-0.010(5)	0.008(5)	-0.022(5)
C(39)	0.038(6)	0.038(6)	0.027(5)	-0.003(4)	0.007(4)	-0.022(5)
C(40)	0.036(5)	0.042(6)	0.015(4)	0.002(4)	0.006(4)	-0.010(5)
C(41)	0.033(6)	0.062(8)	0.031(6)	-0.006(5)	0.005(4)	-0.027(5)
C(42)	0.035(6)	0.077(9)	0.028(6)	-0.004(6)	0.005(5)	-0.014(6)
C(43)	0.035(6)	0.071(8)	0.025(5)	-0.008(5)	0.011(4)	0.001(5)
C(44)	0.024(5)	0.055(7)	0.028(5)	-0.004(5)	0.002(4)	-0.004(5)

Mass spectrometry proved to be a useful tool to complement the x-ray crystallography results. The full spectrum of the $[Pb(DPP)(ClO_4)(H_2O)](ClO_4)$ crystal is shown in Figure 60 and expanded peaks at m/z = 540, and 641 are shown in Figure 61. The software iMass was used to predict peaks taking into account the abundance of different isotopes. The molecular mass of the complex with no perchlorate or water molecules attached to the lead is 542 g/mol. The summary of data obtained from iMass is shown in Table 41.

Table 41. Calculation of monoisotopic mass (^{208}Pb), average mass, and percent composition by iMass.

Formula	**$C_{22}H_{14}N_4Pb$**
Average Mass	541.5801
Monoisotopic Mass	542.0985

Composition (weight):
N:10.3451% **Pb:** 38.2584% **C:** 48.7909% **H:** 2.6056%

iMass was then used to predict the peak distributions based on the relative abundance of lead isotopes and compared to the mass spectrum of the $[Pb(DPP)(ClO_4)(H_2O)](ClO_4)$. Table 42 is a summary of the relative abundance and masses of the different isotopes of lead (Lide, 1993) and Figure 62 is the predicted mass distributions for a) $[Pb(DPP)]^{2+}$ and b) $[Pb(DPP)ClO_4]^{+}$. There was good agreement between the predicted spectra and the actual spectra. There are four major peaks corresponding to $[Pb(DPP)]^{2+}$ and the relative abundance of these peaks are the same as those predicted by iMass. The same was concluded for the five major peaks corresponding to $[Pb(DPP)ClO_4]^{+}$.

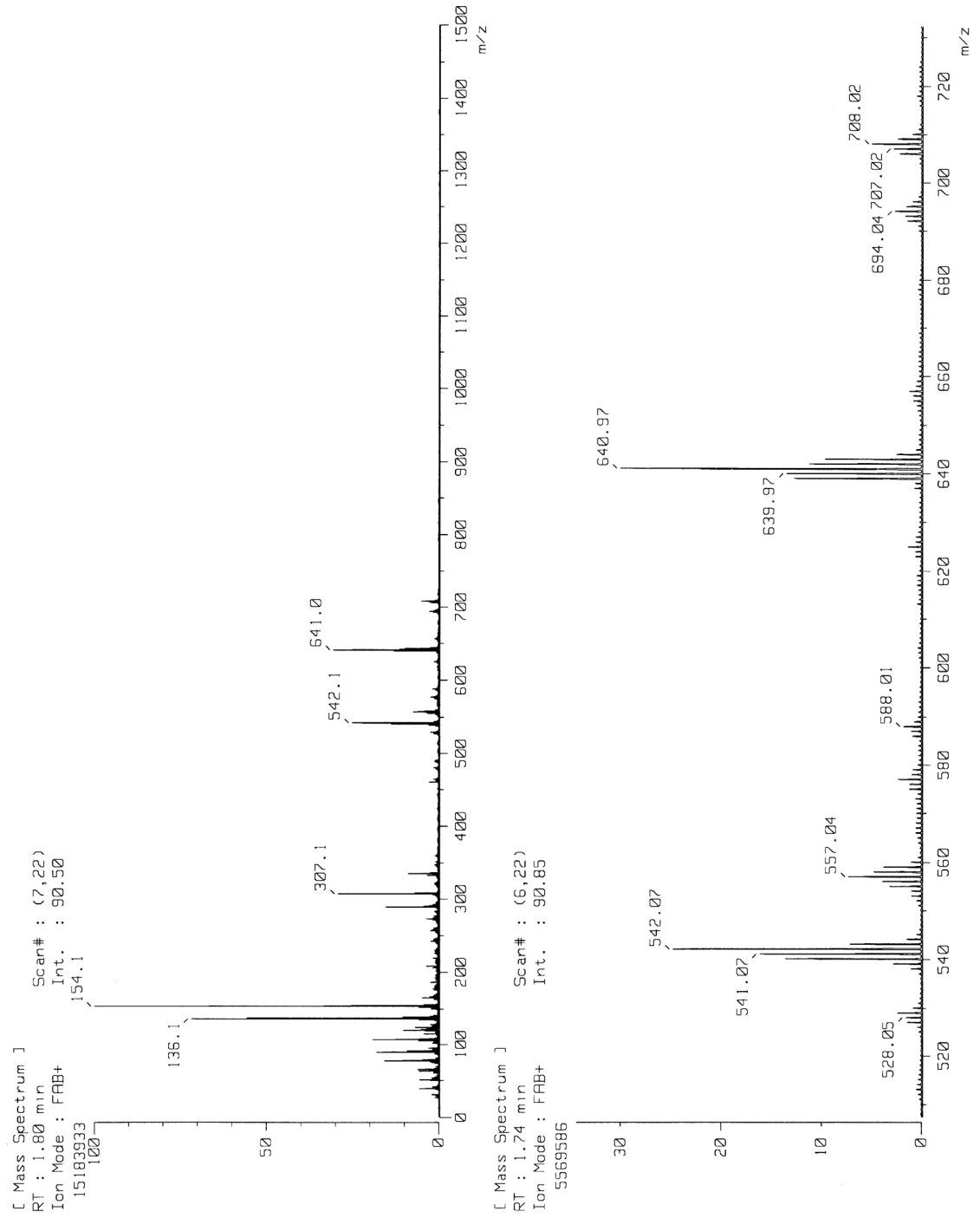

Figure 60. Mass spectrum of $[Pb(DPP)(ClO_4)(H_2O)](ClO_4)$.

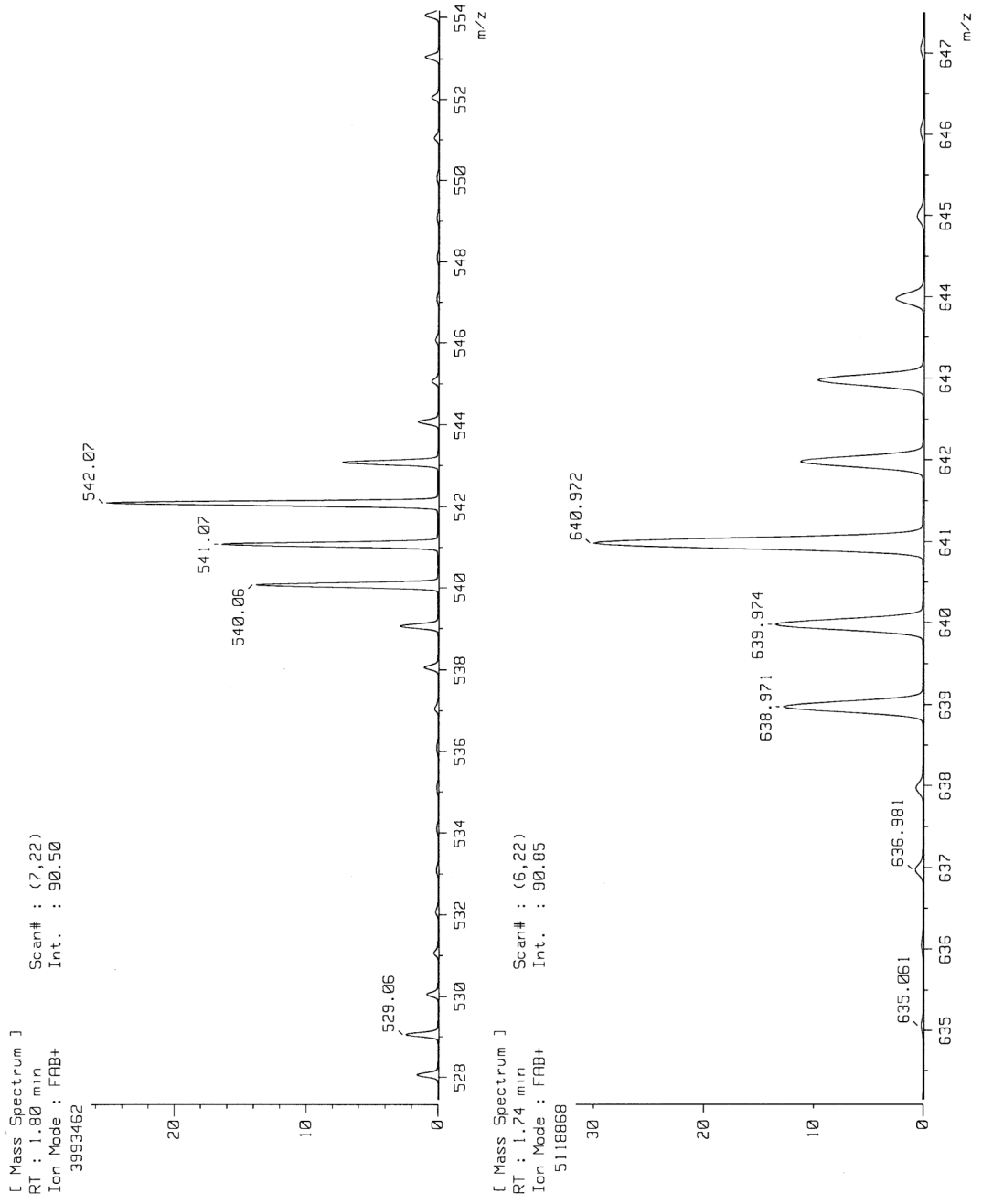

Figure 61. Expanded view of $[Pb(DPP)]^{2+}$ and $[Pb(DPP)ClO_4]^{+}$ mass spectra.

Table 42. Summary of lead isotopes and relative abundance.

#	Abundance	Mass
204	1.4000 %	203.97302000
206	24.1000 %	205.97444000
207	22.1000 %	206.97587200
208	52.4000 %	207.97662700

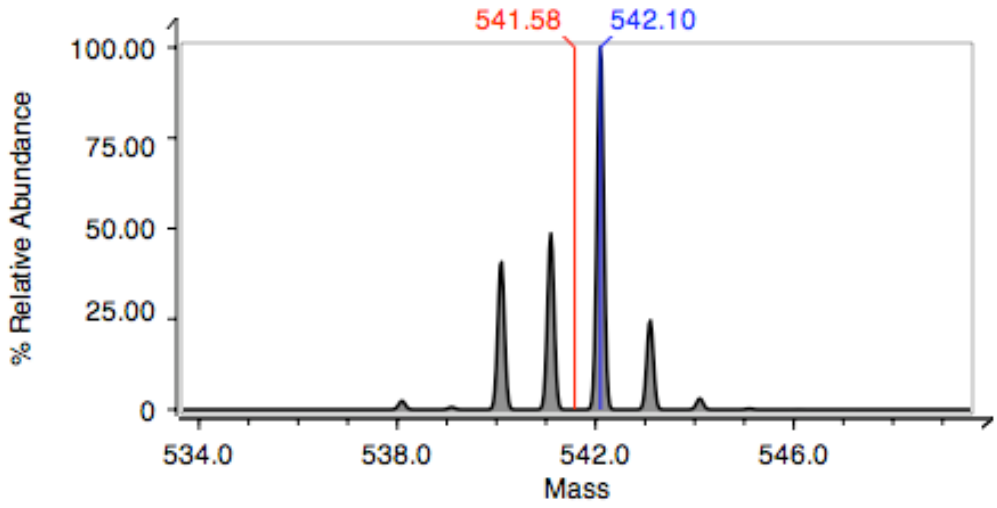

a)

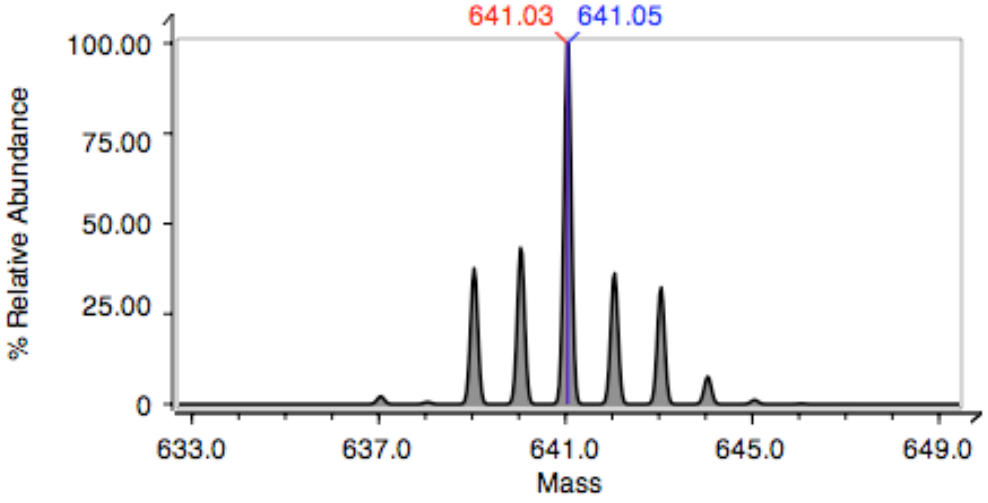

b)

Figure 62. Mass distribution based on relative abundance of isotopes predicted by iMass for a) $[Pb(DPP)]^{2+}$ and b) $[Pb(DPP)ClO_4]^{+}$.

$[Hg_2(DPP)_2(ClO_4)_4]$

The crystals formed on the interface of the butanol/H_2O layers were thin, yellow, and fibrous. Figure 63 is a microscopic photograph of the crystals synthesized. Crystal structures were determined by both x-ray crystallography and mass spectrometry. The crystal structure of $[Hg_2(DPP)_2(ClO_4)_4]$ consists of a mercury metal ion coordinated with one DPP molecule through all four donor atoms along with three perchlorate molecule as in Figure 64. The mercury was coordinated to all four neutral nitrogen donor atoms of DPP, giving it a coordination number of eight including the coordinated perchlorate molecules. A 3D representation of the mercury complex is shown in Figure 65 to show how the three perchlorate molecules are bound to the mercury ion.

The crystal data and structural refinement parameters for the $[Hg_2(DPP)_2(ClO_4)_4]$ complex are listed in Table 43. The bond distances and angles for the complex are shown in Table 44 and 45 respectively. In addition, the spatial coordinates of the atoms for the $[Hg_2(DPP)_2(ClO_4)_4]$ complex are given in Tables 46 and 47. The bond distances between the mercury and nitrogens of DPP were 2.249, 2.258, 2.397, and 2.425 Å. These were compared to an average Hg-N bond length of 2.4 ± 0.1 Å determined by 19 structures containing bipyridyl and mercury from the Cambridge Crystallographic Database. The measured Hg-N bond lengths were in good agreement with the expected average bond length.

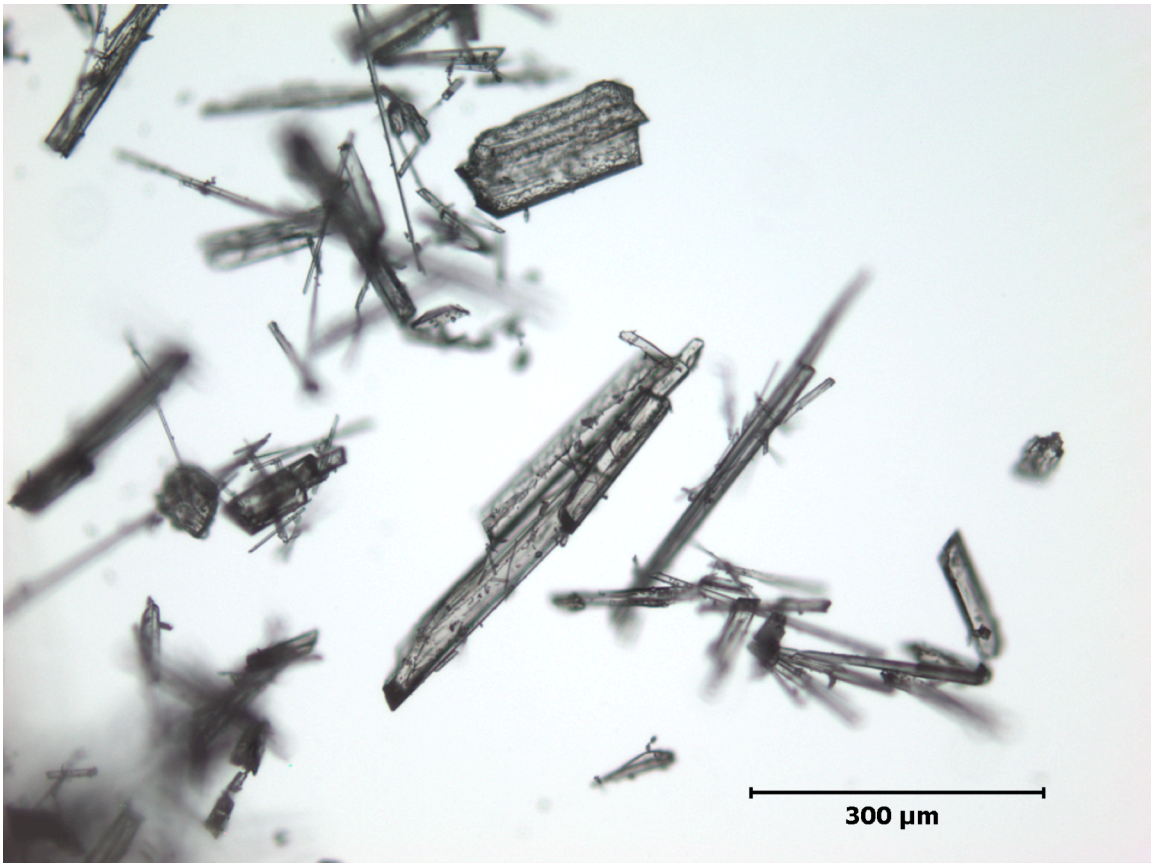

Figure 63. Microscopic view (10x) of crystals formed from equimolar amounts of DPP and $Hg(ClO_4)_2$.

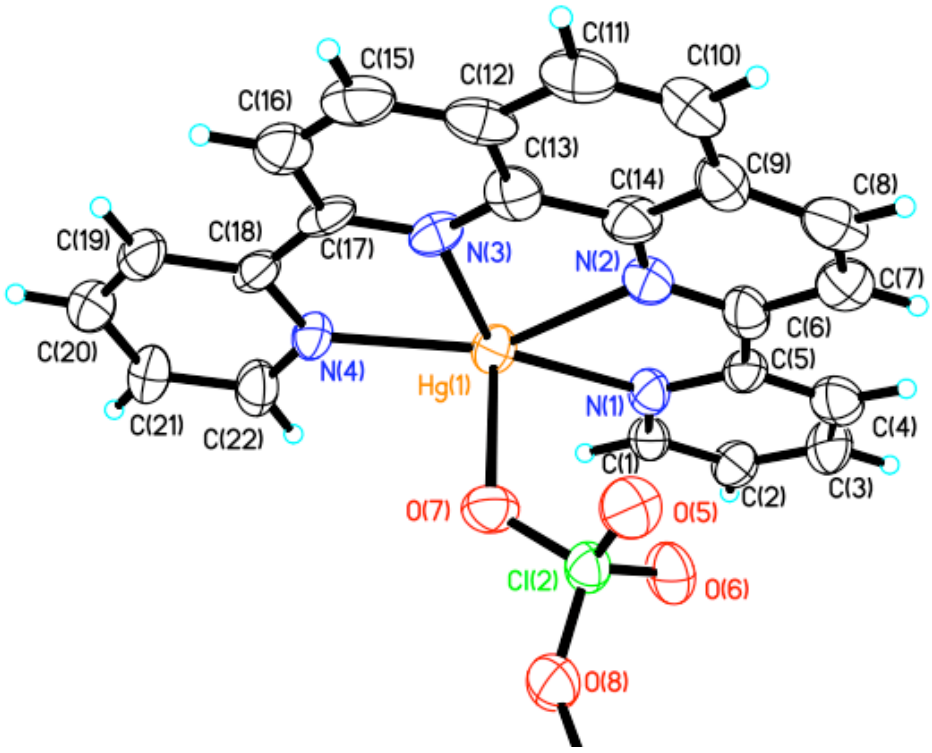

Figure 64. Structure of $[Hg_2(DPP)_2(ClO_4)_4]$ as determined by X-ray crystallography.

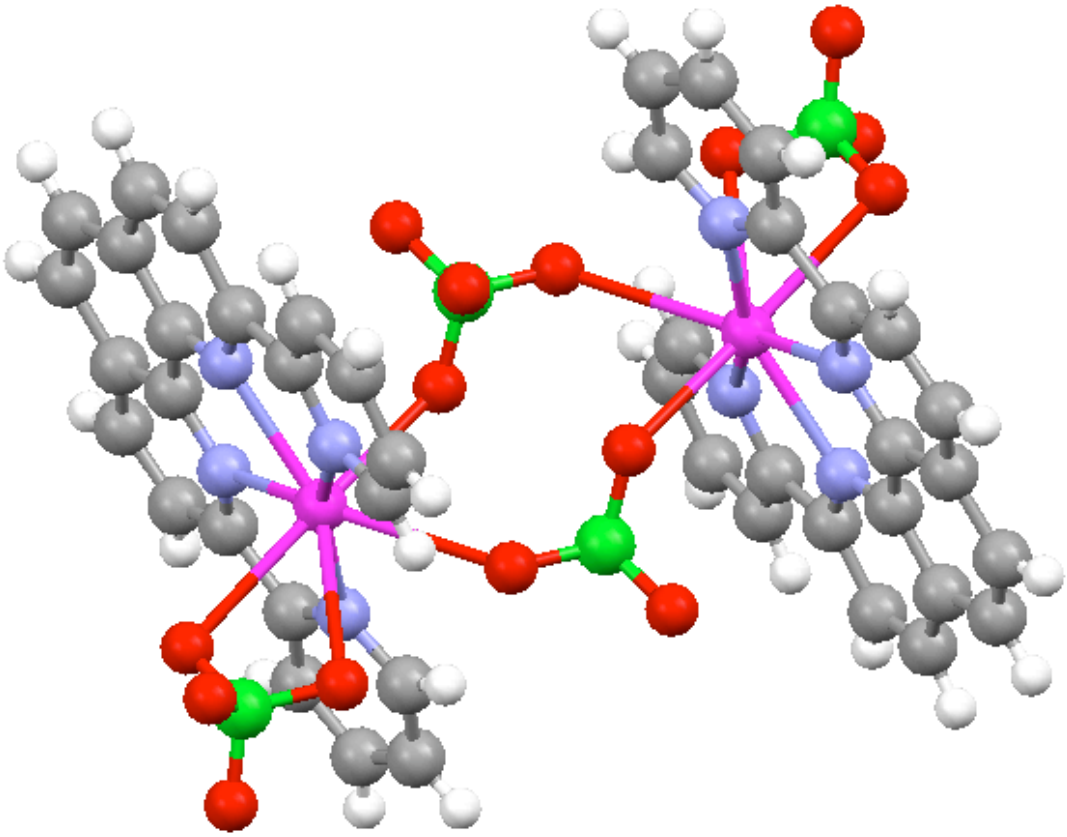

Figure 65. Three-dimensional view of mercury crystals to better show coordinated perchlorate molecules.

Table 43. Crystal data and structure refinement for the $[Hg_2(DPP)_2(ClO_4)_4]$ complex.

Identification code	dpphg	
Empirical formula	C22 H14 Cl2 Hg N4 O8.50	
Formula weight	741.86	
Temperature	153(2) K	
Wavelength	0.71073 Å	
Crystal system	Monoclinic	
Space group	P 2_1/c	
Unit cell dimensions	a = 13.651(3) Å	α= 90.00°
	b = 11.338(2) Å	β= 107.58(3)°
	c = 15.033(3) Å	γ = 90.00°
Volume	2218.1(8) $Å^3$	
Z	4	
Density (calculated)	2.222 Mg/m^3	
Absorption coefficient	0.724 mm^{-1}	
F(000)	1424	
Theta range for data collection	3.52 to 25.05°	
Index ranges	$-16 \leq h \leq 16$, $-13 \leq k \leq 13$, $-17 \leq l \leq 15$	
Reflections collected	3920	
Independent reflections	3179 [R(int) = 0.0871]	
Completeness to theta = 25.05°	99.7 %	
Absorption correction	Semi-empirical from equivalents	
Max. and min. transmission	0.9283 and 0.9148	
Refinement method	Full-matrix least-squares on F^2	
Data / restraints / parameters	3920 / 0 / 344	
Goodness-of-fit on F^2	1.113	
Final R indices [I>2sigma(I)]	R1 = 0.0652, wR2 = 0.1622	
R indices (all data)	R1 = 0.0803, wR2 = 0.1791	
Largest diff. peak and hole	4.029 and -2.310 $e.Å^{-3}$	

Table 44. Bond lengths of $[Hg_2(DPP)_2(ClO_4)_4]$ complex.

Bond	Bond Length (Å)
Hg(1)-N(1)	2.249(10)
Hg(1)-N(4)	2.258(10)
Hg(1)-N(3)	2.397(9)
Hg(1)-N(2)	2.425(11)
Hg(1)-O(7)	2.653(8)
N(1)-C(1)	1.342(15)
N(1)-C(5)	1.354(15)
N(2)-C(6)	1.306(17)
N(2)-C(14)	1.326(16)
N(3)-C(17)	1.316(16)
N(3)-C(13)	1.340(17)
N(4)-C(22)	1.349(18)
N(4)-C(18)	1.356(15)
C(1)-C(2)	1.368(18)
C(2)-C(3)	1.378(19)
C(3)-C(4)	1.37(2)
C(4)-C(5)	1.378(19)
C(5)-C(6)	1.496(18)
C(6)-C(7)	1.426(18)
C(7)-C(8)	1.34(2)
C(8)-C(9)	1.45(2)
C(9)-C(14)	1.399(18)
C(9)-C(10)	1.436(19)
C(10)-C(11)	1.33(2)
C(11)-C(12)	1.44(2)
C(12)-C(13)	1.402(19)
C(12)-C(15)	1.40(2)
C(13)-C(14)	1.447(19)
C(15)-C(16)	1.34(2)
C(16)-C(17)	1.402(17)
C(17)-C(18)	1.510(19)
C(18)-C(19)	1.407(18)
C(19)-C(20)	1.36(2)
C(20)-C(21)	1.40(2)
C(21)-C(22)	1.384(18)

Table 45. Bond angles of $[Hg_2(DPP)_2(ClO_4)_4]$.

Bond	Bond Angle (°)	Bond	Bond Angle (°)
N(1)-Hg(1)-N(4)	155.2(4)	N(1)-C(5)-C(4)	121.5(11)
N(1)-Hg(1)-N(3)	135.3(4)	N(1)-C(5)-C(6)	116.4(10)
N(4)-Hg(1)-N(3)	68.9(3)	C(4)-C(5)-C(6)	122.2(11)
N(1)-Hg(1)-N(2)	68.9(4)	N(2)-C(6)-C(7)	120.0(13)
N(4)-Hg(1)-N(2)	135.7(4)	N(2)-C(6)-C(5)	114.7(11)
N(3)-Hg(1)-N(2)	66.8(4)	C(7)-C(6)-C(5)	125.3(12)
N(1)-Hg(1)-O(7)	97.5(3)	C(8)-C(7)-C(6)	118.1(14)
N(4)-Hg(1)-O(7)	90.4(3)	C(7)-C(8)-C(9)	123.0(13)
N(3)-Hg(1)-O(7)	82.5(3)	C(14)-C(9)-C(10)	117.5(12)
N(2)-Hg(1)-O(7)	82.9(3)	C(14)-C(9)-C(8)	112.9(12)
O(5)-Cl(2)-O(6)	111.1(6)	C(10)-C(9)-C(8)	129.6(12)
O(5)-Cl(2)-O(7)	108.9(6)	C(11)-C(10)-C(9)	121.8(13)
O(6)-Cl(2)-O(7)	109.7(6)	C(10)-C(11)-C(12)	123.4(13)
O(5)-Cl(2)-O(8)	109.3(6)	C(13)-C(12)-C(15)	117.4(12)
O(6)-Cl(2)-O(8)	109.6(6)	C(13)-C(12)-C(11)	115.7(14)
O(7)-Cl(2)-O(8)	108.2(5)	C(15)-C(12)-C(11)	126.9(13)
Cl(2)-O(7)-Hg(1)	126.3(5)	N(3)-C(13)-C(12)	120.8(13)
Cl(2)-O(8)-O(9)	142.5(9)	N(3)-C(13)-C1(4)	117.6(11)
C(1)-N(1)-C(5)	117.3(10)	C(12)-C(13)-C(14)	121.5(13)
C(1)-N(1)-Hg(1)	121.2(8)	N(2)-C(14)-C(9)	123.9(13)
C(5)-N(1)-Hg(1)	121.5(8)	N(2)-C(14)-C(13)	116.2(12)
C(6)-N(2)-C(14)	122.1(12)	C(9)-C(14)-C1(3)	119.8(12)
C(6)-N(2)-Hg(1)	117.7(9)	C(16)-C(15)-C(12)	120.4(14)
C(14)-N(2)-Hg(1)	119.7(9)	C(15)-C(16)-C(17)	119.3(14)
C(17)-N(3)-C(13)	121.0(11)	N(3)-C(17)-C(16)	121.0(12)
C(17)-N(3)-Hg(1)	119.3(8)	N(3)-C(17)-C(18)	114.1(10)
C(13)-N(3)-Hg(1)	119.4(8)	C(16)-C(17)-C(18)	124.9(12)
C(22)-N(4)-C(18)	118.5(11)	N(4)-C(18)-C(19)	122.4(13)
C(22)-N(4)-Hg(1)	119.6(8)	N(4)-C(18)-C(17)	115.6(11)
C(18)-N(4)-Hg(1)	121.8(8)	C(19)-C(18)-C(17)	122.1(12)
N(1)-C(1)-C(2)	124.2(11)	C(20)-C(19)-C(18)	118.0(13)
C(1)-C(2)-C(3)	117.6(12)	C(19)-C(20)-C(21)	120.2(13)
C(4)-C(3)-C(2)	119.7(12)	C(22)-C(21)-C(20)	119.2(13)
C(3)-C(4)-C(5)	119.7(13)	N(4)-C(22)-C(21)	121.5(13)

Symmetry transformations used to generate equivalent atoms

1: -x, -y+½, z+½ **2:** -x, -y+½, z-½ **3:** -x, -y+1, z

Table 46. Atomic coordinates and equivalent isotropic displacement parameters ($Å^2$) for $[Hg_2(DPP)_2(ClO_4)_4]$. U(eq) is defined as one third of the trace of the orthogonalized U^{ij} tensor.

	x	y	z	U(eq)
Hg(1)	0.26450(3)	0.56437(4)	-0.12026(3)	0.0350(3)
Cl(2)	0.5246(2)	0.6820(3)	-0.00663(19)	0.0358(6)
O(5)	0.5101(7)	0.8062(8)	-0.0079(7)	0.049(2)
O(6)	0.5369(8)	0.6414(9)	-0.0930(6)	0.048(2)
O(7)	0.4368(6)	0.6253(7)	0.0093(6)	0.043(2)
O(8)	0.6151(7)	0.6513(9)	0.0697(6)	0.050(2)
N(1)	0.3304(8)	0.5455(9)	-0.2398(7)	0.036(2)
N(2)	0.2857(8)	0.7551(10)	-0.1850(7)	0.040(2)
N(3)	0.1956(7)	0.7238(8)	-0.0532(7)	0.033(2)
N(4)	0.1980(7)	0.4986(9)	-0.0089(7)	0.035(2)
C(1)	0.3470(9)	0.4389(10)	-0.2711(8)	0.033(2)
C(2)	0.3869(10)	0.4210(11)	-0.3433(9)	0.041(3)
C(3)	0.4147(11)	0.5192(13)	-0.3841(9)	0.046(3)
C(4)	0.4002(10)	0.6292(12)	-0.3528(10)	0.047(3)
C(5)	0.3558(9)	0.6409(11)	-0.2822(8)	0.034(2)
C(6)	0.3348(10)	0.7588(12)	-0.2472(8)	0.041(3)
C(7)	0.3598(10)	0.8697(11)	-0.2795(9)	0.043(3)
C(8)	0.3341(11)	0.9682(12)	-0.2421(10)	0.051(3)
C(9)	0.2777(10)	0.9665(12)	-0.1747(9)	0.043(3)
C(10)	0.2403(12)	1.0629(11)	-0.1322(10)	0.048(3)
C(11)	0.1897(11)	1.0454(12)	-0.0706(10)	0.051(4)
C(12)	0.1733(10)	0.9305(10)	-0.0368(10)	0.045(3)
C(13)	0.2088(10)	0.8349(12)	-0.0777(8)	0.042(3)
C(14)	0.2582(10)	0.8522(11)	-0.1494(10)	0.042(3)
C(15)	0.1277(11)	0.9050(14)	0.0331(10)	0.053(4)
C(16)	0.1180(10)	0.7929(12)	0.0581(9)	0.044(3)
C(17)	0.1538(8)	0.7015(12)	0.0133(8)	0.037(3)
C(18)	0.1499(9)	0.5721(12)	0.0357(8)	0.038(3)
C1(9)	0.1007(10)	0.5308(15)	0.0996(8)	0.048(3)
C(20)	0.1016(10)	0.4128(13)	0.1158(10)	0.047(3)
C(21)	0.1547(10)	0.3369(12)	0.0735(9)	0.042(3)
C(22)	0.2029(10)	0.3827(13)	0.0122(9)	0.046(3)

Table 47. Anisotropic displacement parameters ($Å^2$) for $[Hg_2(DPP)_2(ClO_4)_4]$. The anisotropic displacement factor exponent takes the form: $-2\pi^2[h^2 a^{*2}U^{11} + ... + 2 h k a^* b^* U^{12}]$.

	U^{11}	U^{22}	U^{33}	U^{23}	U^{13}	U^{12}
Hg(1)	0.0370(4)	0.0369(3)	0.0332(3)	-0.00315(17)	0.0140(2)	-0.00127(17)
Cl(1)	0.0370(15)	0.0431(15)	0.0359(15)	-0.0044(12)	0.0124(12)	0.0036(12)
O(5)	0.052(5)	0.035(4)	0.062(6)	0.000(4)	0.017(5)	-0.003(4)
O(6)	0.060(6)	0.058(5)	0.028(4)	0.000(4)	0.015(4)	-0.002(5)
O(7)	0.033(4)	0.043(5)	0.049(5)	0.004(4)	0.005(4)	-0.001(4)
O(8)	0.043(5)	0.071(6)	0.033(5)	0.004(4)	0.008(4)	-0.005(5)
N(1)	0.034(5)	0.051(6)	0.023(5)	0.001(4)	0.008(4)	-0.003(4)
N(2)	0.035(5)	0.047(6)	0.035(5)	0.005(4)	0.006(4)	0.002(4)
N(3)	0.024(4)	0.033(5)	0.042(6)	-0.006(4)	0.008(4)	-0.002(4)
N(4)	0.035(5)	0.047(6)	0.029(5)	0.000(4)	0.016(4)	0.002(4)
C(1)	0.037(6)	0.041(6)	0.023(5)	-0.001(4)	0.011(5)	0.004(5)
C(2)	0.043(7)	0.045(7)	0.039(7)	-0.001(5)	0.019(6)	0.008(5)
C(3)	0.052(8)	0.060(8)	0.033(7)	-0.004(6)	0.022(6)	0.002(7)
C(4)	0.040(7)	0.053(8)	0.040(7)	0.004(6)	0.002(6)	-0.004(6)
C(5)	0.031(6)	0.046(6)	0.028(6)	0.000(5)	0.011(5)	0.004(5)
C(6)	0.037(7)	0.051(7)	0.030(6)	0.006(5)	0.003(5)	-0.010(5)
C(7)	0.035(6)	0.045(7)	0.043(7)	-0.004(5)	0.001(5)	-0.009(5)
C(8)	0.045(8)	0.041(7)	0.055(9)	0.006(6)	-0.002(6)	0.001(6)
C(9)	0.043(7)	0.042(6)	0.038(7)	0.006(5)	0.004(5)	-0.004(5)
C(10)	0.060(8)	0.038(7)	0.038(7)	0.003(5)	0.006(6)	0.007(6)
C(11)	0.044(7)	0.052(8)	0.042(8)	-0.010(6)	-0.006(6)	0.008(6)
C(12)	0.035(7)	0.038(7)	0.047(8)	-0.004(5)	-0.010(6)	0.002(5)
C(13)	0.042(7)	0.052(7)	0.028(6)	-0.007(5)	0.002(5)	0.000(6)
C(14)	0.045(7)	0.036(6)	0.047(7)	-0.003(5)	0.016(6)	0.014(5)
C(15)	0.037(7)	0.066(9)	0.047(8)	-0.010(7)	0.000(6)	0.012(6)
C(16)	0.031(6)	0.058(8)	0.038(7)	-0.001(6)	0.004(5)	-0.001(5)
C(17)	0.022(5)	0.059(7)	0.028(6)	-0.018(5)	0.005(4)	0.010(5)
C(18)	0.023(5)	0.067(8)	0.025(6)	-0.004(5)	0.008(5)	0.007(5)
C(19)	0.034(6)	0.084(10)	0.025(6)	-0.005(6)	0.010(5)	0.005(7)
C(20)	0.039(7)	0.058(8)	0.047(8)	0.009(6)	0.016(6)	-0.001(6)
C(21)	0.046(7)	0.046(7)	0.039(7)	-0.005(5)	0.021(6)	-0.012(6)
C(22)	0.044(7)	0.064(8)	0.031(6)	0.000(6)	0.014(6)	-0.009(6)

Mass spectrometry was again utilized to complement the x-ray crystal structure. The full spectrum of the $[Hg_2(DPP)_2(ClO_4)_4]$ crystal is shown in Figure 66 and expanded peaks at m/z = 540 are shown in Figure 67. The software iMass was used to predict peaks taking into account the abundance of different isotopes. The molecular mass of the complex with no perchlorate molecules attached to the lead is 536 g/mol. The summary of data obtained from iMass is shown in Table 48.

Table 48. Calculation of monoisotopic mass (^{202}Hg), average mass, and percent composition of [Hg(DPP)] by iMass.

Formula	**$C_{22}H_{14}N_4Hg$**
Average Mass	534.9701
Monoisotopic Mass	536.0925

Composition (weight):
N: 10.4729% **Hg:** 37.4956% **C:** 49.3938% **H:** 2.6377%

iMass was then used to predict the peak distributions based on the relative abundance of mercury isotopes and compared to the mass spectrum of the $[Hg_2(DPP)_2(ClO_4)_4]$. Table 49 is a summary of the relative abundance and masses of the different isotopes of mercury (Lide, 1993) and Figure 68 is the predicted mass distributions for $[Hg(DPP)]^{2+}$. There was good agreement between the predicted spectra and the actual spectra. There are seven major peaks corresponding to $[Hg(DPP)]^{2+}$ and the relative abundance of these peaks are the same as those predicted by iMass.

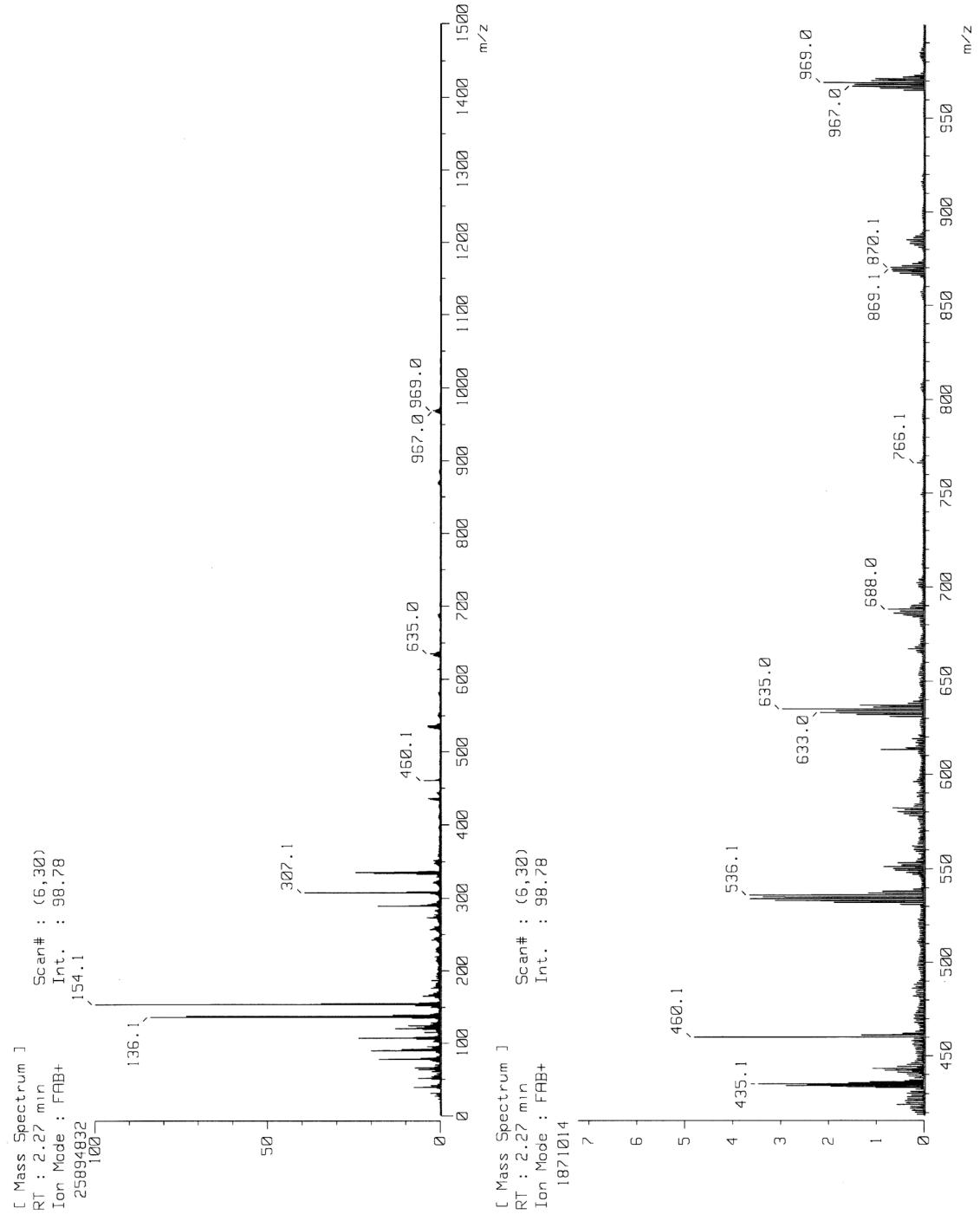

Figure 66. $[Hg_2(DPP)_2(ClO_4)_4]$.

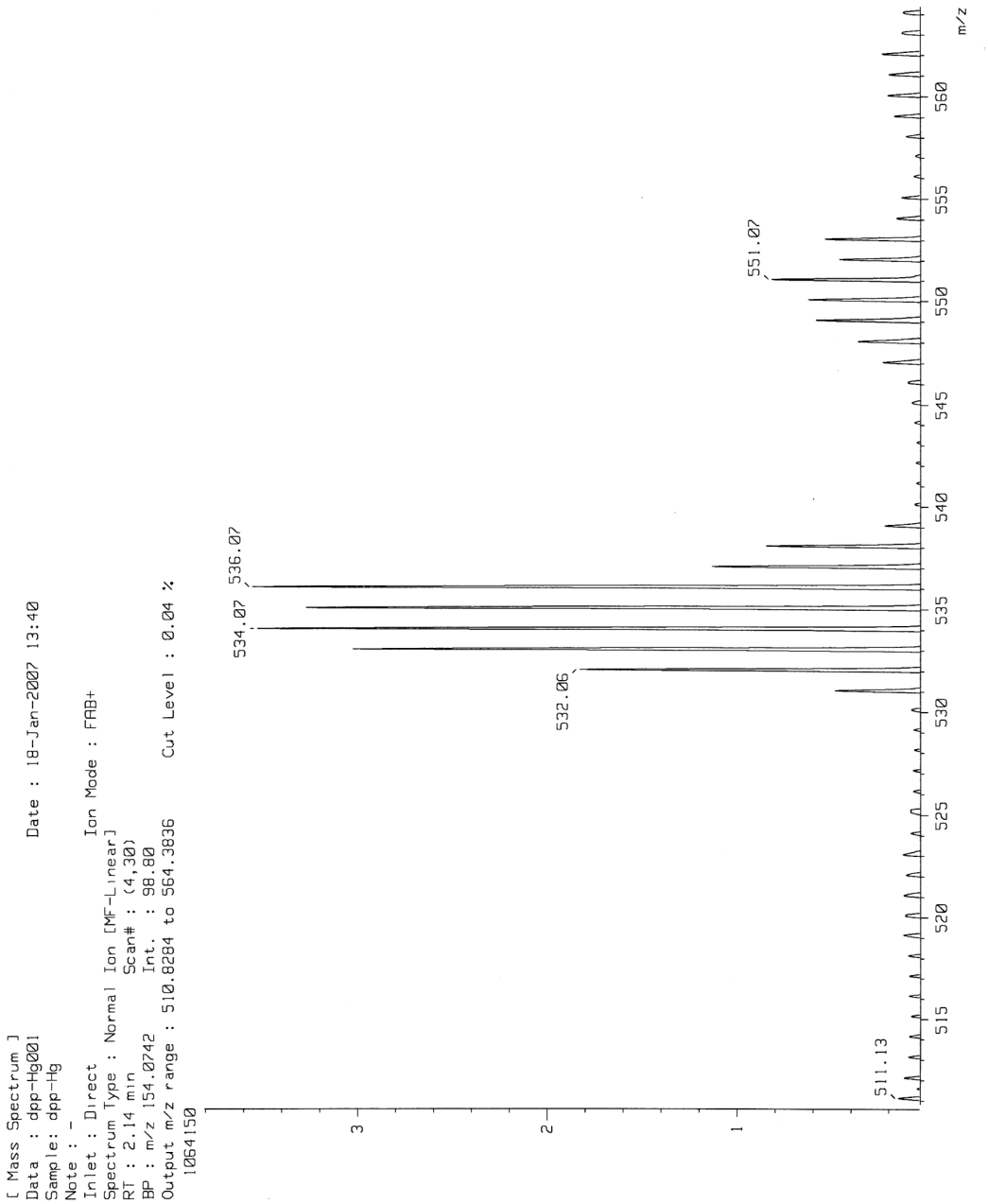

Figure 67. Expanded view of $[Hg(DPP)]^{2+}$ mass spectrum.

Table 49. Summary of mercury isotopes and relative abundance.

#	Abundance	Mass
196	0.1500 %	195.96580700
198	9.9700 %	197.96674300
199	16.8700 %	198.96825400
200	23.1000 %	199.96830000
201	13.1800 %	200.97027700
202	29.8600 %	201.97061700
204	6.8700 %	203.97346700

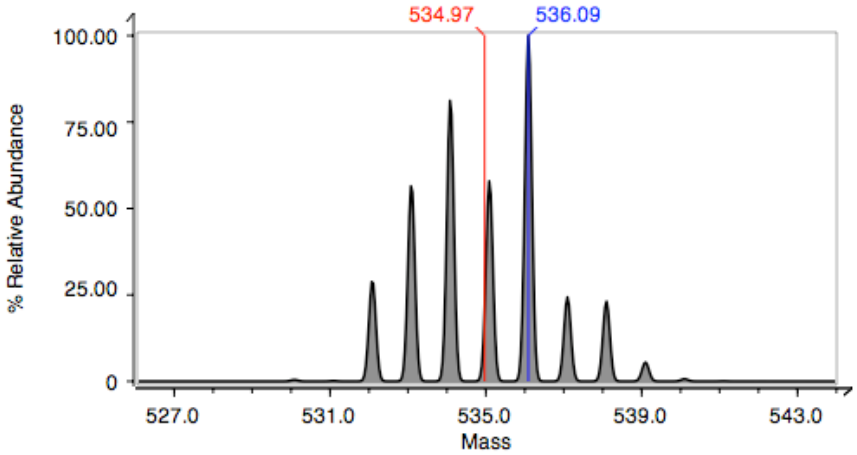

Figure 68. Mass distribution based on relative abundance of isotopes predicted by iMass for $[Hg(DPP)]^{2+}$.

$[Cd(DPP)_2](ClO_4)_2$

The crystals formed on the interface of the butanol/H_2O layers were yellow and cubic. Figure 69 is a microscopic photograph of the crystals synthesized. Crystal structures were determined by both x-ray crystallography and mass spectrometry. The crystal structure of $[Cd(DPP)_2](ClO_4)_2$ consists of a cadmium metal ion coordinated to two DPP molecules through all eight donor atoms as in Figure 70. The cadmium was coordinated to all eight neutral nitrogen donor atoms of the two DPP molecules, giving it a coordination number of eight. A 3D representation of the cadmium complex is shown in Figure 71. From this view the effect the van der wals forces have on the molecule are apparent. The two DPP molecules do not attach flat onto the molecule like the structures for lead and mercury. Van der Wals forces between the pyridine rings and the phenantholine backbone of the other molecule make the conformation of the structure twisted or propeller-like. Figure 72 and 73 are views of the unit cell showing the ionic radii spacefill model and the arrangement of molecules respectively.

The crystal data and structural refinement parameters for the $[Cd(DPP)_2](ClO_4)_2$ complex are listed in Table 50. The bond distances and angles for the $[Cd(DPP)_2](ClO_4)_2$ complex are shown in Table 51 and 52 respectively. In addition, the spatial coordinates of the atoms for the $[Cd(DPP)_2](ClO_4)_2$ complex are given in Tables 53 and 54. The bond distances between the cadmium and nitrogens of one DPP were 2.412 Å, and 2.559 Å for the second DPP molecule. These were compared to an average Cd-N bond length of 2.36 $\pm$ 0.05 Å determined by 84 structures containing bipyridyl and cadmium from the Cambridge Crystallographic Database. The measured Cd-N bond lengths were in good agreement with the expected average bond length.

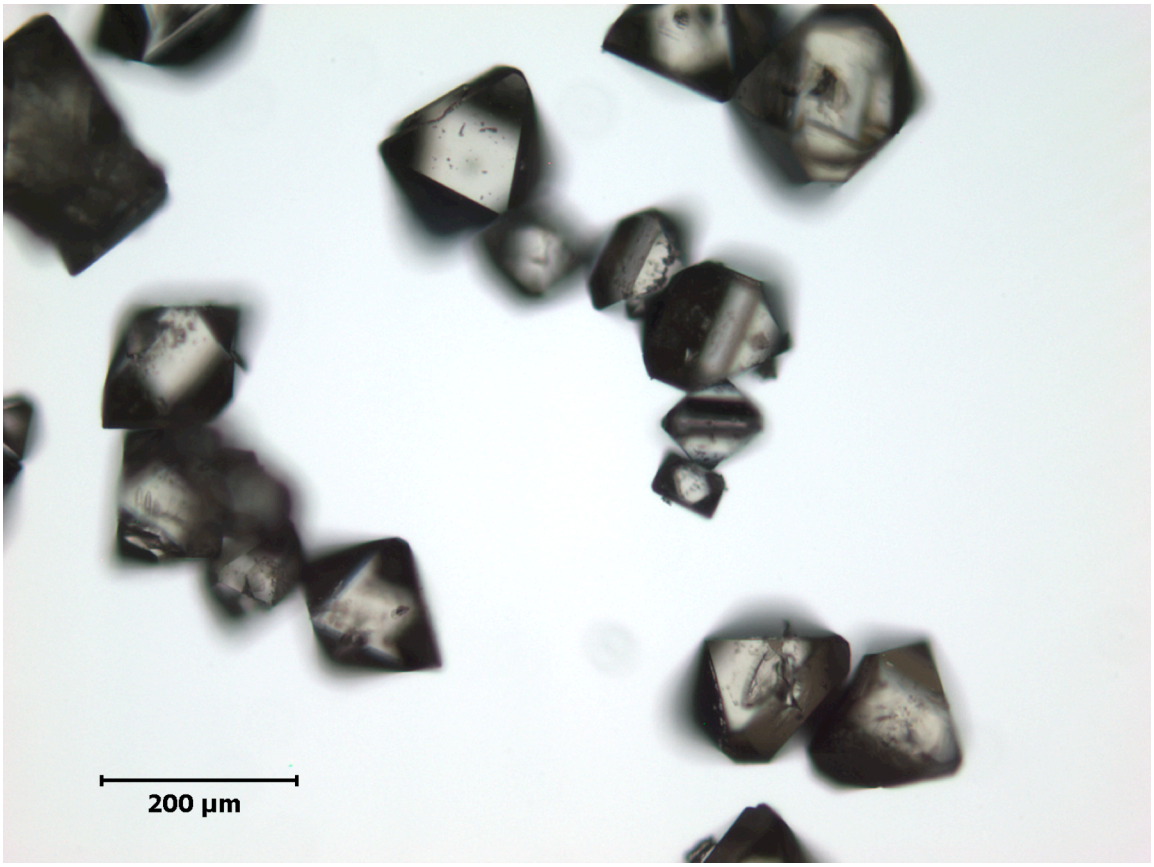

Figure 69. Microscopic view (10x) of crystals formed with equimolar amounts of DPP and $Cd(ClO_4)_2$

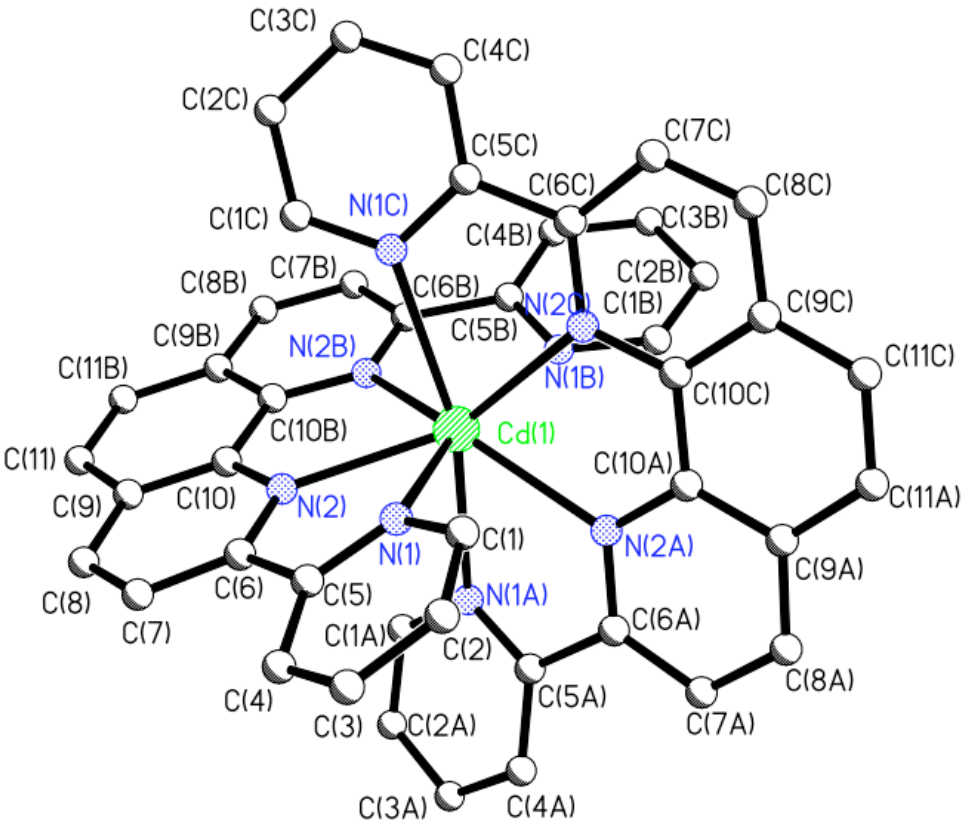

Figure 70. Molecular structure of $[Cd(DPP)_2](ClO_4)_2$ as determined by x-ray crystallography.

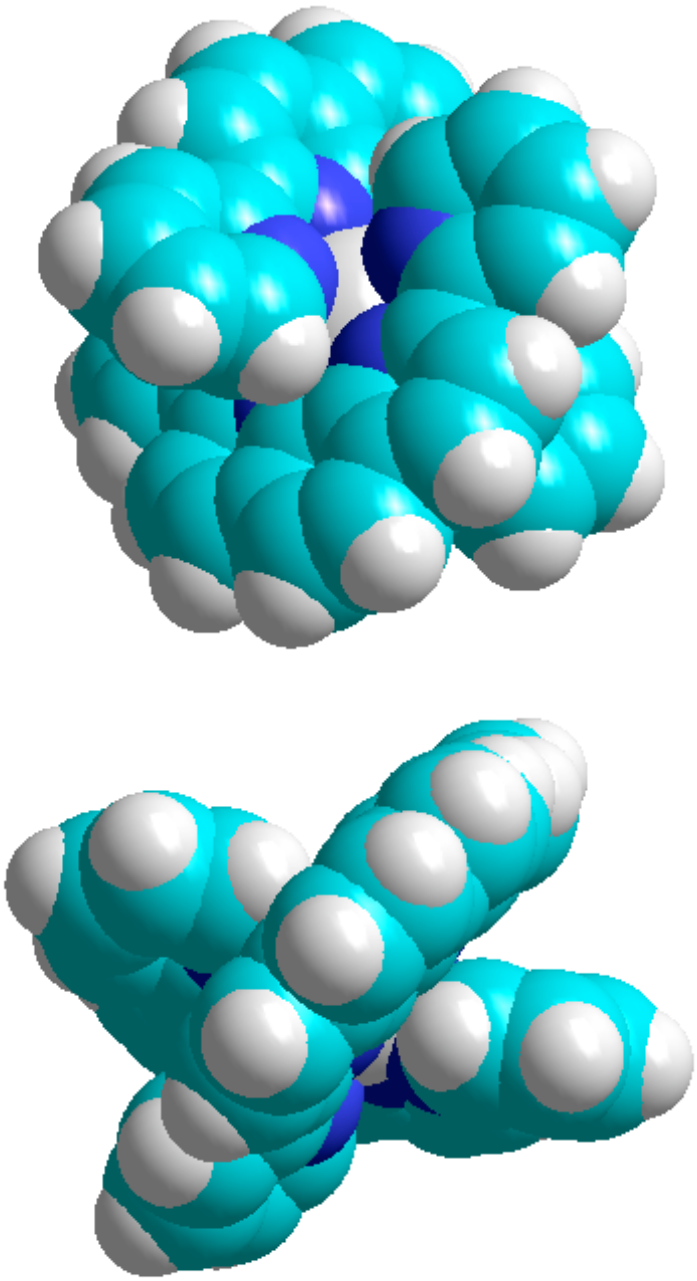

Figure 71. Three dimensional view of $[Cd(DPP)_2](ClO_4)_2$ crystal structure without perchlorate counter ions from two different angels to show structural properties.

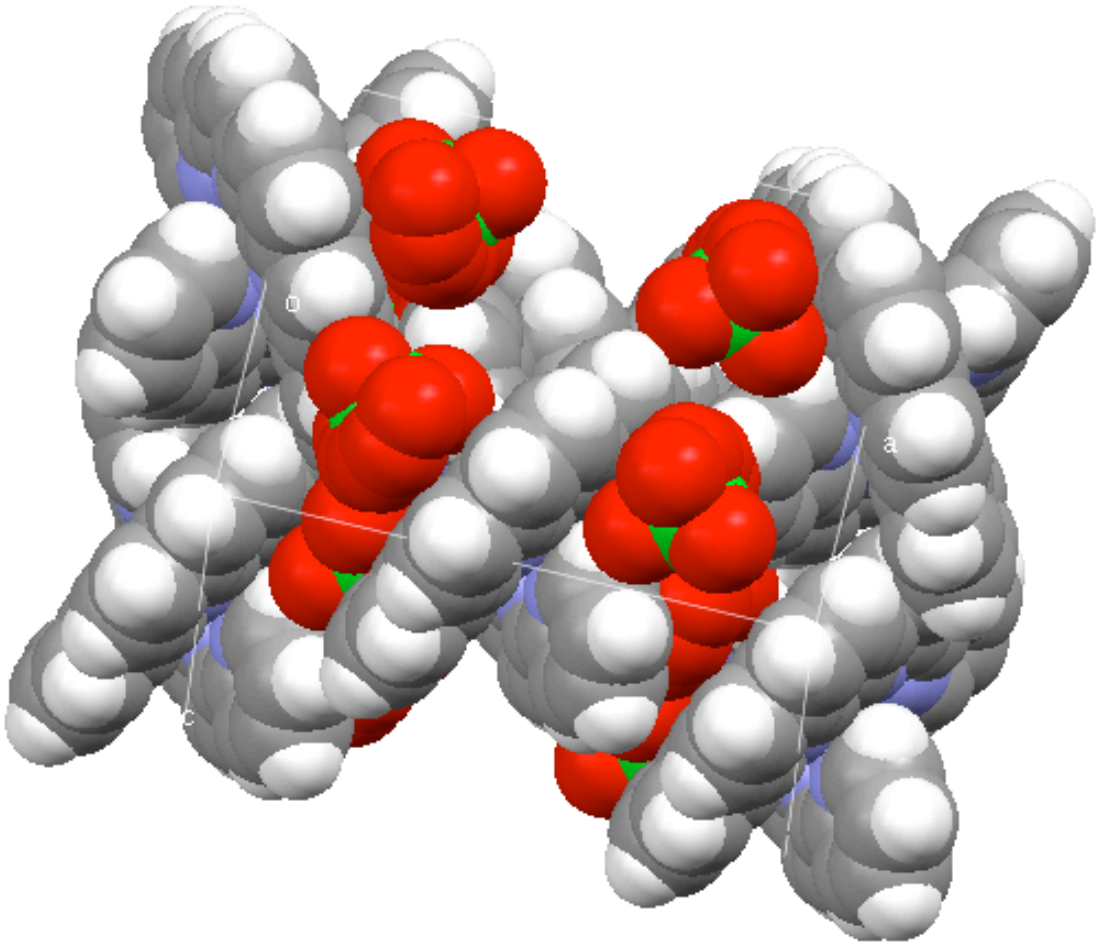

Figure 72. Space filling view of $[Cd(DPP)_2](ClO_4)_2$ unit cell along x axis.

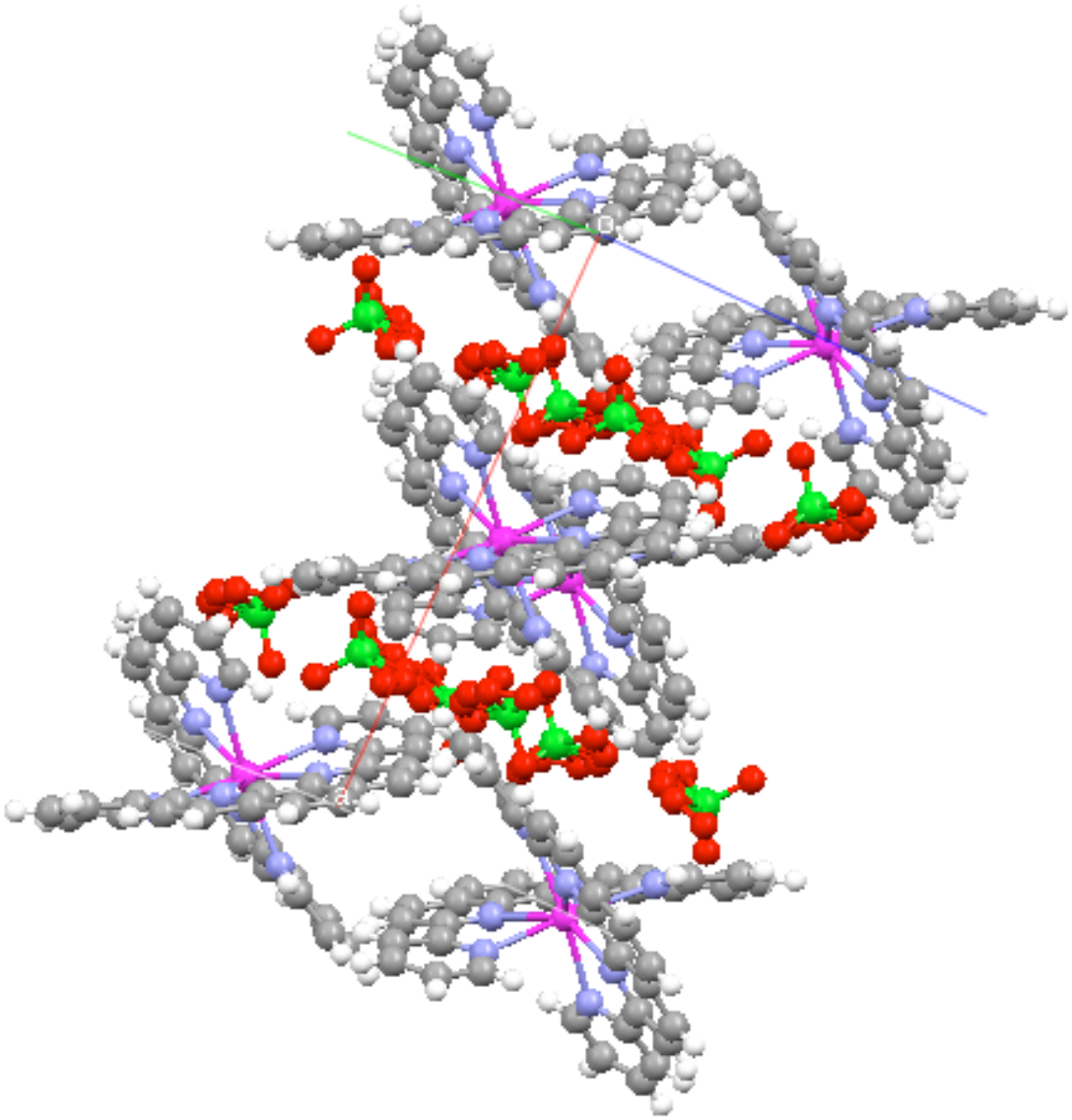

Figure 73. View along y axis of unit cell to display arrangement of complex and perchlorate ions.

Table 50. Crystal data and structure refinement for the $[Cd(DPP)_2](ClO_4)_2$ complex.

Identification code	dppcd	
Empirical formula	C44 H28 Cd Cl2 N8 O8	
Formula weight	980.04	
Temperature	163(2) K	
Wavelength	0.71073 Å	
Crystal system	Orthorhombic	
Space group	Ccca	
Unit cell dimensions	a = 16.617(3) Å	α= 90.00°
	b = 19.661(4) Å	β= 90.00°
	c = 12.120(2) Å	γ = 90.00°
Volume	3959.7(14) $Å^3$	
Z	4	
Density (calculated)	1.644 Mg/m^3	
Absorption coefficient	0.755 mm^{-1}	
F(000)	1976	
Crystal size	0.12 x 0.12 x 0.10 mm^3	
Theta range for data collection	3.36 to 25.09°	
Index ranges	$-19 \leq h \leq 19$, $-23 \leq k \leq 23$, $-13 \leq l \leq 14$	
Reflections collected	1753	
Independent reflections	1625 [R(int) = 0.0455]	
Completeness to theta = 25.09°	99.2 %	
Absorption correction	Semi-empirical from equivalents	
Max. and min. transmission	0.9283 and 0.9148	
Refinement method	Full-matrix least-squares on F^2	
Data / restraints / parameters	1753 / 0 / 159	
Goodness-of-fit on F^2	1.138	
Final R indices [I>2sigma(I)]	R1 = 0.0321, wR2 = 0.0705	
R indices (all data)	R1 = 0.0367, wR2 = 0.0734	
Largest diff. peak and hole	0.331 and -0.369 $e.Å^{-3}$	

Table 51. Bond lengths of $[Cd(DPP)_2](ClO_4)_2$ complex.

Bond	Bond Length (Å)
Cd(1)-N(2)	2.412(2)
Cd(1)-N(2A)	2.412(2)
Cd(1)-N(2B)	2.412(2)
Cd(1)-N(2C)	2.412(2)
Cd(1)-N(1)	2.559(2)
Cd(1)-N(1A)	2.559(2)
Cd(1)-N(1B)	2.559(2)
Cd(1)-N(1C)	2.559(2)
C(6)-N(2)	1.334(3)
C(6)-C(7)	1.407(4)
C(6)-C(5)	1.489(4)
C(7)-C(8)	1.369(4)
C(8)-C(9)	1.404(4)
C(9)-C(10)	1.413(4)
C(9)-C(11)	1.433(4)
C(10)-N(2)	1.350(3)
C(10)-C(10)	1.445(5)
C(11)-C(11)	1.358(6)
C(1)-N(1)	1.348(4)
C(1)-C(2)	1.389(4)
C(2)-C(3)	1.382(4)
C(3)-C(4)	1.379(4)
C(4)-C(5)	1.400(4)
C(5)-N(1)	1.342(3)

Table 52. Bond Angles of $[Cd(DPP)_2](ClO_4)_2$ complex.

Bond	Bond Angle (°)	Bond	Bond Angle (°)
N(2)-Cd(1)-N(2)	142.44(10)	N(1)-Cd(1)-N(1)	162.88(10)
N(2)-Cd(1)-N(2)	68.22(10)	N(2)-C(6)-C(7)	121.6(2)
N(2)-Cd(1)-N(2)	125.34(10)	N(2)-C(6)-C(5)	116.0(2)
N(2)-Cd(1)-N(2)	125.34(10)	C(7)-C(6)-C(5)	122.3(2)
N(2)-Cd(1)-N(2)	68.22(10)	C(8)-C(7)-C(6)	119.5(3)
N(2)-Cd(1)-N(2)	142.44(10)	C(7)-C(8)-C(9)	120.2(2)
N(2)-Cd(1)-N(1)	77.07(7)	C(8)-C(9)-C(10)	116.7(2)
N(2)-Cd(1)-N(1)	132.08(7)	C(8)-C(9)-C(11)	123.5(2)
N(2)-Cd(1)-N(1)	88.70(7)	C(10)-C(9)-C(11)	119.8(2)
N(2)-Cd(1)-N(1)	64.93(7)	N(2)-C(10)-C(9)	122.9(2)
N(2)-Cd(1)-N(1)	88.70(7)	N(2)-C(10)-C(10)	117.79(14)
N(2)-Cd(1)-N(1)	64.93(7)	C(9)-C(10)-C(10)	119.29(15)
N(2)-Cd(1)-N(1)	77.07(7)	C(11)-C(11)-C(9)	120.88(16)
N(2)-Cd(1)-N(1)	132.08(7)	C(6)-N(2)-C(10)	119.1(2)
N(1)-Cd(1)-N(1)	162.88(10)	C(6)-N(2)-Cd(1)	122.75(17)
N(2)-Cd(1)-N(1)	132.08(7)	C(10)-N(2)-Cd(1)	118.06(16)
N(2)-Cd(1)-N(1)	77.07(7)	N(1)-C(1)-C(2)	123.0(3)
N(2)-Cd(1)-N(1)	64.93(7)	C(3)-C(2)-C(1)	118.3(3)
N(2)-Cd(1)-N(1)	88.70(7)	C(4)-C(3)-C(2)	119.4(3)
N(1)-Cd(1)-N(1)	92.21(11)	C(3)-C(4)-C(5)	119.2(3)
N(1)-Cd(1)-N(1)	90.33(11)	N(1)-C(5)-C(4)	121.8(3)
N(2)-Cd(1)-N(1)	64.93(7)	N(1)-C(5)-C(6)	115.9(2)
N(2)-Cd(1)-N(1)	88.70(7)	C(4)-C(5)-C(6)	122.3(2)
N(2)-Cd(1)-N(1)	132.08(7)	C(5)-N(1)-C(1)	118.3(2)
N(2)-Cd(1)-N(1)	77.07(7)	C(5)-N(1)-Cd(1)	115.91(17)
N(1)-Cd(1)-N(1)	90.33(11)	C(1)-N(1)-Cd(1)	123.39(18)
N(1)-Cd(1)-N(1)	92.21(11)		

Symmetry transformations used to generate equivalent atoms

1: -x, -y+½, z+½ **2:** -x, -y+½, z-½ **3:** -x, -y+1, z

Table 53. Atomic coordinates and equivalent isotropic displacement parameters ($Å^2$) for $[Cd(DPP)_2](ClO_4)_2$. U(eq) is defined as one third of the trace of the orthogonalized U^{ij} tensor.

	x	y	z	U(eq)
Cd(1)	0.0000	0.7500	0.2500	0.01970(18)
N(1)	-0.10679(14)	0.76938(11)	0.3989(2)	0.0252(5)
N(2)	-0.04673(13)	0.64843(11)	0.34136(18)	0.0201(5)
C(1)	-0.13603(18)	0.83126(14)	0.4251(3)	0.0294(6)
C(2)	-0.17442(18)	0.84494(15)	0.5244(2)	0.0318(7)
C(3)	-0.1812(2)	0.79302(16)	0.6007(2)	0.0346(7)
C(4)	-0.15301(19)	0.72907(15)	0.5743(2)	0.0305(7)
C(5)	-0.11683(16)	0.71852(14)	0.4714(2)	0.0224(6)
C(6)	-0.09017(16)	0.65001(13)	0.4338(2)	0.0217(6)
C(7)	-0.11196(17)	0.59005(14)	0.4896(2)	0.0269(6)
C(8)	-0.08981(17)	0.52834(14)	0.4471(2)	0.0271(6)
C(9)	-0.04506(16)	0.52504(13)	0.3490(2)	0.0226(6)
C(10)	-0.02393(15)	0.58770(13)	0.2998(2)	0.0196(5)
C(11)	-0.02113(17)	0.46249(13)	0.2979(2)	0.0284(6)

Table 54. Anisotropic displacement parameters ($Å^2$) for $[Cd(DPP)_2](ClO_4)_2$. The anisotropic displacement factor exponent takes the form:
$-2\pi^2[h^2 a^{*2} U^{11} + ... + 2 h k a^* b^* U^{12}]$.

	U^{11}	U^{22}	U^{33}	U^{23}	U^{13}	U^{12}
Cd(1)	0.0234(2)	0.0149(2)	0.0209(2)	0.000	0.000	0.000
C(6)	0.0246(14)	0.0219(13)	0.0185(12)	0.0007(10)	-0.0013(11)	-0.0013(11)
C(7)	0.0294(15)	0.0278(14)	0.0234(14)	0.0054(12)	0.0024(11)	-0.0013(12)
C(8)	0.0281(15)	0.0243(14)	0.0289(14)	0.0078(11)	0.0000(12)	-0.0020(11)
C(9)	0.0212(13)	0.0199(13)	0.0267(14)	0.0029(11)	-0.0049(10)	-0.0013(10)
C(10)	0.0212(13)	0.0168(12)	0.0208(12)	0.0006(10)	-0.0030(10)	-0.0003(9)
C(11)	0.0335(16)	0.0162(13)	0.0354(15)	0.0028(11)	-0.0036(12)	-0.0021(11)
N(2)	0.0229(11)	0.0180(11)	0.0192(11)	0.0008(9)	-0.0017(9)	-0.0008(9)
C(1)	0.0319(15)	0.0188(14)	0.0374(16)	0.0003(12)	0.0079(13)	-0.0004(11)
C(2)	0.0298(16)	0.0271(14)	0.0385(17)	-0.0123(13)	0.0055(13)	-0.0021(12)
C(3)	0.0406(17)	0.0378(17)	0.0253(15)	-0.0086(13)	0.0044(13)	-0.0018(14)
C(4)	0.0390(17)	0.0319(15)	0.0207(14)	-0.0009(11)	0.0032(12)	0.0007(12)
C(5)	0.0233(14)	0.0230(13)	0.0209(13)	-0.0012(11)	-0.0001(10)	-0.0021(11)
N(1)	0.0266(12)	0.0202(12)	0.0290(12)	0.0003(9)	0.0055(10)	-0.0003(9)

Mass spectrometry was again utilized to complement the x-ray crystal structure. The full spectrum of the $[Cd(DPP)_2](ClO_4)_2$ crystal and an expansion of m/z = 770 – 890 are shown in Figure 74. The software iMass was used to predict peaks taking into account the abundance of different isotopes. The molecular mass of the complex with no perchlorate ions is 782 g/mol. The summary of data obtained from iMass is shown in Table 55.

Table 55. Calculation of monoisotopic mass (^{114}Cd), average mass, and percent composition of $[Cd(DPP)_2]^{2+}$ by iMass.

Formula	**$C_{44}H_{28}N_8Cd$**
Average Mass	781.1712
Monoisotopic Mass	782.1470

Composition (weight):
N: 14.3443% **Cd:** 14.3901% **C:** 67.6528% **H:** 3.6128%

iMass was then used to predict the peak distributions based on the relative abundance of cadmium isotopes and compared to the mass spectrum of the $([Cd(DPP)_2]ClO_4)^+$. Table 56 is a summary of the relative abundance and masses of the different isotopes of cadmium (Lide, 1993) and Figure 75 is the predicted mass distributions for a) $[Cd(DPP)_2]^{2+}$ and b) $([Cd(DPP)_2]ClO_4)^+$. There was good agreement between the predicted spectra and the actual spectra. There are seven major peaks corresponding to $[Cd(DPP)_2]^{2+}$ and the relative abundance of these peaks are the same as those predicted by iMass. The eight major peaks correspond to $([Cd(DPP)_2]ClO_4)^+$ and the relative abundance of these peaks are the same as those predicted.

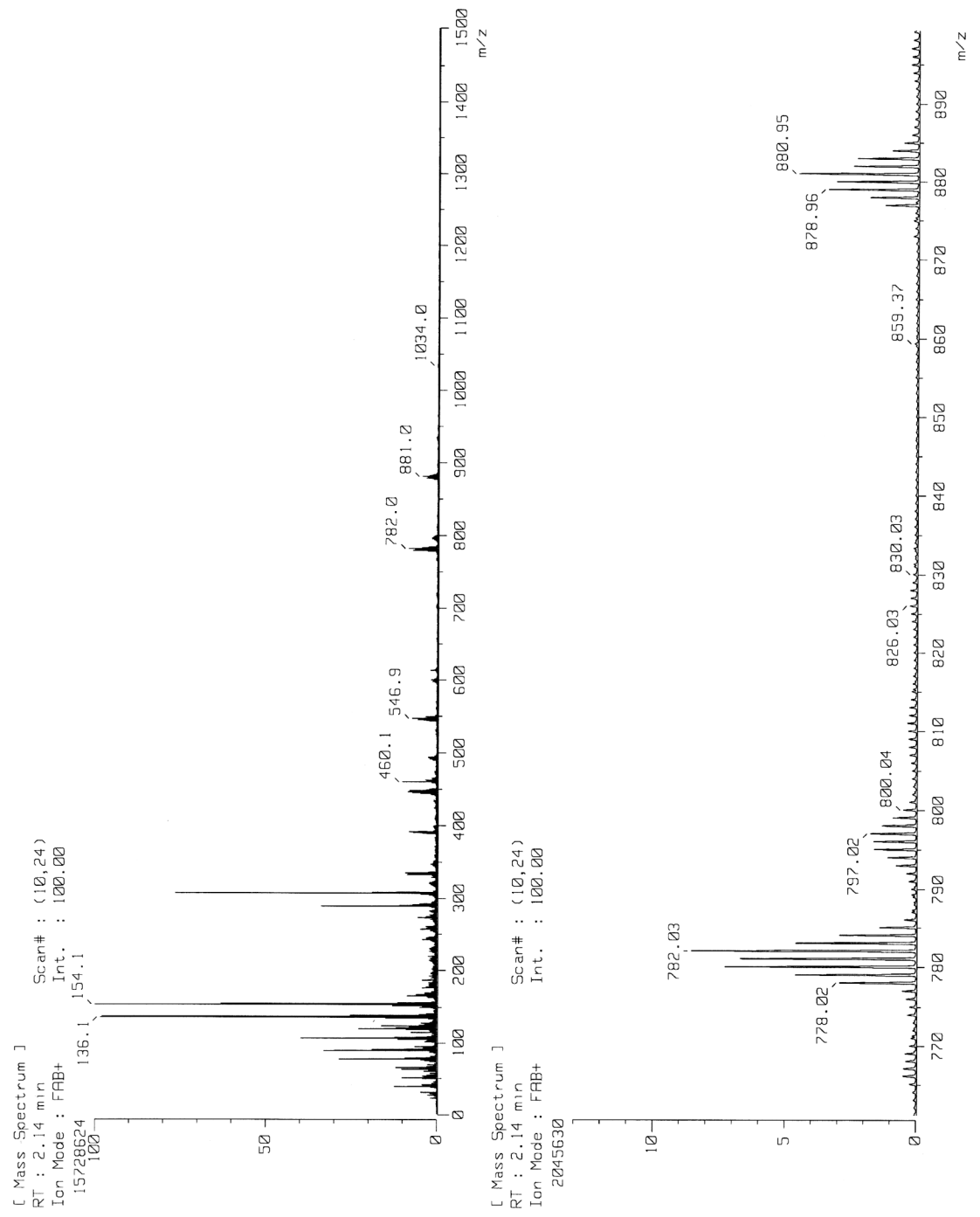

Figure 74. Mass spectrum of $[Cd(DPP)_2](ClO_4)_2$ crystals.

Table 56. Summary of cadmium isotopes and relative abundance.

#	Abundance	Mass
106	1.2500 %	105.90646100
108	0.8900 %	107.90417600
110	12.4900 %	109.90300500
111	12.8000 %	110.90418200
112	24.1300 %	111.90275800
113	12.2200 %	112.90440000
114	28.7300 %	113.90335700
116	7.4900 %	115.90475400

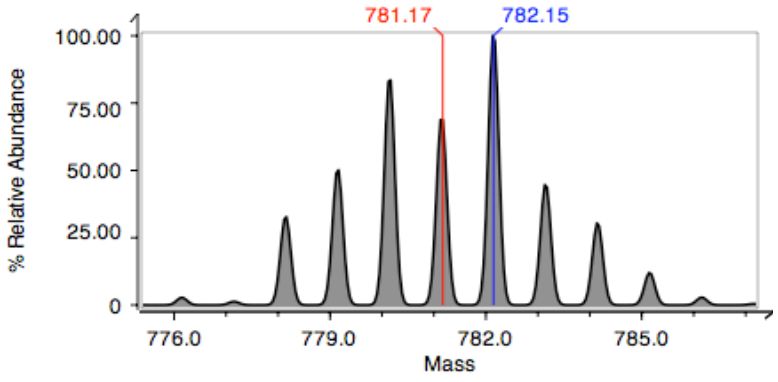

a)

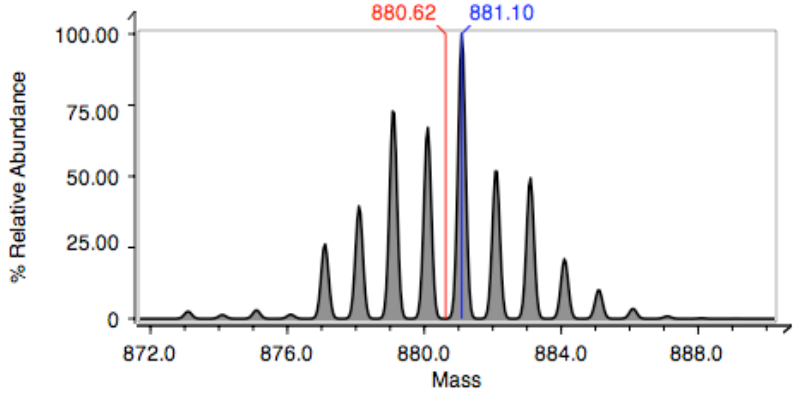

b)

Figure 75. Mass distribution based on relative abundance of isotopes predicted by iMass for a) $[Cd(DPP)_2]^{2+}$ and b) $([Cd(DPP)_2]ClO_4)^{+}$.

$[Zn(DPP)_2](ClO_4)_2$

The crystals formed on the interface of the butanol/H_2O layers were colorless and cubic. Only one crystal was obtained from the synthesis and Figure 76 is a microscopic photograph of the crystal synthesized. Crystal structure was determined by x-ray crystallography, but mass spectrometry was unable to be utilized because of the limited amount of crystals formed. The crystal structure of $[Zn(DPP)_2](ClO_4)_2$ consists of a zinc metal ion coordinated to two DPP molecules through only six donor atoms as in Figure 77. The zinc was coordinated to six neutral nitrogen donor atoms of the two DPP molecules, giving it a coordination number of six. A 3D representation of the zinc complex is shown in Figure 78. The three dimensional representation shows the zinc bound to the two nitrogens of the phenanthroline backbone and only one pyridine ring as previously discussed for energy minimization calculations. The other pyridine ring is π-stacked to the backbone of the second phenanthroline. One non-bonded pyridine ring is not π-stacked but appears to almost bond to the zinc ion. The Cambridge Crystallographic Database was used to find the average Zn-N bond length of 2.13 ± 0.05 Å from 333 different structures containing bipyridyl zinc bonds. The distance between Zn(1) to atom N(8) is 3.23 Å, which is too far to form a bond. The average Zn-N bond length was in good agreement with the measured bond lengths of the complex. Figure 79 is a view of the showing the arrangement of zinc complexes and perchlorate ions.

The crystal data and structural refinement parameters for the $[Zn(DPP)_2](ClO_4)_2$ complex are listed in Table 57. The bond distances and angles for the complex are shown in Table 58 and 59 respectively. In addition, the spatial coordinates of the atoms for the complex are given in Tables 60 and 61.

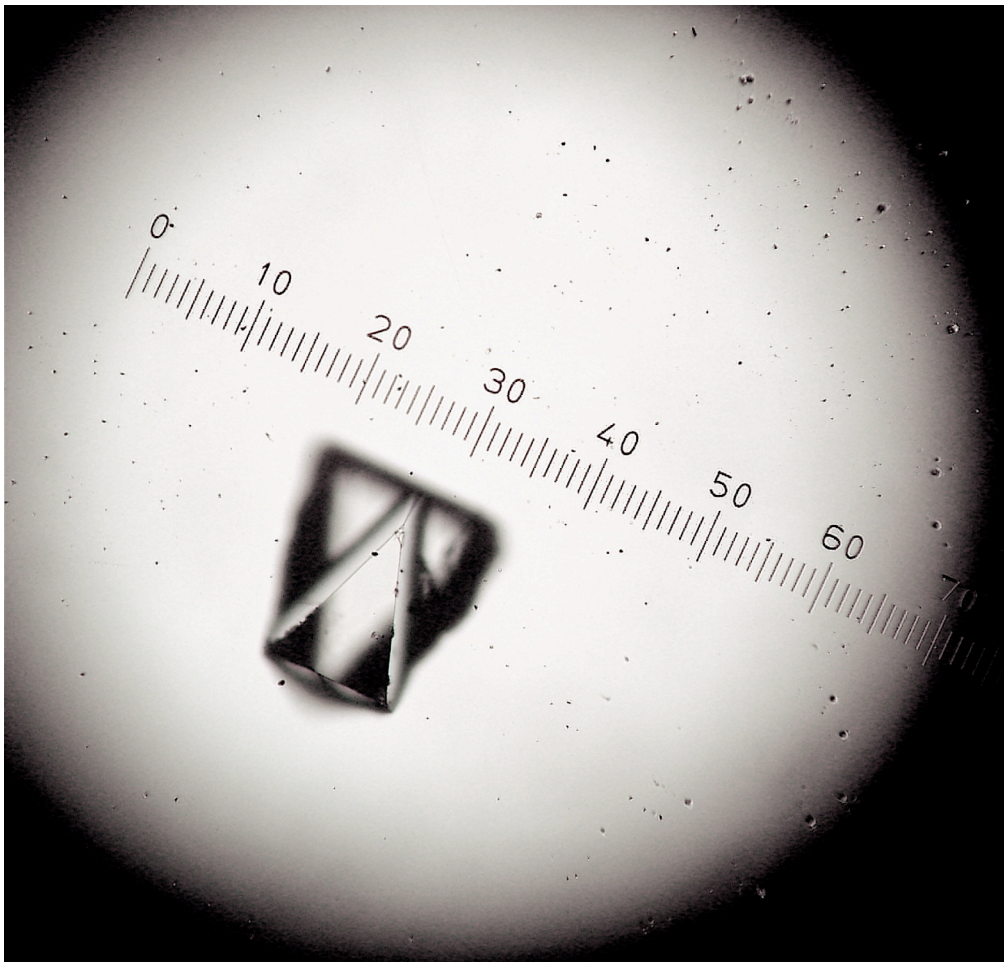

Figure 76. Microscopic view (10x) of crystal formed from equimolar amounts of DPP and $Zn(ClO_4)_2$.

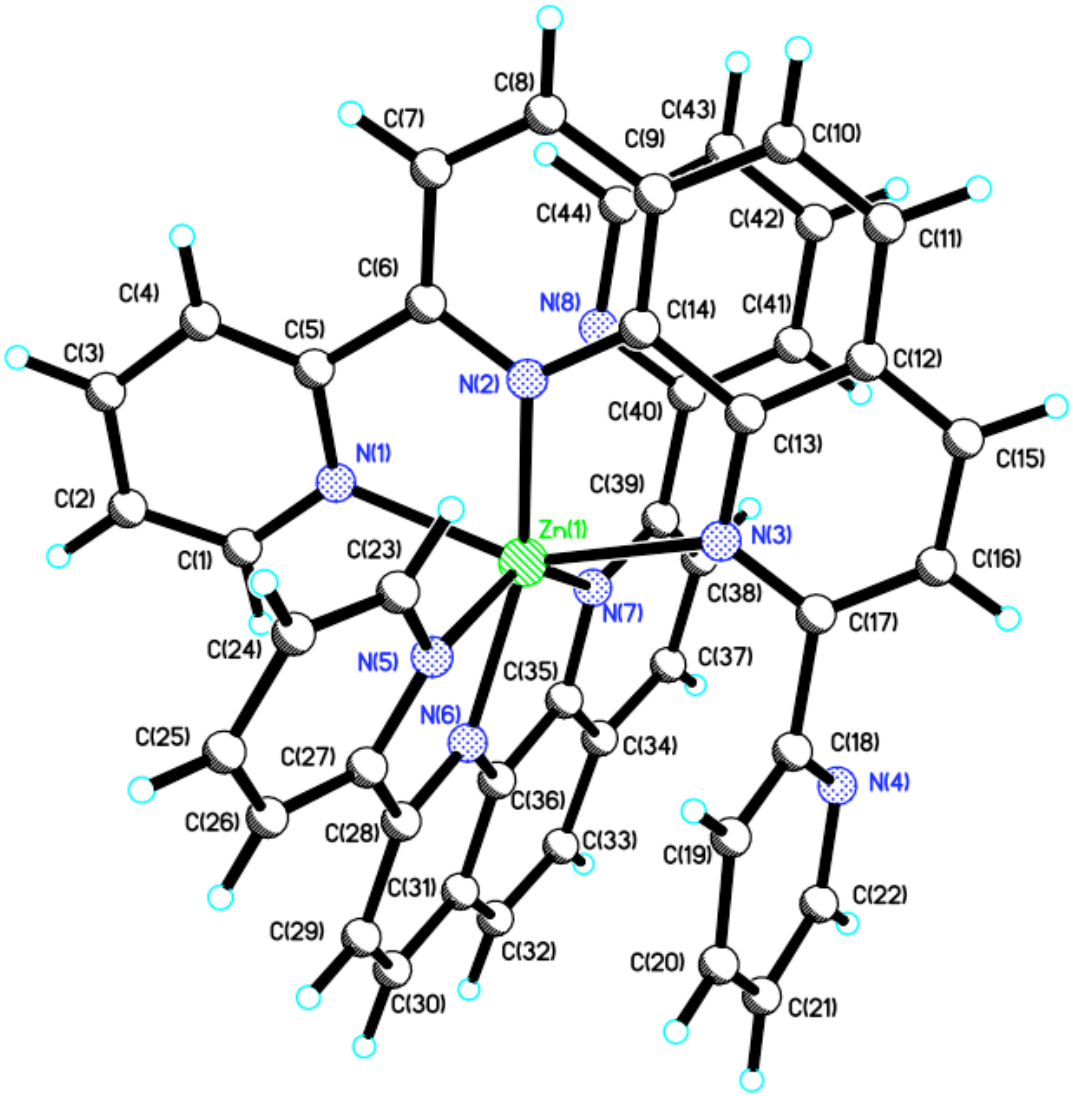

Figure 77. Structure of $[Zn(DPP)_2](ClO_4)_2$ determined by X-ray crystallography.

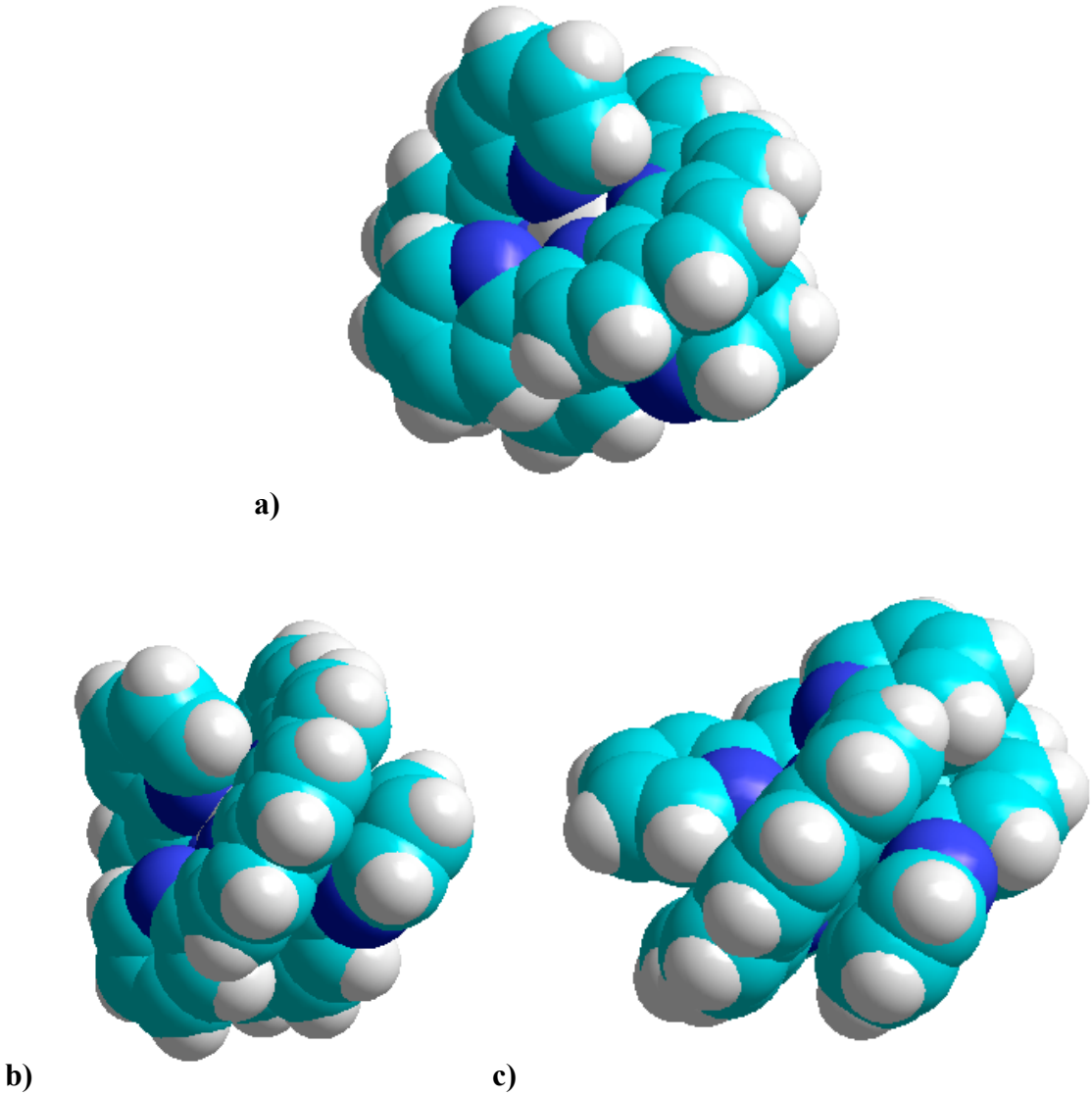

Figure 78. Three-dimensional view of zinc complex to show a) coordination of metal ion and b), c) orientation noncoordinated pyridine rings. Note the π-stacking that occurs between the pyridines and phenanthroline backbone.

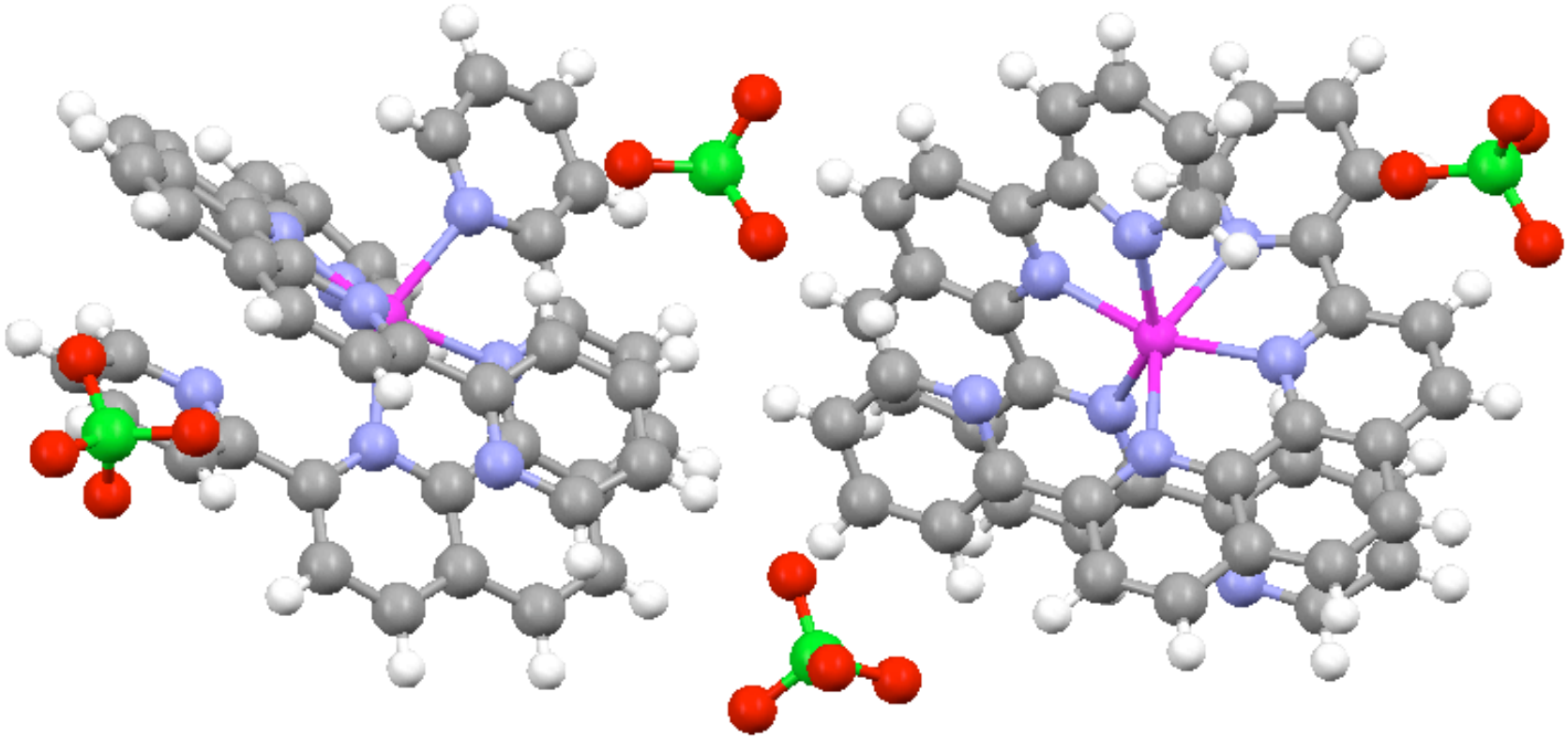

Figure 79: Three-dimensional view to show orientation of zinc complex and perchlorate ions.

Table 57. Crystal data and structure refinement for the $[Zn(DPP)_2](ClO_4)_2$ complex.

Identification code	dppzn	
Empirical formula	C44 H28 Cl2 N8 O8 Zn	
Formula weight	933.01	
Temperature	153(2) K	
Wavelength	0.71073 Å	
Crystal system	Triclinic	
Space group	P-1	
Unit cell dimensions	a = 7.8346(16) Å	α= 79.51(3)°.
	b = 10.333(2) Å	β= 80.43(3)°.
	c = 23.502(5) Å	γ = 76.10(3)°.
Volume	1801.1(6) $Å^3$	
Z	2	
Density (calculated)	1.72 Mg/m^3	
Absorption coefficient	0.906 mm^{-1}	
F(000)	952	
Crystal size	0.13 x 0.12 x 0.06 mm^3	
Theta range for data collection	2.67 to 25.15 °	
Index ranges	$-9 \leq h \leq 8$, $-12 \leq k \leq 12$, $-28 \leq l \leq 26$	
Reflections collected	10399	
Independent reflections	8226 [R(int) = 0.0679]	
Completeness to theta = 25.15°	98.5 %	
Absorption correction	Semi-empirical from equivalents	
Max. and min. transmission	0.9477 and 0.8913	
Refinement method	Full-matrix least-squares on F^2	
Data / restraints / parameters	10399 / 3 / 1135	
Goodness-of-fit on F^2	1.003	
Final R indices [I>2sigma(I)]	R1 = 0.0507, wR2 = 0.0950	
R indices (all data)	R1 = 0.0679, wR2 = 0.1062	
Largest diff. peak and hole	0.672 and -0.518 $e.Å^{-3}$	

Table 58. Bonds lengths of $[Zn(DPP)_2](ClO_4)_2$ complex

Bond	Bond Length (Å)	Bond	Bond Length (Å)
Zn(1)-N(1)	2.125	C(12)-C(15)	1.298
Zn(1)-N(2)	2.067	C(13)-C(14)	1.362
Zn(1)-N(3)	2.133	C(15)-C(16)	1.393
Zn(1)-N(5)	2.263	C(16)-C(17)	1.296
Zn(1)-N(6)	2.056	C(17)-C(18)	1.488
Zn(1)-N(7)	2.217	C(18)-C(19)	1.326
N(1)-C(1)	1.295	C(19)-C(20)	1.377
N(1)-C(5)	1.353	C(20)-C(21)	1.301
N(2)-C(6)	1.269	C(21)-C(22)	1.341
N(2)-C(14)	1.293	C(23)-C(24)	1.28
N(3)-C(13)	1.366	C(24)-C(25)	1.354
N(3)-C(17)	1.257	C(25)-C(26)	1.387
N(4)-C(18)	1.286	C(26)-C(27)	1.261
N(4)-C(22)	1.339	C(27)-C(28)	1.47
N(5)-C(23)	1.319	C(28)-C(29)	1.384
N(5)-C(27)	1.326	C(29)-C30)	1.371
N(6)-C(28)	1.278	C(30)-C(31)	1.319
N(6)-C(36)	1.359	C(31)-C(32)	1.412
N(7)-C(35)	1.372	C(31)-C(36)	1.401
N(7)-C(39)	1.252	C(32)-C(33)	1.272
N(8)-C(40)	1.257	C(33)-C(34)	1.424
N(8)-C(44)	1.355	C(34)-C(35)	1.374
C(1)-C(2)	1.258	C(34)-C(37)	1.322
C(2)–C(3)	1.369	C(35)-C(36)	1.351
C(3)-C(4)	1.331	C(37)-C(38)	1.383
C(4)–C(5)	1.248	C(38)-C(39)	1.353
C(5)-C(6)	1.422	C(39)-C(40)	1.481
C(6)-C(7)	1.409	C(40)-C(41)	1.269
C(7)-C(8)	1.32	C(41)-C(42)	1.368
C(8)-C(9)	1.323	C(42)-C(43)	1.293
C(9)-C(10)	1.361	C(43)-C(44)	1.271
C(9)-C(14)	1.401		
C(10)-C(11)	1.279		
C(11)-C(12)	1.44		
C(12)-C(13)	1.309		

Table 59. Bond angles of $[Zn(DPP)_2](ClO_4)_2$.

Bond	Bond Angle (°)	Bond	Bond Angle (°)	Bond	Bond Angle (°)
N(6)-Zn(1)-N(2)	161.6(2)	C(4)-C(3)-C(2)	123.9(7)	C(23)-C(24)-C(25)	116.3(7)
N(6)-Zn(1)-N(1)	93.6(2)	C(5)-C(4)-C(3)	115.6(7)	C(24)-C(25)-C(26)	121.5(7)
N(2)-Zn(1)-N(1)	74.8(2)	C(4)-C(5)-N(1)	121.7(7)	C(27)-C(26)-C(25)	118.3(7)
N(6)-Zn(1)-N(3)	116.8(2)	C(4)-C(5)-C(6)	120.1(7)	C(26)-C(27)-N(5)	120.2(6)
N(2)-Zn(1)-N(3)	74.4(2)	N(1)-C(5)-C(6)	118.1(6)	C(26)-C(27)-C(28)	120.3(6)
N(1)-Zn(1)-N(3)	149.06(19)	N(2)-C(6)-C(7)	121.3(6)	N(5)-C(27)-C(28)	119.3(6)
N(6)-Zn(1)-N(7)	74.1(2)	N(2)-C(6)-C(5)	111.8(6)	N(6)-C(28)-C(29)	120.1(6)
N(2)-Zn(1)-N(7)	121.8(2)	C(7)-C(6)-C(5)	127.0(6)	N(6)-C(28)-C(27)	112.5(5)
N(1)-Zn(1)-N(7)	102.38(19)	C(8)-C(7)-C(6)	121.7(7)	C(29)-C(28)-C(27)	127.2(6)
N(3)-Zn(1)-N(7)	92.0(2)	C(7)-C(8)-C(9)	117.0(6)	C(30)-C(29)-C(28)	122.8(6)
N(6)-Zn(1)-N(5)	74.59(19)	C(8)-C(9)-C(10)	120.8(7)	C(31)-C(30)-C(29)	118.0(6)
N(2)-Zn(1)-N(5)	90.20(19)	C(8)-C(9)-C(14)	118.4(7)	C(30)-C(31)-C(36)	117.0(6)
N(1)-Zn(1)-N(5)	85.90(19)	C(10)-C(9)-C(14)	120.5(7)	C(30)-C(31)-C(32)	122.0(6)
N(3)-Zn(1)-N(5)	96.25(19)	C(11)-C(10)-C(9)	115.9(7)	C(36)-C(31)-C(32)	121.0(6)
N(7)-Zn(1)-N(5)	148.03(18)	C(10)-C(11)-C(12)	123.9(7)	C(33)-C(32)-C(31)	118.5(6)
C(1)-N(1)-C(5)	121.6(6)	C(15)-C(12)-C(13)	113.5(6)	C(32)-C(33)-C(34)	121.0(6)
C(1)-N(1)-Zn(1)	123.6(4)	C(15)-C(12)-C(11)	125.3(6)	C(37)-C(34)-C(35)	114.4(6)
C(5)-N(1)-Zn(1)	112.2(4)	C(13)-C(12)-C(11)	121.3(7)	C(37)-C(34)-C(33)	123.5(6)
C(6)-N(2)-C(14)	117.0(6)	C(12)-C(13)-C(14)	114.9(6)	C(35)-C(34)-C(33)	122.1(6)
C(6)-N(2)-Zn(1)	121.6(4)	C(12)-C(13)-N(3)	125.6(6)	C(36)-C(35)-N(7)	118.3(6)
C(14)-N(2)-Zn(1)	120.8(4)	C(14)-C(13)-N(3)	119.5(6)	C(36)-C(35)-C(34)	116.6(6)
C(17)-N(3)-C(13)	119.8(6)	N(2)-C(14)-C(13)	112.6(6)	N(7)-C(35)-C(34)	125.0(6)
C(17)-N(3)-Zn(1)	125.6(4)	N(2)-C(14)-C(9)	124.4(6)	C(35)-C(36)-N(6)	115.1(6)
C(13)-N(3)-Zn(1)	111.3(4)	C(13)-C(14)-C(9)	122.9(6)	C(35)-C(36)-C(31)	120.5(6)
C(18)-N(4)-C(22)	118.9(7)	C(12)-C(15)-C(16)	121.0(6)	N(6)-C(36)-C(31)	124.5(6)
C(23)-N(5)-C(27)	121.4(6)	C(17)-C(16)-C(15)	122.2(7)	C(34)-C(37)-C(38)	119.8(6)
C(23)-N(5)-Zn(1)	125.4(4)	N(3)-C(17)-C(16)	117.7(7)	C(39)-C(38)-C(37)	122.5(6)
C(27)-N(5)-Zn(1)	108.5(4)	N(3)-C(17)-C(18)	120.9(6)	N(7)-C(39)-C(38)	119.2(6)
C(28)-N(6)-C(36)	117.5(5)	C(16)-C(17)-C(18)	121.3(7)	N(7)-C(39)-C(40)	119.6(6)
C(28)-N(6)-Zn(1)	122.4(4)	N(4)-C(18)-C(19)	120.8(7)	C(38)-C(39)-C(40)	121.1(6)
C(36)-N(6)-Zn(1)	120.1(4)	N(4)-C(18)-C(17)	118.3(6)	N(8)-C(40)-C(41)	117.9(7)
C(39)-N(7)-C(35)	119.0(5)	C(19)-C(18)-C(17)	120.8(7)	N(8)-C(40)-C(39)	118.7(6)
C(39)-N(7)-Zn(1)	128.2(4)	C(18)-C(19)-C(20)	118.9(7)	C(41)-C(40)-C(39)	123.3(7)
C(35)-N(7)-Zn(1)	112.3(4)	C(21)-C(20)-C(19)	121.9(8)	C(40)-C(41)-C(42)	122.0(7)
C(40)-N(8)-C(44)	119.6(6)	C(20)-C(21)-C(22)	115.7(7)	C(43)-C(42)-C(41)	121.0(7)
C(2)-C(1)-N(1)	119.9(7)	N(4)-C(22)-C(21)	123.7(8)	C(44)-C(43)-C(42)	114.4(7)
C(1)-C(2)-C(3)	117.2(7)	C(24)-C(23)-N(5)	122.3(6)	C(43)-C(44)-N(8)	124.9(7)

Symmetry transformations used to generate equivalent atoms

1: -x, -y+½, z+½ **2:** -x, -y+½, z-½ **3:** -x, -y+1, z

Table 60. Atomic coordinates and equivalent isotropic displacement parameters ($Å^2$) for $[Zn(DPP)_2](ClO_4)_2$. U(eq) is defined as one third of the trace of the orthogonalized U^{ij} tensor.

	x	y	z	U(eq)
Zn(1)	-0.26945(8)	-0.18175(6)	-0.78352(3)	0.02063(18)
N(1)	-0.0865(7)	-0.1027(5)	-0.7500(2)	0.0203(12)
N(2)	-0.3808(7)	-0.1549(5)	-0.6992(2)	0.0179(11)
N(3)	-0.5089(6)	-0.2534(5)	-0.7697(2)	0.0180(11)
N(4)	-0.4143(9)	-0.4105(6)	-0.8893(3)	0.0365(15)
N(5)	-0.3920(6)	0.0354(5)	-0.8159(2)	0.0201(11)
N(6)	-0.1549(6)	-0.1453(5)	-0.8685(2)	0.0191(11)
N(7)	-0.1078(6)	-0.3788(5)	-0.8046(2)	0.0195(12)
N(8)	-0.1517(7)	-0.4270(6)	-0.6812(2)	0.0228(13)
C(1)	0.0469(8)	-0.0609(7)	-0.7818(3)	0.0246(15)
C(2)	0.1189(9)	0.0178(8)	-0.7638(3)	0.0290(17)
C(3)	0.0553(9)	0.0506(7)	-0.7092(3)	0.0335(17)
C(4)	-0.0829(9)	0.0103(8)	-0.6760(3)	0.0308(17)
C(5)	-0.1507(8)	-0.0650(7)	-0.6970(3)	0.0239(14)
C(6)	-0.3044(9)	-0.1084(7)	-0.6664(3)	0.0238(15)
C(7)	-0.3742(9)	-0.1003(7)	-0.6076(3)	0.0295(16)
C(8)	-0.5191(9)	-0.1434(7)	-0.5837(3)	0.0276(16)
C(9)	-0.5958(9)	-0.1957(8)	-0.6174(3)	0.0261(17)
C(10)	-0.7365(8)	-0.2532(7)	-0.5950(3)	0.0278(16)
C(11)	-0.7841(8)	-0.3185(7)	-0.6287(3)	0.0270(16)
C(12)	-0.7051(8)	-0.3264(7)	-0.6882(3)	0.0236(15)
C(13)	-0.5815(8)	-0.2609(7)	-0.7125(3)	0.0228(14)
C(14)	-0.5198(8)	-0.2008(7)	-0.6755(3)	0.0216(14)
C(15)	-0.7441(8)	-0.3975(7)	-0.7224(3)	0.0278(16)
C(16)	-0.6662(8)	-0.3937(7)	-0.7803(3)	0.0235(16)
C(17)	-0.5535(8)	-0.3189(7)	-0.8028(3)	0.0228(15)
C(18)	-0.4882(8)	-0.3036(8)	-0.8663(3)	0.0275(15)
C(19)	-0.5143(9)	-0.1834(8)	-0.8990(3)	0.0313(17)
C(20)	-0.4612(10)	-0.1747(9)	-0.9582(3)	0.0318(18)
C(21)	-0.3810(11)	-0.2804(9)	-0.9825(3)	0.0392(19)
C(22)	-0.3577(12)	-0.3982(9)	-0.9466(4)	0.048(2)
C(23)	-0.4899(9)	0.1234(7)	-0.7829(3)	0.0238(15)
C(24)	-0.4973(9)	0.2502(7)	-0.7964(3)	0.0295(17)
C(25)	-0.4002(9)	0.2900(7)	-0.8470(3)	0.0356(18)
C(26)	-0.2994(9)	0.1978(7)	-0.8822(3)	0.0327(17)
C(27)	-0.2981(8)	0.0745(7)	-0.8657(3)	0.0218(14)
C(28)	-0.1807(8)	-0.0279(6)	-0.8987(3)	0.0185(13)
C(29)	-0.0933(9)	-0.0073(7)	-0.9547(3)	0.0274(15)
C(30)	0.0207(8)	-0.1091(7)	-0.9807(3)	0.0251(15)
C(31)	0.0465(8)	-0.2317(7)	-0.9508(3)	0.0233(15)
C(32)	0.1569(9)	-0.3435(8)	-0.9747(3)	0.0305(16)
C(33)	0.1683(9)	-0.4597(7)	-0.9443(3)	0.0309(17)
C(34)	0.0745(8)	-0.4771(7)	-0.8871(3)	0.0246(15)
C(35)	-0.0247(8)	-0.3698(7)	-0.8609(3)	0.0213(14)
C(36)	-0.0440(8)	-0.2473(7)	-0.8942(3)	0.0217(14)
C(37)	0.0780(9)	-0.5959(6)	-0.8543(3)	0.0255(15)
C(38)	-0.0115(9)	-0.6035(7)	-0.7983(3)	0.0283(16)
C(39)	-0.1017(8)	-0.4928(7)	-0.7746(3)	0.0225(15)
C(40)	-0.1809(8)	-0.5036(7)	-0.7126(3)	0.0226(14)
C(41)	-0.2741(9)	-0.5887(7)	-0.6890(3)	0.0297(16)
C(42)	-0.3378(9)	-0.6009(8)	-0.6309(3)	0.0317(17)
C(43)	-0.3072(9)	-0.5243(8)	-0.5977(3)	0.0329(17)
C(44)	-0.2117(8)	-0.4421(7)	-0.6234(3)	0.0257(15)

Table 61. Anisotropic displacement parameters ($Å^2$) for $[Zn(DPP)_2](ClO_4)_2$. The anisotropic displacement factor exponent takes the form: $-2\pi^2[h^2 a^{*2} U^{11} + ... + 2 h k a^* b^* U^{12}]$.

	U^{11}	U^{22}	U^{33}	U^{23}	U^{13}	U^{12}
Zn(1)	0.0273(4)	0.0179(4)	0.0192(4)	-0.0035(3)	0.0004(3)	-0.0116(3)
N(1)	0.026(3)	0.012(3)	0.027(3)	-0.001(2)	-0.007(2)	-0.009(2)
N(2)	0.026(3)	0.013(3)	0.017(3)	0.000(2)	-0.002(2)	-0.009(2)
N(3)	0.019(3)	0.019(3)	0.016(3)	0.006(2)	-0.004(2)	-0.008(2)
N(4)	0.064(4)	0.020(3)	0.035(4)	-0.011(3)	-0.004(3)	-0.023(3)
N(5)	0.021(3)	0.022(3)	0.019(3)	-0.002(2)	-0.003(2)	-0.009(2)
N(6)	0.024(3)	0.015(3)	0.022(3)	-0.009(2)	-0.002(2)	-0.007(2)
N(7)	0.019(3)	0.017(3)	0.025(3)	-0.011(2)	-0.002(2)	-0.006(2)
N(8)	0.028(3)	0.021(3)	0.021(3)	-0.001(2)	0.001(2)	-0.012(2)
C(1)	0.022(3)	0.026(4)	0.032(4)	-0.009(3)	-0.009(3)	-0.010(3)
C(2)	0.025(4)	0.025(4)	0.043(5)	-0.003(3)	-0.011(3)	-0.014(3)
C(3)	0.042(4)	0.029(4)	0.041(4)	-0.009(4)	-0.013(3)	-0.023(3)
C(4)	0.038(4)	0.029(4)	0.031(4)	-0.006(3)	-0.008(3)	-0.012(3)
C(5)	0.028(3)	0.021(4)	0.028(4)	-0.008(3)	-0.012(3)	-0.005(3)
C(6)	0.037(4)	0.018(4)	0.020(3)	0.000(3)	-0.012(3)	-0.009(3)
C(7)	0.047(4)	0.024(4)	0.021(3)	-0.007(3)	-0.008(3)	-0.009(3)
C(8)	0.031(4)	0.033(4)	0.015(3)	0.000(3)	0.001(3)	-0.005(3)
C(9)	0.031(4)	0.023(4)	0.020(4)	0.003(3)	0.001(3)	-0.004(3)
C(10)	0.023(3)	0.029(4)	0.026(4)	0.006(3)	0.001(3)	-0.007(3)
C(11)	0.027(3)	0.027(4)	0.023(4)	0.007(3)	-0.001(3)	-0.007(3)
C(12)	0.022(3)	0.025(4)	0.024(4)	0.001(3)	0.001(3)	-0.011(3)
C(13)	0.026(3)	0.018(4)	0.025(3)	-0.008(3)	0.000(3)	-0.005(3)
C(14)	0.020(3)	0.020(4)	0.026(4)	0.002(3)	-0.007(3)	-0.008(3)
C(15)	0.023(3)	0.034(4)	0.029(4)	0.006(3)	-0.009(3)	-0.017(3)
C(16)	0.018(3)	0.016(4)	0.041(4)	0.000(3)	-0.013(3)	-0.007(3)
C(17)	0.019(3)	0.020(4)	0.026(4)	0.005(3)	-0.007(3)	-0.002(3)
C(18)	0.028(3)	0.033(4)	0.028(4)	-0.001(3)	-0.012(3)	-0.015(3)
C(19)	0.033(4)	0.027(4)	0.034(4)	0.001(3)	0.001(3)	-0.014(3)
C(20)	0.038(4)	0.032(5)	0.027(4)	0.004(4)	-0.004(3)	-0.017(3)
C(21)	0.062(5)	0.047(5)	0.016(4)	0.003(4)	-0.014(3)	-0.028(4)
C(22)	0.081(6)	0.033(5)	0.037(5)	-0.014(4)	-0.002(4)	-0.024(4)
C(23)	0.029(3)	0.015(4)	0.027(4)	-0.001(3)	-0.001(3)	-0.007(3)
C(24)	0.040(4)	0.019(4)	0.029(4)	-0.007(3)	0.002(3)	-0.007(3)
C(25)	0.041(4)	0.020(4)	0.040(4)	0.004(3)	0.003(3)	-0.009(3)
C(26)	0.041(4)	0.019(4)	0.035(4)	-0.003(3)	0.005(3)	-0.009(3)
C(27)	0.025(3)	0.021(4)	0.022(3)	-0.003(3)	-0.002(3)	-0.011(3)
C(28)	0.023(3)	0.014(3)	0.026(3)	-0.005(3)	-0.004(3)	-0.017(2)
C(29)	0.042(4)	0.018(4)	0.025(4)	0.005(3)	-0.004(3)	-0.016(3)
C(30)	0.033(4)	0.030(4)	0.015(3)	-0.001(3)	-0.002(3)	-0.014(3)
C(31)	0.028(3)	0.025(4)	0.017(3)	-0.007(3)	-0.001(3)	-0.006(3)
C(32)	0.038(4)	0.037(5)	0.018(3)	-0.008(3)	0.004(3)	-0.014(3)
C(33)	0.034(4)	0.028(4)	0.029(4)	-0.009(3)	0.005(3)	-0.006(3)
C(34)	0.032(4)	0.024(4)	0.021(3)	-0.012(3)	-0.003(3)	-0.008(3)
C(35)	0.023(3)	0.026(4)	0.019(3)	-0.009(3)	-0.003(3)	-0.010(3)
C(36)	0.027(3)	0.017(4)	0.027(4)	-0.005(3)	-0.005(3)	-0.012(3)
C(37)	0.037(4)	0.011(3)	0.031(4)	-0.008(3)	-0.006(3)	-0.005(3)
C(38)	0.047(4)	0.017(4)	0.021(3)	-0.004(3)	-0.004(3)	-0.007(3)
C(39)	0.033(4)	0.016(4)	0.021(3)	-0.001(3)	-0.006(3)	-0.009(3)
C(40)	0.029(3)	0.017(4)	0.024(3)	-0.005(3)	-0.004(3)	-0.008(3)
C(41)	0.035(4)	0.022(4)	0.034(4)	0.006(3)	-0.007(3)	-0.014(3)
C(42)	0.035(4)	0.029(4)	0.034(4)	0.004(3)	-0.005(3)	-0.019(3)
C(43)	0.033(4)	0.039(5)	0.028(4)	0.002(3)	0.007(3)	-0.024(3)
C(44)	0.024(3)	0.031(4)	0.022(3)	-0.005(3)	0.000(3)	-0.008(3)

Copper Crystals

The crystals formed on the interface of the butanol/H_2O layers were thin, green, and fibrous. Figure 80 is a microscopic photograph of the crystals synthesized. Crystal structures were sent to be studied by x-ray crystallography. The crystal data and structural refinement parameters for the copper crystals are pending.

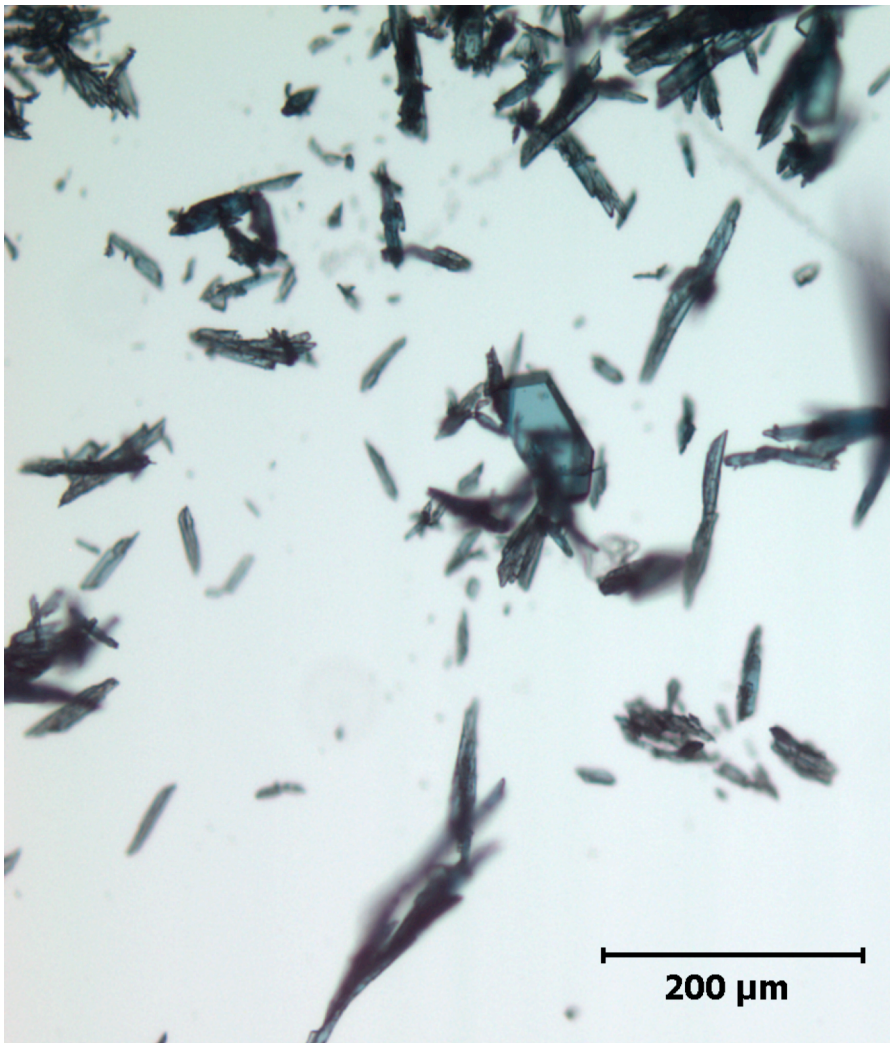

Figure 80. Microscopic view (10x) of crystals formed from equimolar amounts of DPP and $Cu(ClO_4)_2$.

3-D Fluorescence

DPP is a ligand where chelation enhanced fluorescence (CHEF) was observed. As previously discussed DPP fluoresces weakly as the free ligand. The fluorescence spectra of the free ligand are shown in Figure 81. The reason it fluoresces so weakly is because of a quenching effect caused by the lone pairs of electrons on the nitrogens. The free ligand has a weak emission at 315 nm when excited at 260 nm. This molecule is extremely rigid and has high aromaticity, which are properties that are optimal for fluorescence. The concentration of the free ligand was 1×10^{-8} M. This was because the free ligand at 1×10^{-6} M fluoresced so strongly that it was off-scale. This is important because it allows a very low concentration of metal to be detected.

To illustrate the CHEF effect, fluorescence spectra of 1×10^{-8} M DPP at a pH=1 were taken. At this pH the ligand was fully protonated and all of the lone pairs were coordinated to a proton. Figure 82 is the spectra of DPP at pH=1. The intensity of the spectra increases to QSE=25 and the emission spectrum maximum shifts to 450 nm. The increase in fluorescence once the lone pairs are coordinated means that the same effect will be observed when DPP binds a metal ion, if not stronger because of the added rigidity a metal complex will have.

The basis for choosing metals to study the fluorescent properties of their complexes was the stability constant data previously reported. Lead and mercury were studied because of their toxic properties and potential health risks. The fluorescence spectra of zinc were studied because it is a metal commonly found in the body and could potentially compete when trying to detect calcium. Cadmium was obviously studied because of its high stability with DPP.

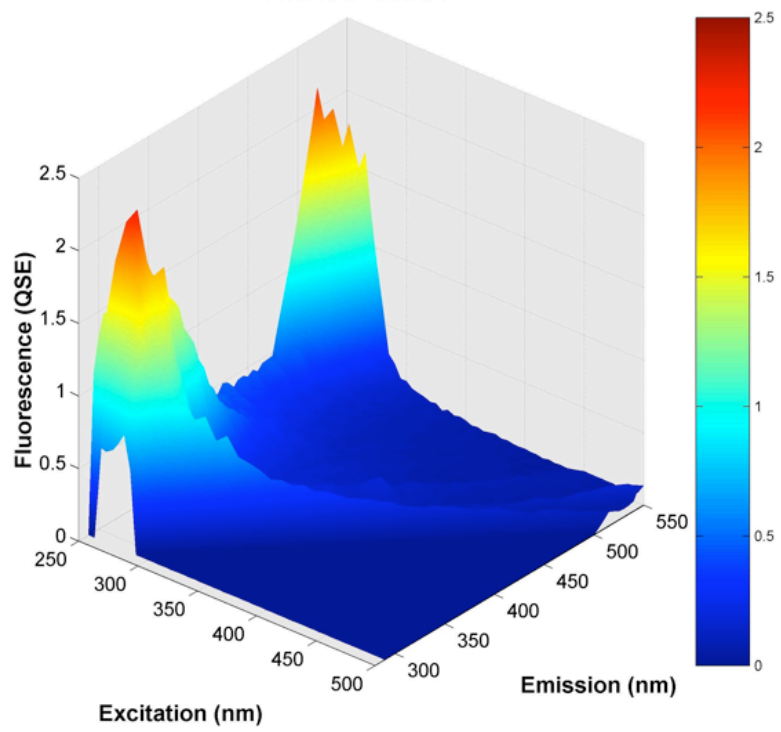

a)

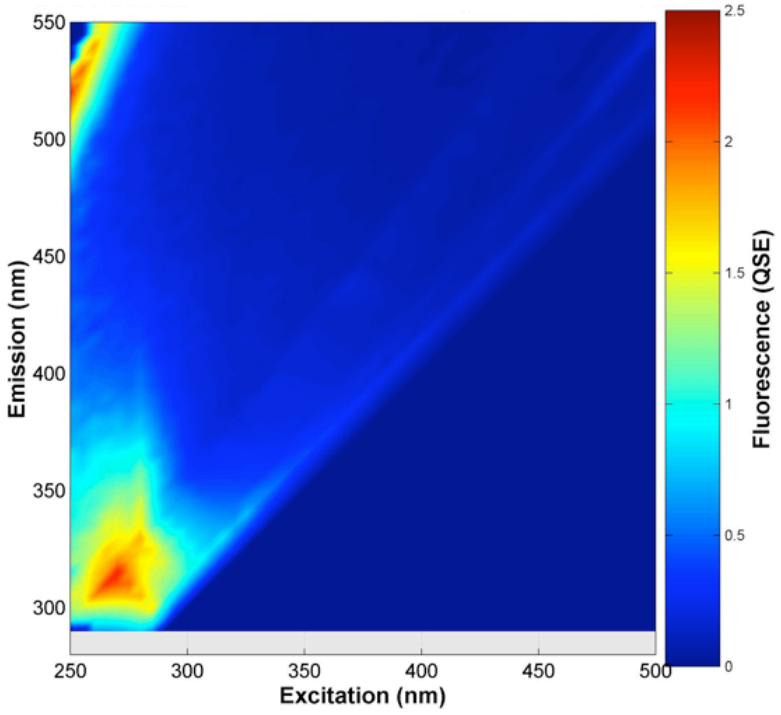

b)

Figure 81. a) 3-dimensional fluorescence spectrum of solution of 1 x 10^{-8} M DPP at pH=7. **b)** 2-dimensional fluorescence spectrum of same solution.

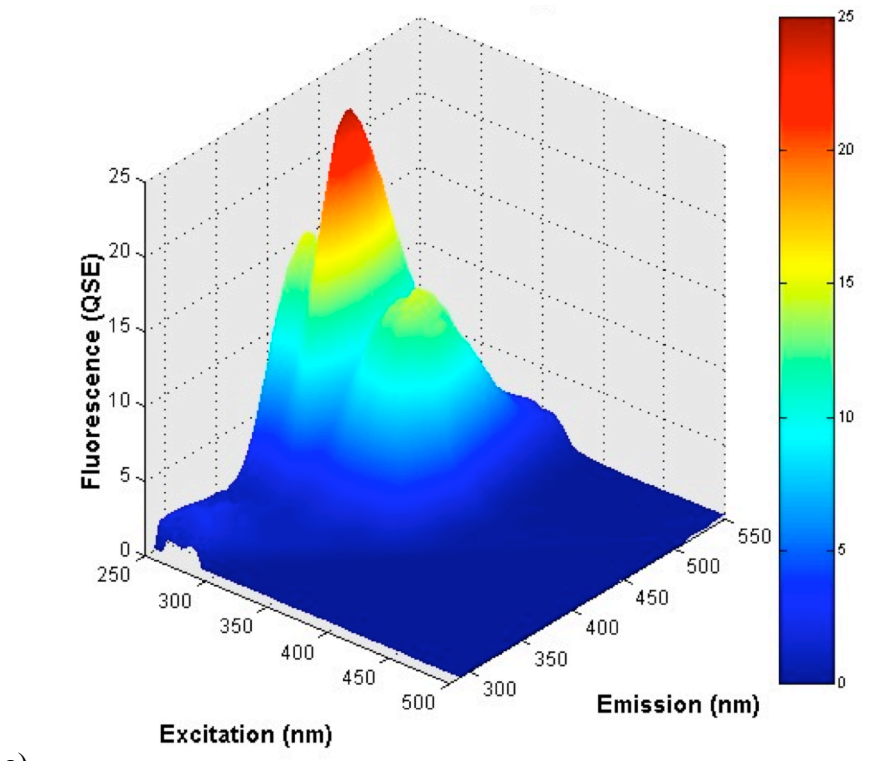

a)

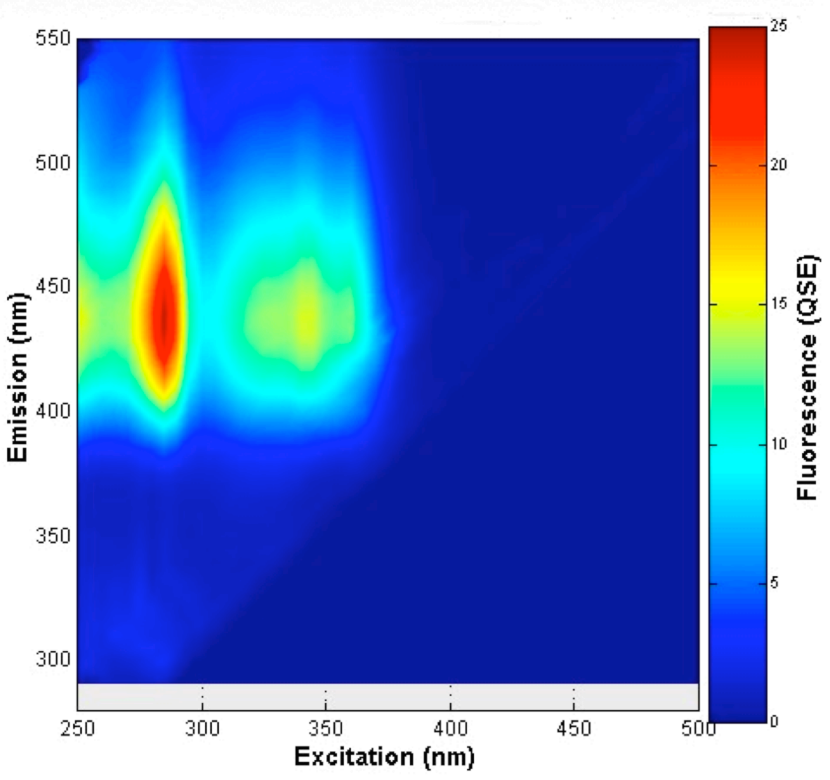

b)

Figure 82. a) 3-dimensional fluorescence spectrum of solution of 1 x 10^{-8} M DPP at pH=1. **b)** 2-dimensional fluorescence spectrum of same solution.

Fluorescence of Cadmium Complex

Cadmium was one of the metals studied that had high stability with DPP (log K_1 = 12.2). The significant difference in log K_1 between cadmium and other metal ions means that cadmium can be detected in an aqueous solution containing other metals. Several solutions of DPP with various cadmium concentrations were prepared to construct a calibration curve of fluorescent intensity versus cadmium concentration. Table 62 summarizes the experimental design and the QSE at an excitation wavelength of 280 nm and an emission wavelength of 385 nm.

Table 62. Experimental design of cadmium complex fluorescence.

[DPP] (M)	[Cd^{2+}] (M)	Fluorescence (QSE)
1 X 10^{-8}	1 x 10^{-6}	15.565
1 X 10^{-8}	1 x 10^{-7}	14.916
1 X 10^{-8}	1 x 10^{-8}	6.2895
1 X 10^{-8}	1 x 10^{-9}	4.9
1 X 10^{-8}	1 x 10^{-10}	1.3947

The fluorescence spectra for each cadmium concentration are shown below in Figures 83-87 respectively. The calibration curve constructed from the data collected is shown in Figure 88. Figure 89 shows the emission spectrum of the free ligand and various cadmium concentrations at an excitation wavelength of 280 nm.

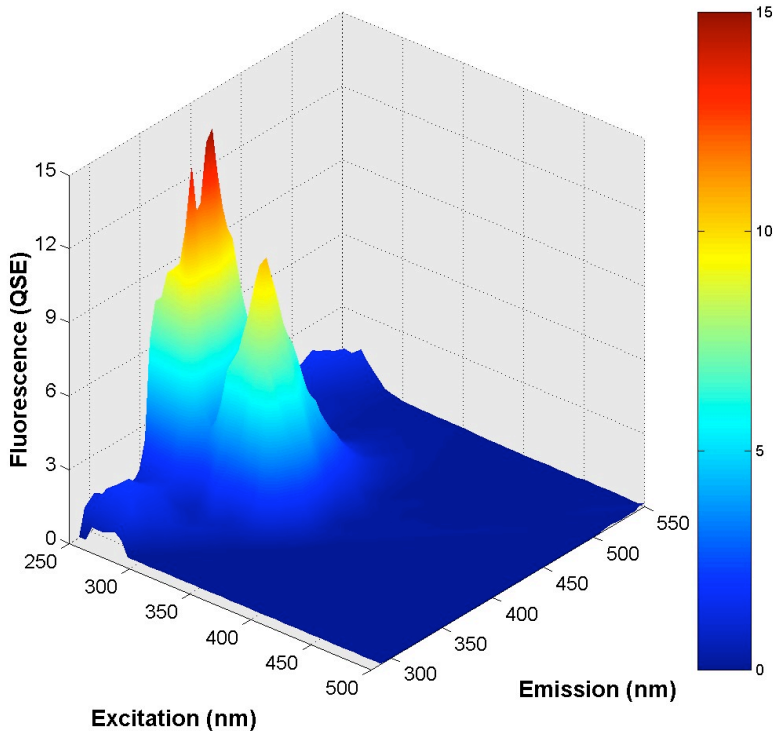

a)

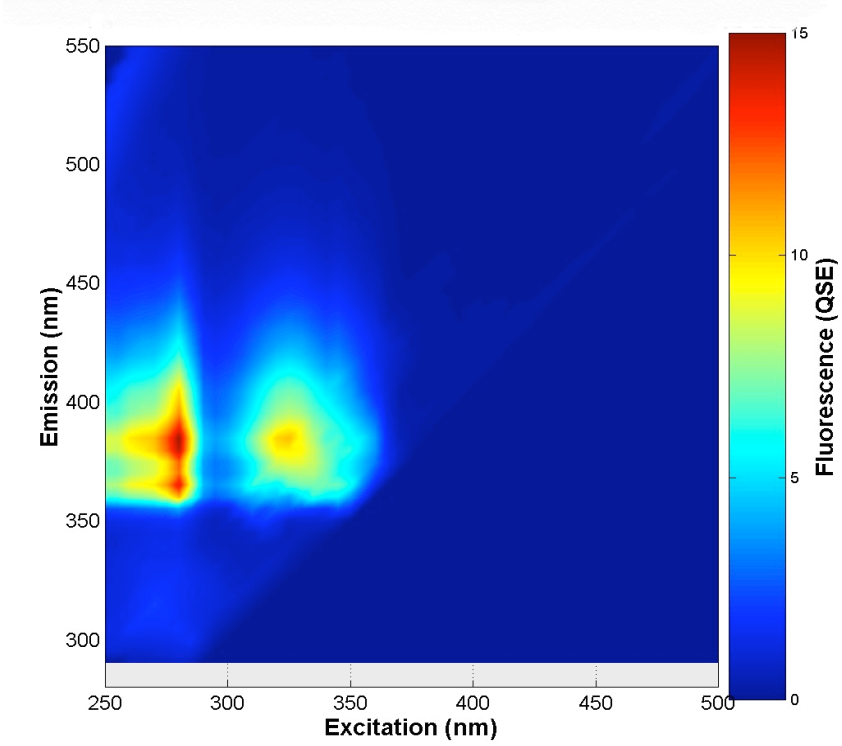

b)

Figure 83. a) 3-dimensional fluorescence spectrum of solution of 1 x 10^{-8} M DPP and 1 x 10^{-6} M $Cd(ClO_4)_2$. **b)** 2-dimensional fluorescence spectrum of same solution.

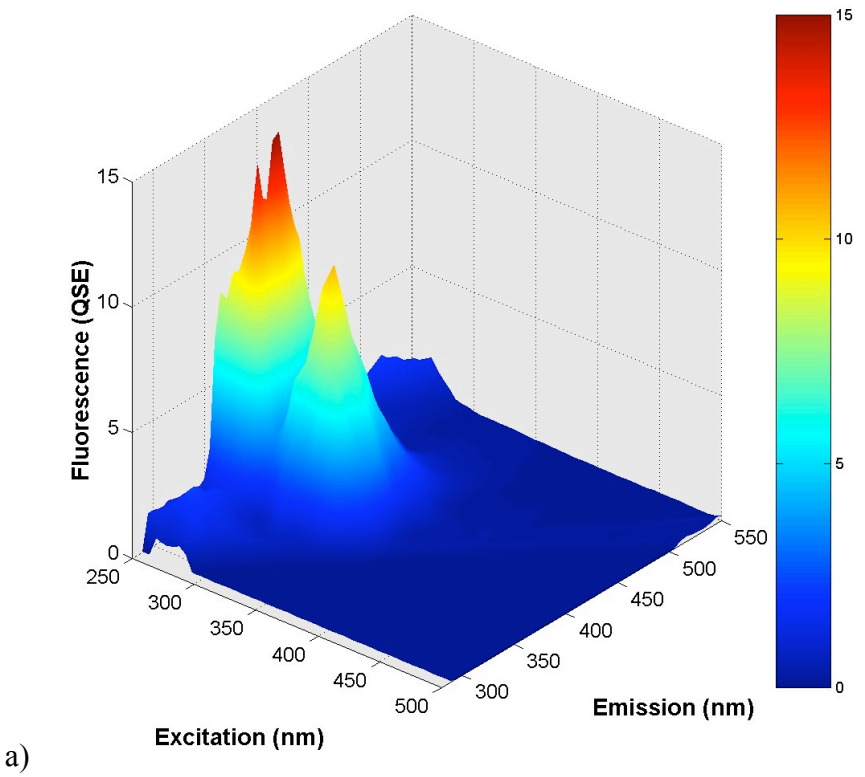

a)

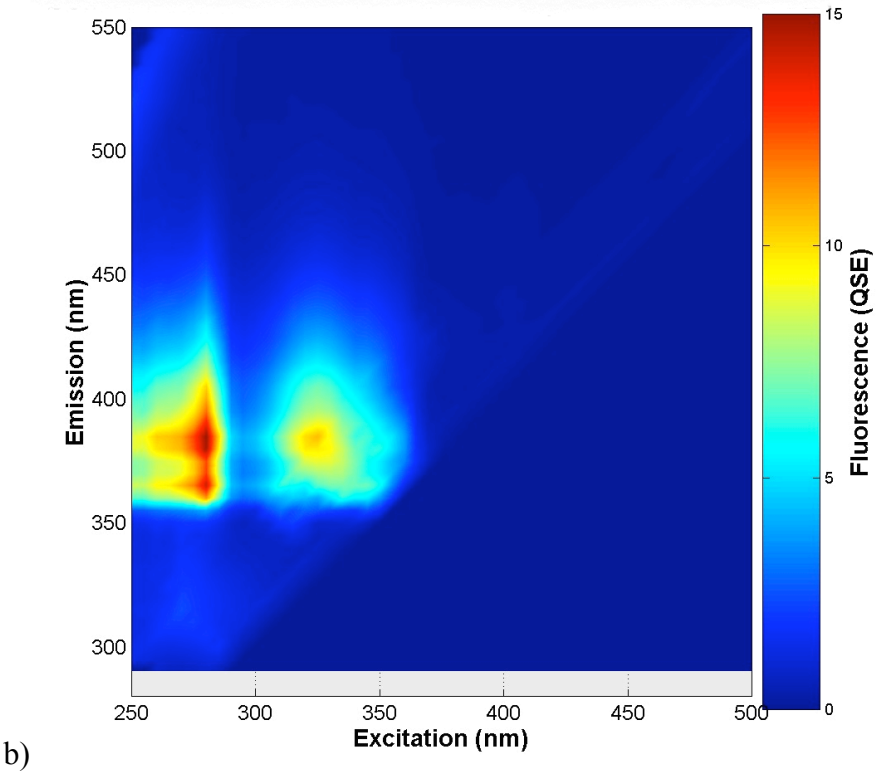

b)

Figure 84. a) 3-dimensional fluorescence spectrum of solution of 1 x 10^{-8} M DPP and 1 x 10^{-7} M $Cd(ClO_4)_2$. **b)** 2-dimensional fluorescence spectrum of same solution.

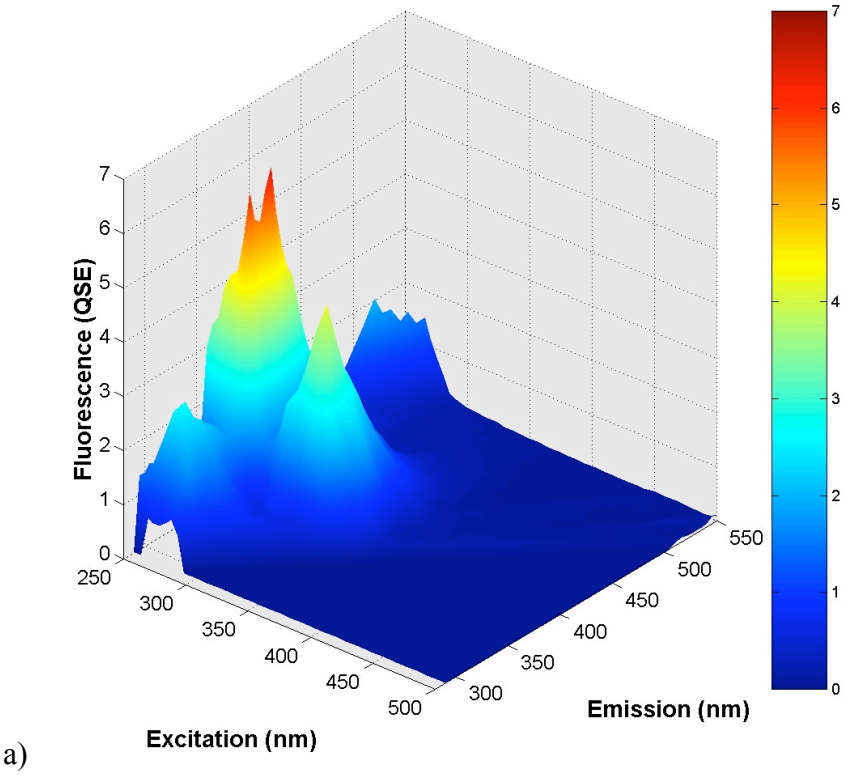

a)

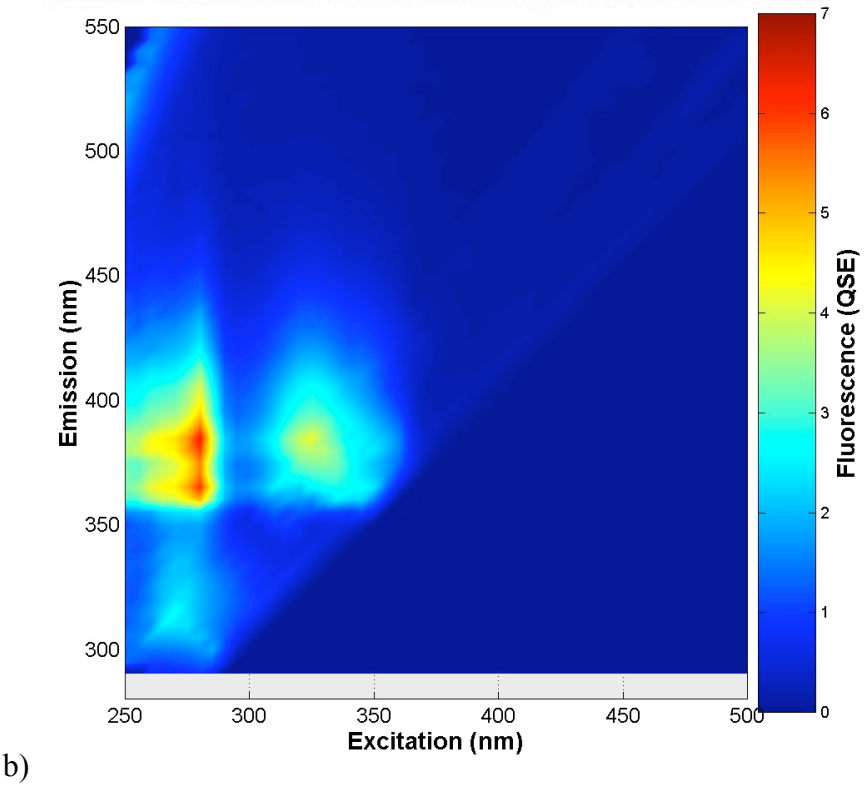

b)

Figure 85. a) 3-dimensional fluorescence spectrum of solution of 1 x 10^{-8} M DPP and 1 x 10^{-8} M $Cd(ClO_4)_2$. **b)** 2-dimensional fluorescence spectrum of same solution.

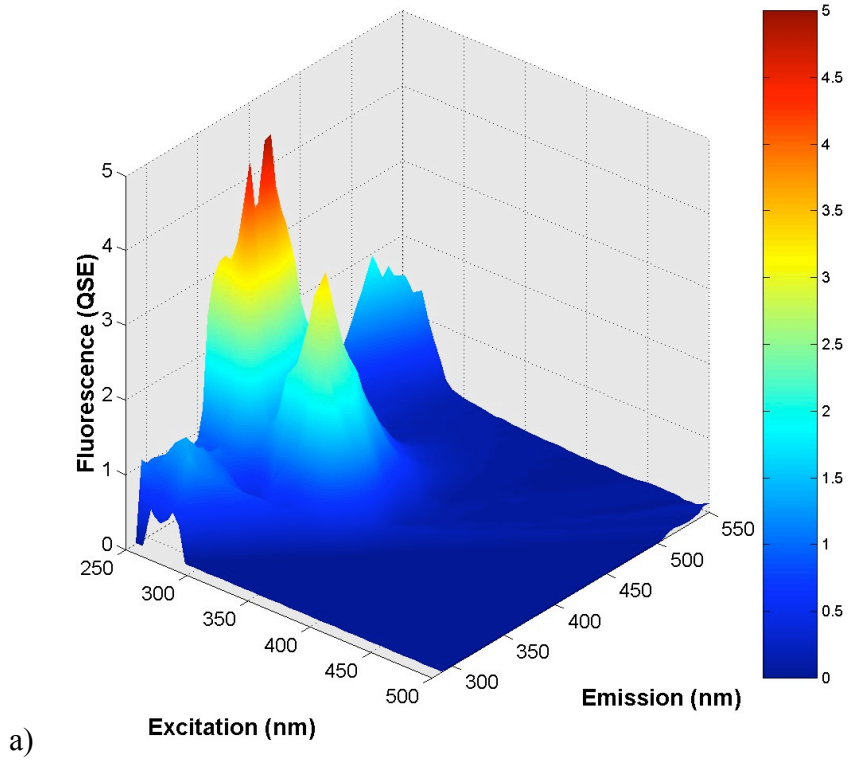

a)

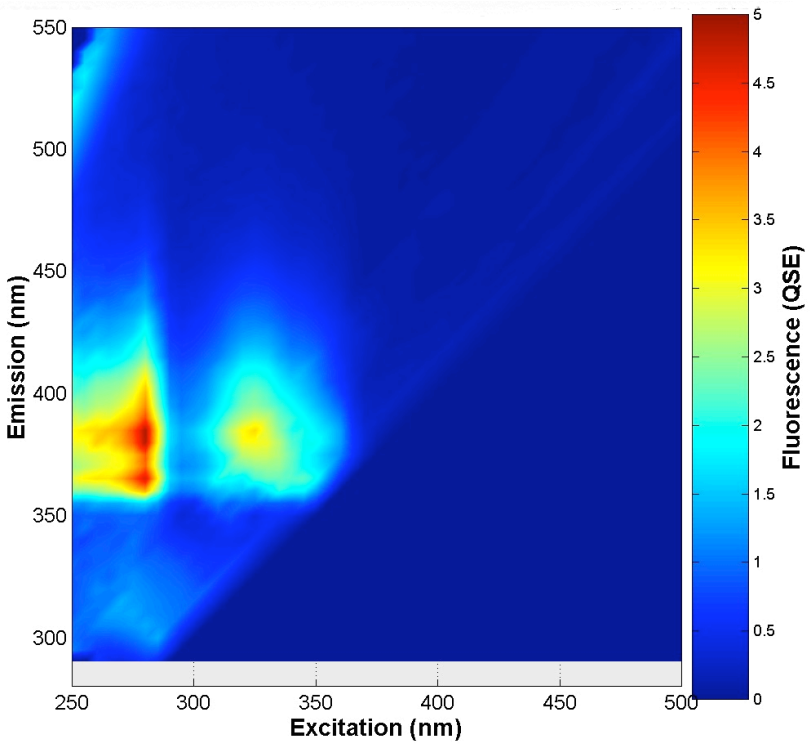

b)

Figure 86. a) 3-dimensional fluorescence spectrum of solution of 1 x 10^{-8} M DPP and 1 x 10^{-9} M $Cd(ClO_4)_2$. **b)** 2-dimensional fluorescence spectrum of same solution.

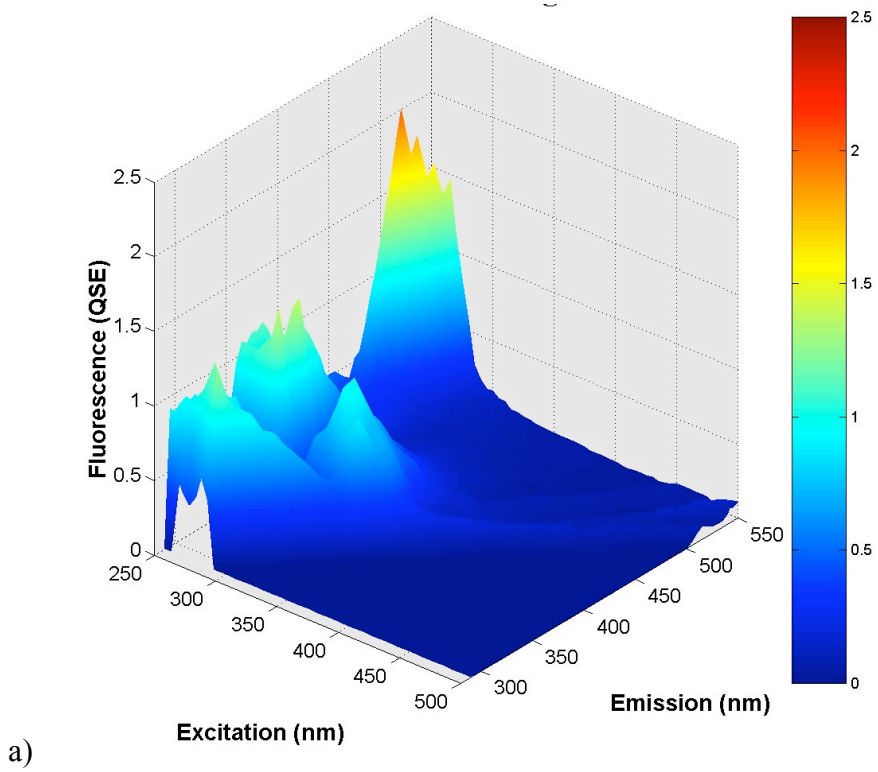

a)

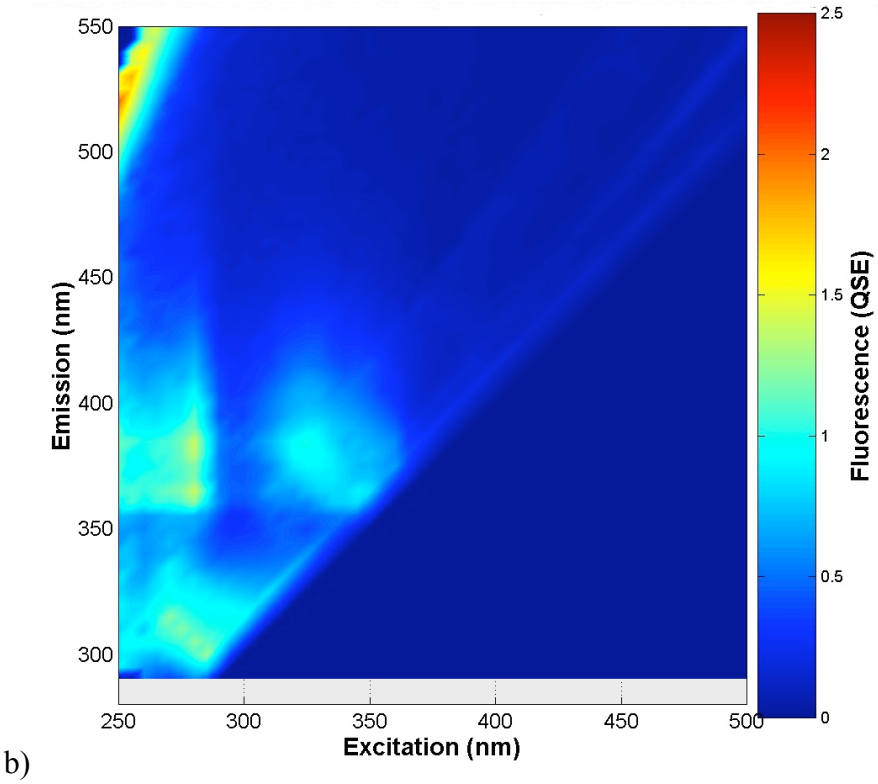

b)

Figure 87. a) 3-dimensional fluorescence spectrum of solution of 1 x 10^{-8} M DPP and 1 x 10^{-10} M $Cd(ClO_4)_2$. **b)** 2-dimensional fluorescence spectrum of same solution.

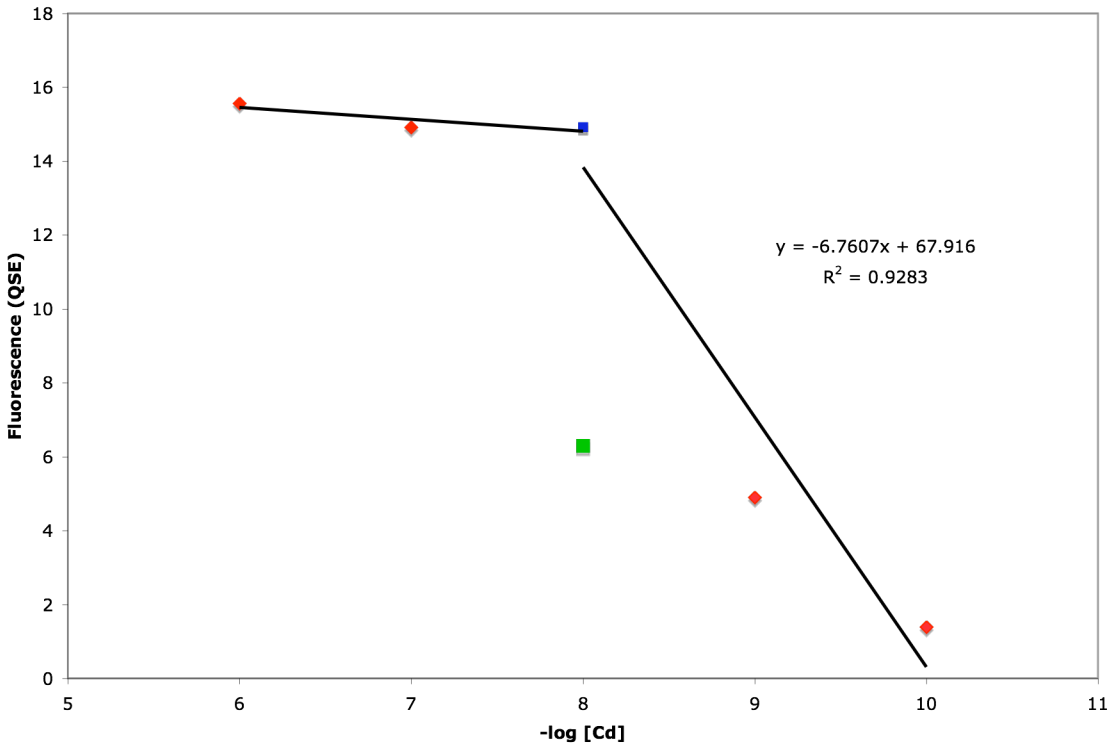

Figure 88. Calibration curve of intensity versus cadmium concentration for fluorescence experiment. Blue data point is theoretical intensity at 1:1 concentrations. Green data point is actual measured fluorescence.

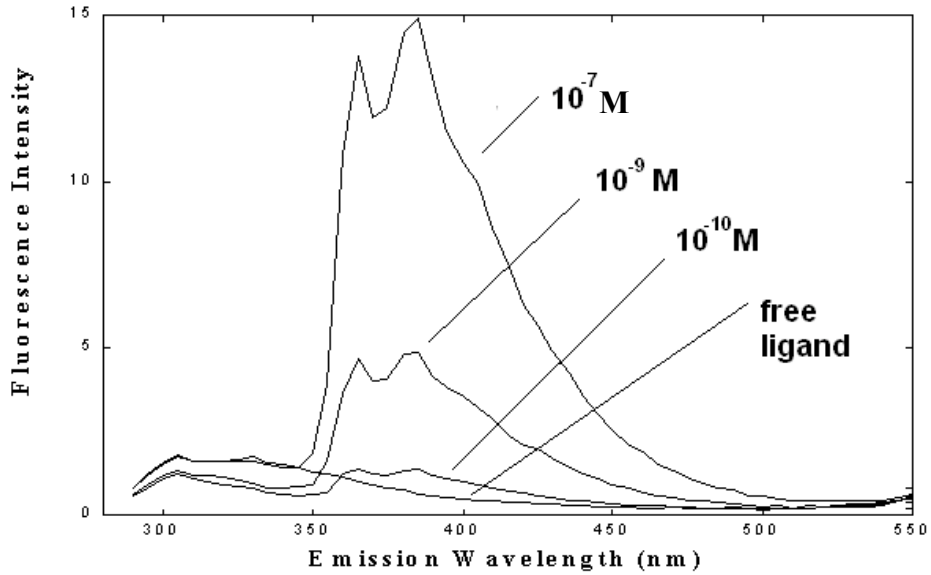

Figure 89. Emissions spectra of cadmium complex at different concentrations and free ligand as a baseline at an excitation wavelength of 280 nm.

The plot has linear characteristics but does not have a good fit. The data point corresponding to the ligand and metal concentrations in a one to one ratio was lower in intensity than expected (green data point). A one to one cadmium DPP solution should have a full signal, i.e. about the same QSE as the solutions with cadmium excess (blue data point). This experiment was run in triplicate with the same results. One explanation for the quenching of the fluorescent signal is π-stacking and electrostatic interactions (Neelakandan, 2006). A calibration curve constructed from experiments correcting for π-stacking is predicted to yield a stronger linear relationship. Although quantitative data was poor due to possible π-stacking, Figures 83-87 are qualitatively significant because of the increase in intensity compared to the free ligand spectra (Figure 81). Figure 89 shows that there is a significant difference in fluorescence intensity between the free ligand and a cadmium concentration of 1×10^{-10} M. More studies need to be conducted to determine the limit of detection but this initial data shows that cadmium can be detected at very low concentrations, which demonstrates DPP to be highly sensitive. The selectivity of DPP for use as a fluorescent detector was explored by studying fluorescent properties of other DPP-metal complexes.

Fluorescence of Calcium Complex

Calcium was tested with DPP because it is a common metal ion found in the body. Tracking calcium as it travels between cells is important to discover cellular activity. Calcium is also abundant in seawater and could potentially displace a small amount of cadmium at high concentrations and fluoresce. Two solutions of DPP and calcium were made. The first solution was 0.01 M calcium and the second was 0.001 M

calcium. DPP had a concentration of 1 x 10^{-8} M in both solutions. The fluorescence spectra are shown in Figures 90 and 91.

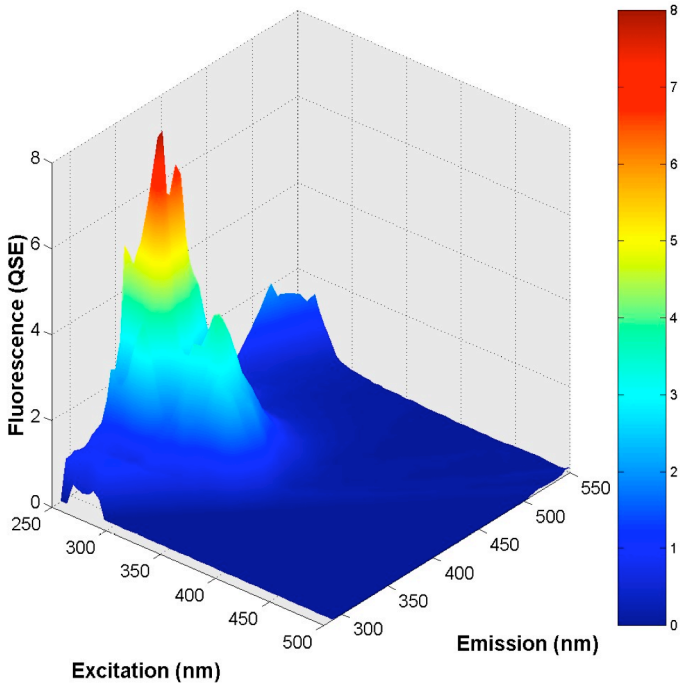

a)

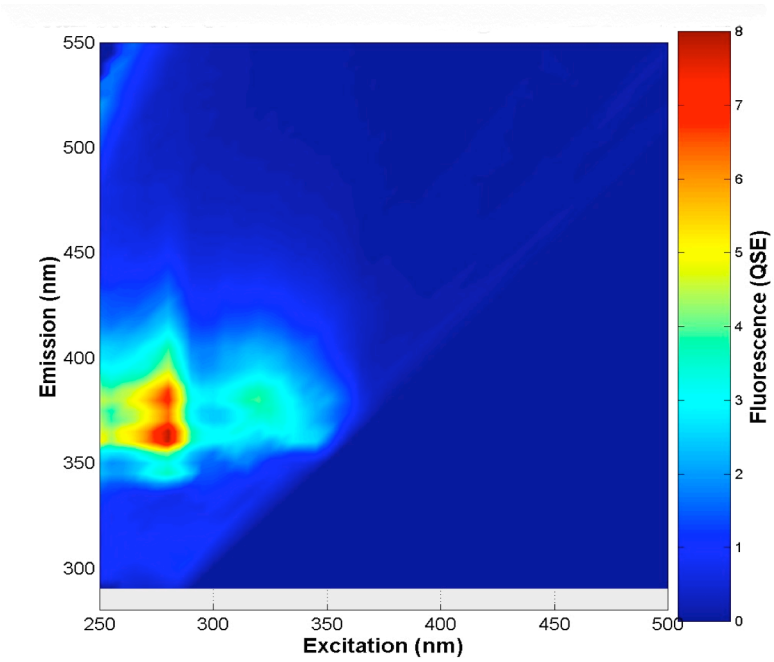

b)

Figure 90. a) 3-dimensional fluorescence spectrum of solution of 1 x 10^{-8} M DPP and 1 x 10^{-2} M $Ca(ClO_4)_2$. **b)** 2-dimensional fluorescence spectrum of same solution.

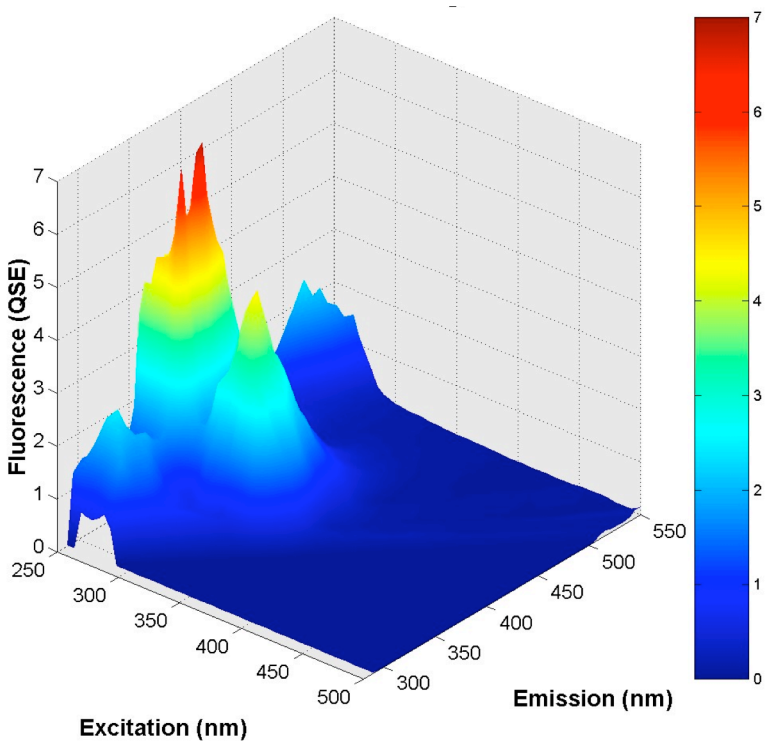

a)

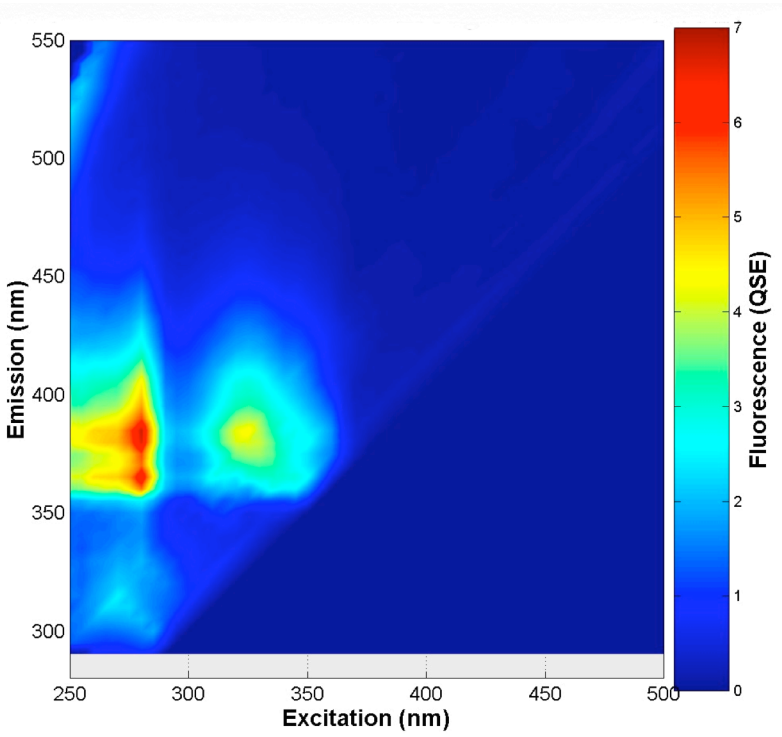

b)

Figure 91. a) 3-dimensional fluorescence spectrum of solution of 1 x 10^{-8} M DPP and 1 x 10^{-3} M $Ca(ClO_4)_2$. **b)** 2-dimensional fluorescence spectrum of same solution.

At an excitation wavelength of 280 nm and an emission wavelength of 365 nm the intensity of the 0.01 M and 0.0001 M DPP-calcium solutions were 7.944 QSE and 6.5265 QSE respectively. This is in good agreement with the log K_1 data previously reported. The decrease in fluorescent intensity with decreasing calcium concentration from 0.01 M to 0.0001 M is consistent with a log K_1 of about 2. The fluorescence spectra of a third solution of 1 x 10^{-5} M calcium and 1 x 10^{-8} M DPP were analyzed to explore the sensitivity of the DPP-calcium complex. The spectra are shown in Figure 92. At low concentrations, calcium cannot be detected by DPP because the fluorescence spectra resemble those of the free ligand. This means at lower concentrations calcium would not displace cadmium but could be detected by fluorescence at higher concentrations. Since DPP has high selectivity of cadmium over calcium, it may prove to be an excellent cadmium detector in seawater.

Fluorescence of Zinc Complex

Zinc is a metal ion that is commonly found in biological systems. Zinc has a higher log K_1 with DPP than calcium, which could be problematic if zinc fluoresces with DPP. A solution of 1 x 10^{-8} M DPP and 1x 10^{-8} $Zn(ClO_4)_2$ was prepared and the fluorescence spectrum was analyzed. The spectrum of the Zn-DPP complex is shown in Figure 93. The spectrum shows that there is no change in fluorescence between the free ligand and the zinc complex. As previously reported zinc does not span the cavity created by DPP and cannot bind to all four donor atoms. This means that one of the pyridine rings is non-bonded, so there is still a lone pair that quenches the fluorescence to some extent, and the rigidity of the complex is not as high as metals that bind completely.

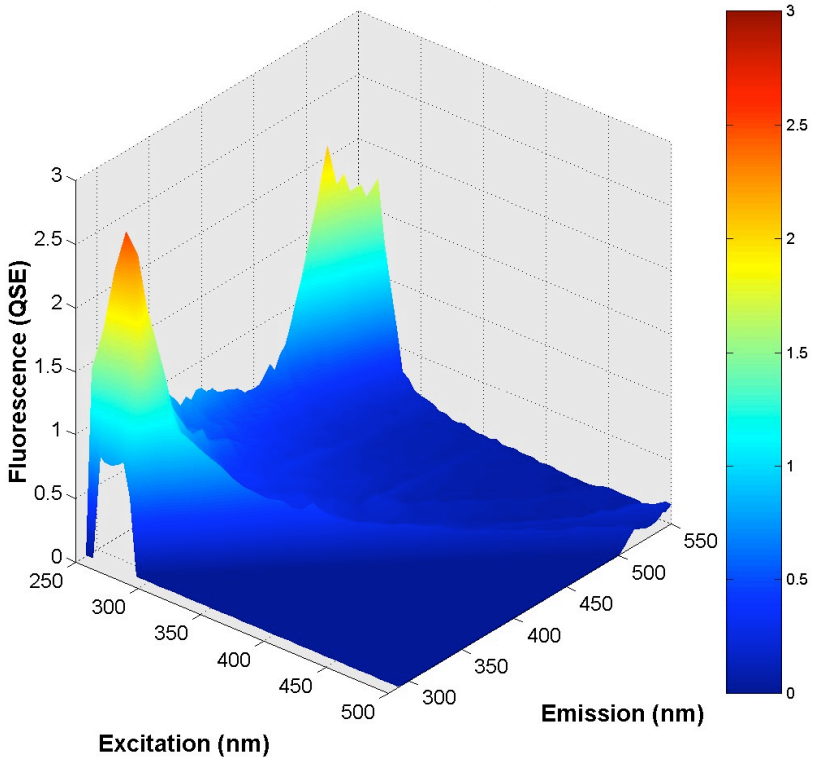

a)

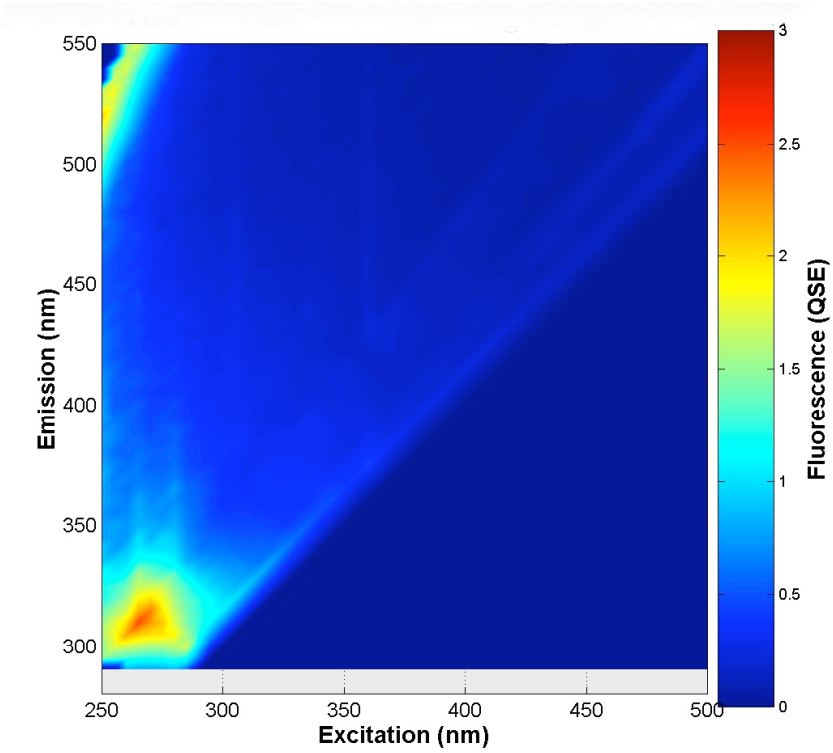

b)

Figure 92. a) 3-dimensional fluorescence spectrum of solution of 1 x 10^{-8} M DPP and 1 x 10^{-5} M $Ca(ClO_4)_2$. **b)** 2-dimensional fluorescence spectrum of same solution.

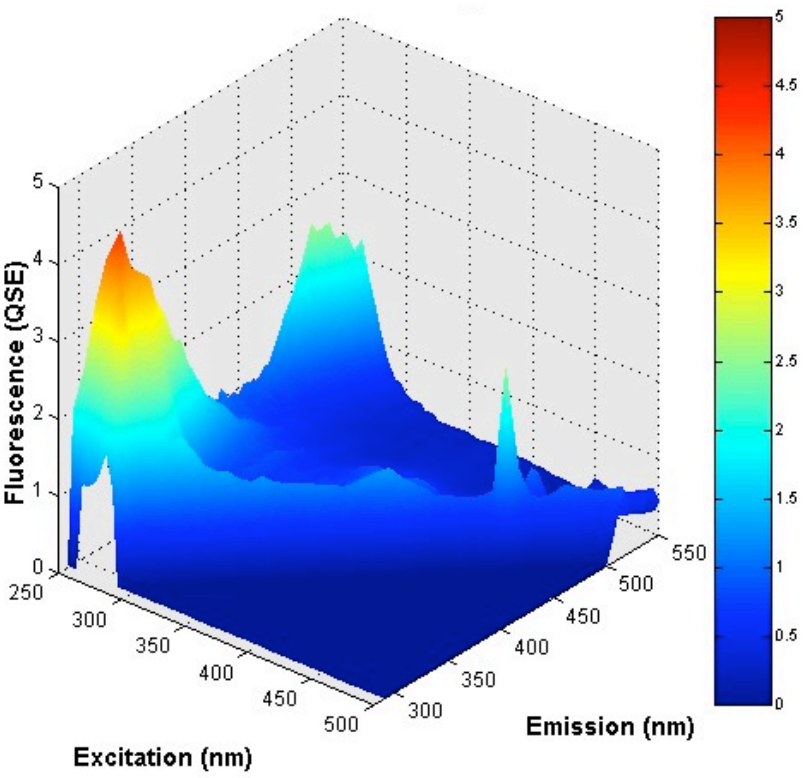

a)

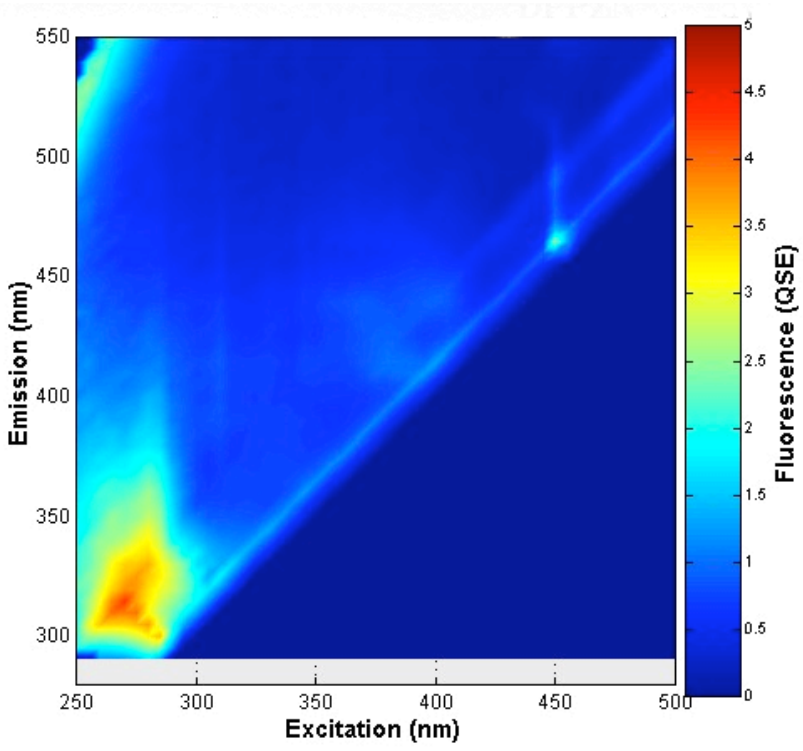

b)

Figure 93. a) 3-dimensional fluorescence spectrum of solution of 1 x 10^{-8} M DPP and 1 x 10^{-8} M $Zn(ClO_4)_2$. **b)** 2-dimensional fluorescence spectrum of same solution.

Fluorescence of Mercury and Lead Complexes

Lead and mercury were two of the heavier metal ions that were studied to test the selectivity of DPP. A solution of 1 x 10^{-8} M DPP and 1x 10^{-8} $Hg(ClO_4)_2$ was prepared and the fluorescence spectra were analyzed. The spectrum of the Hg-DPP complex is shown in Figure 94. The spectrum shows that there is no significant difference in fluorescence between the free ligand and the mercury complex. To test the fluorescence of the Pb-DPP complex, a 1 x 10^{-8} M DPP and 1 x 10^{-8} M $Pb(ClO_4)_2$ solution was prepared. The fluorescence spectrum is shown in Figure 95. There was no difference in the Pb-DPP spectrum and the free ligand. The significance of these fluorescence results is that these two metals that DPP has a high affinity for do not cause any change in fluorescence. In the presence of mercury, cadmium would not be detected. This is because mercury has a large log K_1 with DPP and would displace the cadmium. Fluorescence would not be observed in this solution. High concentrations of lead could displace the cadmium from DPP, but again no fluorescence would be observed.

Cadmium was the only heavy metal that was tested that had a significant change in the fluorescence. The only metal that poses a problem in high concentrations is calcium since fluorescence increases much like the Cd-DPP spectrum. More studies need to be conducted on other possible metals for fluorescence detection.

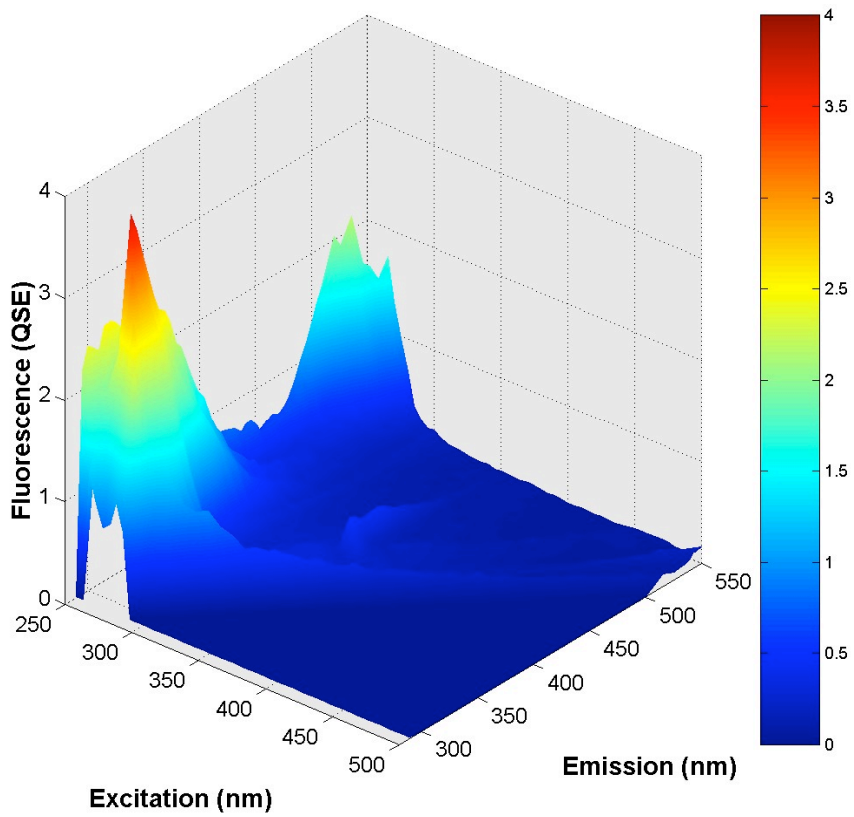

a)

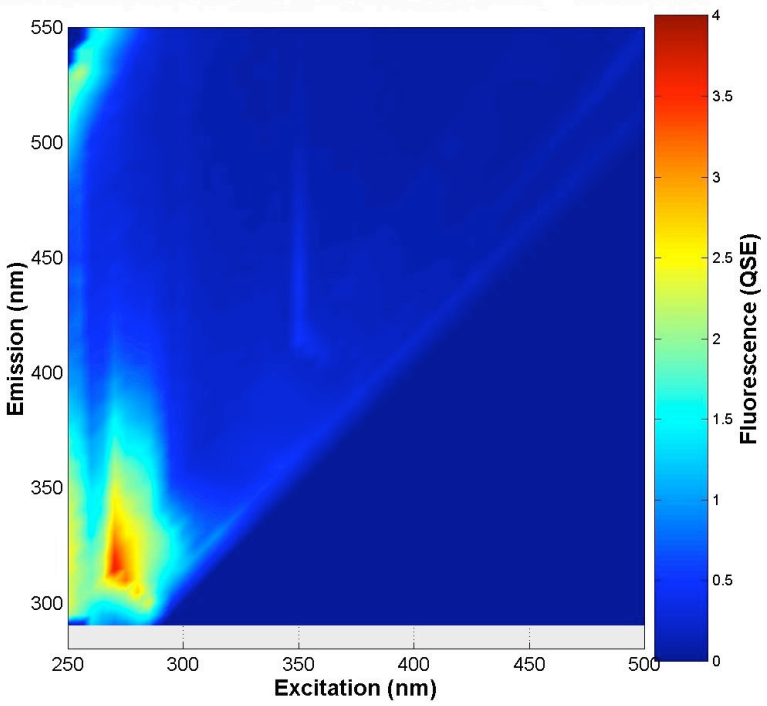

b)

Figure 94. a) 3-dimensional fluorescence spectrum of solution of 1 x 10^{-8} M DPP and 1 x 10^{-8} M $Hg(ClO_4)_2$. **b)** 2-dimensional fluorescence spectrum of same solution.

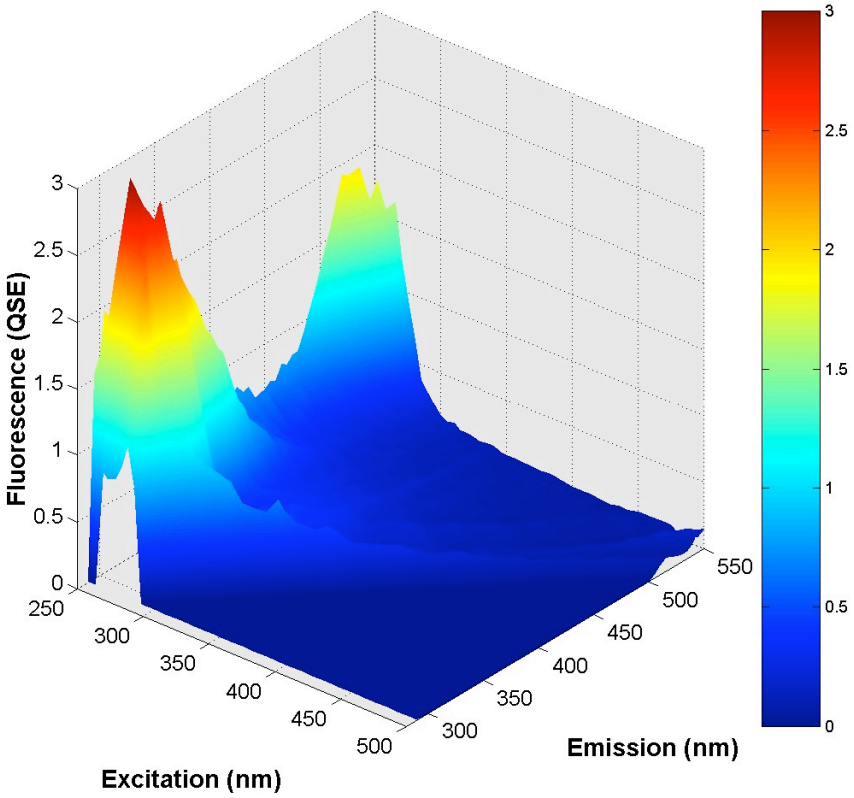

a)

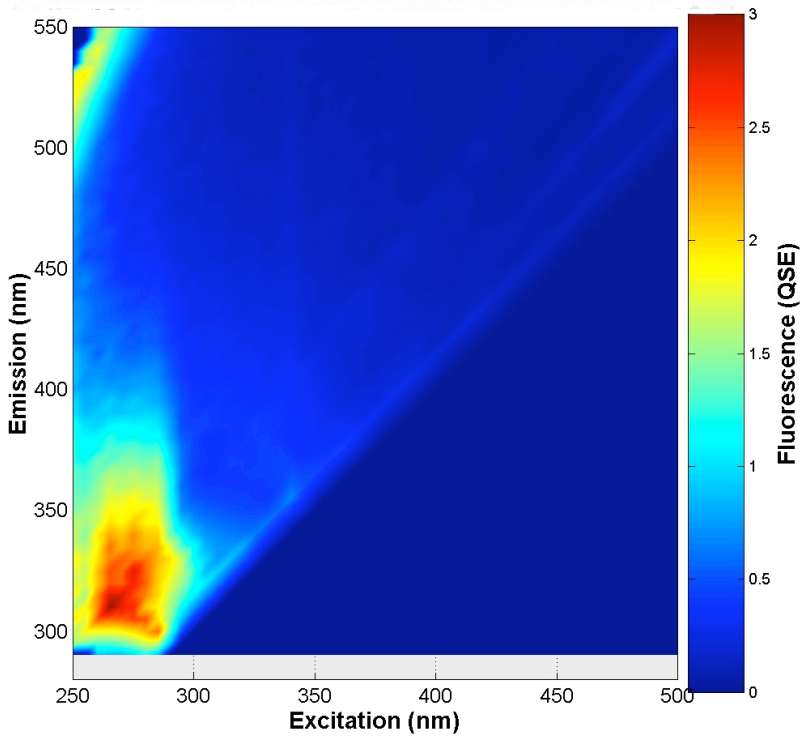

b)

Figure 95. a) 3-dimensional fluorescence spectrum of solution of 1 x 10^{-8} M DPP and 1 x 10^{-8} M $Pb(ClO_4)_2$. **b)** 2-dimensional fluorescence spectrum of same solution.

Fluorescence of Sodium Complex

Sodium was the last of the metal ions studied by fluorescent spectroscopy. The reason sodium was studied was because all UV titrations were conducted in 0.10 M $NaClO_4$. The UV spectra of the free ligand had no complex characteristics and indicated that sodium did not form any complex with DPP at that concentration. However, sodium has an ionic radius of 1.00 Å and is about the perfect size to bind DPP. Sodium is a monovalent cation and a hard acid. These are not optimal characteristics to bind DPP, but because of its size sodium is predicted to make a complex with weak stability. To test the formation of a sodium complex, a 1 x 10^{-8} M DPP solution was prepared in 1 M $NaClO_4$ and the fluorescent spectrum was analyzed. The spectrum of this solution is shown in Figure 96. There was an obvious complex formation based on the spectra as indicated by the increased intensity. This spectrum also has similar characteristics to the previously reported spectra of calcium and cadmium. Although the spectra are similar, the intensity of the sodium spectrum was not as high as the cadmium spectrum. This puts into perspective just how weakly sodium binds to DPP because the sodium solution was 100 million times more concentrated than the cadmium solution and had weaker fluorescence. This also confirms the UV data previously reported for the free ligand that no sodium complex was observed at pH=2, as it would have easily been displaced by a proton.

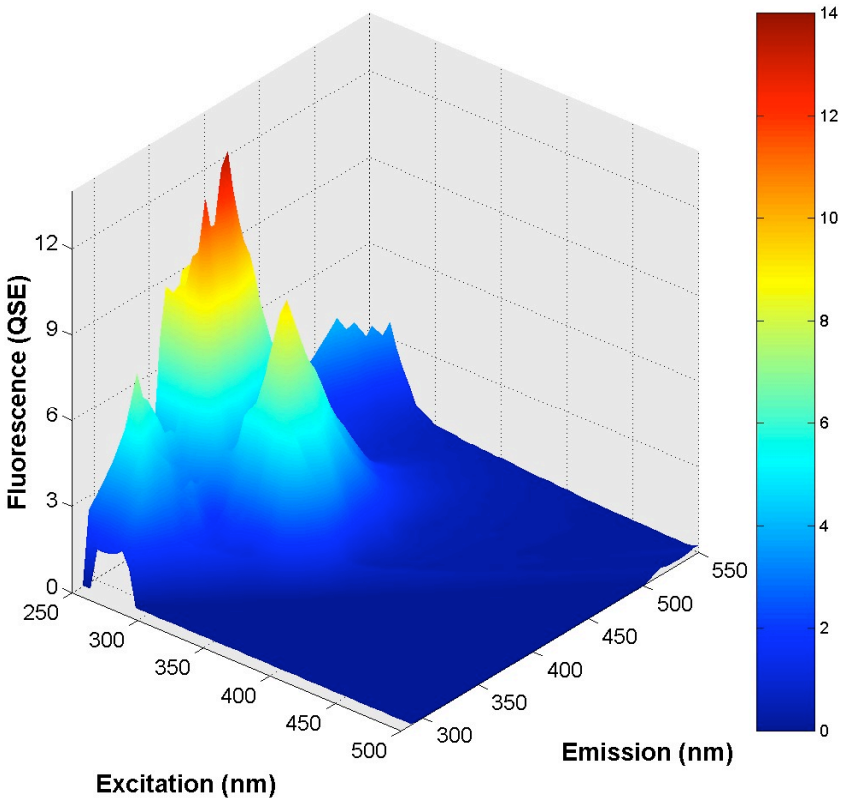

a)

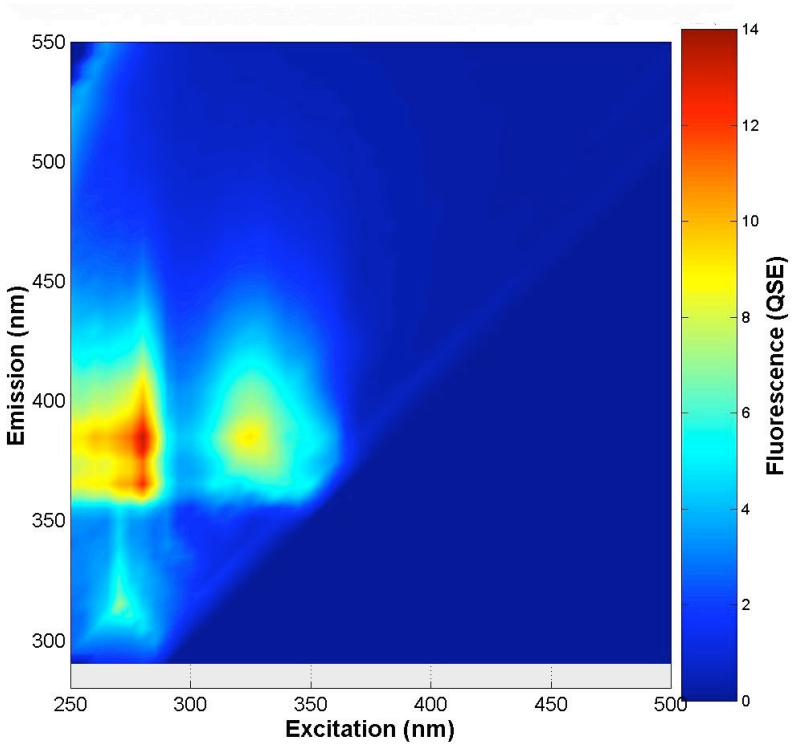

b)

Figure 96. a) 3-dimensional fluorescence spectrum of solution of 1 x 10^{-8} M DPP and 1 M $NaClO_4$. **b)** 2-dimensional fluorescence spectrum of same solution.

CONCLUSIONS

Both sensitivity and selectivity are important characteristics in fluorescent sensors. DPP possesses both properties for cadmium. This has proven to be an excellent ligand for cadmium and can be used for several of the purposes described previously. The fact that lead and mercury do not fluoresce upon forming complexes means that cadmium could be detected in an aqueous solution containing other metals. The solubility of DPP is not a problem as a sensor because of its sensitivity. A very small amount of DPP was proven to still give a fluorescent signal. Although this does not pose a problem for use as a cadmium sensor, the ligand would need to be altered to increase its solubility for uses in biological systems. This could include a number of substituents added to the phenanthroline backbone like ketone groups. These subtituents would not change the binding properties or the stability of the metal-ligand complexes.

Heavier metal ions are toxic as previously discussed. Metals like lead, mercury, and cadmium that can find their way easily into biological systems pose severe health risks. The affinity DPP has for these three heavier metals shows that a more soluble variation of DPP could be used for chelation therapy. Mercury is especially important, because of its increasing concentration in fish. DPP has a very high affinity for mercury and a log K_1 could not be calculated with available materials. This means that DPP could mask the toxicity of mercury introduced in a biological system without being displaced by any other metal ions.

ADDITIONAL RESEARCH FOR FUTURE STUDIES

The research reported in this paper is just one out of many 1,10-phenanthroline derivatives studied. Additional research done coinciding with this project was the synthesis of 1,10-phenanthroline-2,9-dicarboxaldehyde (PDALD). Previous studies have claimed synthesis of PDALD but have reported an impure product (Chandler, 1981). The reported melting point was 232°C and IR peaks at 1720 cm^{-1} and 1700 cm^{-1}. This impurity is expected to be a carboxylic acid derivative (PDA) due to over-oxidation. PDA was not a desired product because it has been extensively studied (Melton, 2005).

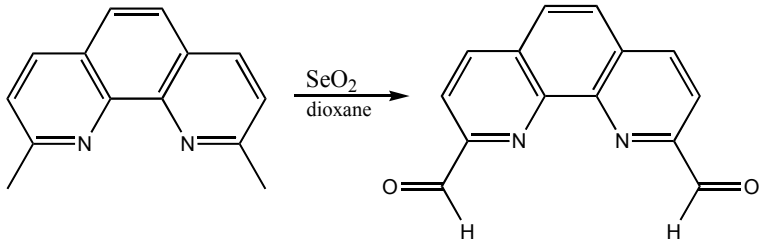

Figure 97. Synthesis of PDALD from 2,9-dimethyl-1,10-phenanthroline and selenium dioxide.

No reaction temperature was reported in the paper. The product of this reaction was a yellow solid, which was recrystallized in THF. The IR of the recrystallized product is shown in Figure 98. The IR shown agrees with the IR obtained by Chandler *et al,* as well as the melting point. Experiments were conducted by varying reaction temperatures and times to minimize the impurity in the product before recrystallization.

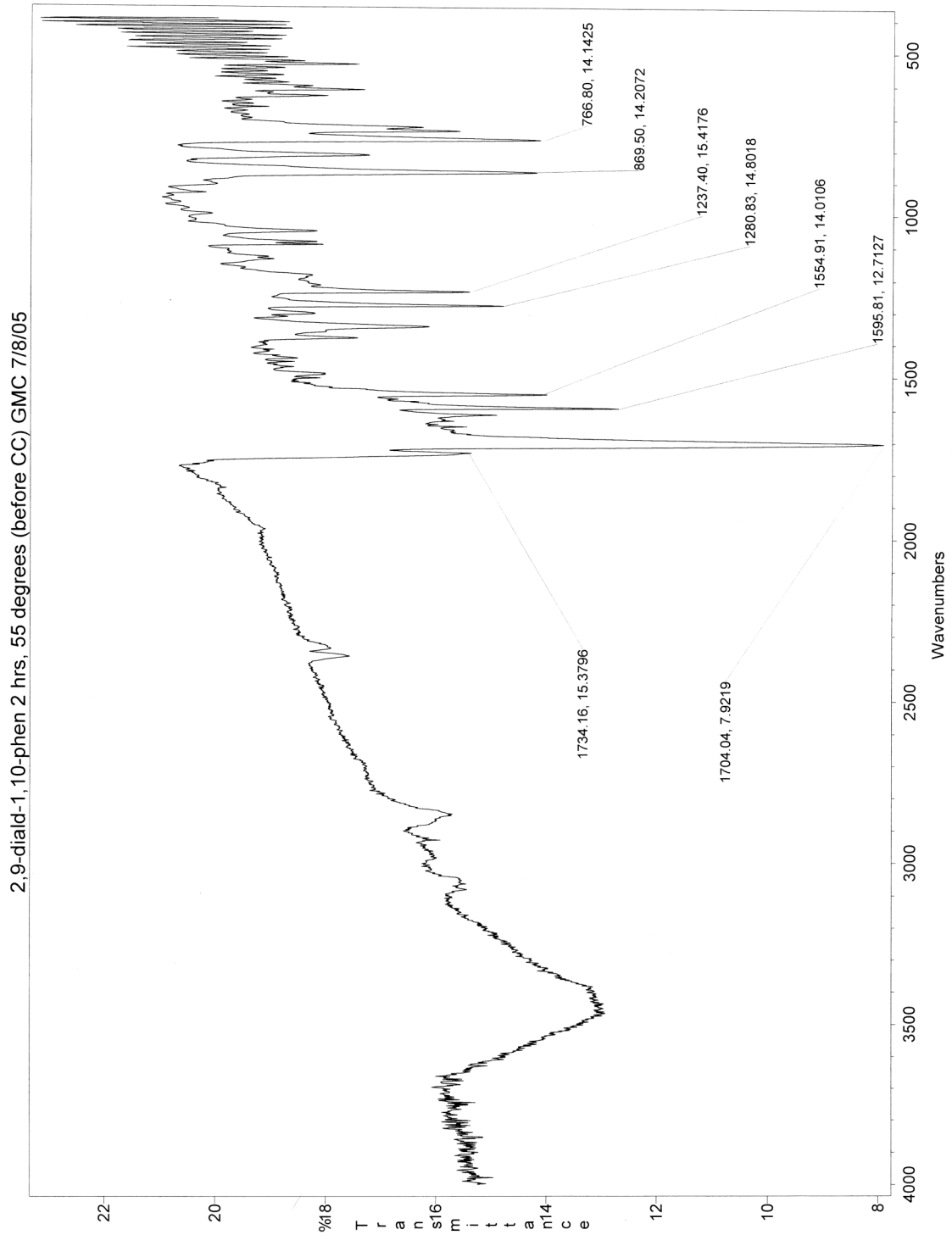

Figure 98. IR spectrum of impure aldehyde product before column chromatography

After several experiments, 60°C for 2 hours was determined to be the optimal temperature and time for the reaction. Traces of carboxylic acid were still present in both IR and NMR spectroscopy. Thin layer chromatography was used to test different solvent systems for the best separation. The TLC plate developed in 10:1 CH_2Cl_2/MeOH mobile phase had the best separation between the aldehyde and carboxylic acid products. Figure 99 shows the TLC plate.

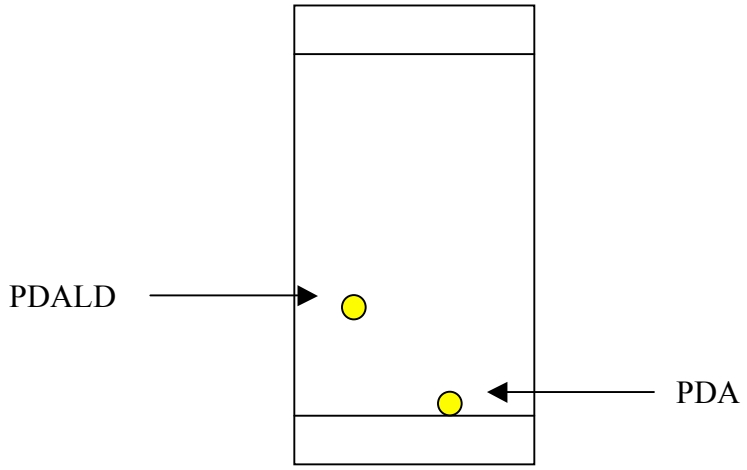

Figure 99. TLC plate of PDALD and PDA in 10:1 CH_2Cl_2/MeOH mobile phase.

Column chromatography was used to completely purify the product. A 10:1 CH_2Cl_2/MeOH solvent system efficiently separated PDALD and the impurity. A tan solid was obtained from the fractions of PDALD collected. The pure PDALD had a melting point range of 269-271°C. The IR spectrum, shown in Figure 100, did not have the extra peak at 1720 cm^{-1}. NMR, shown in Figure 101, analysis of the product confirms the purity of PDALD.

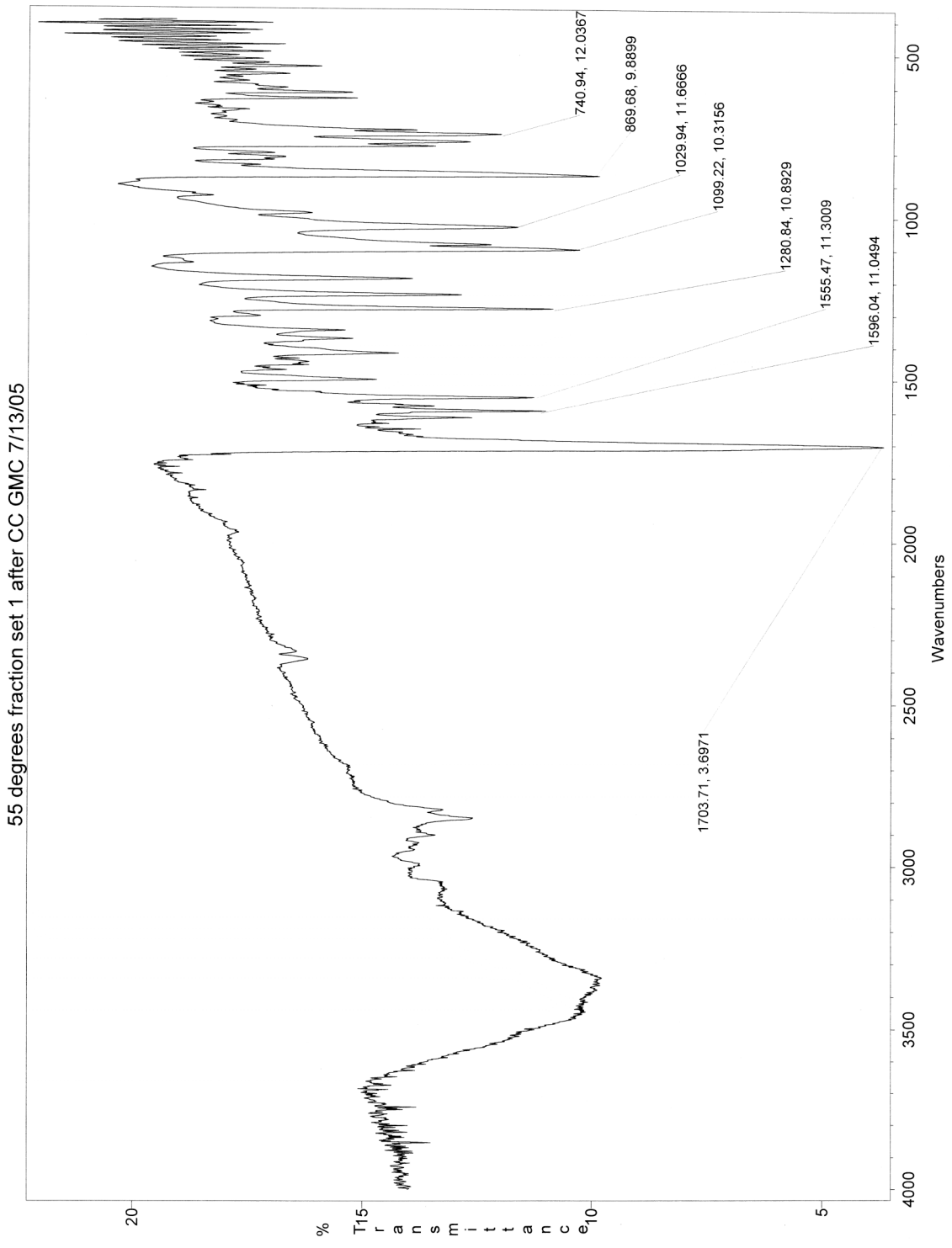

Figure 100. IR spectrum of pure aldehyde product after column chromatography

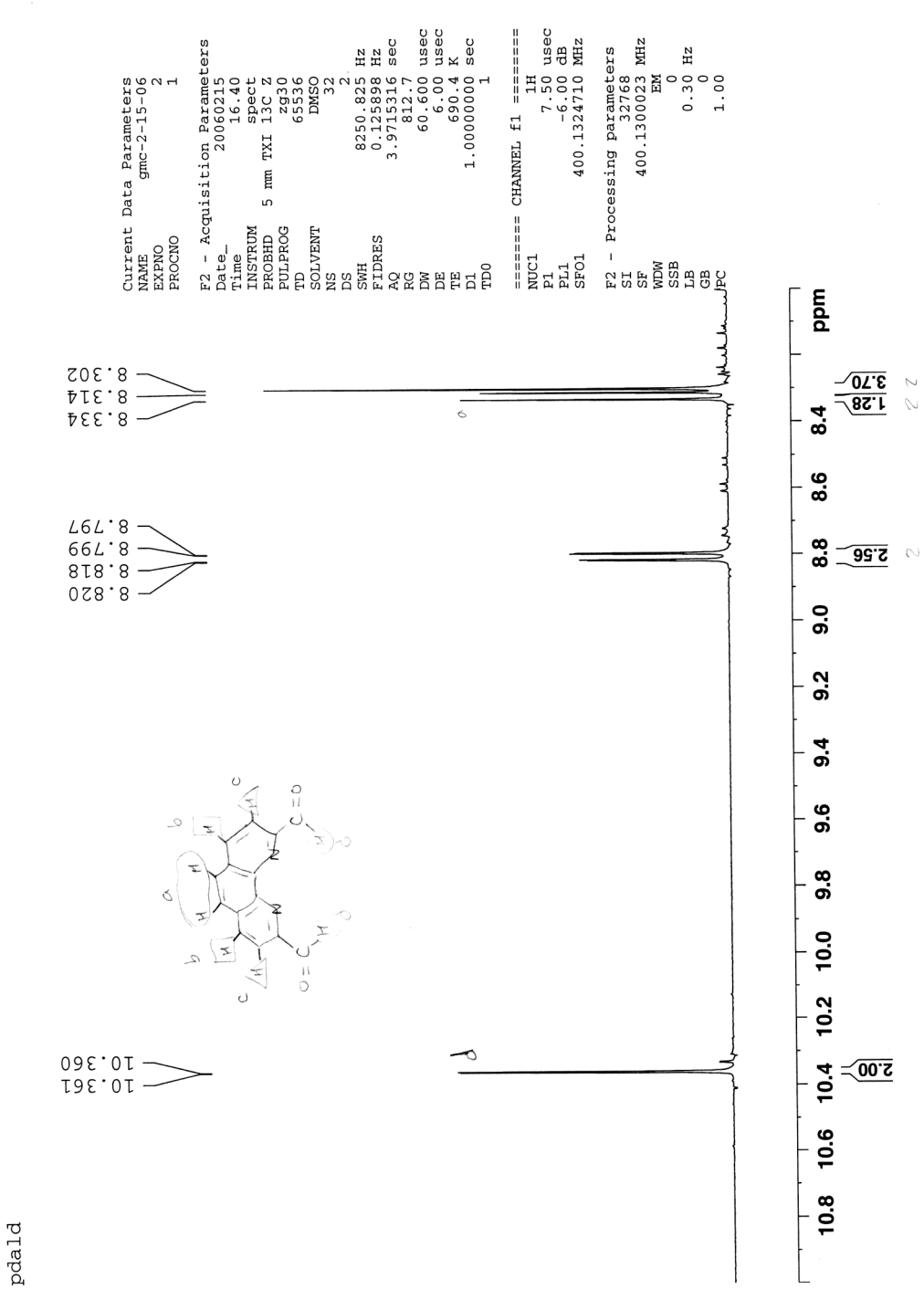

Figure 101. NMR spectrum of pure aldehyde product after column chromatography.

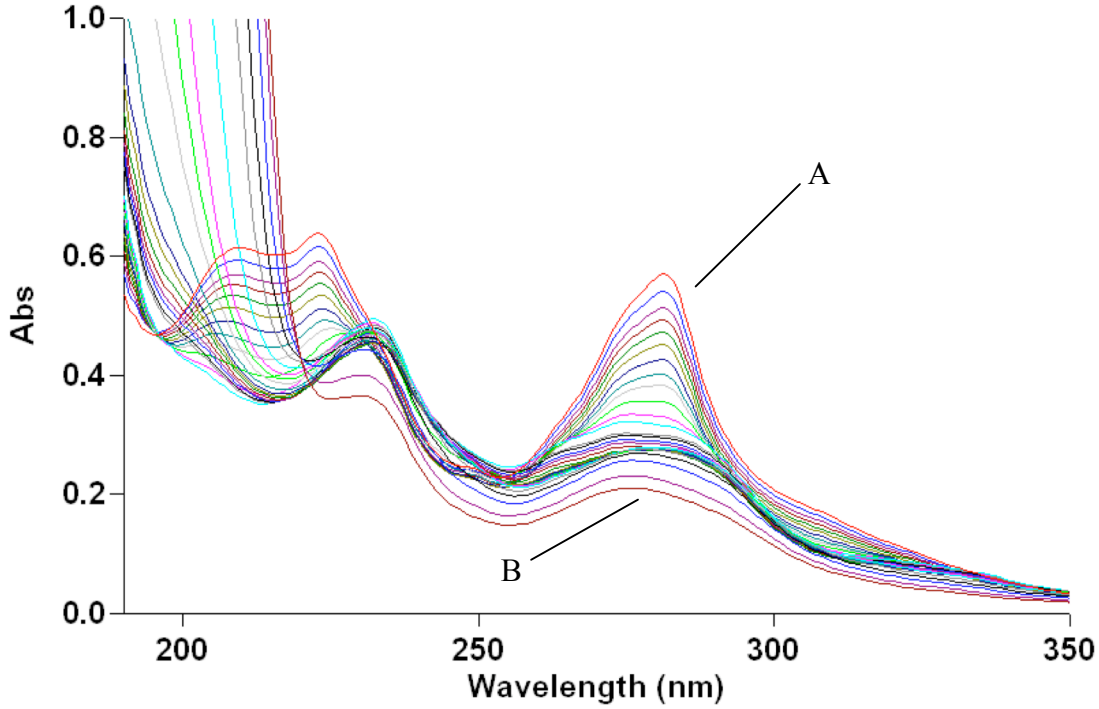

Figure 102. UV spectra of 2 x 10^{-5} M PDALD in 0.01 M $HClO_4$ and 0.09 M $NaClO_4$. (A) Initial spectrum of fully protonated ligand at pH = 1.62. (B) Final spectrum of deprotonated ligand at pH = 12.59.

REFERENCES

Billo, E. J. *EXCEL for Chemists: A Comprehensive Guide*, 2nd Edition, Wiley-VCH, New York, **2001**.

Caravan, P.; Astashkin, A. V.; Raitsimring, A. M. The gadolinium(III)- water hydrogen distance in MRI contrast agents. *Inorg. Chem.* **2003**, 42, 3972-3974.

Chandler, C. J.; Deady, L. W.; Reiss, J. A. Synthesis of some 2,9-disubstituted-1,10-phenanthrolines. *J. Heterocyclic Chem*. **1981,** 18, 599-601.

Cram, D. J. The design of molecular hosts, guests, and their complexes. *Science*. **1988,** 760.

Gomperts, B. D.; Kramer I. M.; Tatham, P. E. R. *Signal Transduction*, Elsevier, San Diego, **2002,** 171-187.

Hancock, R. D.; Martell, A. E. Ligand design for selective complexation. *Chem. Rev.* **1989,** 89, 1875-1914.

Hancock, Robert D. Chelate ring size and metal ion selection. *Journal of Chemical Education.* **1992,** 69, 615-620.

Hancock, R. D.; Cukrowski, I.; Antunes, I.; Cukrowska, E.; Mashishi, J.; Brown, K. Complexation of Bi^{3+} by nitrogen donor ligands. A polarographic study. *Polyhedron*, **1995,** 14(13), 1699-1707.

Hancock, R. D.; Melton, D M.; Harrington, J. M.; Dean, N. E.; McDonald, F. C.; Gephart, R. T.; Boone, L. L.; Jones, S. B.; Whitehead, J. R.; Cockrell, G. M. Metal ion recognition in aqueous solutions by highly preorganized non-macrocyclic ligands. *Coord. Chem. Reviews*, **2006**.

Hood, E. Low-level cadmium exposure and osteoporosis. *Environmental Health Perspectives.* **2006,** 114.

Lide, D.R. *CRC Handbook of Chemistry and Physics,* 74th Ed., CRC Press, Boca Raton, FL, **1993.**

Lim, N.C.; Schuster, V. J.; Porto, M. C.; Tanudra, M. A.; Yao, L.; Freake, H. C.; Bruckner, C. Coumarin-based chemosensors for zinc(II): toward the determination of the design algorithm for CHEF-type and ratiometric probes. *Inorg. Chem.* **2005**, 44, 2018-2030.

Mattson, M. P.; Pedersen, W. A. Effects of amyloid precursor protein derivatives and oxidative stress on basal forebrain cholinergic systems in alzheimer's disease. *Int. J. Devl Neuroscience.* **1998,** 16, 737-753.

Martel, A. E.; Smith, R. M. *Critical Stability Constant Database, 46*; National Institute of Science and Technology (NIST): Gaithersburg, MD, **2003.**

Melton, D. L.; VanDerveer, D. G.; Hancock, R. D. Complexes of greatly enhanced thermodynamic stability and metal ion size-based selectivity, formed by the highly preorganized non-macrocyclic ligand 1,10-phenanthroline-2,9-dicarboxylic acid. A thermodynamic and crystallogrphic study. *Inorg. Chem.* **2006,** 45, 9306-9314.

Neelakandan, P. P.; Hariharan, M.; Ramaiah, D. A supramolecular on-off-on fluorescence assay for selective recognition of GTP. *J. Am. Chem. Soc.* **2006,** 128(35), 11334-11335.

Pearson, Ralph G. Hard and soft acids and bases. *J. Am. Chem. Soc.* **1963,** 85, 3533-3539.

Pierre, V.C.; Botta, M.; Aime, S.; Raymond, K. N. Turning the coordination number of hydroxypyridonate-based gadolinium complexes: implications for MRI contrast agents. *J. Am. Chem. Soc.* **2006**, 128, 5344-5345.

Rockwood, A. L.; Van Orden, S. L.; Smith, R. D. Rapid calculation of isotope distribution, *Anal. Chem.* **1995,** 67(15), 2699.

U.S. Environmental Protection Agency; Cadmium Compounds, **2000**, Technology Transfer Air Toxics Website.

U.S. Environmental Protection Agency; Lead Compounds, **2000**, Technology Transfer Air Toxics Website.

U.S. Environmental Protection Agency; Mercury Compounds, **2000**, Technology Transfer Air Toxics Website.

Wang, E. E. MD; Mahajan, N. MD; Willis B. DO, Leikin, J. MD. Successful treatment of potentially fatal heavy metal poisonings. *Journal of Emergency Medicine.* **2007,** doi:10.1016/j.jemermed.2006.12.013.

APPENDIX

2,9-di-(2'-pyridyl)-1,10-phenanthroline (DPP)

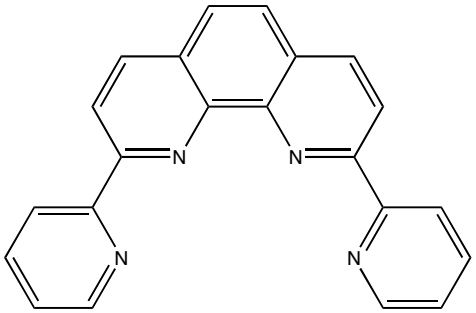

Dipyridoacridine (DPA)

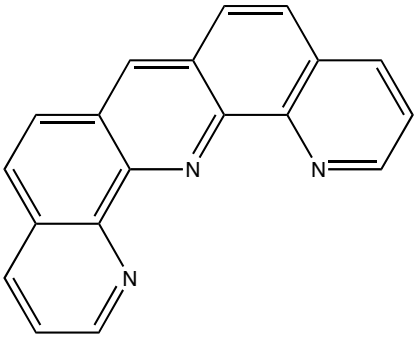

2,6-di-(2-pyridyl)pyridine (TERPY)

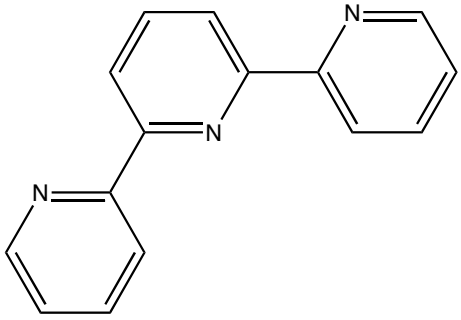

Bis-2,2'-6',2"-6",2"'-quaterpyridine (QUATERPY)

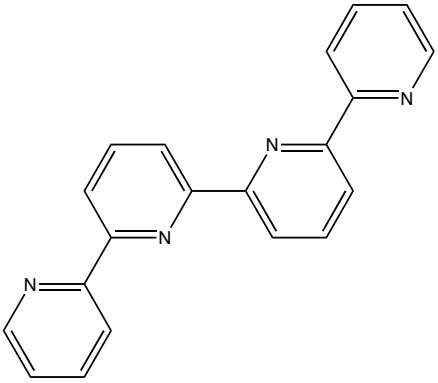

1,10-phenanthroline-2,9-dicarboxaldehyde (PDALD)

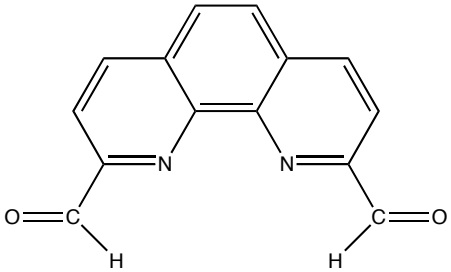

1,10-phenanthroline-2,9-dicarboxylate (PDA)

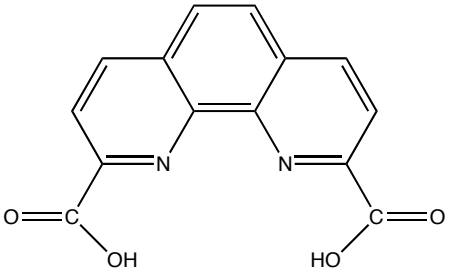

287 nm									
Amount of base	**Total base**	**pH**	**abs.**	**corr. Abs.**	**L(func)1**	**L(func)2**	**L(func)4**	**A(theor)**	**diff**
0	0	2.02	0.1353431	0.1353431	25.33150067	47.61137003	73.9428707	0.135314758	8.03274E-10
1.5	1.5	2.18	0.1188009	0.122364927	17.5251167	22.78823444	41.31335114	0.122317173	2.28048E-09
1	2.5	2.32	0.1046347	0.109866435	12.69582474	11.95943544	25.65526018	0.110317731	2.03668E-07
1	3.5	2.55	0.08582406	0.091831744	7.47585585	4.146776977	12.62263283	0.091092701	5.46185E-07
0.5	4	2.73	0.07241005	0.078202854	4.939248979	1.810133803	7.749382782	0.077975435	5.17193E-08
0.3	4.3	2.89	0.06225843	0.067612655	3.417125416	0.866384509	5.283509926	0.068511474	8.07876E-07
0.3	4.6	3.14	0.05341569	0.058329933	1.921590835	0.273974838	3.195565673	0.058235533	8.91154E-09
0.15	4.75	3.36	0.04859528	0.053211832	1.157872978	0.099474251	2.257347229	0.0531788	1.09107E-09
0.1	4.85	3.6	0.04653708	0.051051177	0.666286354	0.03293902	1.699225374	0.050626906	1.80006E-07
0.1	4.95	4.19	0.04528959	0.049773259	0.171261963	0.002176259	1.173438223	0.049852953	6.3511E-09
0.02	4.97	4.55	0.04515423	0.04964256	0.074758559	0.000414678	1.075173236	0.050149421	2.56908E-07
0.02	4.99	5.63	0.04559491	0.050145282	0.006218146	2.86887E-06	1.006221015	0.050507996	1.31561E-07
0.02	5.01	6.41	0.04657817	0.051245303	0.001031955	7.90152E-08	1.001032034	0.050540967	4.96088E-07
		pK1	3.423660919					$SS_{residuals}$	2.69345E-06
		pK2	2.29404976						
		Abs(0)	0.050547633						
		Abs(1)	0.044071226						
		Abs(2)	0.185641029						

DPP-Ni spreadsheet.

287 nm									
Amount of base	**Total base**	**pH**	**abs.**	**corr. Abs.**	**L(func)1**	**L(func)2**	**L(func)4**	**A(theor)**	**diff**
0	0	1.86	0.1479013	0.1479013	4.71882972	2.114357502	7.833187222	0.147423428	2.28362E-07
1.5	1.5	2.05	0.1187625	0.115303398	3.046732365	0.881410908	4.928143273	0.11462454	4.60848E-07
1	2.5	2.24	0.09443693	0.089939933	1.967135636	0.367433222	3.334568858	0.090526196	3.43704E-07
1	3.5	2.55	0.07272893	0.067970963	0.963461369	0.088141091	2.05160246	0.068383333	1.70049E-07
0.5	4	2.85	0.06489365	0.060086713	0.482874538	0.022140041	1.505014579	0.0606176	2.81841E-07
0.175	4.175	3.03	0.0635204	0.058625196	0.319032044	0.009664478	1.328696522	0.059224878	3.59618E-07
0.15	4.325	3.27	0.06459161	0.05944925	0.183583779	0.00320021	1.186783989	0.058927848	2.7186E-07
0.1	4.425	3.52	0.06540295	0.060085393	0.103236746	0.001011995	1.104248741	0.059250911	6.9636E-07
0.05	4.475	3.74	0.06599589	0.060574475	0.062206291	0.000367433	1.062573724	0.059594747	9.59865E-07
0.03	4.505	3.95	0.06639266	0.06090511	0.038356088	0.000139694	1.038495782	0.05985795	1.09654E-06
0.025	4.53	4.26	0.06594553	0.060467202	0.018785999	3.35103E-05	1.01881951	0.060111543	1.26493E-07
0.015	4.545	4.64	0.06551398	0.060054982	0.007831308	5.82342E-06	1.007837131	0.060269083	4.5839E-08
0.015	4.56	5.71	0.06506886	0.059630554	0.000666552	4.2187E-08	1.000666595	0.060378393	5.59264E-07
0.005	4.565	6.17	0.06452842	0.059129863	0.000231118	5.07199E-09	1.000231123	0.060385199	1.57587E-06
		pK1	2.533834306					$SS_{residuals}$	7.17651E-06
		pK2	1.511344115						
		Abs(0)	0.060388819						
		Abs(1)	0.04471371						
		Abs(2)	0.41781492						

Zn-DPP complex.

287 nm									
Amount of base	**Total base**	**pH**	**abs.**	**corr. Abs.**	**L(func)1**	**L(func)2**	**L(func)4**	**A(theor)**	**diff**
0	0	1.98	0.1760086	0.1760086	6.64989033	44.2210414	51.87093173	0.179125455	9.71479E-06
1.5	1.5	2.13	0.1703814	0.175492842	4.707761826	22.16302141	27.87078323	0.174444074	1.09991E-06
1	2.5	2.27	0.1619917	0.170091285	3.410471958	11.63131898	16.04179093	0.168317651	3.14578E-06
1	3.5	2.48	0.1470725	0.157367575	2.102879963	4.42210414	7.524984103	0.155104816	5.12008E-06
0.5	4	2.62	0.1331988	0.143854704	1.523401865	2.320753243	4.844155108	0.143513362	1.16515E-07
0.3	4.3	2.75	0.1193139	0.129574895	1.129313404	1.275348765	3.404662169	0.131289938	2.94137E-06
0.3	4.6	2.9	0.1063817	0.116168816	0.799492664	0.639188519	2.438681183	0.116683433	2.6483E-07
0.15	4.75	3.01	0.09743623	0.106692672	0.620603875	0.38514917	2.005753045	0.106546505	2.13646E-08
0.1	4.85	3.11	0.08913842	0.097784847	0.49296318	0.243012697	1.735975878	0.098258914	2.2474E-07
0.1	4.95	3.23	0.08032324	0.088275241	0.373950814	0.139839211	1.513790025	0.089792569	2.30229E-06
0.075	5.025	3.35	0.07462307	0.082122689	0.283670702	0.080469067	1.364139769	0.083002796	7.7459E-07
0.075	5.1	3.52	0.06950998	0.076599998	0.191784932	0.03678146	1.228566392	0.075940989	4.34293E-07
0.05	5.15	3.69	0.06538308	0.072117537	0.129662527	0.016812371	1.146474899	0.071209126	8.25211E-07
0.05	5.2	3.96	0.06333581	0.069922734	0.0696329	0.004848741	1.074481641	0.06678929	9.81847E-06
0.025	5.225	4.2	0.06036213	0.066669973	0.040069552	0.001605569	1.041675121	0.064706035	3.85705E-06
0.01	5.235	4.35	0.05862343	0.064761303	0.02836707	0.000804691	1.029171761	0.063903714	7.3546E-07
0.01	5.245	4.59	0.05657358	0.062508149	0.016323545	0.000266458	1.016590003	0.063093012	3.42065E-07
0.01	5.255	5.06	0.05538774	0.061208991	0.005531138	3.05935E-05	1.005561731	0.06238049	1.37241E-06
0.01	5.265	6.12	0.05331699	0.058931269	0.000481742	2.32075E-07	1.000481974	0.062051935	9.73855E-06
		pK1	2.802814483					**$SS_{residuals}$**	5.28498E-05
		pK2	2.802814483						
		Abs(0)	0.062020754						
		Abs(1)	0.126714873						
		Abs(2)	0.189655043						

Mn-DPP complex

287 nm									
Amount of base	**Total base**	**pH**	**abs.**	**corr. Abs.**	**L(func)1**	**L(func)2**	**L(func)4**	**A(theor)**	**diff**
0	0	2.05	0.1855323	0.1855323	14.14039211	15.84881352	30.98920564	0.186436869	8.18245E-07
1.5	1.5	2.21	0.1766469	0.181946307	9.782761203	7.585719081	18.36848028	0.181828502	1.38781E-08
1	2.5	2.36	0.1682401	0.176652105	6.925664553	3.801865561	11.72753011	0.176066193	3.43293E-07
1	3.5	2.58	0.1542992	0.165100144	4.173125566	1.380373952	6.553499519	0.164560717	2.90982E-07
0.5	4	2.76	0.142008	0.15336864	2.757156719	0.602555085	4.359711804	0.152204	1.35639E-06
0.3	4.3	2.92	0.1282168	0.139243445	1.90748641	0.288400996	3.195887406	0.139174976	4.68802E-09
0.3	4.6	3.18	0.1052015	0.114880038	1.048241749	0.087095708	2.135337457	0.115468008	3.45709E-07
0.15	4.75	3.41	0.08502231	0.093099429	0.617250503	0.030199292	1.647449795	0.094602288	2.25858E-06
0.1	4.85	3.67	0.06747894	0.074024397	0.339204381	0.00912004	1.348324421	0.074479656	2.07261E-07
0.05	4.9	3.91	0.05535996	0.060785236	0.195191748	0.003019929	1.198211677	0.060645374	1.95613E-08
0.025	4.925	4.1	0.04631968	0.050882168	0.126026377	0.001258916	1.127285293	0.052840505	3.83508E-06
0.025	4.95	4.52	0.03890648	0.042758222	0.047913892	0.000181969	1.048095861	0.042889634	1.72692E-08
0.015	4.965	5.12	0.03853013	0.042356172	0.012035426	1.14815E-05	1.012046907	0.037848192	2.03219E-05
0.015	4.98	6.45	0.03145242	0.034585081	0.000562939	2.51187E-08	1.000562964	0.036166442	2.5007E-06
		pK1	3.200461453					**$SS_{residuals}$**	3.23335E-05
		pK2	2.099535303						
		Abs(0)	0.036083014						
		Abs(1)	0.18436083						
		Abs(2)	0.197775879						

In-DPP complex

287 nm										
Amount of base	**Total base**	**pH**	**abs.**	**corr. Abs.**	**L(func)1**	**L(func)2**	**L(func)3**	**L(func)4**	**A(theor)**	**diff**
0	0	1.67	0.1548933	0.1548933	3075.236477	28663.17296	35645.44899	67384.85843	0.153835643	1.11864E-06
1.5	1.5	1.82	0.1362069	0.140293107	2177.1007	14365.61636	12647.48257	29191.19963	0.142059842	3.12135E-06
1	2.5	1.98	0.1227199	0.128855895	1506.185691	6875.816287	4187.975086	12570.97706	0.129516389	4.36252E-07
1	3.5	2.22	0.1065665	0.114026155	866.7193996	2276.796758	798.0022015	3942.518359	0.112513823	2.28715E-06
0.5	4	2.42	0.09540937	0.10304212	546.8629708	906.4091153	200.4490902	1654.721176	0.101201873	3.38651E-06
0.3	4.3	2.59	0.08569958	0.093069744	369.7247444	414.3089016	61.9446908	846.9783368	0.093889042	6.71249E-07
0.3	4.6	2.87	0.07803173	0.085210649	194.0343041	114.1101469	8.953731966	318.098183	0.085846969	4.04903E-07
0.15	4.75	3.12	0.07245889	0.079342485	109.1135077	36.08479683	1.59222372	147.7905283	0.081671742	5.42544E-06
0.15	4.9	3.67	0.07108013	0.078045983	30.75236477	2.866317296	0.035645449	34.65432752	0.077148416	8.05627E-07
0.05	4.95	4.29	0.06738866	0.074060137	7.376978495	0.164939345	0.000492044	8.542409883	0.072908945	1.32524E-06
0.015	4.965	4.88	0.05896567	0.064820961	1.896175441	0.010897434	8.35611E-06	2.907081232	0.064551299	7.27179E-08
0.005	4.97	5.27	0.050921	0.055982547	0.772464478	0.001808524	5.64942E-07	1.774273567	0.056655029	4.52232E-07
0.005	4.975	5.7	0.04453051	0.048961296	0.286997767	0.000249646	2.89737E-08	1.287247442	0.049016024	2.99519E-09
0.005	4.98	6.06	0.04118656	0.045288741	0.125279069	4.7569E-05	2.40993E-09	1.12532664	0.045015951	7.44144E-08
0.005	4.985	6.38	0.0390976	0.042995631	0.059962332	1.08974E-05	2.64243E-10	1.05997323	0.043055938	3.63693E-09
		pK1	5.157878517						**$SS_{residuals}$**	1.95884E-05
		pK2	2.639445747							
		pK3	1.764679825							
		Abs(0)	0.041032205							
		Abs(1)	0.076797142							
		Abs(2)	0.091861286							
		Abs(3)	0.210319884							

Gd-DPP complex

287 nm									
Amount of base	**Total base**	**pH**	**abs.**	**corr. Abs.**	**L(func)1**	**L(func)2**	**L(func)4**	**A(theor)**	**diff**
0	0	2.02	0.1658937	0.1658937	8.963416587	6.724580522	16.68799711	0.165896581	8.29952E-12
1.5	1.5	2.18	0.1409734	0.145202602	6.2011692	3.218586596	10.4197558	0.145717311	2.64926E-07
1	2.5	2.33	0.1216615	0.127744575	4.390091594	1.613114512	7.003206106	0.128142921	1.58679E-07
1	3.5	2.55	0.1010495	0.108122965	2.645291774	0.585686479	4.230978253	0.10590281	4.92909E-06
0.5	4	2.72	0.08495053	0.091746572	1.788436733	0.267710372	3.056147105	0.091911351	2.71521E-08
0.3	4.3	2.87	0.07484383	0.081280399	1.266116246	0.134173021	2.400289267	0.081769771	2.39484E-07
0.3	4.6	3.09	0.06483669	0.070801665	0.762910481	0.048715279	1.81162576	0.070172629	3.95687E-07
0.15	4.75	3.26	0.05627969	0.061626261	0.515790788	0.022267179	1.538057967	0.06346916	3.39628E-06
0.15	4.9	3.55	0.0495883	0.054447953	0.264529177	0.005856865	1.270386042	0.05559098	1.30651E-06
0.1	5	3.95	0.04613543	0.050748973	0.105310962	0.000928251	1.106239213	0.04979273	9.144E-07
0.05	5.05	4.45	0.04320864	0.047572713	0.03330225	9.28251E-05	1.033395075	0.046888449	4.68217E-07
0.025	5.075	5.52	0.04257952	0.046901341	0.002834481	6.72458E-07	1.002835154	0.045595388	1.70551E-06
0.01	5.085	6.44	0.04249835	0.046820432	0.00034078	9.71998E-09	1.000340789	0.045487716	1.77613E-06
0.01	5.095	7.18	0.04056389	0.04469735	6.20117E-05	3.21859E-10	1.000062012	0.045475661	6.05768E-07
0.005	5.1	7.27	0.03964126	0.043684669	5.0405E-05	2.1265E-10	1.000050405	0.045475159	3.20586E-06
		pK1	2.972473581					**$SS_{residuals}$**	1.93937E-05
		pK2	1.895191617						
		Abs(0)	0.045472979						
		Abs(1)	0.088723803						
		Abs(2)	0.286670711						

Th-DPP complex

282 nm									
Amount of base	**Total base**	**pH**	**abs.**	**corr. Abs.**	**L(func)1**	**L(func)2**	**L(func)4**	**A(theor)**	**diff**
0	0	3.04	0.1573073	0.1573073	0.239283421	0.000330563	1.239613984	0.161527377	1.78091E-05
0.005	0.005	2.67	0.1395213	0.139535252	0.560935091	0.001816577	1.562751669	0.136247508	1.08093E-05
0.005	0.01	2.48	0.1250487	0.12507371	0.868785592	0.004357666	1.873143257	0.120346333	2.23481E-05
0.005	0.015	2.34	0.108432	0.10846453	1.19925796	0.008303361	2.207561321	0.108373676	8.25437E-09
0.005	0.02	2.23	0.09638959	0.096428146	1.54494353	0.013780148	2.558723678	0.099317987	8.35118E-06
0.005	0.025	2.14	0.08940539	0.089450093	1.900695777	0.020857099	2.921552876	0.092385801	8.61839E-06
0.01	0.035	2.01	0.0829201	0.082978144	2.563968055	0.037953681	3.601921735	0.083452961	2.25451E-07
0.01	0.045	1.92	0.07846618	0.0785368	3.154369827	0.05744522	4.211815047	0.078179135	1.27924E-07
0.01	0.055	1.83	0.0747117	0.074793883	3.88072269	0.086946859	4.967669549	0.073745403	1.09931E-06
0.015	0.07	1.74	0.07156066	0.071660845	4.774331933	0.131599397	5.90593133	0.070206301	2.1157E-06
0.02	0.09	1.64	0.06924184	0.069366475	6.010527795	0.208570988	7.219098783	0.067366861	3.99846E-06
0.03	0.12	1.52	0.06764322	0.067805564	7.923418768	0.362454835	9.285873603	0.065524974	5.20109E-06
0.045	0.165	1.4	0.06701341	0.067234554	10.44510018	0.629874313	12.0749745	0.065443092	3.20934E-06
0.075	0.24	1.25	0.06783274	0.068158337	14.75409617	1.25676448	17.01086065	0.067926724	5.36446E-08
0.1	0.34	1.11	0.07211912	0.07260953	20.36632219	2.394715348	23.76103753	0.073004065	1.55658E-07
0.15	0.49	0.97	0.07716501	0.077921227	28.11335067	4.563036027	33.6763867	0.080957136	9.21674E-06
0.2	0.69	0.85	0.08529183	0.086468857	37.06061397	7.929647789	45.99026176	0.090217115	1.40494E-05
0.3	0.99	0.73	0.09656486	0.098476844	48.8554041	13.7801485	63.6355526	0.101815422	1.11461E-05
0.5	1.49	0.6	0.1125225	0.115875671	65.90412675	25.07574806	91.9798748	0.116985161	1.23097E-06
1	2.49	0.45	0.1320322	0.138607404	93.09205337	50.03269512	144.1247485	0.137529869	1.16108E-06
1	3.49	0.38	0.1419273	0.151833826	109.3736259	69.06434505	179.4379709	0.148030704	1.44637E-05
		pK1	2.41891261					$SS_{residuals}$	0.000135399
		pK2	0.180341288						
		Abs(0)	0.191040967						
		Abs(1)	0.037964527						
		Abs(2)	0.321714052						

Cd-DPP complex

282 nm										
Amount of base	**Total base**	**pH**	**abs.**	**corr. Abs.**	**L(func)1**	**L(func)2**	**L(func)3**	**L(func)4**	**A(theor)**	**diff**
0	0	1.94	0.1459215	0.1459215	4410.963321	19511.65876	86308.77198	110232.3941	0.146822478	8.11761E-07
1.5	1.5	2.09	0.1385598	0.142716594	3122.722888	9778.994276	30623.50791	43526.22507	0.141974005	5.51438E-07
1	2.5	2.22	0.1311342	0.13769091	2314.906458	5373.95706	12475.41316	20165.27668	0.1369928	4.87358E-07
1	3.5	2.41	0.1212768	0.129766176	1494.629144	2240.238166	3357.800871	7093.668181	0.128962208	6.46365E-07
0.5	4	2.55	0.1133846	0.122455368	1082.763099	1175.693702	1276.600286	3536.057088	0.123228824	5.98234E-07
0.3	4.3	2.66	0.1088793	0.11824292	840.4917336	708.4255107	597.1108152	2147.028059	0.119324125	1.16901E-06
0.3	4.6	2.8	0.1049171	0.114569473	608.882436	371.786993	227.0152004	1208.684629	0.115501831	8.69291E-07
0.15	4.75	2.9	0.1037106	0.113563107	483.6525105	234.5817338	113.7771203	833.0113646	0.113622081	3.47794E-09
0.15	4.9	3.02	0.102594	0.112648212	366.8879486	134.9876982	49.66551434	552.5411611	0.112200588	2.00367E-07
0.1	5	3.12	0.1020666	0.11227326	291.4294565	85.17147961	24.89172174	402.4926579	0.111563252	5.04112E-07
0.1	5.1	3.25	0.1015779	0.111938846	216.0396408	46.80520933	10.14039652	273.9852466	0.111238235	4.90855E-07
0.05	5.15	3.34	0.1013548	0.111794344	175.6036127	30.92389514	5.445715357	212.9732232	0.111219394	3.30568E-07
0.05	5.2	3.45	0.1014197	0.111967349	136.311798	18.63348945	2.547152442	158.4924399	0.111313706	4.27249E-07
0.05	5.25	3.59	0.1009072	0.111502456	98.74916828	9.778994276	0.968400349	110.4965629	0.111496733	3.27479E-11
0.025	5.275	3.68	0.1009964	0.11165152	80.26633742	6.460917446	0.520061779	88.24731665	0.111603753	2.28172E-09
0.05	5.325	3.96	0.1001826	0.110852047	42.12437269	1.779484428	0.075171798	44.97902891	0.111690458	7.02934E-07
0.025	5.35	4.22	0.09905834	0.109657582	23.14906458	0.537395706	0.012475413	24.6989357	0.111258455	2.56279E-06
0.025	5.375	4.83	0.0951655	0.105395791	5.68242152	0.032381293	0.000184525	6.714987339	0.107021306	2.6423E-06
0.01	5.385	5.45	0.08761371	0.097049707	1.36311798	0.001863349	2.54715E-06	2.364983876	0.09551089	2.36796E-06
0.005	5.39	5.77	0.08201055	0.090851287	0.652429285	0.000426869	2.7929E-07	1.652856433	0.087808288	9.25984E-06
0.005	5.395	6.01	0.07577574	0.083951942	0.375433867	0.000141349	5.32176E-08	1.375575269	0.082647509	1.70155E-06
0.005	5.4	6.2	0.07156432	0.079293267	0.242400464	5.89243E-05	1.43237E-08	1.242459402	0.079350604	3.28763E-09
0.01	5.41	6.44	0.06697952	0.074226704	0.139486908	1.95117E-05	2.72932E-09	1.139506422	0.076272027	4.18335E-06
0.02	5.43	6.8	0.06553561	0.072652777	0.060888244	3.71787E-06	2.27015E-10	1.060891962	0.07351861	7.49667E-07
0.025	5.455	6.9	0.06541561	0.072552453	0.048365251	2.34582E-06	1.13777E-10	1.048367597	0.073041794	2.39455E-07
		pK1	5.584533446						$SS_{residuals}$	3.15055E-05
		pK2	2.585760745							
		pK3	2.585760745							
		Abs(0)	0.071088197							
		Abs(1)	0.113433504							
		Abs(2)	0.091157717							
		Abs(3)	0.161113784							

Lu-DPP complex

287 nm									
Amount of base	**Total base**	**pH**	**abs.**	**corr. Abs.**	**L(func)1**	**L(func)2**	**L(func)4**	**A(theor)**	**diff**
0	0	1.96	0.1392069	0.1392069	82.63650068	41.17727258	124.8137733	0.13912202	7.20459E-09
1.5	1.5	2.1	0.1197919	0.123385657	59.86485271	21.61013984	82.47499255	0.122681054	4.96465E-07
1	2.5	2.24	0.103664	0.1088472	43.36825204	11.34116261	55.70941465	0.108518605	1.07975E-07
1	3.5	2.47	0.08439057	0.09029791	25.53712006	3.932399003	30.46951906	0.090431738	1.79098E-08
0.5	4	2.65	0.07225181	0.078031955	16.8722079	1.716554423	19.58876233	0.080336401	5.31047E-06
0.3	4.3	2.81	0.06619575	0.071888585	11.67271598	0.821594602	13.49431058	0.073774985	3.55851E-06
0.3	4.6	3.06	0.06150829	0.067167053	6.564050571	0.259811026	7.823861596	0.066867291	8.98573E-08
0.15	4.75	3.26	0.05943523	0.065081577	4.141635917	0.103432632	5.245068549	0.063356531	2.97578E-06
0.1	4.85	3.49	0.05589363	0.061315312	2.438776033	0.035863905	3.474639938	0.0606999	3.78732E-07
0.075	4.925	3.79	0.05396205	0.059277312	1.222283413	0.009008606	2.231292019	0.058547513	5.32607E-07
0.05	4.975	4.24	0.05245525	0.057674547	0.43368252	0.001134116	1.434816637	0.056781521	7.97496E-07
0.015	4.99	4.54	0.05190571	0.0570859	0.217356143	0.000284877	1.21764102	0.056157005	8.62845E-07
0.005	4.995	4.73	0.05121988	0.056336746	0.140336913	0.000118757	1.140455669	0.055906548	1.8507E-07
0.01	5.005	5.37	0.04995085	0.05495093	0.032149329	6.23243E-06	1.032155562	0.055520235	3.24108E-07
0.01	5.015	6.15	0.04868768	0.053571054	0.005335461	1.71655E-07	1.005335632	0.055416956	3.40735E-06
		pK1	3.877171918					$SS_{residuals}$	1.90524E-05
		pK2	1.657485659						
		Abs(0)	0.055395999						
		Abs(1)	0.059336943						
		Abs(2)	0.301271798						

Ca-DPP complex

287 nm									
Amount of base	**Total base**	**pH**	**abs.**	**corr. Abs.**	**L(func)1**	**L(func)2**	**L(func)4**	**A(theor)**	**diff**
0	0	1.94	0.1416331	0.1416331	1.997965128	3.991864653	6.989829782	0.141877357	5.96615E-08
1.5	1.5	2.1	0.1224779	0.126152237	1.382254154	1.910626548	4.292880702	0.125252062	8.10316E-07
1	2.5	2.24	0.104685	0.10991925	1.001354615	1.002711066	3.004065681	0.110662628	5.5261E-07
1	3.5	2.45	0.08492223	0.090866786	0.617430251	0.381220115	1.998650366	0.092081502	1.47553E-06
0.5	4	2.6	0.07897241	0.085290203	0.437107143	0.191062655	1.628169798	0.082671786	6.85611E-06
0.3	4.3	2.72	0.07049348	0.076555919	0.331579677	0.109945082	1.441524759	0.077474818	8.44376E-07
0.3	4.6	2.88	0.06671757	0.072855586	0.22939709	0.052623025	1.282020115	0.073098686	5.90972E-08
0.15	4.75	3	0.06475315	0.070904699	0.174015488	0.03028139	1.204296878	0.071173216	7.21012E-08
0.15	4.9	3.16	0.06344976	0.069667836	0.120389304	0.014493585	1.134882889	0.069726389	3.42838E-09
0.1	5	3.31	0.0627251	0.06899761	0.0852291	0.007264	1.0924931	0.069050591	2.80697E-09
0.05	5.05	3.41	0.06266122	0.068990003	0.067699881	0.004583274	1.072283155	0.068806084	3.38263E-08
0.075	5.125	3.63	0.06206192	0.068423267	0.040793212	0.001664086	1.042457298	0.068562287	1.93267E-08
0.05	5.175	3.88	0.0619959	0.068412476	0.022939709	0.00052623	1.023465939	0.068494788	6.7754E-09
0.05	5.225	4.44	0.06185789	0.06832204	0.00631812	3.99186E-05	1.006358039	0.068504105	3.31477E-08
0.01	5.235	4.93	0.06187496	0.068353268	0.002044504	4.18E-06	1.002048684	0.068518196	2.72012E-08
0.005	5.24	5.23	0.06171634	0.068184212	0.001024679	1.04997E-06	1.001025729	0.068522281	1.14291E-07
0.005	5.245	5.52	0.06203492	0.068542383	0.000525518	2.7617E-07	1.000525795	0.068524383	3.24002E-10
0.005	5.25	5.69	0.06234093	0.068886728	0.000355294	1.26234E-07	1.00035542	0.068525115	1.30764E-07
0.01	5.26	6.01	0.06252019	0.069097314	0.000170054	2.89185E-08	1.000170083	0.068525921	3.2649E-07
		pK1	2.240587904					**$SS_{residuals}$**	1.14282E-05
		pK2	2.240587904						
		Abs(0)	0.068526668						
		Abs(1)	0.064107256						
		Abs(2)	0.199177055						

La-DPP complex

287 nm										
Amount of base	**Total base**	**pH**	**abs.**	**corr. Abs.**	**L(func)1**	**L(func)2**	**L(func)3**	**L(func)4**	**A(theor)**	**diff**
0	0	1.91	0.1436712	0.1436712	6636.299811	262772.9092	122006.7536	391416.9626	0.143264962	1.65029E-07
1.5	1.5	2.04	0.1244644	0.128198332	4919.557015	144404.4542	49703.14517	199028.1564	0.128924884	5.27878E-07
1	2.5	2.17	0.1110109	0.116561445	3646.917998	79356.14993	20248.08109	103252.149	0.116484738	5.88391E-09
1	3.5	2.37	0.09586792	0.102578674	2301.049695	31592.25232	5086.088015	38980.39003	0.101172118	1.9784E-06
0.5	4	2.51	0.0857629	0.092623932	1666.963145	16579.8497	1933.676732	20181.48958	0.092992194	1.35617E-07
0.3	4.3	2.64	0.0795423	0.086382938	1235.736851	9111.305093	787.7417643	11135.78371	0.086980811	3.57453E-07
0.2	4.5	2.74	0.07546348	0.082255193	981.5806717	5748.844867	394.8061156	7126.231654	0.083225035	9.40593E-07
0.15	4.65	2.85	0.07252762	0.079272689	761.9491662	3464.021583	184.6646943	4411.635444	0.079813588	2.92573E-07
0.15	4.8	2.98	0.06958347	0.076263483	564.8407202	1903.621448	75.22875446	2544.690923	0.076568545	9.30625E-08
0.15	4.95	3.17	0.06682503	0.073440708	364.6917998	793.5614993	20.24808109	1179.50138	0.072975506	2.16413E-07
0.125	5.075	3.43	0.06429125	0.070816812	200.4130503	239.6517415	3.360345027	444.4251369	0.069537097	1.63767E-06
0.1	5.175	3.88	0.06068086	0.066961329	71.10923363	30.17036674	0.150101099	102.4297015	0.065820798	1.30081E-06
0.05	5.225	4.7	0.05465824	0.060370026	10.76281804	0.691163172	0.000520456	12.45450167	0.061211764	7.08523E-07
0.01	5.235	5.35	0.04799711	0.053022407	2.409494826	0.034640216	5.83961E-06	3.444140882	0.053981169	9.19224E-07
0.005	5.24	5.8	0.04158555	0.045943716	0.854921026	0.004360945	2.60846E-07	1.859282231	0.045850511	8.68719E-09
0.005	5.245	6.22	0.035728	0.039475867	0.325031909	0.000630348	1.43345E-08	1.325662271	0.038778616	4.86159E-07
0.01	5.255	7.06	0.02893434	0.031975339	0.046981405	1.31698E-05	4.32896E-11	1.046994575	0.032230823	6.52719E-08
		pK1	5.731925998						$SS_{residuals}$	9.83925E-06
		pK2	3.507654591							
		pK3	1.576803282							
		Abs(0)	0.030767748							
		Abs(1)	0.063361348							
		Abs(2)	0.071604592							
		Abs(3)	0.301951101							

Pb-DPP complex